Publishing House ASV

begell house, inc. publishers

PAACH

Scientific coordination is carried out by the Russian Academy of Architecture and Construction Sciences (RAACS)

Volume 17 • Issue 3 • 2021

ISSN 2588-0195 (Online)
ISSN 2587-9618 (Print) Continues ISSN 1524-5845

International Journal for

Computational Civil and Structural Engineering

Международный журнал по расчету гражданских и строительных конструкций

http://raasn.ru/public.php
http://ijccse.iasv.ru/

DOI: 10.22337/2587-9618
GICID: 71.0000.1500.2830

PUBLISHER

ASV Publishing House
(ООО «Издательство АСВ»)
19/1,12, Yaroslavskoe Shosse, 120338, Moscow, Russia
Tel. +7(925)084-74-24; E-mail: iasv@iasv.ru; Интернет-сайт: http://iasv.ru/

ADVISORY EDITORIAL BOARD

TECHNICAL EDITOR

EDITORIAL TEAM

INVITED REVIEWERS

AIMS AND SCOPE

The aim of the Journal is to advance the research and practice in structural engineering through the application of computational methods. The Journal will publish original papers and educational articles of general value to the field that will bridge the gap between high-performance construction materials, large-scale engineering systems and advanced methods of analysis.

The scope of the Journal includes papers on computer methods in the areas of structural engineering, civil engineering materials and problems concerned with multiple physical processes interacting at multiple spatial and temporal scales. The Journal is intended to be of interest and use to researches and practitioners in academic, governmental and industrial communities.

ОБЩАЯ ИНФОРМАЦИЯ О ЖУРНАЛЕ

International Journal for Computational Civil and Structural Engineering

(Международный журнал по расчету гражданских и строительных конструкций)

Международный научный журнал "International Journal for Computational Civil and Structural Engineering (Международный журнал по расчету гражданских и строительных конструкций)" (IJCCSE) является ведущим научным периодическим изданием по направлению «Инженерные и технические науки», издаваемым, начиная с 1999 года (ISSN 2588-0195 (Online); ISSN 2587-9618 (Print) Continues ISSN 1524-5845). В журнале на высоком научно-техническом уровне рассматриваются проблемы численного и компьютерного моделирования в строительстве, актуальные вопросы разработки, исследования, развития, верификации, апробации и приложений численных, численно-аналитических методов, программно-алгоритмического обеспечения и выполнения автоматизированного проектирования, мониторинга и комплексного наукоемкого расчетно-теоретического и экспериментального обоснования напряженно-деформированного (и иного) состояния, прочности, устойчивости, надежности и безопасности ответственных объектов гражданского и промышленного строительства, энергетики, машиностроения, транспорта, биотехнологий и других высокотехнологичных отраслей.

В редакционный совет журнала входят известные российские и зарубежные деятели науки и техники (в том числе академики, члены-корреспонденты, иностранные члены, почетные члены и советники Российской академии архитектуры и строительных наук). Основной критерий отбора статей для публикации в журнале − их высокий научный уровень, соответствие которому определяется в ходе высококвалифицированного рецензирования и объективной экспертизы, поступающих в редакцию материалов.

Журнал входит в Перечень ВАК РФ ведущих рецензируемых научных изданий, в которых должны быть опубликованы основные научные результаты диссертаций на соискание ученой степени кандидата наук, на соискание ученой степени доктора наук по научным специальностям и соответствующим им отраслям науки:

- 01.02.04 – Механика деформируемого твердого тела (технические науки),
- 05.13.18 – Математическое моделирование численные методы и комплексы программ (технические науки),
- 05.23.01 – Строительные конструкции, здания и сооружения (технические науки),
- 05.23.02 – Основания и фундаменты, подземные сооружения (технические науки),
- 05.23.05 – Строительные материалы и изделия (технические науки),
- 05.23.07 – Гидротехническое строительство (технические науки),
- 05.23.17 – Строительная механика (технические науки).

В Российской Федерации журнал индексируется Российским индексом научного цитирования (РИНЦ).

Журнал входит в базу данных Russian Science Citation Index (RSCI), полностью интегрированную с платформой Web of Science. Журнал имеет международный статус и высылается в ведущие библиотеки и научные организации мира.

Издатели журнала – *Издательство Ассоциации строительных высших учебных заведений /АСВ/* (Россия, г. Москва) и до 2017 года *Издательский дом Begell House Inc*. (США, г. Нью-Йорк). Официальными партнерами издания является *Российская академия архитектуры и строительных наук* (РААСН), осуществляющая научное курирование издания, и *Научно-исследовательский центр СтаДиО* (ЗАО НИЦ СтаДиО).

Цели журнала – демонстрировать в публикациях российскому и международному профессиональному сообществу новейшие достижения науки в области вычислительных методов

решения фундаментальных и прикладных технических задач, прежде всего в области строительства.

Задачи журнала:

• предоставление российским и зарубежным ученым и специалистам возможности публиковать результаты своих исследований;

• привлечение внимания к наиболее актуальным, перспективным, прорывным и интересным направлениям развития и приложений численных и численно-аналитических методов решения фундаментальных и прикладных технических задач, совершенствования технологий математического, компьютерного моделирования, разработки и верификации реализующего программно-алгоритмического обеспечения;

• обеспечение обмена мнениями между исследователями из разных регионов и государств.

Тематика журнала. К рассмотрению и публикации в журнале принимаются аналитические материалы, научные статьи, обзоры, рецензии и отзывы на научные публикации по фундаментальным и прикладным вопросам технических наук, прежде всего в области строительства. В журнале также публикуются информационные материалы, освещающие научные мероприятия и передовые достижения Российской академии архитектуры и строительных наук, научно-образовательных и проектно-конструкторских организаций.

Тематика статей, принимаемых к публикации в журнале, соответствует его названию и охватывает направления научных исследований в области разработки, исследования и приложений численных и численно-аналитических методов, программного обеспечения, технологий компьютерного моделирования в решении прикладных задач в области строительства, а также соответствующие профильные специальности, представленные в диссертационных советах профильных образовательных организациях высшего образования.

Редакционная политика. Политика редакционной коллегии журнала базируется на современных юридических требованиях в отношении авторского права, законности, плагиата и клеветы, изложенных в законодательстве Российской Федерации, и этических принципах, поддерживаемых сообществом ведущих издателей научной периодики.

За публикацию статей плата с авторов не взымается. Публикация статей в журнале бесплатная. На платной основе в журнале могут быть опубликованы материалы рекламного характера, имеющие прямое отношение к тематике журнала.

Журнал предоставляет непосредственный открытый доступ к своему контенту, исходя из следующего принципа: свободный открытый доступ к результатам исследований способствует увеличению глобального обмена знаниями.

Индексирование. Публикации в журнале входят в системы расчетов индексов цитирования авторов и журналов. «Индекс цитирования» – числовой показатель, характеризующий значимость данной статьи и вычисляющийся на основе последующих публикаций, ссылающихся на данную работу.

Авторам. Прежде чем направить статью в редакцию журнала, авторам следует ознакомиться со всеми материалами, размещенными в разделах сайта журнала (интернет-сайт Российской академии архитектуры и строительных наук (http://raasn.ru); подраздел «Издания РААСН» или интернет-сайт Издательства АСВ (http://iasv.ru); подраздел «Журнал IJCCSE»): с основной информацией о журнале, его целями и задачами, составом редакционной коллегии и редакционного совета, редакционной политикой, порядком рецензирования направляемых в журнал статей, сведениями о соблюдении редакционной этики, о политике авторского права и лицензирования, о представлении журнала в информационных системах (индексировании), информацией о подписке на журнал, контактными данными и пр. Журнал работает по лицензии Creative Commons типа cc by-nc-sa (Attribution Non-Commercial Share Alike) – Лицензия «С указанием авторства – Некоммерческая – Копилефт».

Рецензирование. Все научные статьи, поступившие в редакцию журнала, проходят обязательное двойное слепое рецензирование (рецензент не знает авторов рукописи, авторы рукописи не знаю рецензентов).

Заимствования и плагиат. Редакционная коллегия журнала при рассмотрении статьи проводит проверку материала с помощью системы «Антиплагиат». В случае обнаружения многочисленных заимствований редакция действует в соответствии с правилами COPE.

Подписка. Журнал зарегистрирован в Федеральном агентстве по средствам массовой информации и охраны культурного наследия Российской Федерации. Индекс в общероссийском каталоге РОСПЕЧАТЬ − 18076.

По вопросам подписки на международный научный журнал “International Journal for Computational Civil and Structural Engineering (Международный журнал по расчету гражданских и строительных конструкций)” обращайтесь в Агентство «Роспечать» (Официальный сайт в сети Интернет: http://www.rosp.ru/) или в издательство Ассоциации строительных вузов (АСВ) в соответствии со следующими контактными данными:

ООО «Издательство АСВ»

Юридический адрес: 129337, Россия, г. Москва, Ярославское ш., д. 26, офис 705;

Фактический адрес: 129337, Россия, г. Москва, Ярославское ш., д. 19, корп. 1, 5 этаж, офис 12 (ТЦ Соле Молл);

Телефоны: +7 (925) 084-74-24, +7 (926) 010-91-33;

Интернет-сайт: www.iasv.ru. Адрес электронной почты: iasv@iasv.ru.

Контактная информация. По всем вопросам работы редакции, рецензирования, согласования правки текстов и публикации статей следует обращаться к главному редактору журнала члену-корреспонденту РААСН *Сидорову Владимиру Николаевичу* (адреса электронной почты: sidorov.vladimir@gmail.com, sidorov@iasv.ru, iasv@iasv.ru, sidorov@raasn.ru) или к техническому редактору журнала советнику РААСН *Кайтукову Таймуразу Батразовичу* (адреса электронной почты: tkaytukov@gmail.com; kaytukov@raasn.ru). Кроме того, по указанным вопросам, а также по вопросам размещения в журнале рекламных материалов можно обращаться к генеральному директору ООО «Издательство АСВ» *Никитиной Надежде Сергеевне* (адреса электронной почты: iasv@iasv.ru, nsnikitina@mail.ru, ijccse@iasv.ru).

Журнал становится технологичнее. Издательство АСВ с сентября 2016 года является членом Международной ассоциации издателей научной литературы (Publishers International Linking Association (PILA)), осуществляющей свою деятельность на платформе CrossRef. Оригинальным статьям, публикуемым в журнале, будут присваиваться уникальные номера (индексы DOI – Digital Object Identifier), что значительно облегчит поиск метаданных и местонахождение полнотекстового произведения. DOI – это система определения научного контента в сети Интернет.

С октября 2016 года стал возможен прием статей на рассмотрение и рецензирование через онлайн систему приема статей Open Journal Systems на сайте журнала (электронная редакция): http://ijccse.iasv.ru/index.php/IJCCSE.

Автор имеет возможность следить за продвижением статьи в редакции журнала в личном кабинете Open Journal Systems и получать соответствующие уведомления по электронной почте.

В феврале 2018 года журнал был зарегистрирован в Directory of open access journals (DOAJ) (это один из самых известных поисковых сервисов в мире, который предоставляет открытый доступ к материалам и индексирует не только заголовки журналов, но и научные статьи), в сентябре 2018 года включен в продукты EBSCO Publishing.

В ноябре 2020 года журнал начал индексироваться в международной базе Scopus.

International Journal for
Computational Civil and Structural Engineering
(Международный журнал по расчету гражданских и строительных конструкций)
Volume 17, Issue 3 ***2021***

Scientific coordination is carried out by the Russian Academy of Architecture and Construction Sciences (RAACS)

CONTENTS

International Journal for
Computational Civil and Structural Engineering
(Международный журнал по расчету гражданских и строительных конструкций)
Volume 17, Issue 3 ***2021***

Scientific coordination is carried out by the Russian Academy of Architecture and Construction Sciences (RAACS)

СОДЕРЖАНИЕ

DOI:10.22337/2587-9618-2021-17-3-14-23

MODELING OF THE SUBWAY DYNAMIC INFLUANCE ON THE GROUND STRUCTURE

Maria S. Barabash, Bogdan Y. Pysarevskiy
«LIRA SAPR» Ltd, Kiev, UKRAINE
National Aviation University, Kiev, UKRAINE

Abstract: The article discusses a new approach to modeling the behavior of structures under the influence of dynamic loads, including loads from ground and underground transport. The approach is to apply the direct integration method, as well as the SBFEM method to calculate the forces in load-bearing building structures under dynamic influences, taking into account a number of factors - the damping properties of the subgrade, physical nonlinearity of soils and the passage of waves in the soil space. The article presents the main theoretical premises, the results of a numerical experiment of a real monolithic building, built in the zone of influence of the subway.

Keywords: dynamic influences, finite elements, structural modeling, internal forces, vibration acceleration, vibration velocity, subway, vibration, soil, boundary conditions, design, dynamic characteristics, damping

МОДЕЛИРОВАНИЕ ДИНАМИЧЕСКОГО ВОЗДЕЙСТВИЯ МЕТРОПОЛИТЕНА НА НАЗЕМНОЕ СООРУЖЕНИЕ

М.С. Барабаш, Б.Ю. Писаревский
ООО «ЛИРА САПР», г. Киев, УКРАИНА
Национальный авиационный университет, г. Киев, УКРАИНА

Аннотация: В статье рассматривается новый подход к моделированию поведения конструкций при влиянии динамических нагрузок, в том числе и нагрузок от наземного и подземного транспорта. Подход заключается в применении метода прямого интегрирования, а также метода SBFEM для вычисления усилий в несущих строительных конструкциях при динамических воздействиях с учетом ряда факторов - демпфирующих свойств грунтового основания, физической нелинейности грунтов и прохождения волн в грунтовом пространстве. В статье приводятся основные теоретические предпосылки, приводятся результаты численного эксперимента реального монолитного здания, построенного в зоне влияния метрополитена.

Ключевые слова: динамические воздействия, конечные элементы, моделирование конструкций, внутренние усилия, виброускорения, виброскорости, метрополитен, вибрация, грунт, граничные условия, проектирование, динамические характеристики, демпфирование

In recent decades, the world has experienced urbanization and intense urban growth. At the same time, in order to unload the traffic flow in cities, underground space is being developed and new metro lines are being built. However, the underground is a source of increased vibration and noise levels. As a rule, new tunnels are laid in the formed urban development, which causes an increase in vibration and noise in buildings and structures adjacent or located above metro lines, as well as new construction is carried out near existing metro stations and tunnels. Constantly acting vibration loads from the movement of the subway affect the physical and mechanical properties of soils and the bearing capacity of structures in operation, erected and reconstructed buildings and structures [1]. It is not possible to provide a complete and reliable assessment of these actions only by instrumental methods.

Therefore, it is very important to develop complex numerical modeling tools that will allow obtaining

objective and comprehensive information about the actual stress-strain state (SSS) of load-bearing structures of buildings and structures under vibration effects. In the future, this will make it possible to develop a set of measures to counteract vibration effects in order to prevent damage and further destruction of structures.

The purpose

The purpose of the article is to assess the effect of vibration loads on the stress-strain state of the bearing structures of buildings and structures.

In addition, a methodology for modeling the behavior of buildings under the constant influence of the subway is presented.

Formulation of the problem

When designing buildings and structures of increased responsibility, regulatory documents regulate the calculation of the system "ground part - foundation - foundation" for dynamic effects. This problem can be solved by numerical modeling methods, which make it possible to take into account such factors as the damping properties of the subgrade, physical nonlinearity of soils and the passage of waves in an infinite half-space of the subgrade.

The development of new calculation methods for dynamic effects and the improvement of existing ones are especially important in the design of multi-storey buildings.

Direct integration of equations of motion (method of central differences)

Calculation under the influence of dynamic loads is based on solving differential equations:

$$M\ddot{\bar{u}}(t) + C\dot{\bar{u}}(t) + K\bar{u}(t) = \bar{q}(t) \qquad (1)$$

$$\bar{q}(t) = -\sum_{i=1}^{3}\left(M\vec{v}_i u_g^i(t)\right) - \sum_{i=4}^{6}\left(M\vec{v}_i u_g^i(t)\right) \qquad (2)$$

where M, C, K are – accordingly matrices of masses, damping and system stiffness respectively;

$\bar{u}(t), \dot{\bar{u}}(t), \ddot{\bar{u}}(t)$ are vectors of nodal displacements, velocities and accelerations at the moment of time *t*;

$\bar{q}(t)$ are loads corresponding to the moment in time *t*.

For accelerations at time t, using the method of central differences, we can write the expression in the following form:

$$\ddot{\bar{u}}(t) = \frac{\bar{u}(t+\Delta t) - 2\bar{u}(t) + \bar{u}(t-\Delta t)}{\Delta t^2} \qquad (3)$$

The calculation error by formula (3) is of the order of Δt^2, and the following expressions are used to calculate velocities and displacements with errors of the same order:

$$\dot{\bar{u}}(t) = \frac{\bar{u}(t+\Delta t) - \bar{u}(t-\Delta t)}{2\Delta t};$$
$$\bar{u}(t) = \frac{\bar{u}(t+\Delta t) + \bar{u}(t-\Delta t)}{2}. \qquad (4)$$

Substituting expressions (4) into expression (1) and determining the vector $\bar{u}(t+\Delta t) + \bar{u}(t-\Delta t)$, we obtain the following equation:

$$\left[\frac{2M}{\Delta t^2} + \frac{C}{\Delta t} + K\right](\bar{u}(t+\Delta t) + \bar{u}(t-\Delta t)) = 2\left(q(t) + \frac{2M}{\Delta t^2}\bar{u}(t) + \frac{C}{\Delta t}\bar{u}(t-\Delta t)\right) \qquad (5)$$

In the process of performing the calculation, displacements at the control points of the building are determined with a gradual application of a dynamic load to the building:

$$\left[\frac{M}{\Delta t^2} + \frac{C}{2\Delta t} + \frac{K}{2}\right](u(t+\Delta t) = q(t) + \frac{2M}{\Delta t^2}u(t) - \left[\frac{M}{\Delta t^2} - \frac{C}{2\Delta t} + \frac{K}{2}\right]u(t-\Delta t) \qquad (6)$$

Obtained displacements $\bar{u}(t+\Delta t)$ can be determined taking in account previously found displacement $\bar{u}(t)$ and $\bar{u}(t-\Delta t)$ from equations (1,2).
After entering the initial parameters of the computational model and calculating the mass matrix, the subroutine for calculating the total vector of forces and the critical time step is launched. Based on the obtained vector, the calculation of nodal accelerations, velocities and displacements is carried out.

Damping factor accounting when calculating structures for dynamic effects
The damping matrix [C] in the Rayleigh model [2] is defined as a linear combination of the system stiffness matrix [K] and the system mass matrix [M]:

$$[C]=\beta[K]+\alpha[M] \tag{7}$$

where α is a mass proportionality factor (C-1);
β is a proportionality factor (C).
The orthogonal transformation of the damping matrix (7) brings the matrix [C] to the form:

$$2\xi_i\omega_i=\alpha+\beta\omega_i^2 \tag{8}$$

Let us divide (9) by and express the dependence of the damping coefficient on frequency in the form:

$$\xi_i=\frac{\alpha}{2\omega_i}+\frac{\beta\omega_i}{2} \tag{9}$$

In order to determine the Rayleigh coefficients, a modal analysis of the structure (or its part) is carried out and by specifying empirical damping coefficients for the material at the two lowest natural frequencies, the coefficients are determined by the formulas:

$$\alpha=\frac{2\xi_i\xi_j\omega_i\omega_j}{\xi_i\omega_i+\xi_j\omega_j},\ \beta=\frac{2\xi_i\xi_j}{\xi_i\omega_i+\xi_j\omega_j}, \tag{10}$$

where $\omega_i\omega_j$ are natural frequencies;
$\xi_i\xi_j$ is a modal damping for the first and second natural modes, given as a percentage of the critical damping.

Modeling the passage of waves in an infinite half-space of a subgrade
There are two general approaches to solving this problem - the direct method and the subsystem method.
The inconsistency of the problem under consideration lies in the fact that the propagation of waves occurs in an infinite half-space, and a limited section of a soil half-space can be included in a specific calculation. Both methods differ in the boundary conditions imposed on the boundaries of the soil half-space. In the direct method, constraints are imposed on the boundaries of the selected area, which cause the reflection of waves and the return of energy. In order to reduce the influence of this negative factor, it is necessary to increase the size of the allocated area so that the waves reach the boundaries less than the time of the dynamic impact. This technique is ineffective, since it requires a significant increase in the time of the problem being solved, especially for three-dimensional problems.
In the subsystem method, two parts working together are modeled as two substructures, which are separated by a generalized interaction line. One part includes a building and a foundation with additional boundary conditions, this part can have non-linearity in both structure models and soil models. The other part includes the rest of the soil, which stretches indefinitely (Fig. 1).
The combination of the two subsystems is carried out using the interaction vector $r_b(t)$ acting in both directions - on the building and on the soil massif. The interaction vector in the direct dynamic problem is represented as a convolution vector:

$$r_b(t)=\int_0^t M_b^{\infty}(t)\{u(t-\tau)\}d\tau, \tag{11}$$

where $M_b^{\infty}(t)$ is acceleration response matrix. Index b denotes nodes lying on the interaction line, which belong to both the structure and the ground.

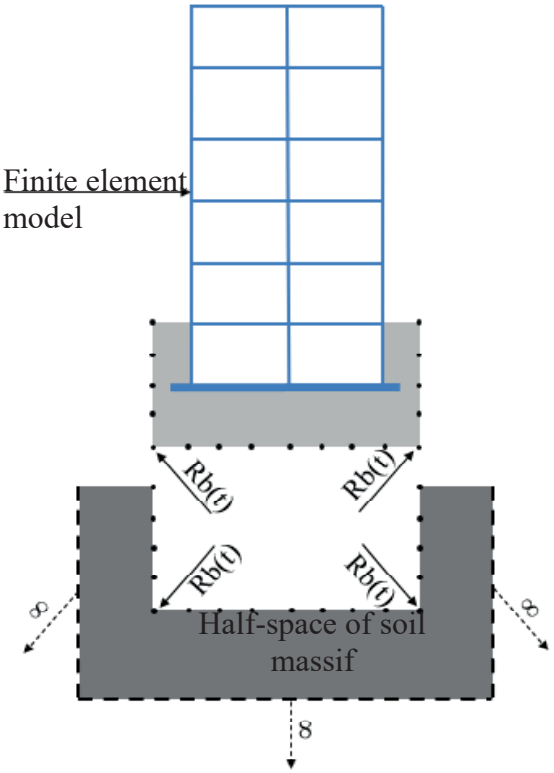

Figure 1. Schematic representation of the subsystem method

The equations of motion in the problem of integration in time can be written as:

$$\begin{bmatrix} M_{ss} & M_{sb} \\ M_{bs} & M_{bb} \end{bmatrix} \begin{Bmatrix} \ddot{u}_s(t) \\ \ddot{u}_b(t) \end{Bmatrix} + \begin{bmatrix} C_{ss} & C_{sb} \\ C_{bs} & C_{bb} \end{bmatrix} \begin{Bmatrix} \dot{u}_s(t) \\ \dot{u}_b(t) \end{Bmatrix} + \\ + \begin{bmatrix} K_{ss} & K_{sb} \\ K_{bs} & K_{bb} \end{bmatrix} \begin{Bmatrix} u_s(t) \\ u_b(t) \end{Bmatrix} = \begin{Bmatrix} p_s(t) \\ p_b(t) \end{Bmatrix} - \begin{Bmatrix} 0 \\ r_b(t) \end{Bmatrix} \quad (12)$$

where K, C and M are matrices of stiffness, damping and mass of the structure, respectively, $\dot{u}(t)$ and $\ddot{u}(t)$ are vectors of displacements, velocities and accelerations;

$p(t)$ is vector of forces that act directly on the structure. The index s denotes the nodes belonging to the structure. To solve this equation, you need to know the vector of forces of interaction between the soil and the structure $r_b(t)$. In other words, you need to define the acceleration response matrix $M_b^{\infty}(t)$.

Equation of SBFEM [3] takes the form:

$$\int_0^t [m^{\infty}(\tau - t)][m^{\infty}(\tau)]d\tau + \\ + t\int_0^t [m^{\infty}(\tau)]d\tau + [e^1]\int_0^t\int_0^{\tau} [m^{\infty}(\tau)]dtd\tau + \\ + [e^1]^T \int_0^t\int_0^{\tau} [m^{\infty}(\tau)]dtd\tau - \frac{t^3}{6}[e^2]H(t) - t[m^0]H(t) = 0, \quad (13)$$

where H(t) is Heaviside function

$$\left[m^{\infty}(t)\right] = \left(\left[U\right]^{-1}\right)^T \left[M^{\infty}(t)\right]\left[U\right]^{-1}\right) \quad (14)$$

Methodology for the formation of calculation schemes in which there are limitless areas

The finite element design scheme of a limited part of the model is formed according to standard rules (limited subsystem).

No boundary conditions are imposed on the bounded subsystem. Both the structure model and the foundation model can have linear and physically non-linear elements. There may be additional links in a limited subsystem.

Next, a finite element diagram of the unlimited part of the model is formed. To do this, along the line of delimitation of the limited and unlimited parts, finite elements are installed, with the help of which infinity is modeled. Depending on the type of system, these can be two-node, three-node, or four-node elements. In the LIRA-SAPR software package, these are finite elements FE - 67, FE - 68 and FE - 69.

Then the system loads are simulated. The load can only be applied to a limited subsystem. The load can be static or dynamic.

Further work - the calculation and analysis of the calculation results are carried out according to the usual scheme.

Algorithm for assessing the dynamic influence of the subway on the supporting structures

Fig. 2 shows a block diagram of the algorithm for assessing the dynamic influence of the subway on the supporting structures:

1. A computational model of the building is formed and its calculation for the given influences is carried out in a linear setting, as a result of which the following are determined: the values of the concentrated masses at each level along the height; frequency and period of natural oscillations; ordinates of natural vibration modes; the magnitude of inertial forces at each height level; and also the design calculation is performed, the areas of reinforcement for reinforced concrete structures are selected.
2. A numerical soil model is created based on geological survey data. The dynamic characteristics of the soil are modeled using finite elements (FE) 281-284, namely the physically nonlinear rectangular, triangular and universal rectangular FE of the plane problem (soil). This FE is designed to simulate the one-sided work of the soil in compression, taking into account shear according to the planar deformation scheme.
3. Further, the linear computational model is transformed into a physically nonlinear one. To take into account the effect of damping, the Rayleigh coefficients for materials of construction and soil are determined and set. Boundary finite elements FE-67 in the foundation model are set, creating an infinite soil mass. This type of FE is intended for modeling a flat endless soil massif located outside the design model. This function is implemented to prevent the effect of reflection when imposing boundary conditions on the ground and in accordance with the Mohr-Coulomb law. It is used in a nonlinear stepper processor for calculating mine workings and tunnel penetrations.
4. The loading history of the design model is formed, which sequentially includes full vertical load; horizontal dynamic forces are added step by step. General dynamic actions in the system are formed from the coordinated matrix of masses of static actions using the "Dynamics in time" module in the LIRA-SAPR software package.
5. To take into account the influence of the time factor on the propagation of vibrations, the "Dynamics in time" module is used. The load is modeled using a graph of dynamic vibration accelerations generalized over the entire frequency range. The accelerogram of actions, the step and the integration time are set, on the basis of which the minimum number of moments will be obtained, for each of which the results will be generated.

Numerical experiment in SP LIRA-SAPR

A number of numerical experiments have been carried out in the LIRA-SAPR software package [4]. They prove the reliability of the fact of the influence of the underground, both shallow and deep, on the supporting structures of various buildings and structures.

The article presents the results of one of the experiments - the calculation of a high-rise building on the influence of the shallow underground [5], taking into account the real geological situation using the PC "LIRA-SAPR". The preliminary assessment and analysis of the vibration effects of the subway on a high-rise building were carried out in a linear and non-linear formulation, as well as taking into account the modeling of the real work of the soil massif and unlimited FE.

For the numerical experiment, a 27-storey monolithic building was taken as a basis (Fig. 3), which is located near the Svyatoshino-Brovarskaya line of the Kiev metro, which is shallow. Concrete class C25 / 30, working reinforcement class A400C. The thickness of the monolithic floor is 200 mm, the thickness of the vertical supporting structures is 300 mm. The foundation is a solid monolithic reinforced concrete slab on a pile field.

The calculation was carried out taking into account wind and snow loads according to the construction area. Long-term and short-term

loads on the floor slabs of typical floors, as well as the attic floor, are taken into account.
In the course of the study, a number of calculations were carried out taking into account the nonlinear properties of the soil, taking into account the different frequency ranges caused by the movement of trains.

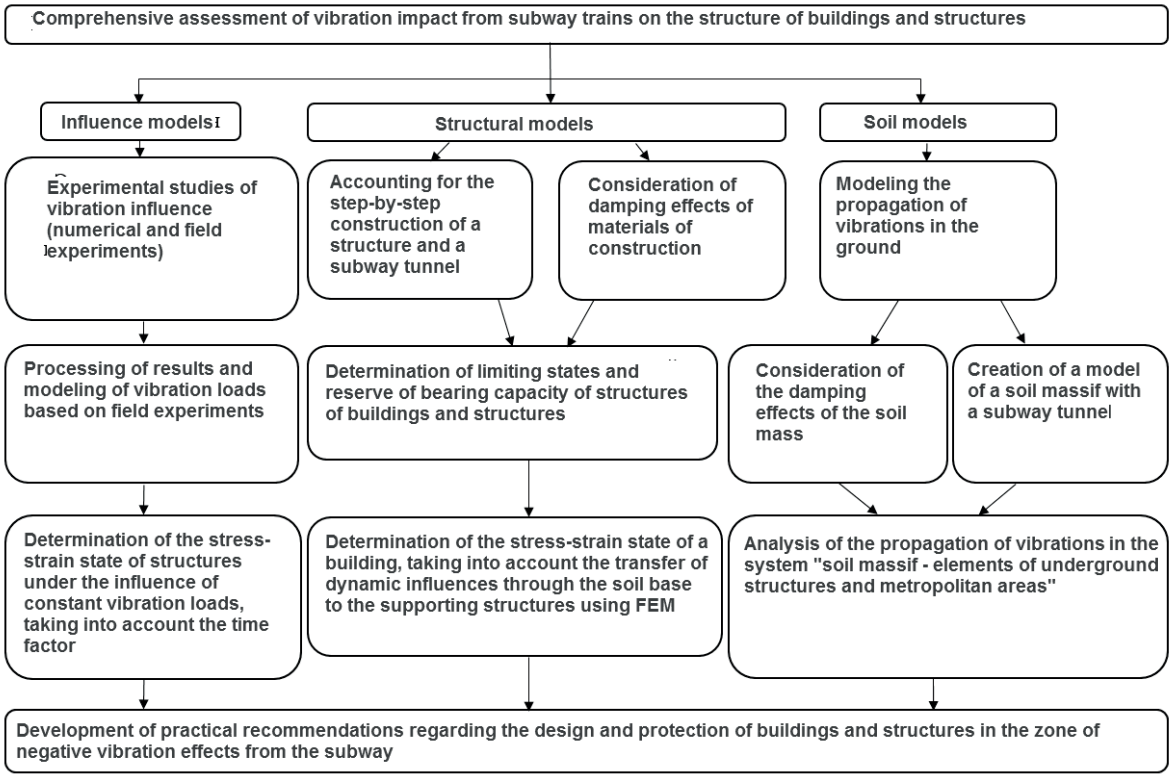

Figure 2. Algorithm for assessing vibration influence

The soil is modeled by flat, physically nonlinear finite elements. For the most accurate assessment of the vibration impact of the metro, we used sensor data from the measurement point, which was located directly at the base of the rail. The method of numerical simulation of dynamic loads in time in the LIRA-SAPR software package provides for setting the actions in the form of an accelerogram of vibration accelerations. For each moment in time, the equation is solved:

$$\sum_{n=0}^{i} a = A_i \sin(\omega_i \cdot t_n) + A_{i+1} \sin(\omega_{i+1} \cdot t_{n+1}) \qquad (15)$$

$$A_i = V_i \cdot \nu, \omega_i = 2\pi\nu \qquad (16)$$

where A_i *is* vibration acceleration, ω_i is cyclic frequency, which are calculated for each frequency from 2 Hz to 100 Hz - time point from 0 to 15 s, step 0.1 s.
The obtained results of dynamic vibration acceleration are set in the form of load accelerogram (Fig. 4) in the LIRA-SAPR software package.
Two types of models were investigated - a model with boundary conditions imposed along the perimeter of a limited soil massif (model 1) and a model using unlimited FE (model 2) [6].

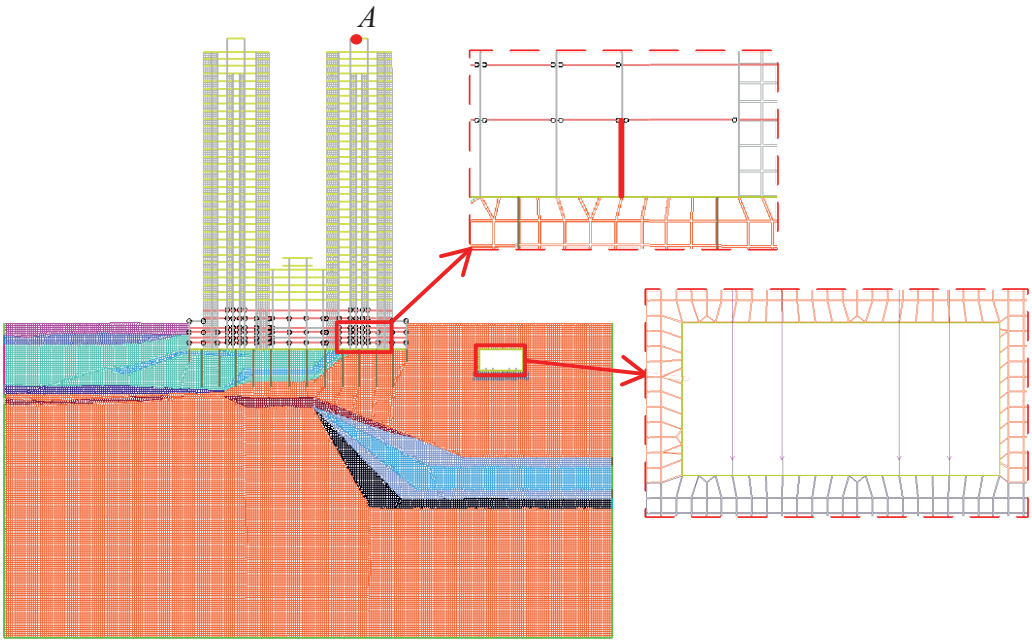

Figure 3. Design scheme of the building to take into account the dynamic influence of the underground

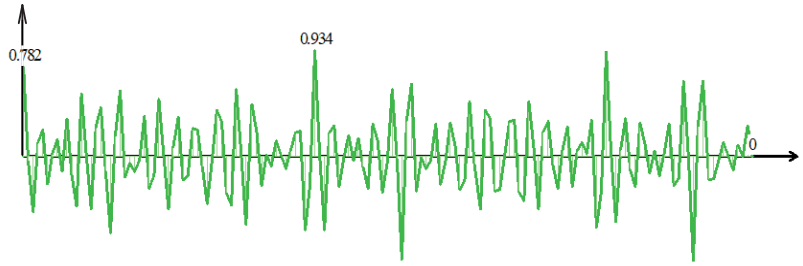

Figure 4. Specified accelerogram per metro track

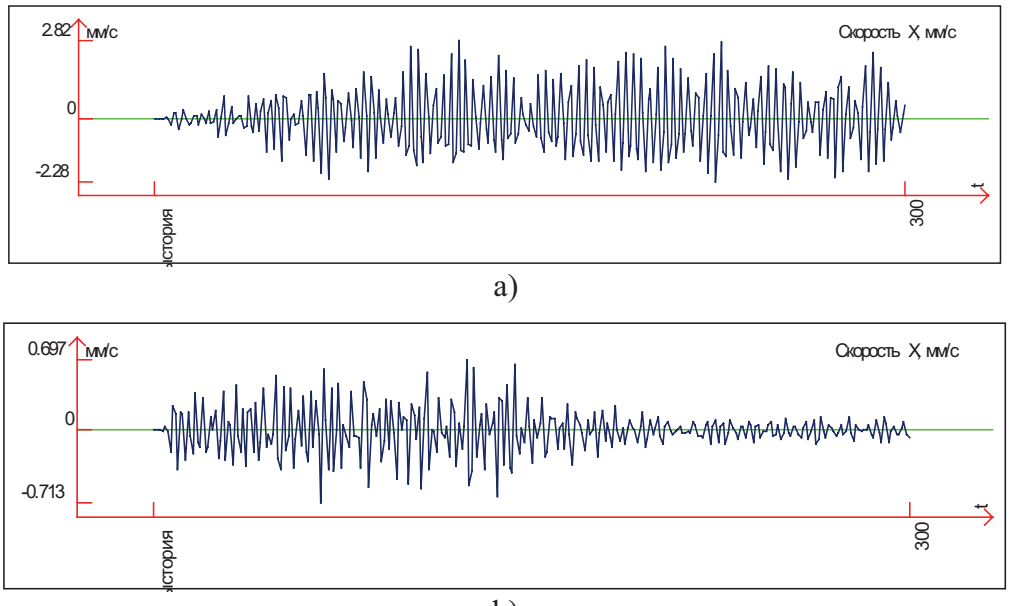

Figure 5. Vibration velocities at the control point (A) of the upper floor: a) model 1; b) model 2

Normative documents [7] regulate that the vibration load transmitted through the soil to the supporting structures of a building or structure (for example, when a track or metro station is located nearby) should not adversely affect the mechanical safety of the supporting and enclosing structures of a building during its life cycle. The estimated value, in accordance with Standard of RF GOST R 52892, is the peak value of the vibration velocity of vibrations at the control points. In our case, this is the top point of the building. The building in question belongs to the 2nd category of structures - "Residential buildings and buildings of similar design or purpose". The limiting values of the peak vibration velocity of vibrations for such buildings is within 5 mm / s. For this numerical experiment, we see that the vibration velocities correspond to the normative ones. However, this is not always the case.

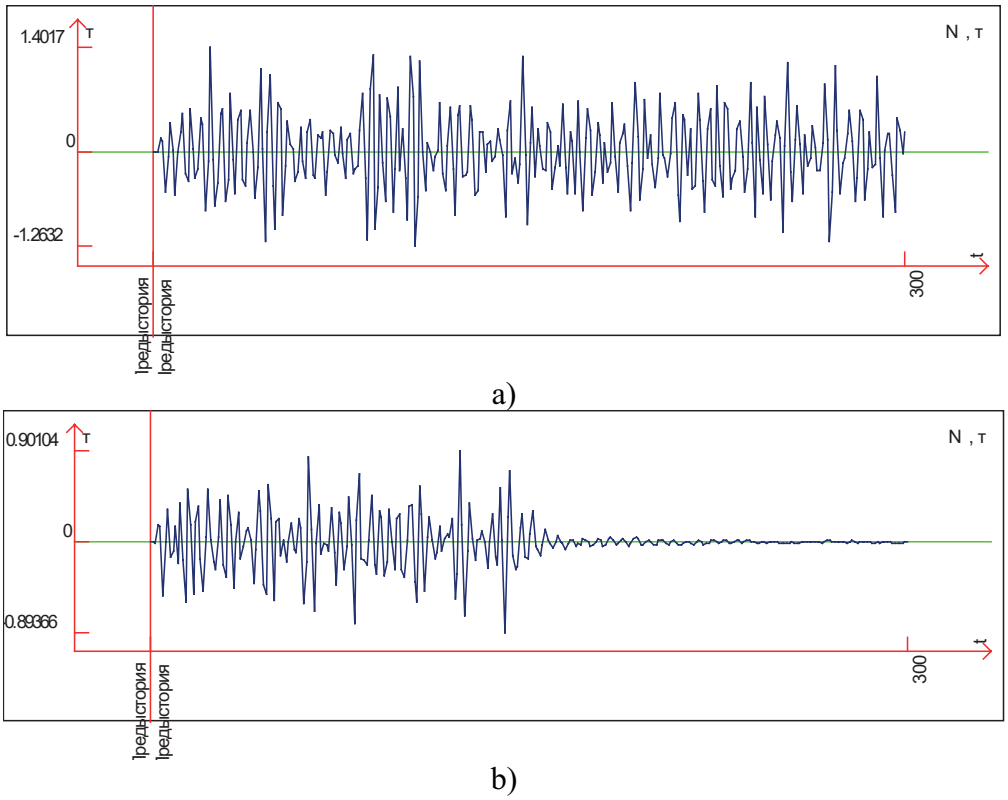

Figure 6. Longitudinal forces in the column from dynamic load: a) model 1; b) model 2

As a result of the calculation, data were obtained from which it can be seen, firstly, that the movement of the subway car creates vibration velocity and vibration acceleration at the control point on the top floor. And, secondly, we can track the damping of vibrations and dissipation of energy and, as a consequence, a decrease in internal forces in the column when using limitless ("transparent") FE, which we see in Figure 6.

Conclusions

A numerical modeling tool has been developed that allows one to assess the influence of the subway on building structures, taking into account many factors.

A method for numerical modeling of the processes of deformation and destruction of structures of buildings and structures under vibration influences of the underground has been developed and theoretically substantiated.

A mathematical and numerical model of vibration impact has been created, taking into account the time factor and the infinity of the soil mass.
A variant of modeling the system "source of vibration loads-soil-base-load-bearing structures of the building" is proposed.
A technique was proposed and implemented in SP LIRA-SAPR, which takes into account the continuous passage of a wave into an infinite region under dynamic influences.
The main recommendations are the use of damping devices in the construction of buildings in the zone of influence of the metro and the adoption of measures to reduce the level of penetrating vibration.

REFERENCES

1. **Clough R., Penziyen J.** Dinamika sooruzheniy [Dynamics of structures]: Translated from english. – Moscow: Stroyizdat, 1979. 320 p.
2. **Barabash M.S.** Manerial damping in dynamic analysis of structures (with LIRA-SAPR programm) / M. Barabash, B. Pisarevskyi, Y. Bashynskyi // Civil and Environmental Engineering, 2020. – Vol. 16, Issue 1, P. 63-70.
3. **Wolf, J.P.** and Song, C. (1996). Finite-Element Modelling of Unbounded Media, John Wiley & Sons Ltd, England
4. **Barabash M.S.** Komp'yuternoye modelirovaniye protsessov zhiznennogo tsikla ob"yektov stroitel'stva [Computer modeling of the life cycle processes of construction objects]: Monograph / Maria Sergeevna Barabash. – Kiyv: "Stal", 2014. – 301 p.
5. **Barabash M.S.** Stress-strain state of the structure in the service area of underground railway / M. Barabash, Ya. Bashinsky , A. Korjakins // IOP Conference Series: Materials Science and Engineering. The 3rd International Conference on Innovative Materials, Structures and Technologies (IMST 2017), 27–29 September 2017. – Riga, (Latvia), 2017. – Vol. 251. – conference 1.
6. **Gorodetskiy A.S.** Modelirovaniye raboty gruntovykh massivov na dinamicheskoye vozdeystviye [Modeling of work of soil massifs on dynamic impact] / A. S. Gorodetskiy, A. V. Pikul', B.YU. Pisarevskiy // International Journal for Computational Civil and Structural Engineering. – 2017. – Vol. 13. – Issue 3. – P.34–41.
7. Building Code of RF SP 465.1325800.2019 Buildings and structures. Protection against vibration of underground lines. Design rules. – [Introduced from 03-06-2020]. – Moscow: Standartinform, 2020. – 40 p.

СПИСОК ЛИТЕРАТУРЫ

1. **Клаф Р., Пензиен Дж**. Динамика сооружений: Пер. с англ. – М.: Стройиздат, 1979. – 320 с.
2. **Barabash M.S.** Manerial damping in dynamic analysis of structures (with LIRA-SAPR programm) / M. Barabash, B. Pisarevskyi, Y. Bashynskyi // Civil and Environmental Engineering, 2020. – Vol. 16, Issue 1, P. 63-70.
3. **Wolf, J.P. and Song, C.** (1996). Finite-Element Modelling of Unbounded Media, John Wiley & Sons Ltd, England
4. **Барабаш М.С.** Компьютерное моделирование процессов жизненного цикла объектов строительства: Монография / Мария Сергеевна Барабаш. – К.: «Сталь», 2014. – 301 с
5. **Barabash M.S.** Stress-strain state of the structure in the service area of underground railway / M. Barabash, Ya. Bashinsky, A. Korjakins // IOP Conference Series: Materials Science and Engineering. The 3rd International Conference on Innovative Materials, Structures and Technologies (IMST 2017), 27–29 September 2017. – Riga, (Latvia), 2017. – Vol. 251. – conference 1.
6. **Городецкий А.С.** Моделирование работы грунтовых массивов на динамическое воз-

действие / А.С. Городецкий, А.В. Пикуль, Б.Ю. Писаревский // International Journal for Computational Civil and Structural Engineering. – 2017.– Vol. 13. – Issue 3. – P. 34–41.

7. Здания и сооружения. Защита от вибрации метрополитена. Правила проектирования: СП 465.1325800.2019. – [Введен в действие с 03-06-2020]. – М: Стандартинформ, 2020. – 40 с. (Свод правил).

Барабаш Мария Сергеевна, академик Академии строительства Украины, доктор технических наук, профессор, профессор кафедры компьютерных технологий строительства Национального авиационного университета, директор ООО «ЛИРА САПР», 04053, Украина, Киев, пер. Кияновский, д.7-а; тел.: +38 (095) 286-39-90; e-mail: bmari@ukr.net, www.liraland.com. ORCID ID: 0000-0003-2157-521X, Researcher ID: R-9181-2016

Писаревский Богдан Юрьевич, аспирант кафедры компьютерные технологии строительства, Национального авиационного университета, инженер-программист компании ООО «ЛИРА САПР», 04053, Украина, Киев, пер. Кияновский, д.7-а, тел.: +38 (044) 590 58 85, e-mail: mikst1234@gmail.com, ORCID ID: 0000-0002-1001-2879

Maria S. Barabash. Academician of the Academy of Construction of Ukraine, Doctor of Technical Sciences, Professor, Professor of Computer Technologies of Construction Department, National Aviation University Director of “LIRA SAPR” Ltd, 7a, Kiyanovsky side street (pereulok), Kiev, 04053, Ukraine; phone: +38 (095) 286-39-90; e-mail: bmari@ukr.net, www.liraland.com. ORCID ID: 0000-0003-2157-521X, Researcher ID: R-9181-2016

Bogdan Y. Pysarevskiy – Postgraduate student; Department of Computer Technology Building, National Aviation University,software engineer «LIRA SAPR» Ltd, 7a, Kiyanovsky side street (pereulok), Kiev, 04053, Ukraine; phone +38 (044) 590 58 85, e-mail: mikst1234@gmail.com ORCID ID: 0000-0002-1001-2879

DOI:10.22337/2587-9618-2021-17-3-24-38

SIMULATION OF AERODYNAMIC INSTABILITY OF BUILDING STRUCTURES ON THE EXAMPLE OF A BRIDGE SECTION. PART 2: SOLUTION OF THE PROBLEM IN A COUPLED AEROELASTIC FORMULATION AND COMPARISON WITH ENGINEERING ESTIMATES

Alexander M. Belostotsky [1,2,3]***, Irina N. Afanasyeva*** [1,4]***, Irina Yu. Negrozova*** [2]***, Oleg S. Goryachevsky*** [1,2]

[1] Scientific Research Center StaDyO, Moscow, RUSSIA
[2] National Research Moscow State University of Civil Engineering, Moscow, RUSSIA
[3] Russian University of Transport (RUT - MIIT), Moscow, RUSSIA
[4] University of Florida, Gainesville, Florida, USA

Abstract: In this paper, we study aerodynamic instability using the example of a two-dimensional problem of flow around a simplified section of a flexible suspension bridge (on the Tacoma River, USA). A direct dynamic coupled calculation was performed to determine the critical speed of manifestation of aerodynamic instability. The results obtained were compared with the results of engineering estimates presented in [40]. This example shows that to solve such problems it is possible to use the lighter des turbulence model instead of the les turbulence model and, therefore, a coarser mesh. In contrast to existing engineering techniques, direct numerical modeling of the interaction between the structure and the air flow allows one to take into account the reverse effect of the structure on the flow, as well as the mutual influence of several types of aerodynamic instability.

Keywords: aerodynamic instability, galloping, divergence, FSI, URANS SST turbulence model, DES SST turbulence model

МОДЕЛИРОВАНИЕ АЭРОДИНАМИЧЕСКОЙ НЕУСТОЙЧИВОСТИ СТРОИТЕЛЬНЫХ КОНСТРУКЦИЙ НА ПРИМЕРЕ СЕЧЕНИЯ МОСТА. ЧАСТЬ 2: РЕШЕНИЕ ЗАДАЧИ В СВЯЗАННОЙ АЭРОУПРУГОЙ ПОСТАНОВКЕ И СОПОСТАВЛЕНИЕ С ИНЖЕНЕРНЫМИ ОЦЕНКАМИ

А.М. Белостоцкий [1,2,3]***, И.Н. Афанасьева*** [1,4]***, И.Ю. Негрозова*** [2]***, О.С. Горячевский*** [1,2]

[1] Научно-исследовательский центр СтаДиО, г. Москва, РОССИЯ
[2] Национальный исследовательский Московский государственный строительный университет, г. Москва, РОССИЯ
[3] Российский университет транспорта (МИИТ), г. Москва, РОССИЯ
[4] Университет Флориды, г. Гейнсвилл, США

Аннотация: В настоящей работе исследуется аэродинамическая неустойчивость на примере двумерной задачи обтекания упрощенного сечения гибкого подвесного моста (на реке Такома, США). Выполнен прямой динамический связанный расчет для определения критической скорости проявления аэродинамической неустойчивости. Полученные результаты сравнивались с результатами инженерных оценок, представленных в [40]. На данном примере показано, что для решения подобных задач можно использовать более «легкую» модель турбулентности DES вместо модели турбулентности LES и, следовательно, более грубую сетку. В отличие от существующих инже-

нерных методик, прямое численное моделирование взаимодействия конструкции и воздушного потока позволяет учесть обратное влияние конструкции на поток, а также взаимное влияние нескольких видов аэродинамической неустойчивости.

Ключевые слова: аэродинамическая неустойчивость, галопирование, дивергенция, FSI, модель турбулентности URANS SST, модель турбулентности DES SST

1. INTRODUCTION

Long span and flexible structures such as bridges with long spans are highly sensitive to wind influences. Such structures are susceptible to aeroelastic phenomena. Over the past 150 years, many such cases have been known and described. Until the 1940s, the wind load was considered secondary and even its static component was not taken into account. This continued until the most famous destruction of the Tacoma Narrows Bridge in the United States. Almost from the very beginning of construction work, problems with the stability of the bridge began to appear, even in light winds. The bridge immediately gained a reputation as an unstable structure. Due to the fact that the windy weather of the bridge swayed, he was given the nickname "Galloping Gertie". Numerous attempts were made to stabilize the structure, but they could not solve this problem – on November 7, 1940, a collapse occurred as a result of the increasing vibrations of the bridge deck in the air stream. This disaster marked the beginning of an intensive and purposeful study of the interaction of flexible structures with wind flow. The first fundamental scientific works on this topic appeared, namely the works of Theodor von Karman [1], Alan Garnett Davenport [2–3], Barshtein M.F. [4], Simiu [5], Scanlan [5–8], Den Hartog [9]. Based on these studies, engineering methods for assessing the occurrence of aerodynamic instability were developed and introduced into regulatory documents [10–12].

In a number of cases, the issues of wind flow around unique buildings and structures during their design are solved experimentally. For this, the testing of models in laboratory conditions is widely used, as a rule, in wind tunnels (WT). Experimental studies of the assessment of the aerodynamic characteristics of structures were carried out by such scientists as M.I. Kazakevich [11], S.M. Gorlin [12], Alan Davenport [2, 15], A. Kareem [16], B. Blocken [17] and others.

The experimental approach, which was practically uncontested 20–30 years ago, has a number of serious drawbacks. A correct analysis of the mutual influence of the air flow and the structure is practically impossible in an experiment in a wind tunnel due to the difficulty of observing the similarity of a scale model of a deformable structure. Almost all modern experimental studies are based on the assumption that the structure behaves as an absolutely rigid body, and fluctuations in the flow and damping are imitated by “springs”. In this case, the reverse effect of the deformed structure on the structure of the air flow has been repeatedly confirmed. Failure to take into account the reverse effect can lead to both an overestimation of the critical wind speeds (at best), and their underestimation (in the worst case).

Due to the rapid development of mathematical modeling, numerical methods and implementing software systems against the background of an impressive growth in computing power, another approach has been actively developing in recent years – mathematical (numerical) modeling, free from the limitations of physical (experimental) modeling methods. Today it is possible to carry out a direct numerical solution of related problems of aero-hydroelasticity and directly simulate the phenomena of aerodynamic instability without resorting to numerous serious assumptions adopted in experimental methods. As a result, more accurate assessments of the criteria for the occurrence of aerodynamic instability of unique and especially critical flexible structures are

obtained and, as a consequence, their mechanical safety is increased. Among the works devoted to the numerical modeling of the phenomena of aeroelasticity, one can single out [18–38].

Despite the advantages of direct numerical modeling, it also has disadvantages. The main one is high computational complexity. Although, along with the further progress of algorithms and computer technology, this drawback will be more and more overcome, now it seems relevant to develop a universal and more economical approach to assessing the aerodynamic stability of structures. The purpose of this study is to develop a universal approach to assessing the aerodynamic instability of bridge structures in an unsteady wind flow using a preliminary engineering estimate and subsequent direct mathematical (numerical) modeling of the structure's behavior in a coupled aeroelastic formulation.

2. FORMULATION OF THE PROBLEM

The problem of interaction of a simplified section of a bridge on the Tacoma River with an air flow is considered. This problem was presented by a team of scientists from China at an international conference (The Seventh International Colloquium on Bluff Body Aerodynamics and Applications (BBAA7) Shanghai, China; September 2-6, 2012). They presented their results in [39], which describes their method for solving the problem using the ANSYS Fluent software package in a related setting with the author's software package. The geometric parameters of the section are shown in Fig. 1.

When modeling the dynamic behavior of the elastic section, the scheme shown in Fig. 2. The parameters of the material are presented in Table 1. The parameters of elastic connections with linear damping are taken from [39] and are also displayed in the table. In the Ox direction, the geometric center of the section is fixed. A torsional elastic link was applied to the entire cross section on average.

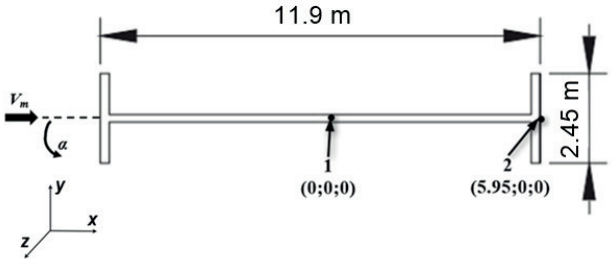

Figure 1. Geometric parameters of the section.

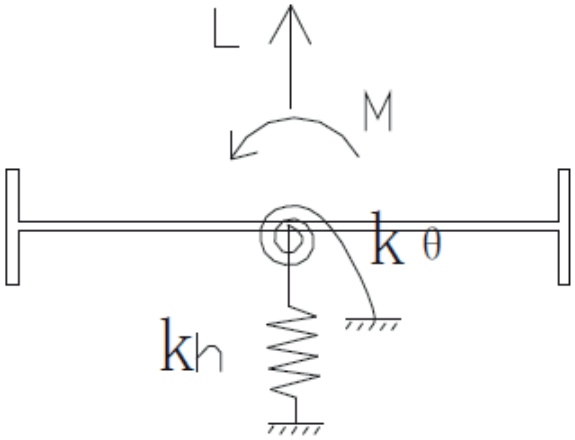

Figure 2. Design model.

Table 1. Material parameters

Material parameters		Parameters of the elastic model of the bridge section	
Density ρ, kg / m^3	1300	Linear weight, kg / m	4250
		Moment of inertia, kgm / m	177 730
Elastic modulus E, Pa	$2.1 \cdot 10^{11}$	Vertical relative damping	0.005
Poisson's ratio v	0.16	Relative damping by torsional degree of freedom	0.005

Air with constant properties at a temperature of 25ºC is considered.

In the course of solving the problem in a related formulation, the following parameters were determined:

• vertical displacements $y_1(t)$ of point 1 and $y_2(t)$ of point 2 (Fig. 1), the position of which changes over time due to wind action on the structure;

• angle of rotation $\theta(t)$, which is calculated as follows:

$$\theta = \arcsin\left(\frac{\Delta y}{L/2}\right) \quad (1)$$

where $\Delta y = y_2 - y_1$ is vertical displacements of point 1 and point 2, respectively.

In order to solve the problem, the ANSYS software package was used. To simulate the fluid – structure interaction (FSI), the "2-way FSI" simulation mode was used – two-way transfer of calculated data between various independent modules in the form of displacements (on the one hand) and loads (on the other side).

3. NUMERICAL SIMULATION METHODOLOGY

3.1. Numerical CFD Setup

The entire computational air domain was divided into finite volumes using the ANSYS Meshing module. Variants of computational grids with indication of the variable parameters were considered in [40]. Model 4 was chosen to simulate the behavior of air (Fig. 3).

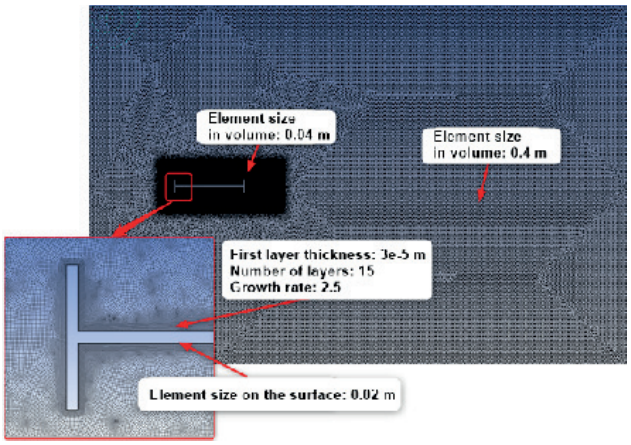

Figure 3. Calculation grid for CFD model: Model 4 (381 894 FE).

The INLET condition ($U = V_{in}$, $V = W = 0$, where U, V, W are the components of the velocity vector, V_{in} is a given constant flow velocity) with a horizontal directional flow velocity uniformly distributed along the height is specified as a boundary condition at the input. On the face opposite from the entrance, "soft" boundary conditions "Opening" were set with the averaged relative pressure equal to zero. On the surface of the streamlined body, the "liquid-structure" interface condition was applied. Symmetry conditions were set on the other faces of the computational domain. Zero flow rate was taken as the initial conditions for the problem.

Since the flow is turbulent at typical Reynolds numbers of ~ 10^6 for this problem, the turbulence model must be used to close the Navier-Stokes equations. In this paper, two turbulence models are considered: URANS k-ω SST and DES SST.

3.2. Numerical CSD Setup

For the Computational Structural Dynamics model (CSD model), a structured finite element model of a bridge section with an element size of 0.05 m was created (Fig. 4).

Figure 4. Computational grid for CSD model: Model 4 (10 913 nodes).

In order to simulate the plane problem, both sides of the section are fixed along the O_z axis, which coincides with the axis of the bridge. The movements of the center point are limited along the O_x axis directed along the wind flow (there are no oscillations in the direction of the flow). The elastic vertical link was modeled by a single spring with damping, one end of which is fixed at the central

point of the section, and the other is motionless (see the parameters of the vertical link in Table 1). The elastic torsional bond is modeled through the so-called Remote Displacement mechanism, when the angle of rotation of the entire section is calculated as the average value of the angles of rotation of all mesh nodes, and, accordingly, this angle and its rate of change cause elastic and viscous components of the reactions, respectively (see the parameters of the torsional bond in Table 1).

3.3. Coupling conditions

The time step size for CFD and CSD solvers is $\Delta t = 0.02$ s. The physical calculation time is 80 s. To ensure the convergence and stability of the solution at each associated time step, it is necessary to set the following calculation parameters:

– the maximum number of iterations at each associated step (maximum number of stagger iterations);

– criterion of convergence for loads and displacements;

Is the under relaxation factor for calculating loads and displacements at each iteration of the associated step:

$$\varphi = \varphi_{pre} + \alpha(\varphi_{new} + \varphi_{pre}) \quad (2)$$

where φ_{new} is the value of the variable calculated at the current iteration, φ_{pre} is the value of the variable calculated at the previous iteration, α is the relaxation coefficient (by default it is 0.75), φ is the corrected value of the desired value at the current iteration.

In this study, the loads were assigned a constant coefficient of lower relaxation $\alpha = 0.5$, while displacements were transferred without lower relaxation. To achieve the convergence criterion, 5 FSI sub-iterations were assigned (the maximum number of iterations at each related step) and the convergence criterion for loads and displacements was set equal to 10-3.

4. RESULTS

4.1. Results of solving the problem taking in account coupling conditions

Below are the results of solving the problem in a coupled aeroelastic formulation. In fig. 5 shows the obtained graphs of the dependences of the

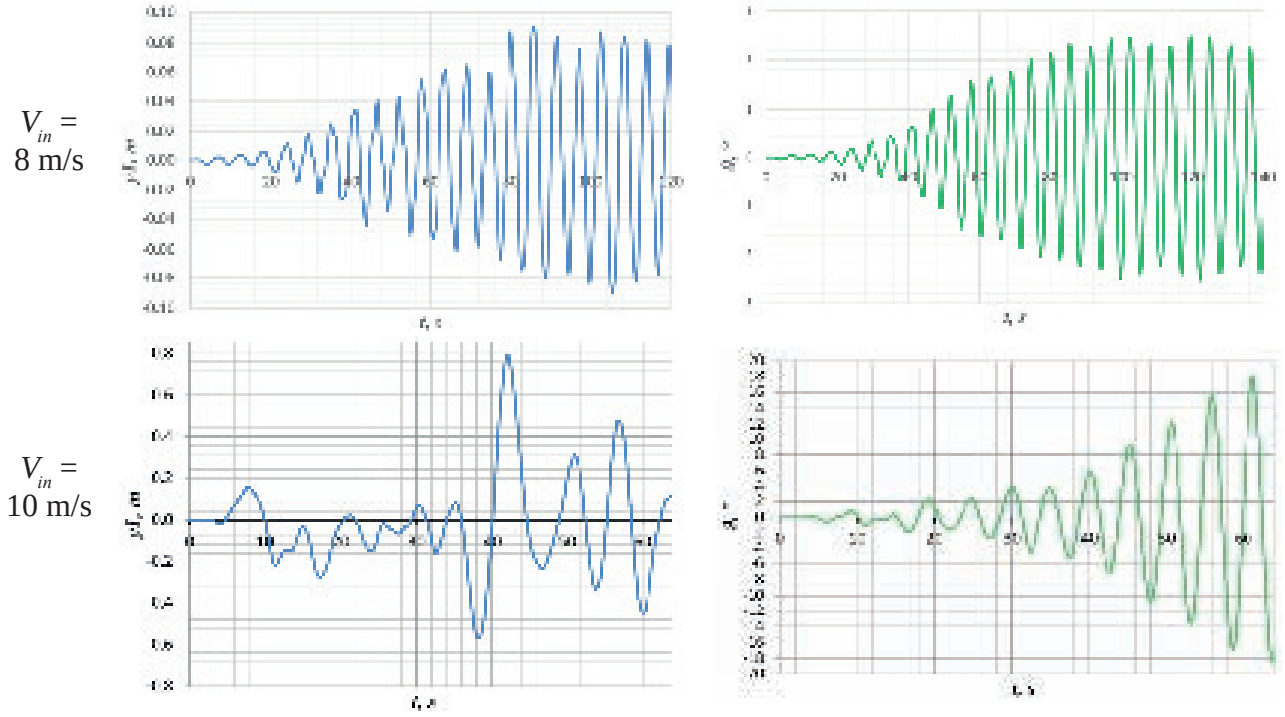

Figure 5. DES SST model: Graphs versus time t, s at different speeds
a - vertical movement of point 1, m; b - angle of rotation ϑ, °

vertical dynamic displacement of point 1 and the angle of rotation ϑ on time t for flow velocities of 8 m / s and 10 m / s for the DES SST turbulence model. Fig. 6 presents graphs of the dependences of the vertical displacement of point 1 and the angle of rotation ϑ on time t for flow velocities V_{in} equal to 10 m / s, 12 m / s and 15 m / s for the URANS *k*-ω SST turbulence model. Fig. 7 shows the velocity fields at different times for the DES SST turbulence model at a flow velocity of 10 m / s. Fig. 8 presents velocity fields at different times for the URANS SST turbulence model at a flow velocity of 15 m / s.

Based on the results of calculations in a coupled formulation for different flow rates, the vertical displacement of *point* 1 and the angle of rotation ϑ from time t were obtained. Loss of stability was determined by an infinitely increasing displacement and / or angle of rotation. Table 2 shows a comparison of the critical velocity values in [39] (experimental and numerical simulation results) and this study.

Comparing the results, it can be noted that the value of the critical velocity for the URANS k-ω SST turbulence model is overestimated, in contrast to the results presented in [39]. This is partly due to the fact that this turbulence model can underestimate the pulsation components of aerodynamic loads, as well as thin out the frequency spectrum, which in turn did not show aerodynamic instability for speeds of 10 m / s and 12 m / s. For the DES SST turbulence model,

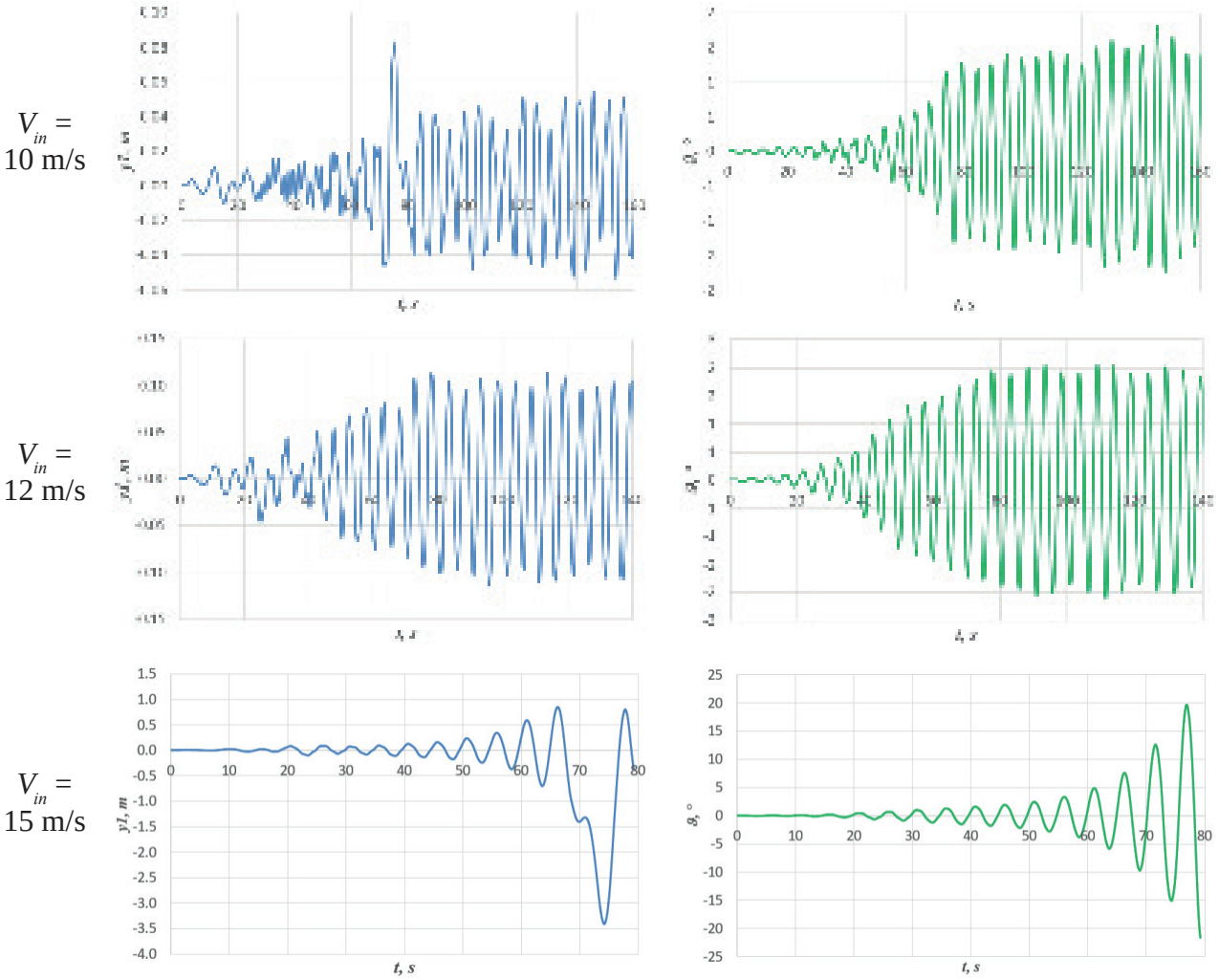

Figure 6. Model URANS k-ω SST: Graphs versus time t, s at different speeds a – vertical movement of point 1, m; b – angle of rotation ϑ, °

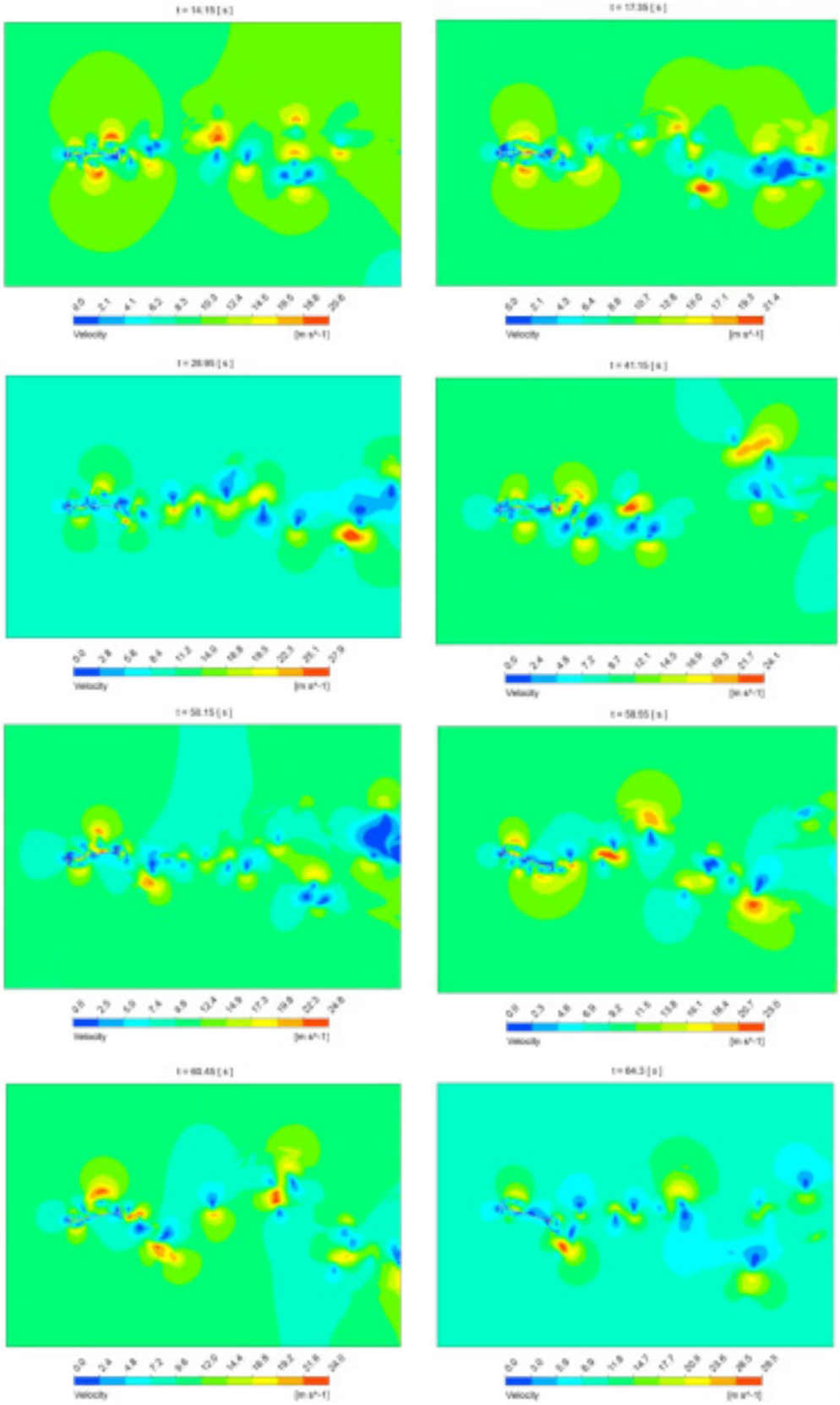

Figure 7. Velocity fields, m / s at different times t, s for a velocity V_{in} = 10 m / s (DES SST turbulence model)

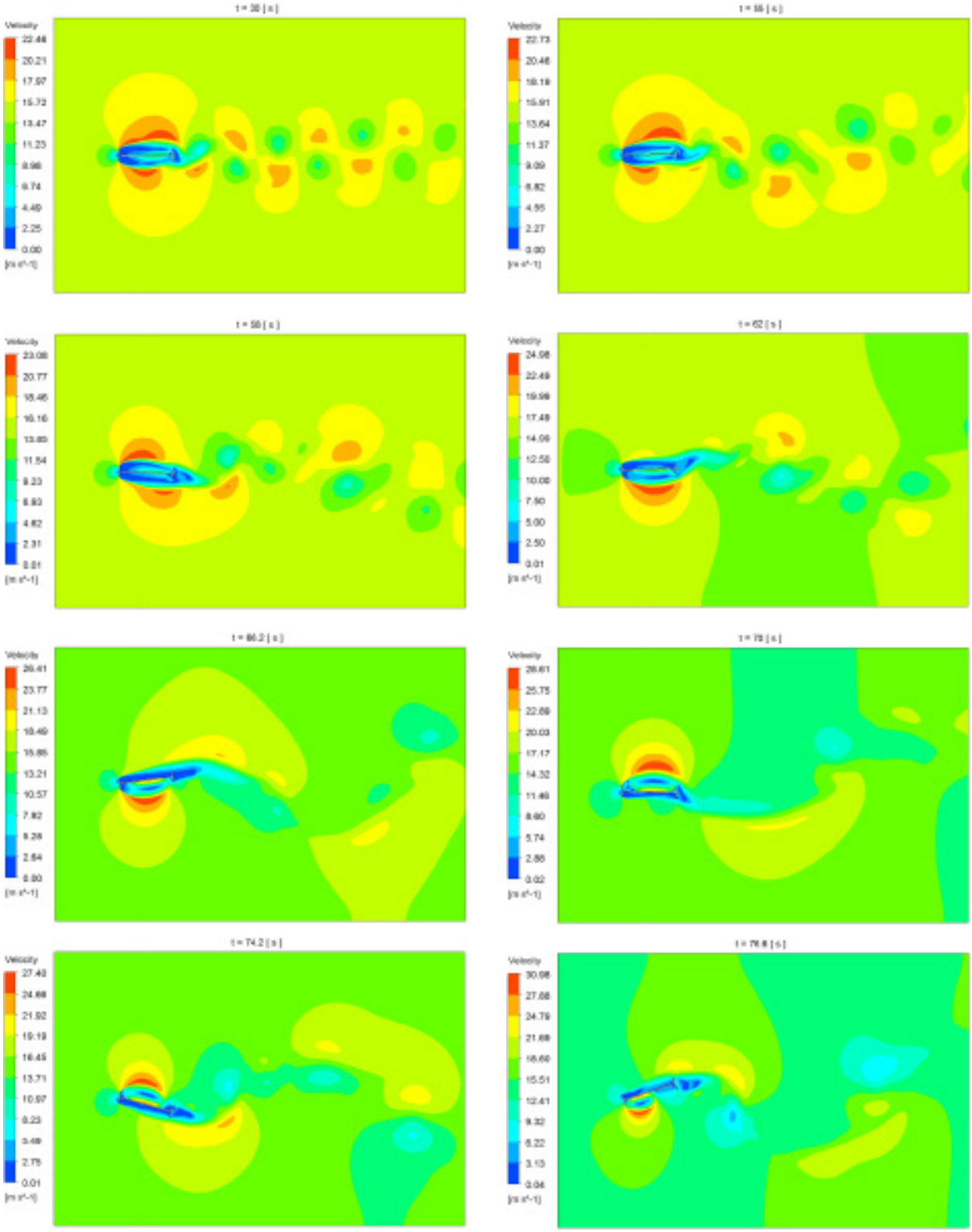

Figure 8. Velocity fields, m / s at different times t, s for a velocity V_{in} = 15 m / s (turbulence model URANS k-ω SST)

the result was similar to the numerical simulation result in [39], where the LES turbulence model was used. The critical speeds can be clarified by additional calculations, but this does not affect the conclusions of this study.

4.2. Comparison of Engineering Estimates and Direct Coupled Calculation

Comparison of the results of direct coupled calculation and engineering estimates [40] revealed the following.

For the DES SST turbulence model:

– according to the engineering estimate of the divergence occurrence [40], at 0 ° the critical speed is 7.91 m / s. The related calculation showed that at an input flow velocity of 8 m / s there was no unlimited increase in the angle of rotation of the section - it was observed at a speed of 10 m / s;

– according to an engineering assessment of the occurrence of galloping [40], this phenomenon should occur at a cross-sectional angle of rotation equal to 10° at a flow velocity of 9.77 m / s. From the graphs of the dependence of the angle of rotation of the section ϑ, ° and the vertical displacement of point 1, m, on time t, s at an input flow rate of 10 m / s, it can be seen that when the angle of rotation of the section approaches 10° (time 38–47 sec) significant jump in vertical displacement. This indicates a possible galloping effect at this moment. Nevertheless, further vertical vibrations of the structure returned to a stable mode (with a rapid increase in the amplitude of the rotation angle). This indicates a complex mutual influence of two aerodynamic instabilities, in which they may not arise, taking into account the vibrations of the structure along other degrees of freedom. In this calculated variant, divergence prevails over galloping.

Table 2. Comparison of the results obtained in the related FSI setting with the results [39]

	V_{CR}, m/s
Experiment [39]	11.5
FSI [39]	10
FSI (turbulence model URANS SST)	15
FSI (turbulence model DES SST)	10

For the turbulence model URANS k-ω SST:

– according to an engineering estimate of the occurrence of divergence [40], at 0 ° the critical speed was 17.18 m / s. A related calculation showed that even at an input flow velocity of 15 m / s, an unlimited increase in the angle of rotation of the section was observed;

– according to an engineering estimate of the occurrence of galloping [40], at a cross-sectional angle of rotation equal to 8 ° at a flow velocity of 5.76 m / s, we should observe this phenomenon. If we look at the graphs of the dependence of the angle of rotation of the section ϑ, ° and the vertical

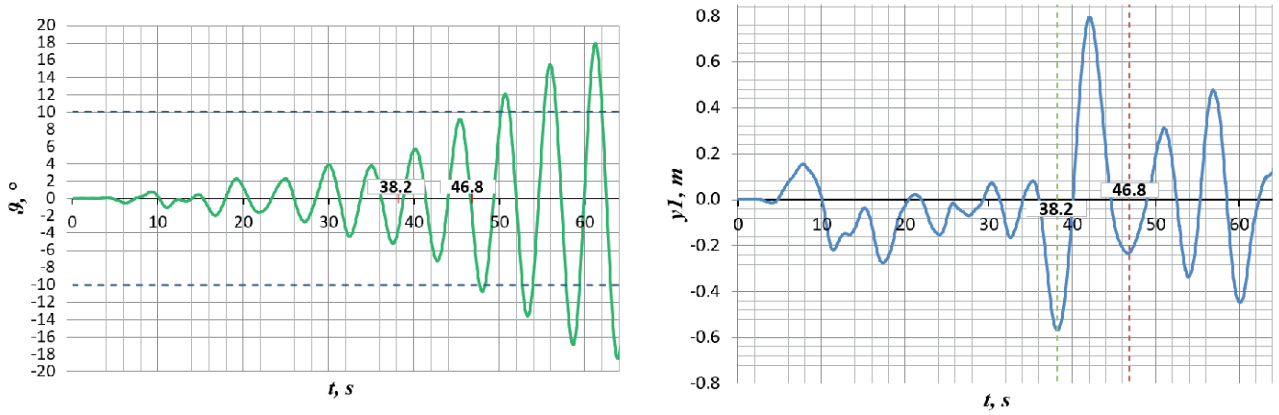

a *b*

Figure 9. Turbulence model DES SST, V_{in} = 10 m / s: Graphs of dependence on time t, s (a) rotation angle ϑ, °; (b) vertical movement of point 1, m

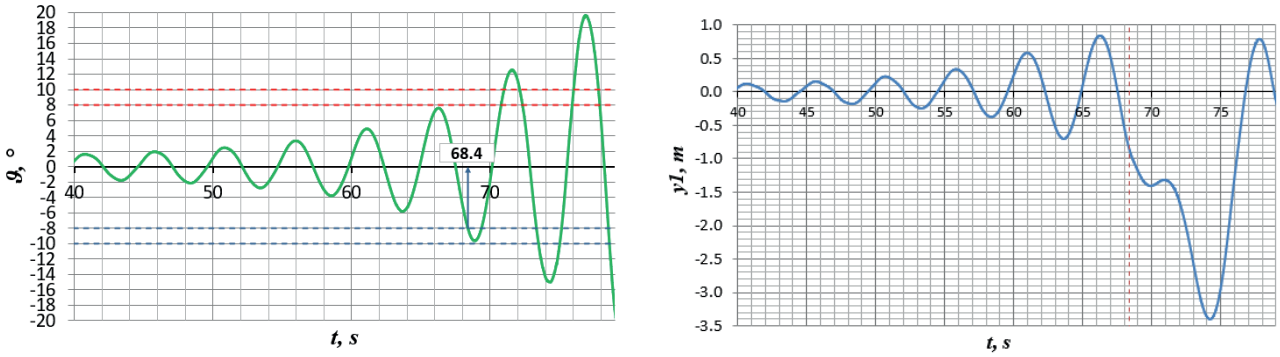

a *b*

Figure 10. Turbulence model URANS k-ω SST, V_{in} = 15 m / s: Graphs of dependence on time t, s (a) rotation angle ϑ, °; (b) vertical movement of point 1, m

displacement of point 1, m on time t, s at an input flow velocity of 15 m / s, we can see that the angle of rotation of the section equal to 8 ° is reached at the moment of time 68.4 s. Therefore, at about this point in time, galloping should be observed. Indeed, at about this moment in time, there is a sharp increase in the amplitude of the vertical displacement of point 1 (the center of the section).

5. CONCLUSION

On the considered two-dimensional problem of aeroelasticity, it is shown that it is quite acceptable to use a lighter, in comparison with LES, DES turbulence model and a coarser mesh (in comparison with "reference" numerical solutions). This will allow in the near future to take an important step towards a full 3D computational model with reasonable computing power.

Also, a test problem with a Tacoma bridge section showed that, although engineering techniques provide estimates of the possible occurrence of aerodynamic instability, they do not take into account the reverse effect of the structure on the flow and the mutual influence of several types of aerodynamic instability. Comparison of the results showed that such inaccuracies both underestimate and overestimate the calculated critical wind flow velocities, which can have detrimental practical consequences.

6. ACKNOWLEDGMENTS

This work was financially supported by the Ministry of Science and Higher Education of the Russian Federation (Project: Theoretical and experimental design of new composite materials to ensure safety during the operation of buildings and structures under conditions of technogenic and biogenic threats #FSWG-2020-0007) (4.1. Results of solving the problem in a related setting) and RFBR, project number 19-31-90128 (4.2. Comparison of Engineering Estimates and Direct Associated Calculation).

REFERENCES

1. **Karman T.** Aerodinamika. Izbrannyye temy v ikh istoricheskom razvitii [Aerodynamics. Selected topics in their historical development]. Izhevsk: NITS "Regulyarnaya i khaoticheskaya dinamika", 2001. 207 p.
2. **Davenport A.G.** The application of statistical concepts to the wind loading of structures. Proceedings of the Institution of Civil Engineers. 1961. 19(4). Pp. 449–472. DOI:10.1680/iicep.1961.11304.
3. **Davenport A.G.** Buffeting of a suspension bridge by storm winds. Journal of structural

Division. 1962. 88(3). Pp. 233–268. DOI:10.4319/lo.2013.58.2.0489.
4. **Barshteyn M.F.** Dinamicheskiy raschet vysokikh sooruzheniy na deystviye vetra [Dynamic calculation of tall structures for the action of the wind]. // In the book: Spravochnik po dinamike sooruzheniy [Reference book on the dynamics of structures]. Under ed. B.G. Korenev, I.M. Rabinovich. Moscow: Stroyizdat, 1972. Pp. 286-321.
5. **Simiu, E., Scanlan, R.H.** Wind effects on structures: an introduction to wind engineering. 1978. DOI:10.1016/0167-6105(80)90031-8.
6. **Scanlan R.H., Stroh S.L., Raggett, J.D**. Methods of wind response investigation employed for the Kap Shui Mun Bridge. Journal of Wind Engineering and Industrial Aerodynamics. 1995. 54–55(C). Pp. 1–11. DOI:10.1016/0167-6105(94)00024-8.
7. **Katsuchi, H., Jones, N.P., Scanlan, R.H., Akiyama, H.** A study of mode coupling in flutter and buffeting of the Akashi-Kaikyo bridge. Structural Engineering/Earthquake Engineering. 1998. 15(2). DOI:10.2208/jscej.1998.598_21.
8. **Scanlan, R.H.** Estimates of skew wind speeds for bridge flutter. Journal of Bridge Engineering. 1999. 4(2). Pp. 95–98. DOI:10.1061/(ASCE)1084-0702(1999)4:2(95).
9. Den Hartog JP Mechanical vibrations // New York; London: McGraw-Hill, 1956. 436 p.
10. EN 1991-1-4. Eurocode 1: Actions on structures - Part 1-4: General actions -Wind actions. European Committee for Standardization. 2005. DOI:ICS 91.010.30; 93.040.
11. ASCE 7-16 Minimum Design Loads and Associated Criteria for Buildings and Other Structures.
12. Building Code of RF SP 20.13330.2016 Nagruzki i vozdeystviya [Loads and actions].
13. **Kazakevich M.I.** Aerodinamika mostov [Aerodynamics of bridges]. Moscow: Transport, 1987. 240 p.
14. **Gorlin S.M.** Eksperimental'naya aerodinamika [Experimental aerodynamics]. Moscow: «Vysshaya shkola», 1970. 423 p.
15. **Davenport A.G.** Gust loading factors. Proc. of American soc. of civil Engineering. Vol. 93 (1), No. ST3 – 1967.
16. **Wei Z., Kareem A.** A benchmark study of flow around a rectangular cylinder with aspect ratio 1:5 at Reynolds number 1.E5. 13th International Conference on Wind Engineering, Proceedings, July 10-15, 2011
17. **Blocken B., Stathopoulos T., Carmeliet J.** CFD simulation of atmospheric boundary layer-wall function problems. Atmospheric Environment, vol. 41 (2), 2007 – pp. 238-252.
18. **Wall, W.A., Ramm, E.** Fluid-structure interaction based upon a stabilized (ALE) finite element method. Computational Mechanics. 1998. Pp. 1–20.
19. **Robertson, I., Sherwin, S.J., Bearman, P.W.** Flutter instability prediction techniques for bridge deck sections. International Journal for Numerical Methods in Fluids. 2003. DOI:10.1002/fld.535.
20. **Costa, C., Borri, C.** Application of indicial functions in bridge deck aeroelasticity. Journal of Wind Engineering and Industrial Aerodynamics. 2006. 94(11). Pp. 859–881. DOI:10.1016/j.jweia.2006.06.007.
21. **Šarkić, A., Höffer, R.** Improved numerical simulation of bridge deck aeroelasticity by model validation. 6th European and African Conference on Wind Engineering, EACWE 2013. 2013.
22. **Wu, T., Kareem, A.** Bridge aerodynamics and aeroelasticity: A comparison of modeling schemes. Journal of Fluids and Structures. 2013. 43. Pp. 347–370. DOI:10.1016/j.jfluidstructs.2013.09.015.
23. **Wu, T., Kareem, A.** Aerodynamics and aeroelasticity of cable-supported bridges: Identification of nonlinear features. Journal of Engineering Mechanics. 2013. 139(12). Pp. 1886–1893. DOI:10.1061/(ASCE)EM.1943-7889.0000615.

24. **Zhan, H., Fang, T., Zhang, Z.** Flutter stability studies of Great Belt East suspension Bridge by two CFD numerical simulation methods. 6th European and African Conference on Wind Engineering, EACWE 2013. 2013.
25. **Xu, Y.L., Hu, L., Kareem, A.** Conditional simulation of nonstationary fluctuating wind speeds for long-span bridges. Journal of Engineering Mechanics. 2014. 140(1). Pp. 61–73. DOI:10.1061/(ASCE)EM.1943-7889.0000589.
26. **Mannini, C., Bartoli, G.** Aerodynamic uncertainty propagation in bridge flutter analysis. Structural Safety. 2015. 52(PA). Pp. 29–39. DOI:10.1016/j.strusafe.2014.07.005.
27. **Xu, F., Wu, T., Ying, X., Kareem, A.** Higher-order self-excited drag forces on bridge decks. Journal of Engineering Mechanics. 2016. 142(3). DOI:10.1061/(ASCE)EM.1943-7889.0001036.
28. **Kavrakov, I., Morgenthal, G.** A synergistic study of a CFD and semi-analytical models for aeroelastic analysis of bridges in turbulent wind conditions. Journal of Fluids and Structures. 2018. 82. Pp. 59–85. DOI:10.1016/j.jfluidstructs.2018.06.013.
29. **Kavrakov, I., Legatiuk, D., Gürlebeck, K., Morgenthal, G.** A categorical perspective towards aerodynamic models for aeroelastic analyses of bridge decks. Royal Society Open Science. 2019. DOI:10.1098/rsos.181848.
30. **Zhang, M., Xu, F., Zhang, Z., Ying, X.** Energy budget analysis and engineering modeling of post-flutter limit cycle oscillation of a bridge deck. Journal of Wind Engineering and Industrial Aerodynamics. 2019. 188. Pp. 410–420. DOI:10.1016/j.jweia.2019.03.010.
31. **Belostotskiy A.M., Akimov P.A., Afanas'yeva I.N.** Vychislitel'naya aerodinamika v zadachakh stroitel'stva [Computational aerodynamics in construction problems]. Moscow: Publishing ASV, 2017, 720 p.
32. Metodicheskoye posobiye «Matematicheskoye (chislennoye) modelirovaniye vetrovykh nagruzok i vozdeystviy» (k SP 20.13330.2016) [Methodological manual "Mathematical (numerical) modeling of wind loads and effects" (to SP 20.13330.2016)], Moscow, FAU FTSS Minstroya Rossii, 2020
33. **Belostotskiy A.M., Afanas'yeva I.N.** Chislennoye modelirovaniye zadach aerouprugosti v stroitel'stve [Numerical modeling of aeroelasticity problems in construction]. Vysotnyye zdaniya. 2015. №1. Pp. 106-109.
34. **Afanas'yeva I.N**. Adaptivnaya metodika chislennogo modelirovaniya trekhmernykh dinamicheskikh zadach stroitel'noy aerogidrouprugosti [An adaptive technique for numerical modeling of three-dimensional dynamic problems of construction aerohydroelasticity]. Diss. Of Candidate of Technical Sciences. M., MGSU, 2014. 200 p.
35. **Belostotsky, A.M., Afanasyeva, I.N., Lantsova, I.Y., Petryashev, S.O., Petryashev, N.O.** Estimation of aerodynamic instability of building structures //Procedia Structural Integrity. – 2017. – Vol. 6. – Pp. 322-329.
36. **Lantsova I., Afanasyeva I.** Investigation of aerodynamic instability of a thin plate //MATEC Web of Conferences. – EDP Sciences, 2017. – Vol. 117. – 00099.
37. **Afanasyeva I. N., Lantsova I. Y.** Numerical simulation of an elastic structure behavior under transient fluid flow excitation. AIP Conference Proceedings. – AIP Publishing LLC, 2017. – Vol. 1800. – No. 1. . 040013
38. **Afanas'yeva I.N.** Modelirovaniye dvumernogo nestatsionarnogo obtekaniya gibkoy uprugoy konstruktsii v svyazannoy postanovke. Chast' 3: verifikatsiya metodiki chislennogo modelirovaniya svyazannoy zadachi aerogidrouprugosti [Simulation of two-dimensional unsteady flow around a flexible elastic structure in a coupled setting. Part 3: verification of the methodology for numerical modeling of the coupled aerohydroelasticity problem]. International Journal for Computational Civil and Structural Engineering. – 2014. – Vol. 10. – No. 3. – Pp. 40-48.

39. **Zhan H, Fang T.** Flutter stability studies of Great Belt East Bridge and Tacoma Narrows Bridge by CFD numerical simulation. Proceedings of the7th International Colloquium on Bluff Body Aerodynamics and Applications (BBAA7). Shanghai, 2012. Pp. 1518-1527.
40. **Lantsova I.YU., Afanas'yeva I.N.** Modelirovaniye aerodinamicheskoy neustoychivosti stroitel'nykh konstruktsiy na primere secheniya mosta chast' 1: otsenka aerodinamicheskoy neustoychivosti secheniya inzhenernymi metodami [Modeling aerodynamic instability of building structures on the example of a bridge section, part 1: estimation of aerodynamic instability of a section by engineering methods]. IJCCSE, vol. 14, issue 1, 2018.

СПИСОК ЛИТЕРАТУРЫ

1. **Карман Т.** Аэродинамика. Избранные темы в их историческом развитии. Ижевск: НИЦ "Регулярная и хаотическая динамика", 2001. 207 стр.
2. **Davenport A.G.** The application of statistical concepts to the wind loading of structures. Proceedings of the Institution of Civil Engineers. 1961. 19(4). Pp. 449–472. DOI:10.1680/iicep.1961.11304.
3. **Davenport A.G**. Buffeting of a suspension bridge by storm winds. Journal of structural Division. 1962. 88(3). Pp. 233–268. DOI:10.4319/lo.2013.58.2.0489.
4. **Барштейн М.Ф.** Динамический расчет высоких сооружений на действие ветра. // В кн.: Справочник по динамике сооружений. Под ред. Б.Г. Коренева, И.М. Рабиновича. М., Стройиздат, 1972–. с. 286-321.
5. **Simiu, E., Scanlan, R.H.** Wind effects on structures: an introduction to wind engineering. 1978. DOI:10.1016/0167-6105(80)90031-8.
6. **Scanlan R.H., Stroh S.L., Raggett, J.D**. Methods of wind response investigation employed for the Kap Shui Mun Bridge. Journal of Wind Engineering and Industrial Aerodynamics. 1995. 54–55(C). Pp. 1–11. DOI:10.1016/0167-6105(94)00024-8.
7. **Katsuchi, H., Jones, N.P., Scanlan, R.H., Akiyama, H.** A study of mode coupling in flutter and buffeting of the Akashi-Kaikyo bridge. Structural Engineering/Earthquake Engineering. 1998. 15(2). DOI:10.2208/jscej.1998.598_21.
8. **Scanlan, R.H.** Estimates of skew wind speeds for bridge flutter. Journal of Bridge Engineering. 1999. 4(2). Pp. 95–98. DOI:10.1061/(ASCE)1084-0702(1999)4:2(95).
9. Den Hartog JP Mechanical vibrations // New York; London: McGraw-Hill, 1956. 436 p.
10. EN 1991-1-4. Eurocode 1: Actions on structures – Part 1–4: General actions – Wind actions. European Committee for Standardization. 2005. DOI:ICS 91.010.30; 93.040.
11. ASCE 7-16 Minimum Design Loads and Associated Criteria for Buildings and Other Structures.
12. СП 20.13330.2016 Нагрузки и воздействия
13. **Казакевич М.И**. Аэродинамика мостов. // М.: Транспорт, 1987. – 240 с.
14. **Горлин С.М**. Экспериментальная аэродинамика. // М.: «Высшая школа», 1970. – 423 с.
15. Davenport A.G. Gust loading factors. Proc. of American soc. of civil Engineering. Vol. 93 (1), No. ST3 – 1967.
16. **Wei Z., Kareem A.** A benchmark study of flow around a rectangular cylinder with aspect ratio 1:5 at Reynolds number 1.E5. 13th International Conference on Wind Engineering, Proceedings, July 10-15, 2011
17. **Blocken B., Stathopoulos T., Carmeliet J.** CFD simulation of atmospheric boundary layer-wall function problems. Atmospheric Environment, vol. 41 (2), 2007 – pp. 238-252.
18. **Wall, W.A., Ramm, E.** Fluid-structure interaction based upon a stabilized (ALE) finite element method. Computational Mechanics. 1998. Pp. 1–20.
19. **Robertson, I., Sherwin, S.J., Bearman, P.W.** Flutter instability prediction techniques for

bridge deck sections. International Journal for Numerical Methods in Fluids. 2003. DOI:10.1002/fld.535.

20. **Costa, C., Borri, C.** Application of indicial functions in bridge deck aeroelasticity. Journal of Wind Engineering and Industrial Aerodynamics. 2006. 94(11). Pp. 859–881. DOI:10.1016/j.jweia.2006.06.007.
21. **Šarkić, A., Höffer, R.** Improved numerical simulation of bridge deck aeroelasticity by model validation. 6th European and African Conference on Wind Engineering, EACWE 2013. 2013.
22. **Wu, T., Kareem, A.** Bridge aerodynamics and aeroelasticity: A comparison of modeling schemes. Journal of Fluids and Structures. 2013. 43. Pp. 347–370. DOI:10.1016/j.jfluidstructs.2013.09.015.
23. **Wu, T., Kareem, A.** Aerodynamics and aeroelasticity of cable-supported bridges: Identification of nonlinear features. Journal of Engineering Mechanics. 2013. 139(12). Pp. 1886–1893. DOI:10.1061/(ASCE)EM.1943-7889.0000615.
24. **Zhan, H., Fang, T., Zhang, Z.** Flutter stability studies of Great Belt East suspension Bridge by two CFD numerical simulation methods. 6th European and African Conference on Wind Engineering, EACWE 2013. 2013.
25. **Xu, Y.L., Hu, L., Kareem, A.** Conditional simulation of nonstationary fluctuating wind speeds for long-span bridges. Journal of Engineering Mechanics. 2014. 140(1). Pp. 61–73. DOI:10.1061/(ASCE)EM.1943-7889.0000589.
26. **Mannini, C., Bartoli, G.** Aerodynamic uncertainty propagation in bridge flutter analysis. Structural Safety. 2015. 52(PA). Pp. 29–39. DOI:10.1016/j.strusafe.2014.07.005.
27. **Xu, F., Wu, T., Ying, X., Kareem, A.** Higher-order self-excited drag forces on bridge decks. Journal of Engineering Mechanics. 2016. 142(3). DOI:10.1061/(ASCE)EM.1943-7889.0001036.
28. **Kavrakov, I., Morgenthal, G.** A synergistic study of a CFD and semi-analytical models for aeroelastic analysis of bridges in turbulent wind conditions. Journal of Fluids and Structures. 2018. 82. Pp. 59–85. DOI:10.1016/j.jfluidstructs.2018.06.013.
29. **Kavrakov, I., Legatiuk, D., Gürlebeck, K., Morgenthal, G.** A categorical perspective towards aerodynamic models for aeroelastic analyses of bridge decks. Royal Society Open Science. 2019. DOI:10.1098/rsos.181848.
30. **Zhang, M., Xu, F., Zhang, Z., Ying, X.** Energy budget analysis and engineering modeling of post-flutter limit cycle oscillation of a bridge deck. Journal of Wind Engineering and Industrial Aerodynamics. 2019. 188. Pp. 410–420. DOI:10.1016/j.jweia.2019.03.010.
31. **Белостоцкий А.М., Акимов П.А., Афанасьева И.Н.** Вычислительная аэродинамика в задачах строительства. М., Издательство АСВ, 2017, 720 с.
32. Методическое пособие «Математическое (численное) моделирование ветровых нагрузок и воздействий» (к СП 20.13330.2016), М., ФАУ ФЦС Минстроя России, 2020
33. **Белостоцкий А.М., Афанасьева И.Н.** Численное моделирование задач аэроупругости в строительстве. Высотные здания №1 (2015), М., 2015. – стр. 106–109.
34. **Афанасьева И.Н.** Адаптивная методика численного моделирования трехмерных динамических задач строительной аэрогидроупругости. Дисс. на соискание ученой степени к.т.н. М., МГСУ, 2014. – 200 с
35. **Belostotsky, A.M., Afanasyeva, I.N., Lantsova, I.Y., Petryashev, S.O., Petryashev, N.O.** Estimation of aerodynamic instability of building structures //Procedia Structural Integrity. – 2017. – Т. 6. – С. 322-329.
36. **Lantsova I., Afanasyeva I.** Investigation of aerodynamic instability of a thin plate //MATEC Web of Conferences. – EDP Sciences, 2017. – Т. 117. – С. 00099.
37. **Afanasyeva I.N., Lantsova I.Y.** Numerical simulation of an elastic structure behavior under transient fluid flow excitation //AIP

Conference Proceedings. – AIP Publishing LLC, 2017. – T. 1800. – №. 1. – C. 040013

38. **Афанасьева И.Н.** Моделирование двумерного нестационарного обтекания гибкой упругой конструкции в связанной постановке. Часть 3: верификация методики численного моделирования связанной задачи аэрогидроупругости //International Journal for Computational Civil and Structural Engineering. – 2014. – Т. 10. – №. 3. – С. 40–48.
39. **Zhan H, Fang T.** Flutter stability studies of Great Belt East Bridge and Tacoma Narrows Bridge by CFD numerical simulation. Proceedings of the7th International Colloquium on Bluff Body Aerodynamics and Applications (BBAA7). Shanghai, 2012. Pp. 1518-1527.
40. **Ланцова И.Ю., Афанасьева И.Н.** Моделирование аэродинамической неустойчивости строительных конструкций на примере сечения моста часть 1: оценка аэродинамической неустойчивости сечения инженерными методами // IJCCSE, vol. 14, issue 1, 2018.

Alexander M. Belostotsky, corresponding member of RAACS, professor, doctor of technical sciences; General Director of CJSC Scientific Research Center StaDiO; Professor of the Department of Informatics and Applied Mathematics of the National Research Center, scientific director of the REC KM named after A.B. Zolotov Moscow State University of Civil Engineering; Professor of the Department of Building Structures, Buildings and Structures of the Russian University of Transport (MIIT); 125040, Russia, Moscow, st. 3rd Yamskogo Polya, 18, office 810; Tel. +7 (499) 706-88-10. E-mail: amb@stadyo.ru

Irina N. Afanasyeva, Candidate of Technical Sciences, Leading Calculation Engineer, JSC Scientific Research Center StaDiO; assistant at the University of Florida (USA); 125040, Russia, Moscow, st. 3rd Yamskogo Polya, 18, 8th floor, office 810, tel. +7 (495) 706-88-10. E-mail: irina.n.afanasyeva@gmail.com.

Irina Yu. Negrozova, Junior Researcher, REC KM named after V.I. A.B. Zolotova and Senior Lecturer of the Department of Informatics and Applied Mathematics of the National Research Moscow State University of Civil Engineering; 129337, Russia, Moscow, Yaroslavskoe shosse, 26. E-mail: LantsovaIYu@mgsu.ru.

Oleg S. Goryachevsky, Lead Structural Engineer, CJSC Research Center StaDiO; Deputy Director of REC KM named after A.B. Zolotov of the National Research Moscow State University of Civil Engineering; 129337, Russia, Moscow, Yaroslavskoe shosse, 26. E-mail: osgoryachevskij@mail.ru

Белостоцкий Александр Михайлович, член-корреспондент РААСН, профессор, доктор технических наук; генеральный директор ЗАО Научно-исследовательский центр СтаДиО; профессор кафедры Информатики и прикладной математики Национального исследовательского, научный руководитель НОЦ КМ им. А.Б. Золотова Московского государственного строительного университета; профессор кафедры «Строительные конструкции, здания и сооружения» Российского университета транспорта (МИИТ); 125040, Россия, Москва, ул. 3-я Ямского Поля, д.18, офис 810; тел. +7 (499) 706-88-10. E-mail: amb@stadyo.ru

Афанасьева Ирина Николаевна, кандидат технических наук, ведущий инженер-расчетчик ЗАО Научно-исследовательский центр СтаДиО; ассистент Флоридского университета (США); 125040, Россия, г. Москва, ул. 3-я Ямского Поля, д.18, 8 этаж, офис 810, тел. +7 (495) 706-88-10. E-mail: irina.n.afanasyeva@gmail.com.

Негрозова Ирина Юрьевна, младший научный сотрудник НОЦ КМ им. А.Б. Золотова и старший преподаватель кафедры Информатики и прикладной математики Национального исследовательского Московского государственного строительного университета; 129337, Россия, г. Москва, Ярославское шоссе, д. 26. E-mail: LantsovaIYu@mgsu.ru.

Горячевский Олег Сергеевич, ведущий инженер-расчетчик ЗАО Научно-исследовательский центр СтаДиО; заместитель директора НОЦ КМ им. А.Б. Золотова Национального исследовательского Московского государственного строительного университета; 129337, Россия, г. Москва, Ярославское шоссе, д. 26. E-mail: osgoryachevskij@mail.ru

DOI:10.22337/2587-9618-2021-17-3-39-47

COMPARISON OF DETERMINATION OF SNOW LOADS FOR ROOFS IN BUILDING CODES OF VARIOUS COUNTRIES

Alexander M. Belostotsky [1,2,3]***, Nikita A. Britikov*** [2,3]***, Oleg S. Goryachevsky*** [1,2]

[1] Scientific Research Center StaDyO, Moscow, RUSSIA
[2] National Research Moscow State University of Civil Engineering, Moscow, RUSSIA
[3] Russian University of Transport (RUT - MIIT), Moscow, RUSSIA

Abstract: The article compares the requirements for calculating the snow load on the coatings of buildings and structures in accordance with the regulations of technically developed countries and associations – Russia, the European Union, Canada and the United States. It was revealed that in these norms the general approaches, the subtleties of calculating the coefficients, the set of standard coatings and the schemes of the form coefficient proposed for them differ significantly. This situation reflects the general problem of determining snow loads – at the moment there is no recognized unified scientifically grounded approach to determining snow loads on coatings of even the simplest form. The difference in the normative schemes of snow loads is clearly demonstrated by the example of a three-level roof.

Keywords: snow loads, regulatory documents, physical modeling, mathematical modeling

СРАВНЕНИЕ НОРМАТИВНЫХ ДОКУМЕНТОВ РАЗЛИЧНЫХ СТРАН В ЧАСТИ НАЗНАЧЕНИЯ СНЕГОВЫХ НАГРУЗОК

А.М. Белостоцкий [1,2,3]***, Н.А. Бритиков*** [2,3]***, О.С. Горячевский*** [1,2]

[1] Научно-исследовательский центр СтаДиО, г. Москва, РОССИЯ
[2] Национальный исследовательский Московский государственный строительный университет, г. Москва, РОССИЯ
[3] Российский университет транспорта (МИИТ), г. Москва, РОССИЯ

Аннотация: В статье сравниваются требования к расчёту снеговой нагрузки на покрытия зданий и сооружений в соответствии с нормативными документами технически развитых стран и объединений – России, Евросоюза, Канады и США. Выявлено, что в этих нормах значительно отличаются общие подходы, тонкости вычисления коэффициентов, набор стандартных покрытий и предлагаемые для них схемы коэффициента формы. Такая ситуация отражает общую проблему определения снеговых нагрузок – на данный момент отсутствует признанный единый научно обоснованный подход к определению снеговых нагрузок на покрытия даже простейшей формы. Различие в нормативных схемах снеговых нагрузок наглядно продемонстрировано на примере трехуровневой кровли.

Ключевые слова: снеговые нагрузки, нормативные документы, физическое моделирование, математическое моделирование

INTRODUCTION

The problem of determining the distribution of snow loads on roofs of various shapes does not lose its relevance to the present day. Very few full-scale tests are carried out all over the world, which does not allow obtaining new load arrangements or clarifying old ones. The physical modeling in wind tunnel or water flumes, regulated by the normative documents of all technically developed countries, makes it possible to simulate only single snow storms, and the problem of simulating the natural phenomenon of snow accumulation and scale models remains unsolvable. Progress in the direction of determining the snow loads on the roofs of

structures is currently observed only in the field of mathematical (numerical) modeling [7].
Despite the development of a large number of mathematical models, their algorithmic and software implementations, the normative documents regarding the determination of snow loads remain conservative and for the most part do not allow the possibility of mathematical modeling.
The conservatism of the norms often causes designers, constructors and other participants in the construction process to misunderstand that all the problems have already been solved, and the provisions set out in the norms are unshakable. The purpose of this article is to show that the regulations in different countries and schemes for the distribution of snow loads, even for the simplest roofs, differ qualitatively and quantitatively.

COMPARISON OF BASIC PROVISIONS

This section compares the main provisions of regulatory documents in terms of determining snow loads according to the standards of Russia (SP 20.13330.2016 [1]), the European Union (EN 1991-1-3 [2]), Canada (National Building Code of Canada [3]) and USA (ASCE / SEI 7-16: Snow Loads [4]).

Similar provisions of the norms:
1) the calculation of the load is carried out according to the same principle - multiplying the characteristic value of snow load on the ground by various coefficients (drift, thermal, etc.), including the snow load shape coefficientof the snow cover of the earth to the snow load on the cover (or several such coefficients).
2) there are maps of snow zoning of varying degrees of detail to determine the characteristic value of snow load on the ground.
3) to determine the coefficient (or coefficients) of the shape, there are load arrangements for the following roofs:
• monopitch and pitched;
• dome and cylindrical;
• multi-level;
• multi-span (sawtooth, etc.)
4) To determine snow loads on other types of roofs that are not regulated by standards, it is recommended to carry out research in satisfying the requirements of wind tunnels [5].

Miscellaneous provisions of the norms:
Each regulatory document has its own set of calculated values, and not all of them can be found analogous; the detailing of zoning maps varies greatly; some norms allow the use of numerical modeling for calculating snow loads, others do not stipulate or directly prohibit due to some circumstances. Also, in some standards there are load arrangements for the transfer coefficients in addition to the above. Let's consider in more detail each of these provisions for each of the mentioned documents.

1) *Bulding Code of Russia SP 20.13330.2016 "Loads and actions" (with amendment 3)* [1] give the following formula for calculating the standard value of the snow load:

$$S = \mu c_e c_t S_g, \tag{1}$$

where μ is the shape coefficient, which takes into account the transition from the weight of the snow cover of the earth to the snow load on the roof, c_e is the exposure coefficient, c_t is the thermal coefficient, S_g is nominal weight of snow cover per square meter of surface. In order to obtain the design load, this expression is multiplied by the load safety factor γ_f, usually equal to 1.4. Amendment 3 in some cases allowed a decrease in the value of the c_e coefficient based on climatic data for the construction site.

Differences from other documents:
In Russian standards, an increase in snow load for roofs abutting and close to taller construction works is considered separately for the windward and leeward sides, while the concept of wind direction itself is absent. There are also load arrangements for specific roofs, which, from

the point of view of other documents, are even redundant. Much attention has been paid to roof lanterns, as there are separate load arrangements presented for longitudal and transversal lanterns in the norms. Also, a special load arrangement for a roof abutting two taller construction works is shown, as well as for arched roofs and vaulted roofs.

Numerical Simulation:
In contrast to wind loads [6], the Russian standards do not say anything about the numerical modeling of snow loads.

2) Eurocode [2] identifies three types of snow load: for persistent / transient design situations (s_1), for the accidental design situations, where exceptional snow load is the accidental action (s_2), and for the accidental design situations, where exceptional snow drift is the accidental action (s_3), and gives the following formulas for calculating the values of each of them:

$$s_1 = \mu C_e C_t s_k,\ s_2 = \mu C_e C_t s_{ad},\ s_3 = \mu s_k, \qquad (2)$$

where μ is the snow load shape coefficient, C_e is the exposure coefficient, C_t is the thermal coefficient, s_k is the characteristic value of snow load on the ground, $s_{ad}=2s_k$.

Differences from other documents:
Similar to Russian standards, an increase in snow load for roofs abutting and close to taller construction works is considered separately for the windward and leeward sides, while the concept of wind direction itself is absent.

Numerical Simulation:
Unlike Russian and Canadian standards, Eurocode allows the use of numerical modeling to refine the shape coefficient along with physical modeling, however, it does not contain any specific requirements for the methods that should be used.

3) *National Building Code of Canada* [3] gives the following formula for calculating the standard value of the snow load:

$$S = I_s S_s (C_b C_w C_s C_a), \qquad (3)$$

where I_s is importance factor for snow load, S_s is 1-in-50-year ground snow load, C_b is the basic roof snow load factor, C_w is the wind exposure factor, C_s is the slope factor, C_a is the accumulation factor. Togethers C_b, C_s and C_a are analogous to μ from the Building Code of Russia and the Eurocode.

Differences from other documents:
In the Canadian standards, wind directions are clearly distinguished, and the load is calculated for each of the sides separately, but then the largest of the obtained values is taken and assigned to both sides in reserve.

Numerical Simulation:
Construction Canada explicitly prohibits the use of numerical simulations of snow accumulation due to insufficient data on the legality of its use and the physicality of the results obtained with its help.

4) *ASCE standard* [4] gives the following formula for calculating the standard value of the snow load:

$$p_f = 0.7 C_e C_t I_s p_g, \qquad (4)$$

where C_e is the exposure factor, C_t is the thermal factor, I_s is the importance factor, p_g is the ground snow load. Also, a minimum roof snow load for low-slope roofs, p_m, shall be obtained using the following formula:

$$p_m = I_s p_g, \qquad (5)$$

For unbalanced load, the following formula is used:

$$p_s = C_s p_f, \qquad (6)$$

where C_s is the roof shape factor.

Differences from other documents:
Similar to the Canadian standards, wind directions are clearly highlighted, and the load is cal-

culated for each of the sides separately, but then the largest of the obtained values is taken and assigned to both sides as a margin. The values of the shape factor depend, as can be seen from formula (4), on the thermal factor.

Numerical Simulation:

American regulations explicitly state that physical modeling results should only be used in conjunction with numerical simulations, that shape factors or load values cannot be generated based on the experiment alone. The Appendix to the ASCE standard [5] contains a classification of numerical methods for modeling snow accumulation. Also, American norms are distinguished by the most detailed map of snow zoning, it contains data for all more or less large settlements in the United States due to the arrangement of meteorological stations near airports.

In general, the differences between different norms are more likely due to the engineering tradition of countries that serve as prerequisites for the compilation of norms, and in all respects: even the standard weight of the snow cover is taken somewhere strongly in reserve, somewhere it is specified as much as possible to prevent unnecessary large loads. A significant drawback of all regulatory documents is observed in terms of legitimization and regulation of mathematical (numerical) modeling of snow loads. This circumstance for all documents is undoubtedly an inhibiting factor in the introduction of mathematical modeling into construction practice, especially considering the increasing need for its use and the increasing pace of scientific research in this direction in other countries, such as China, where in the last 7 years, several dozen articles on research (for example [18-19]), carried out with the support of government grants, were published.

EXAMPLE

In order to demonstrate the differences in the definition of snow loads according to the regulatory documents of Russia [1], the European Union [2], Canada [3] and the USA [4-5], an example of a three-level roof is considered (Fig. 1). Calculation formulas and values of the corresponding parameters and coefficients are presented in table. 1. Figures 2-5 show calculation results.

Table. 1. Calculation formulas for various regulatory documents

Regulatory documents	*Formula for snow load*	*Accepted values in the formula*
Building Code of Russia SP 20.13330.2016 (with amendment 3)	$S = \mu c_e c_t S_g$	$c_e = 0.7$ for the central level, $c_e = 1.0$ for side levels, $c_t = 1.0$, $S_g = 1.5$ kPa
EN 1991-1-3 (2003)	$s = \mu C_e C_t s_k$ (persistent); $s = \mu C_e C_t s_{ad}$ (exceptional snow load) $s = \mu s_{ad}$ (exceptional snow drift)	$C_e = 0.8$, $C_t = 1.0$, $s_k = 1.5$ kPa, $s_{ad} = 2s_k = 3$ kPa
National Building Code of Canada 2015	$S = I_s S_s (C_b C_w C_s C_a)$	$I_s = 1.0$, $C_w = 1.0$, $C_s = 1.0$, $S_s = 1.5$ kPa
ASCE/SEI 7-16: Snow Loads	$p_f = 0.7 C_e C_t I_s p_g$ $p_m = I_s p_g$ (minimum load for low-slope roofs) $p_s = C_s p_f$ (unbalanced load)	$C_e = 0.9, C_t = 1.0, I_s = 1.1$ $p_g = 0.96$ kPa (analogue of S_g)

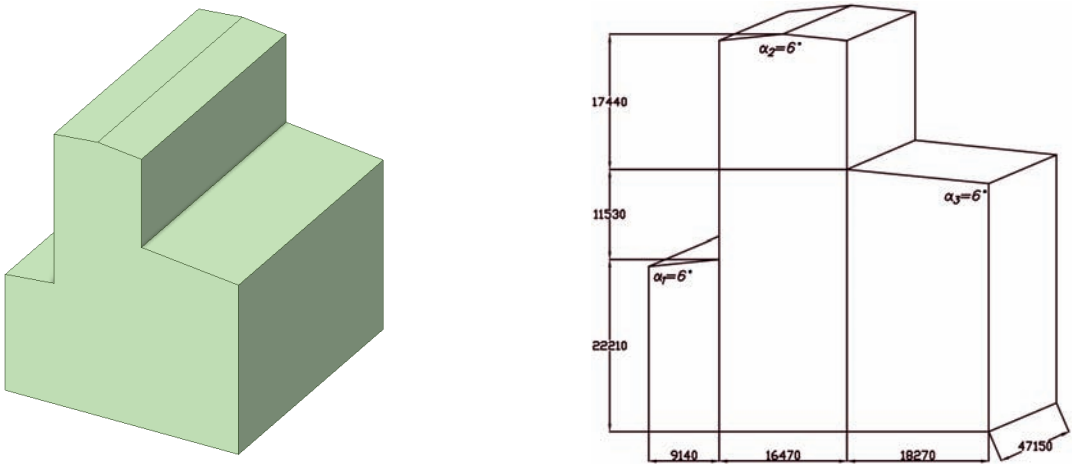

Figure 1. General view and dimensions of the structure

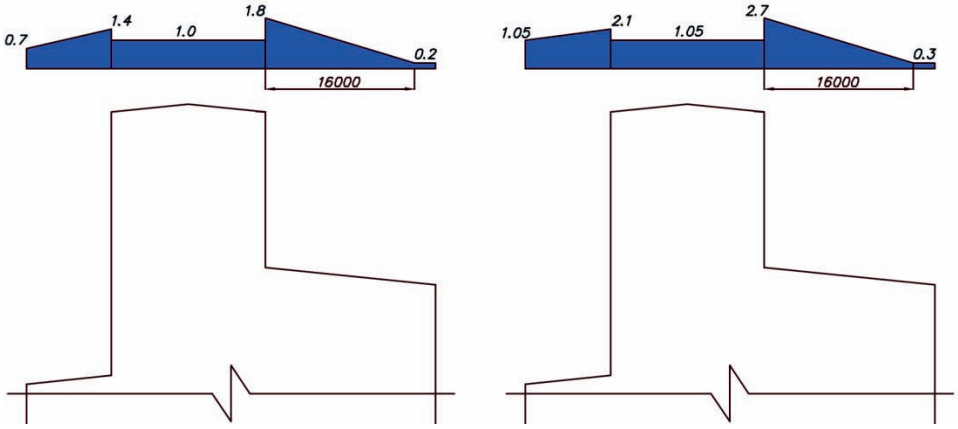

Figure 2. Load arrangement according to the Building Code of Russia SP 20.13330.2016 (with amendment No 3)

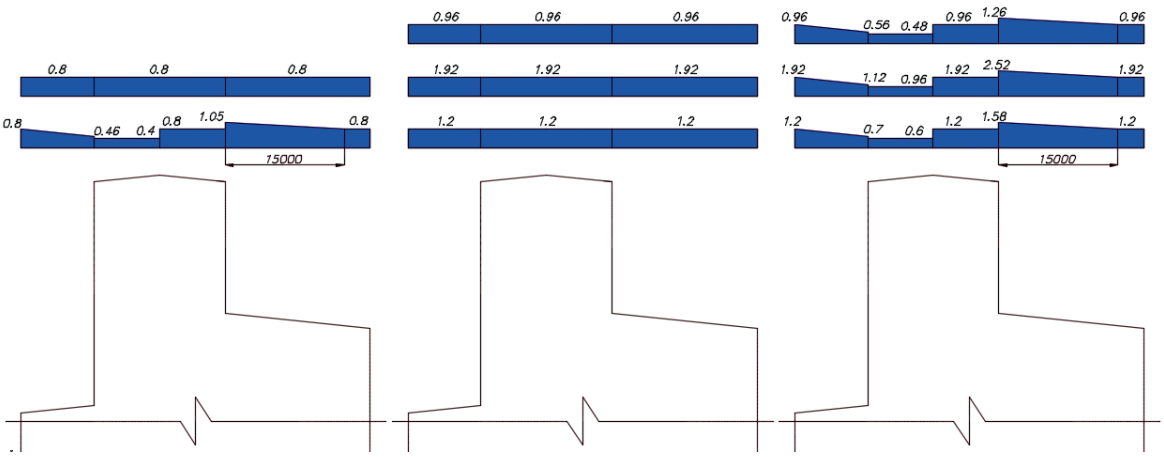

Figure 3. Load arrangement according to EN 1991-1-3 (2003)

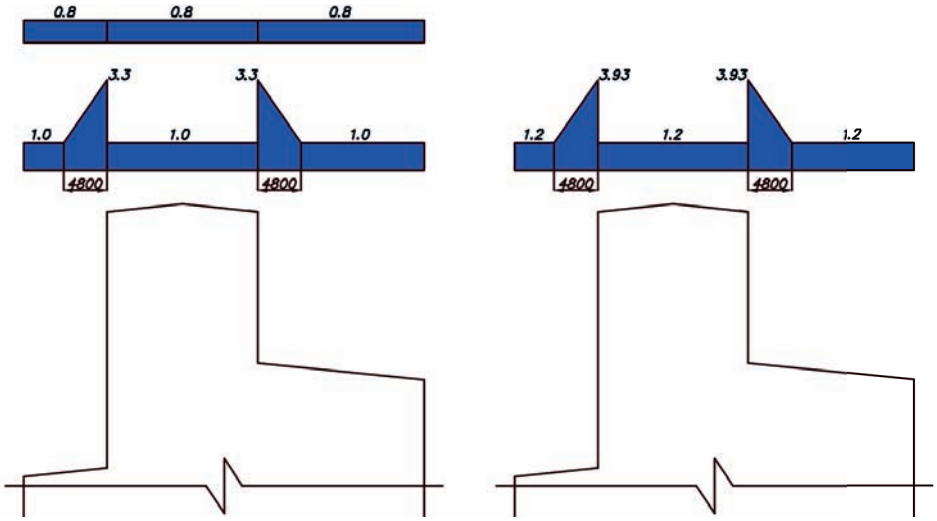

Figure 4. Load arrangement according to the National Building Code of Canada 2015

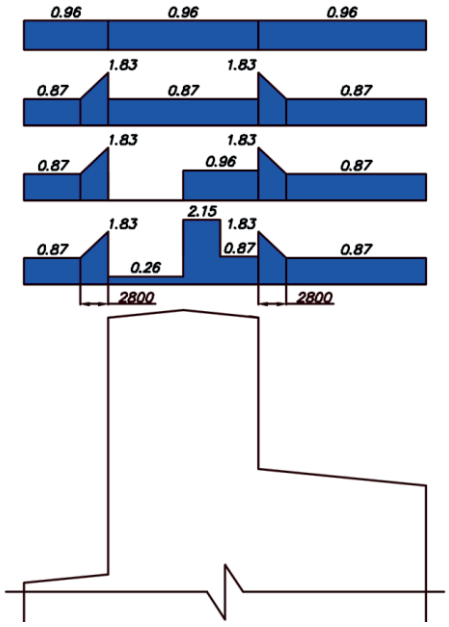

Figure 5. Load arrangement according to ASCE/SEI 7-16: Snow Loads

CONCLUSIONS

Based on the results of the analysis and comparison of the regulatory documents of Russia, the European Union, Canada and the United States in terms of determining snow loads on the roofs of structures, as well as comparing load arrangements using the example of a three-level roof, determined according to the relevant documents, the following conclusions can be drawn:

1. Normative documents of technically advanced countries / associations have their own general approach to determining snow loads, which differ significantly from other countries.

2. All normative documents contain recommendations for carrying out physical modeling of snow loads, but recommendations for mathematical (numerical) modeling are contained only in the norms of the European Union and the United States.
3. Load arrangements, even for the simplest roofs, differ in different documents both qualitatively and quantitatively.
4. This reveals the general problem of the lack of progress in a common understanding of how to determine the snow loads on roofs. We can say that in this matter there is no reliable support even in the norms.

Improvement of Russian normative documents in terms of physical modeling (regulation of requirements and procedure for conducting experiments) and mathematical (numerical) modeling (legitimization and regulation) will help to partially solve the problem of uncertainty in the assignment of snow loads to complex surfaces. Such measures, in particular, will increase the mechanical safety of large-span structures, for which the snow load is one of the determining factors.
The improvement of Russian normative documents in terms of assigning snow loads to simple typical roofs can also be helped by studies based on physical (experimental in wind tunnel) and mathematical (numerical) modeling. This alternative approach seems to be more effective than field experiments and observations, which are very time-consuming, labor-intensive, and financially expensive.

ACKNOWLEDGMENTS

This work was financially supported by the Ministry of Science and Higher Education of the Russian Federation (Project: Theoretical and experimental design of new composite materials to ensure safety during the operation of buildings and structures under conditions of technogenic and biogenic threats #FSWG-2020-0007)

REFERENCES

1. Building Code of RF 20.13330.2016 (with amendments No 1, 2, 3) Load and actions. Moscow: Ministry of Regional Development of Russia, 2021
2. Eurocode 1: Actions on structures – Part 1-3: General actions – Snow loads, CEN, 2003.
3. National Research Council of Canada. National building code of Canada 2015. – National Research Council Canada, 2015.
4. ASCE/SEI 7-16 Minimum Design Loads and Associated Criteria for Building and other Structures. USA: ASCE, 2017
5. ASCE. Wind tunnel testing for buildings and other structures. – American Society of Civil Engineers, 2012.
6. Methodical manual "Mathematical (numerical) modeling of wind loads and impacts" (to SP 20.13330.2016), M., FAU FTSS of the Ministry of Construction of Russia, 2020
7. **Belostotskiy A.M., Akimov P.A., Afanas'yeva I.N.** Vychislitel'naya aerodinamika v zadachakh stroitel'stva [Computational aerodynamics in construction problems]. Moscow: Publishing ASV, 2017, 720 p.
8. **Zhou X., Hu J., Gu M.** Wind tunnel test of snow loads on a stepped flat roof using different granular materials //Natural hazards. – 2014. – T. 74. – №. 3. – C. 1629-1648
9. **Zhou X.** et al. Wind tunnel test on responses of a lightweight roof structure under joint action of wind and snow loads //Cold Regions Science and Technology. – 2016. – T. 132. – C. 19-32.
10. **Kang, L., Zhou, X., Gu, M.,** 2016. A new method for predicting snowdrift on flat roofs. In: Proceedings of the 8th International Conference on Snow Engineering, Nantes, France, C. 137–141 (June 14–17).
11. **Zhou, X., Kang, L., Gu, M., Qiu, L., Hu, J.**, 2016a. Numerical simulation and wind tunnel test for redistribution of snow on a flat roof. J. Wind Eng. Ind. Aerodyn. T. 153, C. 92–105
12. **Sun X., He R., Wu Y.** Numerical simulation of snowdrift on a membrane roof and the mechanical performance under snow loads

//Cold Regions Science and Technology. – 2018. – T. 150. – C. 15-24
13. **Zhou X., Zhang Y., Gu M.** Coupling a snowmelt model with a snowdrift model for the study of snow distribution on roofs // Journal of Wind Engineering and Industrial Aerodynamics. – 2018. – T. 182. – C. 235-251
14. **Wang J.** et al. Modeling snowdrift on roofs using Immersed Boundary Method and wind tunnel test //Building and environment. – 2019. – T. 160. – C. 106208.
15. **Wang J.** et al. Wind tunnel test of wind-induced snowdrift on stepped flat roofs during snowfall //Natural Hazards. – 2020. – T. 104. – №. 1. – C. 731-752.
16. **Zhou X.** et al. RANS CFD simulations can be successfully used for simulating snowdrift on roofs in a long period of snowstorm //Building simulation. – Tsinghua University Press, 2020. – T. 13. – C. 1157-1163.
17. **Qiang S.** et al. A novel snow transport model for analytically investigating effects of wind exposure on flat roof snow load due to saltation //Journal of Wind Engineering and Industrial Aerodynamics. – 2021. – T. 210. – C. 104505
18. **Ma W., Li F., Zhou X.** An empirical model of snowdrift based on field measurements: Profiles of the snow particle size and mass flux //Cold Regions Science and Technology. – 2021. – C. 103312. Ma W. et al. Field measurement and numerical simulation of snow deposition on an embankment in snowdrift //Wind and Structures. – 2021. – T. 32. – №. 5. – C. 453-469.
19. **Zhang G.** et al. Numerical simulations of snowdrift characteristics on multi-span arch roofs //Journal of Wind Engineering and Industrial Aerodynamics. – 2021. – T. 212. – C. 104593.

СПИСОК ЛИТЕРАТУРЫ

1. СП 20.13330.2016 (с изменениями N 1, 2, 3) Нагрузки и воздействия. М.: Минрегион России, 2021
2. Eurocode 1: Actions on structures – Part 1-3: General actions – Snow loads, CEN, 2003.
3. National Research Council of Canada. National building code of Canada 2015. – National Research Council Canada, 2015.
4. ASCE/SEI 7-16 Minimum Design Loads and Associated Criteria for Building and other Structures. USA: ASCE, 2017
5. ASCE. Wind tunnel testing for buildings and other structures. – American Society of Civil Engineers, 2012.
6. Методическое пособие «Математическое (численное) моделирование ветровых нагрузок и воздействий» (к СП 20.13330.2016), М., ФАУ ФЦС Минстроя России, 2020
7. **Белостоцкий А.М., Акимов П.А., Афанасьева И.Н.** Вычислительная аэродинамика в задачах строительства. М., Издательство АСВ, 2017, 720 с.
8. **Zhou X., Hu J., Gu M.** Wind tunnel test of snow loads on a stepped flat roof using different granular materials //Natural hazards. – 2014. – T. 74. – №. 3. – C. 1629-1648
9. **Zhou X.** et al. Wind tunnel test on responses of a lightweight roof structure under joint action of wind and snow loads //Cold Regions Science and Technology. – 2016. – T. 132. – C. 19-32.
10. **Kang, L., Zhou, X., Gu, M.,** 2016. A new method for predicting snowdrift on flat roofs. In: Proceedings of the 8th International Conference on Snow Engineering, Nantes, France, C. 137–141 (June 14–17).
11. **Zhou, X., Kang, L., Gu, M., Qiu, L., Hu, J.**, 2016a. Numerical simulation and wind tunnel test for redistribution of snow on a flat roof. J. Wind Eng. Ind. Aerodyn. T. 153, C. 92–105
12. **Sun X., He R., Wu Y.** Numerical simulation of snowdrift on a membrane roof and the mechanical performance under snow loads //Cold Regions Science and Technology. – 2018. – T. 150. – C. 15-24
13. **Zhou X., Zhang Y., Gu M.** Coupling a snowmelt model with a snowdrift model for the study of snow distribution on roofs //

Journal of Wind Engineering and Industrial Aerodynamics. – 2018. – T. 182. – C. 235-251
14. **Wang J.** et al. Modeling snowdrift on roofs using Immersed Boundary Method and wind tunnel test //Building and environment. – 2019. – T. 160. – C. 106208.
15. **Wang J.** et al. Wind tunnel test of wind-induced snowdrift on stepped flat roofs during snowfall //Natural Hazards. – 2020. – T. 104. – №. 1. – C. 731-752.
16. **Zhou X.** et al. RANS CFD simulations can be successfully used for simulating snowdrift on roofs in a long period of snowstorm //Building simulation. – Tsinghua University Press, 2020. – T. 13. – C. 1157-1163.
17. **Qiang S.** et al. A novel snow transport model for analytically investigating effects of wind exposure on flat roof snow load due to saltation //Journal of Wind Engineering and Industrial Aerodynamics. – 2021. – T. 210. – C. 104505
18. **Ma W., Li F., Zhou X.** An empirical model of snowdrift based on field measurements: Profiles of the snow particle size and mass flux //Cold Regions Science and Technology. – 2021. – C. 103312. Ma W. et al. Field measurement and numerical simulation of snow deposition on an embankment in snowdrift //Wind and Structures. – 2021. – T. 32. – №. 5. – C. 453-469.
19. **Zhang G.** et al. Numerical simulations of snowdrift characteristics on multi-span arch roofs //Journal of Wind Engineering and Industrial Aerodynamics. – 2021. – T. 212. – C. 104593.

Alexander M. Belostotsky, corresponding member of RAACS, professor, doctor of technical sciences; General Director of CJSC Scientific Research Center StaDiO; Professor of the Department of Informatics and Applied Mathematics of the National Research Center, scientific director of the REC KM named after A.B. Zolotov Moscow State University of Civil Engineering; Professor of the Department of Building Structures, Buildings and Structures of the Russian University of Transport (MIIT); 125040, Russia, Moscow, st. 3rd Yamskogo Fields, 18, office 810; Tel. +7 (499) 706-88-10. E-mail: amb@stadyo.ru

Nikita A. Britikov, engineer of the REC KM them. A.B. Zolotov of the National Research Moscow State University of Civil Engineering; postgraduate student of the Russian University of Transport (MIIT); 129337, Russia, Moscow, Yaroslavskoe shosse, 26. E-mail: n.a.britikov@gmail.com

Oleg S. Goryachevsky, Lead Structurel Engineer, CJSC Research Center StaDiO; Deputy Director of REC KM named after A.B. Zolotov of the National Research Moscow State Construction University; 129337, Russia, Moscow, Yaroslavskoe shosse, 26. E-mail: osgoryachevskij@mail.ru

Белостоцкий Александр Михайлович, член-корреспондент РААСН, профессор, доктор технических наук; генеральный директор ЗАО Научно-исследовательский центр СтаДиО; профессор кафедры Информатики и прикладной математики Национального исследовательского, научный руководитель НОЦ КМ им. А.Б. Золотова Московского государственного строительного университета; профессор кафедры «Строительные конструкции, здания и сооружения» Российского университета транспорта (МИИТ); 125040, Россия, Москва, ул. 3-я Ямского Поля, д.18, офис 810; тел. +7 (499) 706-88-10 E-mail: amb@stadyo.ru

Бритиков Никита Александрович, инженер НОЦ КМ им. А.Б. Золотова Национального исследовательского Московского государственного строительного университета; аспирант Российского университета транспорта (МИИТ); 129337, Россия, г. Москва, Ярославское шоссе, д. 26. E-mail: n.a.britikov@gmail.com

Горячевский Олег Сергеевич, ведущий инженер-расчетчик ЗАО Научно-исследовательский центр СтаДиО; заместитель директора НОЦ КМ им. А.Б. Золотова Национального исследовательского Московского государственного строительного университета; 129337, Россия, г. Москва, Ярославское шоссе, д. 26. E-mail: osgoryachevskij@mail.ru

International Journal for Computational Civil and Structural Engineering, 17(3) 48–62 (2021)

DOI:10.22337/2587-9618-2021-17-3-48-62

FINITE ELEMENTS FOR THE ANALYSIS OF REISSNER-MINDLIN PLATES WITH JOINT INTERPOLATION OF DISPLACEMENTS AND ROTATIONS (JIDR)

Viktor S. Karpilovskyi

ScadGroup Ltd., Kyiv, UKRAINE

Abstract: This paper proposes a method for creating finite elements with simultaneous approximation of functions corresponding to displacements and rotations. New triangular and quadrangular finite elements have been created, which can have additional nodes on the sides. No locking effect is observed for all the created elements. All created elements retain the existing symmetry of the design models. The results of numerical experiments are presented.

Keywords: finite elements; Reissner–Mindlin; plate problem; triangular element; rectangular element; quadrangular element

КОНЕЧНЫЕ ЭЛЕМЕНТЫ ДЛЯ РАСЧЕТА ПЛАСТИН РЕЙССНЕРА–МИНДЛИНА С СОВМЕСТНОЙ ИНТЕРПОЛЯЦИЕЙ ПЕРЕМЕЩЕНИЙ И УГЛОВ ПОВОРОТА (JIDR)

В.С. Карпиловский

ООО ScadGroup, г. Киев, УКРАИНА

Аннотация: Предложен метод построения конечных элементов с одновременной аппроксимацией функций, соответствующих перемещениям и углам поворота. Построены новые треугольные и четырехугольные элементы конечные элементы, которые могут иметь дополнительные узлы на сторонах. Для всех построенных элементов отсутствует эффект запирания. Все построенные элементы сохраняют существующую симметрию расчетных схем. Приведены результаты численных экспериментов.

Ключевые слова: конечные элементы; Рейсснер-Миндлин; изгиб плит; треугольный элемент; прямоугольный элемент; четырехугольный элемент

1. INTRODUCTION

Write down the Lagrange functional for Reissner-Mindlin plates as follows [1-3]:

$$\Pi(\mathrm{u}) = \frac{1}{2}\int_{\Omega}(Au)^T DAu d\,\Omega - \int_{\Omega} f^{\mathrm{T}} u d\,\Omega \quad (1)$$

where: Ω – plate of thickness h: solid body with a midplane ***XOY***;

$u(x) = \{w(x), \theta_x(x), \theta_y(x)\}^T$ is the vertical displacement and rotations,

$\boldsymbol{x} = \begin{Bmatrix} x \\ y \end{Bmatrix}$, $f(\boldsymbol{x}) = \begin{Bmatrix} f_z(\boldsymbol{x}) \\ m_x(\boldsymbol{x}) \\ m_y(\boldsymbol{x}) \end{Bmatrix}$ is the area load.

The geometric operator $\boldsymbol{A}$ and the elasticity matrix $\boldsymbol{D}$ (for an isotropic material):

$$\boldsymbol{A} = \begin{bmatrix} \frac{\partial}{\partial x} & \frac{\partial}{\partial y} & 0 & 0 & 0 \\ 0 & -1 & 0 & -\frac{\partial}{\partial y} & -\frac{\partial}{\partial x} \\ 1 & 0 & \frac{\partial}{\partial x} & 0 & \frac{\partial}{\partial y} \end{bmatrix}^T, \quad (2)$$

$$D = \begin{bmatrix} \lambda & & & \\ & \lambda & & \\ & & 1 & \nu \\ & & \nu & 1 \\ & & & & 0.5(1-\nu) \end{bmatrix}, \quad \lambda = \frac{5(1-\nu)}{h^2}$$

E is the Young's modulus, ν is the Poisson's ratio.
Equations of equilibrium:

$$-\Delta w + \frac{\partial \theta_x}{\partial y} - \frac{\partial \theta_y}{\partial x} = \frac{q}{\lambda D}$$
$$\lambda(\theta_x - \frac{\partial w}{\partial y}) - \frac{\partial^2 \theta_x}{\partial y^2} - \frac{1-\nu}{2}\frac{\partial^2 \theta_x}{\partial x^2} + \frac{1+\nu}{2}\frac{\partial^2 \theta_y}{\partial x \partial y} = 0$$
$$\lambda(\frac{\partial w}{\partial x} + \theta_y) - \frac{\partial^2 \theta_y}{\partial x^2} - \frac{1-\nu}{2}\frac{\partial^2 \theta_y}{\partial y^2} + \frac{1+\nu}{2}\frac{\partial^2 \theta_x}{\partial x \partial y} = 0 \quad (3)$$

Classic finite elements have three degrees of freedom in each node: vertical displacement w_i and rotations θ_{xi}, θ_{yi}, i=1,2,…,N, where N is the number of element nodes. Finite elements have $3N$ unknowns, which are arranged in the following order during the generation of a stiffness matrix of the element:

$$\{w_1, \theta_{x1}, \theta_{y1}, ..., w_N, \theta_{xN}, \theta_{yN}\}, \quad (4)$$

which has a corresponding system of approximating functions

$$\{\varphi_{1,1}, \varphi_{1,2}, \varphi_{1,3}, \ldots, \varphi_{N,1}, \varphi_{N,2}, \varphi_{N,3}\} \quad (5)$$

We introduce a generalized displacement vector

$$\tilde{\boldsymbol{u}} = \left\{w, \theta_x, \theta_y, \gamma_{xz}, \gamma_{yz}\right\}^T \quad (6)$$

where :
γ_{xz}, γ_{yz} are shear characteristics depending on the displacement w and rotations θ_x, θ_y.
Then the functional (1) can be written as follows:

$$\Pi(\boldsymbol{u}) = \frac{1}{2}\int_\Omega \left(B\tilde{\boldsymbol{u}}\right)^T DB\tilde{\boldsymbol{u}} d\Omega - \int_\Omega \boldsymbol{f}^T \boldsymbol{u} d\Omega \quad (7)$$

$$\boldsymbol{B} = \begin{bmatrix} \frac{\partial}{\partial x} & 0 & 1 & 1 & 0 \\ \frac{\partial}{\partial y} & -1 & 0 & 0 & 1 \\ 0 & 0 & \frac{\partial}{\partial x} & 0 & 0 \\ 0 & -\frac{\partial}{\partial y} & 0 & 0 & 0 \\ 0 & -\frac{\partial}{\partial x} & \frac{\partial}{\partial y} & 0 & 0 \end{bmatrix} \quad (8)$$

Represent the approximating functions (5) of the element in a five-dimensional space for the generalized displacement vector (6):

$$\boldsymbol{\varphi}_{ij}^r(x,y) = \left\{\varphi_{ij}^1, \varphi_{ij}^2, \varphi_{ij}^3, \varphi_{ij}^4, \varphi_{ij}^5\right\}^T, i=1\div N, j=1,2,3 \quad (9)$$

where i is the node number, and j is the number of its degree of freedom.
Elements with:

- $\varphi_{i1}^1 = \varphi_{i2}^2 = \varphi_{i3}^3$ – the corresponding approximations of the elements of the plane problem of the theory of elasticity;
- $\varphi_{i1}^2 = \varphi_{i1}^3 = \varphi_{i2}^1 = \varphi_{i2}^3 = \varphi_{i3}^1 = \varphi_{i3}^2 = 0$, $i=1\div N$
- $\varphi_{ij}^4 = \varphi_{ij}^5 = 0$, $i=1\div N$, j=1,2,3,

as a rule, provide convergence of the method only for medium thickness plates. The so-called *locking effect* often occurs during the analysis of thin plates, when the calculation results differ significantly from the analytical ones.
The main reason for the locking effect is that it is impossible to set such values of the degrees of freedom of an element so as to ensure constant moments in its area for the corresponding tasks.
There are many methods for eliminating the locking mechanism. The most common elements use:

- *Mixed Interpolation of Tensorial Components, MITC* [2,4];
- *Discrete Shear Gap, DSG* [5];
- hybrid models based on Reissner's functional [6];

and others.

This paper proposes another method for creating finite elements for Reissner-Mindlin plates without the locking effect: *Joint Interpolation of Displacements and Rotations* (*JIDR*). In this method:

- φ_{i1}^1, φ_{i2}^2, φ_{i3}^3 – not necessarily corresponding approximations of the elements of the plane problem of the theory of elasticity. These can be, for example, approximations of finite elements for Kirchhoff-Love plates;
- $\varphi_{i2}^1 = \varphi_{i3}^1$ – nonzero functions depending on φ_{i2}^2, φ_{i3}^3;
- $\varphi_{i1}^2 = \varphi_{i1}^3 = \varphi_{i2}^3 = \varphi_{i3}^2 = 0$, $\varphi_{ij}^4 = \varphi_{ij}^5 = 0$, j=1,2,3
- in addition to approximating functions (5), *up to four* specially constructed functions are introduced corresponding to some internal degrees of freedom of the element:

$$\boldsymbol{\mu}_k = \left\{0, 0, 0, \mu_k^4, \mu_k^5\right\}^T, \; k \le 4 \qquad (10)$$

We will assume that the functions φ_{i1}^1, φ_{i2}^2, φ_{i3}^3 are compatible for the constructed ***JIDR*** elements. Incompatible functions are (10), which may have discontinuities on the element sides.

2. COMPLETENESS AND INCOMPATIBILITY CRITERIA

Consider the residual:

$$\zeta(\boldsymbol{x}) = \begin{Bmatrix} w \\ \theta_x \\ \theta_y \end{Bmatrix} - \boldsymbol{A}_1 \sum_{i=1}^{N} \left(w_i \boldsymbol{\varphi}_{i1} + \theta_{x,i} \boldsymbol{\varphi}_{i2} + \theta_{y,i} \boldsymbol{\varphi}_{i3} \right), \qquad (11)$$

where $\boldsymbol{A}_1$ is the matrix operator that transforms functions in a five-dimensional space into three-dimensional ones:

$$\boldsymbol{A}_1 = \begin{bmatrix} 1 & 0 & 0 & 0 & 0 \\ 0 & 1 & 0 & 0 & 0 \\ 0 & 0 & 1 & 0 & 0 \end{bmatrix}$$

It follows from the equilibrium quations (3) that:

$$\theta_x = \frac{\partial w}{\partial y} + \frac{1}{\lambda}\left(\frac{\partial^2 \theta_x}{\partial y^2} + \frac{1-\nu}{2}\frac{\partial^2 \theta_x}{\partial x^2} - \frac{1+\nu}{2}\frac{\partial^2 \theta_y}{\partial x \partial y} \right) =$$
$$\frac{\partial w}{\partial y} + \frac{1}{\lambda}\left(\frac{\partial^3 w}{\partial y^3} + \frac{1-\nu}{2}\frac{\partial^3 w}{\partial x^2 \partial y} - \frac{1+\nu}{2}\frac{\partial^3 w}{\partial x \partial y^2} \right) + \ldots$$
$$\theta_y = -\frac{\partial w}{\partial x} + \frac{1}{\lambda}\left(\frac{\partial^2 \theta_y}{\partial x^2} + \frac{1-\nu}{2}\frac{\partial^2 \theta_y}{\partial y^2} - \frac{1+\nu}{2}\frac{\partial^2 \theta_x}{\partial x \partial y} \right) =$$
$$-\frac{\partial w}{\partial x} - \frac{1}{\lambda}\left(\frac{\partial^3 w}{\partial x^3} + \frac{1-\nu}{2}\frac{\partial^3 w}{\partial x \partial y^2} - \frac{1+\nu}{2}\frac{\partial^3 w}{\partial x^2 \partial y} \right) + \ldots \qquad (12)$$

Substituting (12) into (11) and expanding the values of displacement w with respect to the origin, we obtain:

$$\zeta(\boldsymbol{x}) = \begin{Bmatrix} w\big|_{\boldsymbol{x}=0} + x w_x\big|_{\boldsymbol{x}=0} + y w_y\big|_{\boldsymbol{x}=0} + \frac{1}{2}x^2 w_{xx}\big|_{\boldsymbol{x}=0} + xy w_{xy}\big|_{\boldsymbol{x}=0} + \frac{1}{2}y^2 w_{yy}\big|_{\boldsymbol{x}=0} + \ldots \\ w_y\big|_{\boldsymbol{x}=0} + x w_{xy}\big|_{\boldsymbol{x}=0} + y w_{yy}\big|_{\boldsymbol{x}=0} + (\frac{1}{2}x^2 + \frac{1}{\lambda}) w_{xxy}\big|_{\boldsymbol{x}=0} + xy w_{xyy}\big|_{\boldsymbol{x}=0} + (\frac{1}{2}y^2 + \frac{1}{\lambda}) w_{yyy}\big|_{\boldsymbol{x}=0} + \ldots \\ -w_x\big|_{\boldsymbol{x}=0} - x w_{xx}\big|_{\boldsymbol{x}=0} - y w_{xy}\big|_{\boldsymbol{x}=0} - (\frac{1}{2}x^2 + \frac{1}{\lambda}) w_{xxx}\big|_{\boldsymbol{x}=0} - xy w_{xxy}\big|_{\boldsymbol{x}=0} - (\frac{1}{2}y^2 + \frac{1}{\lambda}) w_{xyy}\big|_{\boldsymbol{x}=0} + \ldots \end{Bmatrix} -$$
$$\sum_{i=1}^{N} \left(w + x_i w_x + y_i w_y + \frac{1}{2}x_i^2 w_{xx} + x_i y_i w_{xy} + \frac{1}{2}y_i^2 w_{yy} + \ldots \right)\Big|_{\boldsymbol{x}=0} \boldsymbol{A}_1 \boldsymbol{\varphi}_{i1} -$$
$$\sum_{i=1}^{N} \left(w_y + x_i w_{xy} + y_i w_{yy} + (\frac{1}{2}x_i^2 + \frac{1}{\lambda}) w_{xxy} + x_i y_i w_{xyy} + (\frac{1}{2}y_i^2 + \frac{1}{\lambda}) w_{yyy} \right)\Big|_{\boldsymbol{x}=0} \boldsymbol{A}_1 \boldsymbol{\varphi}_{i2} +$$
$$\sum_{i=1}^{N} \left(w_x + x_i w_{xx} + y_i w_{xy} + (\frac{1}{2}x_i^2 + \frac{1}{\lambda}) w_{xxx} + x_i y_i w_{xxy} + (\frac{1}{2}y_i^2 + \frac{1}{\lambda}) w_{yyy} \right)\Big|_{\boldsymbol{x}=0} \boldsymbol{A}_1 \boldsymbol{\varphi}_{i3} + \ldots \qquad (13)$$

Let us equate to zero the coefficients of the corresponding derivatives of w. We obtain the identities of the *completeness criterion* [7-8]:

- of order p=1:

$$\boldsymbol{A}_1\sum_{i=1}^{N}\boldsymbol{\varphi}_{i1}\equiv\begin{Bmatrix}1\\0\\0\end{Bmatrix},\quad \boldsymbol{A}_1\sum_{i=1}^{N}(x_i\boldsymbol{\varphi}_{i1}-\boldsymbol{\varphi}_{i3})\equiv\begin{Bmatrix}x\\0\\-1\end{Bmatrix},$$

$$\boldsymbol{A}_1\sum_{i=1}^{N}(y_i\boldsymbol{\varphi}_{i1}+\boldsymbol{\varphi}_{i2})\equiv\begin{Bmatrix}y\\1\\0\end{Bmatrix} \qquad (14)$$

- of order p=2:

$$\boldsymbol{A}_1\sum_{i=1}^{N}(\frac{x_i^2}{2}\boldsymbol{\varphi}_{i1}-x_i\boldsymbol{\varphi}_{i3})\equiv\left\{\frac{x^2}{2},0,-x\right\}^T,$$

$$\boldsymbol{A}_1\sum_{i=1}^{N}(\frac{y_i^2}{2}\boldsymbol{\varphi}_{i1}+y_i\boldsymbol{\varphi}_{i2})\equiv\left\{\frac{y^2}{2},y,0\right\}^T$$

$$\boldsymbol{A}_1\sum_{i=1}^{N}(x_iy_i\boldsymbol{\varphi}_{i1}+x_i\boldsymbol{\varphi}_{i2}-y_i\boldsymbol{\varphi}_{i3})\equiv\{xy,x,-y\}^T \qquad (15)$$

- of order p=3:

$$\boldsymbol{A}_1\sum_{i=1}^{N}\left(\frac{x_i^3}{6}\boldsymbol{\varphi}_{i1}-(\frac{x_i^2}{2}+\frac{1}{\lambda})\boldsymbol{\varphi}_{i3}\right)\equiv\left\{\frac{x^3}{6},0,-\frac{x^2}{2}-\frac{1}{\lambda}\right\}^T,$$

$$\boldsymbol{A}_1\sum_{i=1}^{N}\left(\frac{x_i^2y_i}{2}\boldsymbol{\varphi}_{i1}+(\frac{x_i^2}{2}+\frac{1}{\lambda})\boldsymbol{\varphi}_{i2}-x_iy_i\boldsymbol{\varphi}_{i3}\right)\equiv$$

$$\left\{\frac{x^2y}{2},\frac{x^2}{2}+\frac{1}{\lambda},-xy\right\}^T$$

$$\boldsymbol{A}_1\sum_{i=1}^{N}\left(\frac{x_iy_i^2}{2}\boldsymbol{\varphi}_{i1}+x_iy_i\boldsymbol{\varphi}_{i2}-(\frac{y_i^2}{2}+\frac{1}{\lambda})\boldsymbol{\varphi}_{i3}\right)\equiv$$

$$\left\{\frac{1}{2}xy^2,xy,-\frac{1}{2}y^2-\frac{1}{\lambda}\right\}^T$$

$$\boldsymbol{A}_1\sum_{i=1}^{N}\left(\frac{y_i^3}{6}\boldsymbol{\varphi}_{i1}+(\frac{y_i^2}{2}+\frac{1}{\lambda})\boldsymbol{\varphi}_{i2}\right)\equiv\left\{\frac{y^3}{6},\frac{y^2}{2}+\frac{1}{\lambda},0\right\}^T \qquad (16)$$

It should be noted that the identities of the completeness criterion (14) and (15) coincide with the corresponding identities of the Kirchhoff-Love thin plate elements. See [7,8,10]. Identities of order p=3 coincide as well if

$$\sum_{i=1}^{N}\varphi_{ij}^{j}=1,\ j=2,3 \qquad (17)$$

The completeness criterion identities of order p=1 are the equations of the rigid body motion of a finite element.

Failure to satisfy the completeness criterion identities of order p = 2, as a rule, leads to the so-called locking effect, when the method does not converge to an analytical solution during the analysis of thin plates.

If the completeness criterion identities of order p=2 are not satisfied, then it is impossible to implement the constant moment tests, and for p=3 – the constant shear tests.

For all the created elements, incompatibility is allowed only for functions (10). Since when constructing the stiffness matrix of a finite element the functional includes the following expressions:

$$\mu_k^4\left(\frac{\partial}{\partial y}\varphi_{ij}^1-\varphi_{ij}^2\right),\quad \mu_k^5\left(\frac{\partial}{\partial x}\varphi_{ij}^1+\varphi_{ij}^3\right), \qquad (18)$$

then *the incompatibility criterion* [7-9] of the minimum order that provides piecewise testing [11] is reduced for this problem to the following equalities:

$$\int_{\Omega_\kappa}\mu_k^j d\Omega=0,\ \mathrm{k}\le 4. \qquad (19)$$

Due to the fact that functions (10) correspond to internal degrees of freedom, they can only increase the order of fulfillment of the completeness criterion identities of the system of functions (5).

According to [7-9], if the completeness criterion identities (14), (15) and the incompatibility criterion equalities (19) are satisfied, the convergence of the method will be ensured.

3. CONSTRUCTION OF APPROXIMATING FUNCTIONS

We will assume that in (9)

$$\varphi_{i1}^1=\varphi_{i2}^2=\varphi_{i3}^3=\chi_i\ ,i=1\div N \qquad (20)$$

where χ_i are classic approximations of the elements of the plane problem of the theory of elasticity, for which the completeness criterion identities of order p=1 are satisfied:

$$\sum_{i=1}^{N}\chi_i \equiv 1,\ \ \sum_{i=1}^{N}x_i\chi_i \equiv x,\ \ \sum_{i=1}^{N}y_i\chi_i \equiv y \qquad (21)$$

Transform the coordinate system for isoparametric elements:

$$x=\sum_{i=1}^{N}x_i\chi_i,\quad y=\sum_{i=1}^{N}y_i\chi_i\,, \qquad (22)$$

Hence, (21) is satisfied as well.
Suppose that the last identity (15) is satisfied. Then, according to (21):

$$\sum_{i=1}^{N}\left(x_iy_i\chi_i+x_i\varphi_{i2}^1-y_i\varphi_{i3}^1\right)\equiv\sum_{i,j=1}^{N}x_iy_j\chi_i\chi_j \qquad (23)$$

Let us set, keeping symmetry:

$$\varphi_{i2}^1=\frac{1}{2}\chi_i\left(y-y_i\right),\ \ \varphi_{i3}^1=-\frac{1}{2}\chi_i\left(x-x_i\right) \qquad (24)$$

Check that all identities (14) and (15) are satisfied for (24), since:

$$\sum_{i=1}^{N}\varphi_{i2}^1=\frac{1}{2}\sum_{i\in\Omega_r}\chi_i\left(y-y_i\right)=0,$$
$$\sum_{i=1}^{N}\varphi_{i3}^1=-\frac{1}{2}\sum_{i\in\Omega_r}\chi_i\left(x-x_i\right)=0 \qquad (25)$$

The fulfillment of (24) ensures the convergence of the method without the locking effect, which is confirmed by the numerical experiments.
Functions (10) are designed to improve the accuracy of elements. To construct them, we use the residuals of the completeness criterion (16) of order p=3:

$$\boldsymbol{\zeta}_1=\left\{\frac{x^3}{6},0,-\frac{x^2}{2}-\frac{1}{\lambda}\right\}^T-\sum_{i=1}^{N}\boldsymbol{A}_1\left(\frac{x_i^3}{6}\boldsymbol{\varphi}_{i1}-(\frac{x_i^2}{2}+\frac{1}{\lambda})\boldsymbol{\varphi}_{i3}\right),$$
$$\boldsymbol{\zeta}_2=\left\{\frac{x^2y}{2},\frac{x^2}{2}+\frac{1}{\lambda},-xy\right\}^T-\sum_{i=1}^{N}\boldsymbol{A}_1\left(\frac{x_i^2y_i}{2}\boldsymbol{\varphi}_{i1}+(\frac{x_i^2}{2}+\frac{1}{\lambda})\boldsymbol{\varphi}_{i2}-x_iy_i\boldsymbol{\varphi}_{i3}\right)$$
$$\boldsymbol{\zeta}_3=\left\{\frac{xy^2}{2},xy,-\frac{y^2}{2}-\frac{1}{\lambda}\right\}^T-\sum_{i=1}^{N}\boldsymbol{A}_1\left(\frac{x_iy_i^2}{2}\boldsymbol{\varphi}_{i1}+x_iy_i\boldsymbol{\varphi}_{i2}-(\frac{y_i^2}{2}+\frac{1}{\lambda})\boldsymbol{\varphi}_{i3}\right)$$
$$\boldsymbol{\zeta}_4=\left\{\frac{y^3}{6},\frac{y^2}{2}+\frac{1}{\lambda},0\right\}^T-\sum_{i=1}^{N}\boldsymbol{A}_1\left(\frac{y_i^3}{6}\boldsymbol{\varphi}_{i1}+(\frac{y_i^2}{2}+\frac{1}{\lambda})\boldsymbol{\varphi}_{i2}\right) \qquad (26)$$

Form the vectors from the residuals (26):

$$\boldsymbol{\omega}_k=\begin{Bmatrix}\frac{\partial}{\partial x}\zeta_k^1+\zeta_k^3\\ \frac{\partial}{\partial y}\zeta_k^1-\zeta_k^2\end{Bmatrix},\ k=1,2,3,4 \qquad (27)$$

Specify the components of functions (10) as follows:

$$\mu_k^4=\omega_k^1+a_k,\quad \mu_k^5=\omega_k^2+b_k\ ,\ k=1,2,3,4 \qquad (28)$$

The constants a_k, b_k in (28) are found from the incompatibility criterion equations (19).
Nonzero functions (28) usually have discontinuities on the element sides.
Analyze the constructed system of functions and supplement the system of approximating functions (5) with *nonzero and linearly independent* functions (10), correlating them with some internal degrees of freedom.
Instead of introducing the internal degrees of freedom, we can "scatter" functions (28) over

the approximations of the element, specifying in (9)

$$\varphi_{ij}^{m} = \sum_{k} c_{ij}^{k} \mu_{k}^{m} \,,\ i=1\div N,\ j=1,2,3,\ \ m=4,5, \quad (29)$$

where c_{ij}^{k} are coefficients which are determined by solving systems of equations based on the completeness criterion identities.

Let high-precision elements be used, for which the completeness criterion identities of order p=2 are satisfied for the approximations χ_i:

$$\sum_{i=1}^{N} x_i^2 \chi_i \equiv x^2,\ \sum_{i=1}^{N} x_i y_i \chi_i \equiv xy,\ \sum_{i=1}^{N} y_i^2 \chi_i \equiv y^2 \quad (30)$$

Then, using the first and last identities (16) and keeping symmetry, we assume:

$$\varphi_{i2}^{1} = \frac{1}{3}\chi_i\left(y-y_i\right),\ \ \varphi_{i3}^{1} = -\frac{1}{3}\chi_i\left(x-x_i\right) \quad (31)$$

It follows from (31) and (30) that:

$$\sum_{i=1}^{N} x_i\varphi_{i2}^{1} = \sum_{i=1}^{N} y_i\varphi_{i2}^{1} = \sum_{i=1}^{N} x_i\varphi_{i3}^{1} = \sum_{i=1}^{N} y_i\varphi_{i3}^{1} = 0 \quad (32)$$

Hence, identities (15) are satisfied.

All identities (16) of the completeness criterion of the 3rd order are satisfied as well:

$$\begin{aligned}
&\sum_{i=1}^{N}\left(\frac{1}{6}x_i^3\varphi_{i1}^{1} - (\frac{1}{2}x_i^2 + \frac{1}{\lambda})\varphi_{i3}^{1}\right) = \frac{1}{6}x^3\\
&\sum_{i=1}^{N}\left(\frac{1}{2}x_i^2 y_i\varphi_{i1}^{1} + (\frac{1}{2}x_i^2 + \frac{1}{\lambda})\varphi_{i2}^{1} - x_i y_i\varphi_{i3}^{1}\right) = \frac{1}{2}x^2 y\\
&\sum_{i=1}^{N}\left(\frac{1}{2}x_i y_i^2\varphi_{i1}^{1} + x_i y_i\varphi_{i2}^{1} - (\frac{1}{2}y_i^2 + \frac{1}{\lambda})\varphi_{i3}^{1}\right) = \frac{1}{2}xy^2\\
&\sum_{i=1}^{N}\left(\frac{1}{6}y_i^3\varphi_{i1}^{1} + (\frac{1}{2}y_i^2 + \frac{1}{\lambda})\varphi_{i2}^{1}\right) = \frac{y^3}{6}
\end{aligned} \quad (33)$$

To construct approximations (5) and (10), we can use the *approximating functions of Kirchhoff-Love thin plate finite elements*.

Let in (9):

$$\begin{aligned}
&\varphi_{ij}^{1} = \psi_{ij},\ \ \varphi_{ij}^{2} = \varphi_{ij}^{3} = \chi_i,\\
&\varphi_{i1}^{2} = \varphi_{i1}^{3} = \varphi_{i2}^{3} = \varphi_{i3}^{2} = \varphi_{ij}^{4} = \varphi_{ij}^{5} = 0,
\end{aligned} \quad (34)$$

i=1÷N, j=1,2,3,

where ψ_{ij} is the system of approximating functions of a Kirchhoff-Love thin plate element corresponding to the degrees of freedom (4). They usually satisfy the second-order, if not third-order completeness criterion identities. In order to ensure consistency they only have to belong to the Sobolev space W_2^1, and not W_2^2;

χ_i is the system of approximating functions of the element of the plane problem of the theory of elasticity.

We construct functions (27) based on residuals (26). Next we calculate the constants in (28) from the equations (19). Then we analyze the constructed system of functions (10) and supplement the system of approximating functions (5) with *nonzero and linearly independent* functions, correlating them with some internal degrees of freedom.

It would be a mistake to define the functions corresponding to the rotations through the derivatives ψ_{ij}:

$$\varphi_{i2}^{j} = \frac{\partial}{\partial y}\psi_{ij},\ \ \varphi_{i3}^{j} = -\frac{\partial}{\partial x}\psi_{ij}\ \ i=1\div N,\ j=1,2,3 \quad (35)$$

The relationship between the approximations of the rotation functions and vertical displacements leads to a significant narrowing of the required space for solving the variational problem. Thus, for example, in the case of analysis of a simply supported plate, we obtain *zero shear forces* with good convergence in displacements and moments.

4. FINITE ELEMENTS

4.1. Three-Node Element (JIDR3)

Let us consider a triangle in the local coordinate system shown in Fig. 1a. After changing the coordinates (36), it is transformed into a right triangle with unit legs shown in Fig. 1b.

$$\xi = \frac{1}{a}\left(x - \frac{b}{c}y\right), \quad \eta = \frac{1}{c}y \tag{36}$$

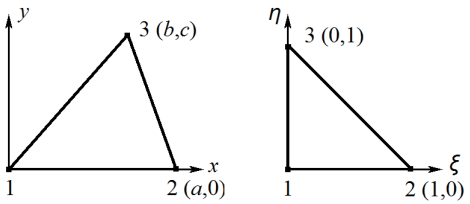

a) b)

Figure 1. Triangle and its master-element

Assume that the functions χ_i in (20) are linear approximations:

$$\chi_1 = 1 - \xi - \eta, \quad \chi_2 = \xi, \quad \chi_3 = \eta, \; i = 1,2,3 \tag{37}$$

Since (21) is satisfied, then using (24):

$$\begin{aligned}
&\varphi^1_{i1} = \varphi^2_{i2} = \varphi^3_{i3} = \chi_i, \quad i = 1,2,3 \\
&\varphi^1_{12} = \frac{c}{2}\eta\chi_1, \qquad \varphi^1_{13} = -\frac{1}{2}(a\xi + b\eta)\chi_1, \\
&\varphi^1_{22} = \frac{c}{2}\xi\eta, \qquad \varphi^1_{23} = -\frac{1}{2}\xi(a\xi + b\eta - a), \\
&\varphi^1_{32} = \frac{c}{2}\eta(\eta - 1), \quad \varphi_{33} = -\frac{1}{2}\eta(a\xi + b\eta - b)
\end{aligned} \tag{38}$$

Construct residuals (26):

$$\boldsymbol{\zeta}_1 = \begin{Bmatrix} \frac{x^3}{6} - \frac{a^3}{6}\xi - \frac{b^3}{6}\eta - \frac{a^2}{4}\xi(x-a) - \frac{b^2}{4}\eta(x-b) \\ 0 \\ -\frac{x^2}{2} + \frac{a^2}{2}\xi + \frac{b^2}{2}\eta \end{Bmatrix}$$

$$\boldsymbol{\zeta}_2 = \begin{Bmatrix} \frac{x^2 y}{2} - \frac{b^2 c}{2}\eta - \frac{a^2}{4}\xi y - \frac{b^2}{4}\eta(y-c) - \frac{bc}{2}\eta(x-b) \\ \frac{x^2}{2} - \frac{a^2}{2}\xi - \frac{b^2}{2}\eta \\ -xy + bc\eta \end{Bmatrix}$$

$$\boldsymbol{\zeta}_3 = \begin{Bmatrix} \frac{xy^2}{2} - \frac{bc^2}{2}\eta - \frac{bc}{2}\eta(y-c) - \frac{c^2}{4}\eta(x-b) \\ xy - bc\eta \\ -\frac{y^2}{2} + \frac{c^2}{2}\eta \end{Bmatrix}$$

$$\boldsymbol{\zeta}_4 = \begin{Bmatrix} \frac{y^3}{6} - \frac{c^3}{6}\eta - \frac{c^2}{4}\eta(y-c) \\ \frac{y^2}{2} - \frac{c^2}{2}\eta \\ 0 \end{Bmatrix} \tag{39}$$

Calculate vectors (27) according to (39):

$$\boldsymbol{\omega}_1 = \frac{1}{12c}\begin{Bmatrix} a^2 c + 3(b-a)by \\ (a-b)(-a^2 + 3bx) \end{Bmatrix}, \quad \boldsymbol{\omega}_2 = \frac{2b-a}{4}\begin{Bmatrix} y \\ -x \end{Bmatrix}$$

$$\boldsymbol{\omega}_3 = \frac{c}{4}\begin{Bmatrix} y \\ -x + b \end{Bmatrix}, \qquad \boldsymbol{\omega}_4 = \frac{c^2}{12}\begin{Bmatrix} 0 \\ -1 \end{Bmatrix} \tag{40}$$

Substituting (40) into (28), we find the values of the constants a_k, b_k from the incompatibility criterion equations (19). Discarding the zero function from the linear independence condition, we obtain only one function (10):

$$\boldsymbol{\mu}_1 = \{0, 0, 0, c(3\eta - 1), a + b - 3(a\xi + b\eta)\}^T, \tag{41}$$

corresponding to the internal degree of freedom.

4.2. Four-Node Isoparametric Element (JIDR4)

Let us consider a convex quadrangular finite element in the local coordinate system shown in Fig. 2a. After an isoparametric transformation of the coordinate system (42), it is transformed into a unit square shown in Fig. 2b.

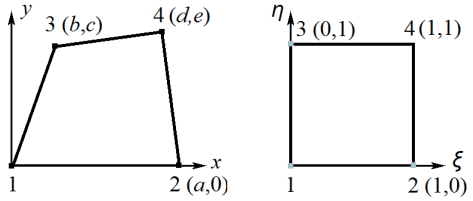

a) b)

Figure 2. Quadrangle and its master-element

$$\begin{aligned}
x &= a\xi(1-\eta) + b(1-\xi)\eta + d\xi\eta, \\
y &= c(1-\xi)\eta + e\xi\eta
\end{aligned} \tag{42}$$

Assume that the functions χ_i in (20) are multilinear approximations:

$$\chi_1=(1-\xi)(1-\eta),\ \ \chi_2=\xi(1-\eta),\\ \chi_3=(1-\xi)\eta,\qquad \chi_4=\xi\eta \tag{43}$$

They were also used for the isoparametric transformation (42).
Since (21) is satisfied, then using (24):

$$\varphi^1_{i1}=\varphi^2_{i2}=\varphi^3_{i3}=\chi_i,\ \ i=1,2,3,4\\ \varphi^1_{12}=\frac{1}{2}y\chi_1,\qquad \varphi^1_{13}=-\frac{1}{2}x\chi_1,\\ \varphi^1_{22}=\frac{1}{2}y\chi_2,\qquad \varphi^1_{23}=-\frac{1}{2}(x-a)\chi_2,\\ \varphi^1_{32}=\frac{1}{2}(y-c)\chi_3,\quad \varphi^1_{33}=-\frac{1}{2}(x-b)\chi_3,\\ \varphi^1_{42}=\frac{1}{2}(y-e)\chi_4,\quad \varphi^1_{43}=-\frac{1}{2}(x-d)\chi_4, \tag{44}$$

Construct residuals (26). To obtain functions (10), we substitute (26) into (27) and find the values of the constants a_k, b_k in (28) from the incompatibility criterion equations (19). There are only two functions left for the rectangle:

$$\boldsymbol{\mu}_1=\{0,0,0,0,\xi(1-\xi)\}^T\\ \boldsymbol{\mu}_2=\{0,0,0,\eta(1-\eta),0\}^T \tag{45}$$

4.3. Six-Node Isoparametric Element (JIDR6)

Let us consider the triangle shown in Fig. 3.

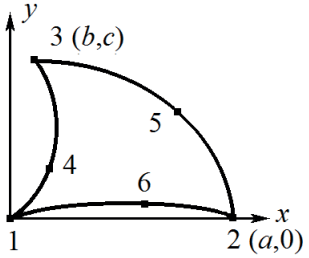

Figure 3. Isoparametric six-node element

Use the functions defined on the master-element in Fig. 1b:

$$\chi_1=(1-\xi-\eta)(1-2\xi-2\eta);\ \chi_2=\xi(2\xi-1);\\ \chi_3=\eta(2\eta-1);\qquad \chi_4=4\eta(1-\xi-\eta);\\ \chi_5=4\xi(1-\xi-\eta);\qquad \chi_6=4\xi\eta. \tag{46}$$

After transforming the coordinate system (22), the element is transformed into a right triangle with unit legs, shown in Fig. 1b.
Use formulas (24) to specify φ^1_{i2}, φ^1_{i3} and construct the residuals (26). To obtain functions (10), we substitute (26) into (27) and find the values of the constants a_k, b_k in (28) from the incompatibility criterion equations (19).
If intermediate nodes are located at the midpoints of the sides of the element, then the Jacobian of the transformation (22) is a linear function. Since functions (46) satisfy the completeness criterion identities of the second order (30), formulas (31) can be used to specify φ^1_{i2}, φ^1_{i3}. All the completeness criterion identities of the third order (16) will be satisfied, and all the residuals (26) will be equal to zero.

4.4. Eight-Node Isoparametric Element (JIDR8)

Let us consider the quadrangle shown in Fig. 4.

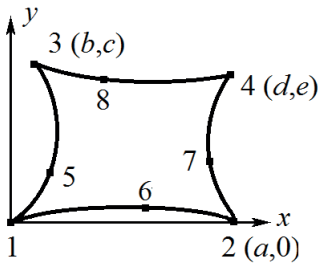

Figure 4. Isoparametric eight-node element

Use the approximations defined on the master-element in Fig. 2b:

$$\chi_1=(1-\xi)(1-\eta)(1-2\xi-2\eta);\\ \chi_2=\xi(1-\eta)(2\xi-2\eta-1);\\ \chi_3=(1-\xi)\eta(2\eta-2\xi-1);\\ \chi_4=\xi\eta(2\eta+2\xi-3);\\ \chi_5=4(1-\xi)\eta(1-\eta);\quad \chi_6=4\xi(1-\xi)(1-\eta);\\ \chi_7=4\xi\eta(1-\eta);\qquad \chi_8=4\xi(1-\xi)\eta. \tag{47}$$

After transforming the coordinate system (22), the element is transformed into the master-element in Fig. 2b.

Use formulas (24) to specify φ_{i2}^1, φ_{i3}^1 and construct the residuals (26). To obtain functions (10), we substitute (26) into (27) and find the values of the constants a_k, b_k in (28) from the incompatibility criterion equations (19).

Suppose that the Jacobian of the transformation (22) is a linear function (rectangle with the nodes at the midpoints of the sides of the element). Since functions (47) satisfy the completeness criterion identities of the second order (30), formulas (31) can be used to specify φ_{i2}^1, φ_{i3}^1. All the completeness criterion identities of the third order (16) will be satisfied, and all the residuals (26) will be equal to zero.

4.5. Four-Node Element with a Piecewise Polynomial Approximation (JIDR4SubAreas)

Let us consider a quadrangular finite element in the local coordinate system shown in Fig. 2a. It is transformed into a quadrangle shown in Fig. 5 by transforming the coordinate system (48). ***A*** is the intersection point of the diagonals of the element.

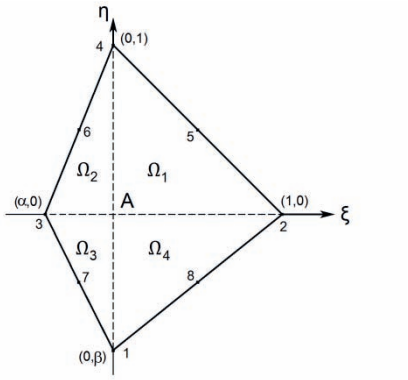

Figure 5. Four-node element in a special coordinate system

$$\begin{cases} x = x_A + (a - x_A)\xi + (d - x_A)\eta \\ y = y_A(1-\xi) + (e - y_A)\eta \end{cases} \tag{48}$$

Consider the functions from [12], which are second degree polynomials in each subdomain Ω_i, i=1,2,3,4 and are *continuous together with their first derivatives* on the diagonals of the element:

$$\chi_i,\ i=1,2,3,4 \tag{49}$$

Use formulas (24) to specify φ_{i2}^1, φ_{i3}^1 and construct the residuals (26). To obtain functions (10), we substitute (26) into (27) and find the values of the constants a_k, b_k in (28) from the incompatibility criterion equations (19).

4.6. Eight-Node Element with a Piecewise Polynomial Approximation (JIDR8SubAreas)

Let us consider a quadrangular finite element in the local coordinate system shown in Fig. 2a. It is transformed into a quadrangle shown in Fig. 5 by transforming the coordinate system (46).

Consider the functions from [12], which are second degree polynomials in each subdomain Ω_i, i=1,2,3,4 and are *continuous together with their first derivatives* on the diagonals of the element:

$$\chi_i,\ i=1\div 8 \tag{50}$$

Since functions (50) satisfy the completeness criterion identities of the second order (30), formulas (31) can be used to specify φ_{i2}^1, φ_{i3}^1. All the completeness criterion identities of the third order (16) will be satisfied, and all the residuals (26) will be equal to zero.

5. TESTS

All calculations were performed in SCAD, which is a part of SCAD Office®.

5.1. Patch Tests

A rectangular plate is shown in Fig. 6. The plate sizes are proportional to those in the Patch Tests considered in [13].

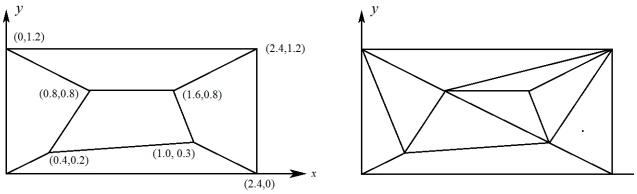

Figure 6. Rectangular plate

Two groups of kinematic loadings with known theoretical values were considered.

The first three load cases are a check of the displacement of a rectangle as a rigid body when moments and shear forces over the entire area of the plate are zero:

- displacement along the OZ axis: $w|_\Gamma=1$, $\theta_x|_\Gamma, \theta_y|_\Gamma=0$;
- rotation about the OX axis: $w|_\Gamma=y$, $\theta_x|_\Gamma=1, \theta_y|_\Gamma=0$;
- rotation about the OY axis: $w|_\Gamma=y$, $\theta_y|_\Gamma=-1, \theta_x|_\Gamma=0$.

The following three load cases provide non-zero constant moments and zero shear forces over the entire area of the plate:

- $w|_\Gamma=x^2$, $\theta_x|_\Gamma=0$, $\theta_y|_\Gamma=-2x$;
- $w|_\Gamma=y^2$, $\theta_x|_\Gamma=2y$, $\theta_y|_\Gamma=0$;
- $w|_\Gamma=xy$, $\theta_x|_\Gamma=x$, $\theta_y|_\Gamma=-y$.

Patch tests are performed in order to check whether the completeness criterion identities (15) are satisfied for all the considered elements:

- stiffness matrices of all the considered finite elements have three eigenvectors corresponding to their *displacement as rigid bodies*;
- the results for plates subjected to constant moments were obtained with an accuracy up to a computational error.

These tests serve only as a criterion for the correctness of the program code.

5.2. Rectangular Plate Simply Supported along the Perimeter Subjected to the Transverse Uniformly Distributed Load

Let us consider a rectangular plate simply supported along the perimeter subjected to the transverse uniformly distributed load shown in Fig. 6. Specify:

$$E = 30000\ kPa,\ \nu = 0.3,\ h = 0.2\ m,$$
$$a = 2.4\ m,\ b = 4.8\ m,\ p = 1.0\ kPa.$$

Specify the boundary conditions:

$$w\big|_\Gamma = 0,\ \theta_x(0,y) = \theta_x(a,y) = \theta_y(x,0) = \theta_y(x,b) = 0$$

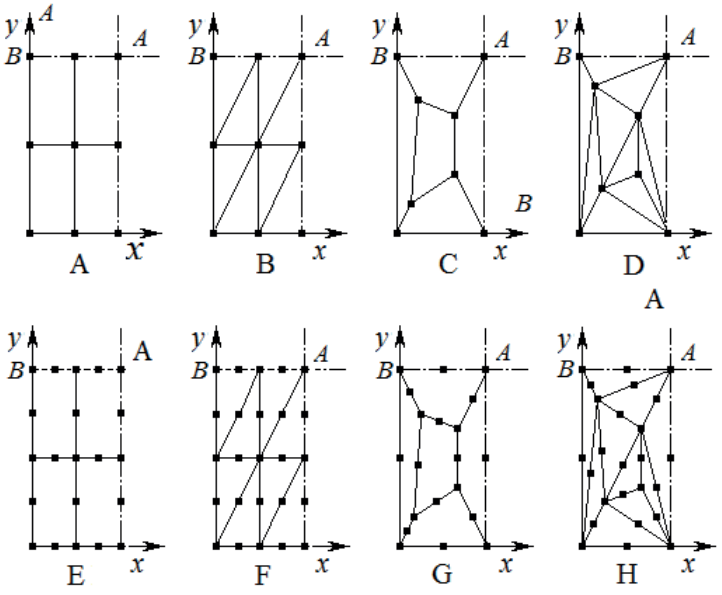

Figure 7. Design models of a rectangular plate

To study the locking effect, the plate thickness varied from h=0.001*m*=*a*/2400 to h=1.2=*a*/2. Experiment design models taking into account the symmetry axes are shown in Fig. 7. Table 1 presents the calculation results for a thin plate when h=0.08*m*=*a*/30. Analytical solution of this problem in the center of the plate (point *A*) and in the middle of the larger side (point *B*) (Analytical solution according to the spatial theory: $w|_A$ = 0.239663*m*; according to the Kirchhoff-Love theory: $w|_A$ = 0.238907 *m*, the values of the moments and shear forces coincide):

$w|_A = 0.239759m$,
$M_x|_A, = 0.585695(kNm/m)$,
$M_y|_A = 0.266978(kNm/\text{m})$,
$Q_x|_B,= 1.11602(kN/m)$

Table 1. Displacements, moments and shear forces in the plate

Mesh type	Element	Displacement w_A (*m*)				Moment $M_{x,A}$ (*kNm/m*)				Shear force $Q_{xz,B}$ (*kN/m*)			
		Mesh				Mesh				Mesh			
		2x2	4x4	8x8	16x16	2x2	4x4	8x8	16x16	2x2	4x4	8x8	16x16
A	*MTC4*	-0.2363	-0.2384	-0.9394	0.9394	0.454	0.5809	0.5845	0.5854	0.8226	0.9676	1.0415	1.0787
	JIDR4	-0.2302	-0.2382	-0.2393	-0.2396	0.585	0.5847	0.5852	0.5856	1.1523	0.9224	1.0376	1.0782
	JIDR4SA	-0.2379	-0.2397	-0.2397	-0.2397	0.6001	0.5616	0.5871	0.586	2.2426	1.3454	1.0611	1.0678
B	*DSG3*	-0.0879	-0.2171	-0.2367	-0.2393	0.2172	0.5315	0.5765	0.5838	1.2419	1.0958	1.0861	1.1369
	JIDR3	-0.1838	-0.2311	-0.2377	-0.2393	0.4276	0.5581	0.5788	0.5841	0.9327	1.0717	1.108	1.1274
C	*MTC4*	-0.2335	-0.2385	-0.2389	-0.2395	0.454	0.5872	0.5852	0.5867	0.7938	0.9263	0.9666	1.0028
	JIDR4	-0.2097	-0.237	-0.2388	-0.2395	0.4737	0.5695	0.5819	0.5854	1.1062	1.1911	0.9985	1.0187
	JIDR4SA	-0.2118	-0.2374	-0.2395	-0.2397	0.4604	0.574	0.5864	0.5862	1.0494	1.9069	1.2488	1.0785
D	*DSG3*	-0.1627	-0.222	-0.2375	-0.2393	0.3379	0.5152	0.5815	0.5861	0.8049	0.9572	1.1442	1.2105
	JIDR3	-0.1941	-0.2317	-0.2379	-0.2393	0.4239	0.5473	0.5802	0.5854	1.5143	0.8798	0.8864	0.9576
E	*JIDR4*	-0.24	-0.2398	-0.2398	-0.2398	0.6077	0.5907	0.5869	0.586	0.8362	0.9553	1.0397	1.0783
	JIDR4SA	-0.2398	-0.2398	-0.2398	-0.2398	0.617	0.5938	0.5878	0.5862	0.8685	0.966	1.0403	1.0784
F	*JIDR6*	-0.2414	-0.2399	-0.2398	-0.2398	0.659	0.6019	0.5894	0.5866	0.8142	1.0022	1.0659	1.0912
	JIDR4	-0.2417	-0.2396	-0.2397	-0.2398	0.6671	0.5985	0.5874	0.5861	0.5796	0.8685	1.0046	1.0616
	JIDR4SA	-0.2425	-0.2398	-0.2398	-0.2398	0.682	0.6056	0.5905	0.587	0.7586	0.9254	1.0077	1.0611
H	*JIDR6*	-0.2424	-0.2398	-0.2398	-0.2398	0.6849	0.604	0.5902	0.587	0.8495	0.9604	1.0436	1.082

5.3. Stress-Strain State of a Clamped Hexagonal Plate Subjected to the Uniformly Distributed Load

Let us consider a regular hexagonal plate clamped along the perimeter subjected to the transverse uniformly distributed load shown in Fig. 8.

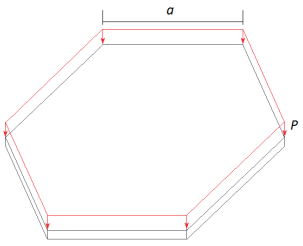

Figure 8. Hexagonal plate

Specify:

$$E = 30000\ kPa,\ \nu = 0.3,\ h = 0.1m,$$
$$a = 1m,\ p = 10\ kPa.$$

and boundary conditions:

$$w\big|_\Gamma = \theta_n\big|_\Gamma = \theta_\tau\big|_\Gamma = 0\,.$$

A numerical solution of this problem was obtained according to the Reissner-Mindlin theory at the center of the plate at point A with a high degree of accuracy:

$$w_A = -38.749(mm),\ M_x|_A = 0.6511(kNm/m).$$

The solutions were obtained for various types of finite elements. The maximum order of the system of equations for which the solution is obtained is 2747925.

The solution of this problem according to thin plate theory is given in [14] and is:

$$w_A = -36.324(mm),\ M_x = 0.64786(kNm/m).$$

The calculation results for the design models in Fig. 9 are given in Table 2.

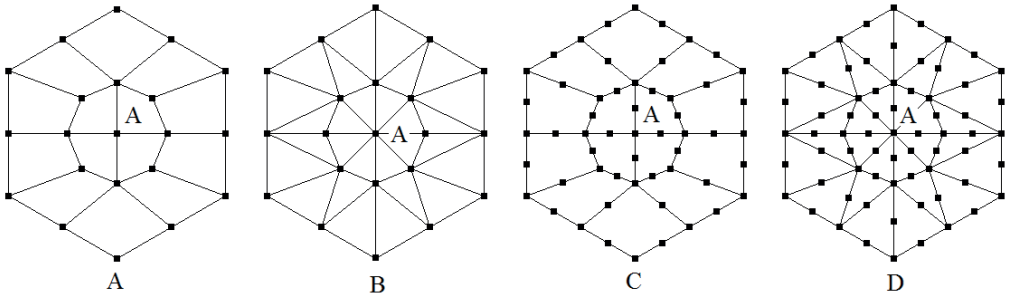

Figure 9. Design models 1x1 of a hexagonal plate

Table 2. Displacements and moments in the clamped plate

Mesh type	Element	Displacement w_A (mm)				Moment $M_{x,A}$ (kHm/m)			
		Mesh				Mesh			
		1x1	2x2	4x4	8x8	1x1	2x2	4x4	8x8
A	*MITC4*	-36.619	-37.916	-38.57	-38.737	0.7259	0.6573	0.656	0.6514
	JIDR4	-27.752	-35.899	-38.081	-38.584	0.5335	0.6405	0.6489	0.6504
	JIDR4SA	-29.89	-35.932	-38.09	-38.586	0.5236	0.6439	0.6478	0.6504
B	*DSG3*	-21.032	-35.274	-38.132	-38.663	0.3751	0.6101	0.6293	0.6429
	JIDR3	-24.194	-35.77	-38.035	-38.565	0.5076	0.6184	0.642	0.6486
C	*JIDR8*	-36.853	-38.559	-38.717	-38.743	0.7235	0.6602	0.654	0.6518
	JIDR8SA	-37.37	-38.614	-38.734	-38.747	0.7317	0.6657	0.6549	0.6521
D	*JIDR6*	-37.47	-38,66	-38.739	-38.747	0.6842	0.6613	0.6538	0.6518

6. CONCLUSIONS

All the created elements:
• have passed all Patch Tests;
• numerical experiments have confirmed that there is no locking effect;
• a good approximation of the numerical solution to the analytical results and the results of high-precision calculations has been obtained.
Elements based on thin plate elements were created. Approximating functions were used for:
• triangular elements [7,15];
• quadrangular elements [16].
Numerical experiments did not increase the accuracy of calculations in comparison with the approximations given in the paper with a significant complication of the algorithm.

REFERENCES

1. **Washizu K.** Variational Methods in Elasticity and Plasticity. Pergamon Press, Oxford New York, 1982, 630 pages.
2. **Bathe K.J.** Finite Element Procedures. New Jersey, Prentice Hall, 1996, 1038 pages.
3. **Slivker V.I.** Stroitelnaya mekhanika. Variatsionnyye osnovy [Construction mechanics. Variational bases]. Moskow, IASV, 2005, 708 pages (in Russian).
4. **Bathe K.J. Dvorkin, E.N.** A four-node plate bending element based on Mindlin/Reissner plate theory and a mixed interpolation. Int. J. Num. Meth. Engrg., 1985, Vol. 21, pp. 367–383. DOI: doi.org/10.1002/nme.1620210213
5. **Bletzinger K.U, Bischoff M, Ramm E.** A unified approach for shear-locking-free triangular and rectangular shell finite elements. Computers & Structures, 2000, Vol. 75, pp. 321-334. DOI:10.1016/S0045-7949(99)00140-6
6. **Zienkiewicz O.C., Taylor R.L.** The Finite Element Method. 3 volumes. Planta Tree, Butterworth-Heinemann, 2000, Vol. 1, 690 pages, Vol. 2, 459 pages, Vol. 3, 334 pages.
7. **Karpilovskyi V.S**. Konstpuipovaniye nesovmestnyx konechnyx elementov [Designing Incompatible Finite Elements]. UkrNIINTI, Kyiv, 1980, 2153, 49 pages (in Russian). https://scadsoft.com/download/Karpil1980.pdf/
8. **Karpilovskyi V.S.** Issledovanie i konstruirovanie nekotorykh tipov konechnykh elementov dlya zadach stroitel`noj mekhaniki. [Study and design of some types of finite elements for the structural mechanics problems]. // PhD diss., National transport university(KADI), Kyiv, 1982, 179 pages (in Russian)
9. **Evzerov I.D.** Oczenki pogreshnosti po peremeshheniyam pri ispol`zovanii nesovmestny`kh konechny`kh e`lementov [Estimates of the error in displacements when using incompatible finite elements] // Chislennye metody mekhaniki sploshnoj sredy [Numerical methods of continuum mechanics], Novosibirsk, 1983, Vol 14(5), pp. 24-31 (in Russian)
10. **Gorodetsky A.S., Karpilovskyi V.S**. Metodicheskiye pekomendatsii po issledovaniyu i konstpuipovaniyu konechnyx elementov [Methodological recommendations for the study and construction of finite elements]. Kyiv, NIIASS, 1981. 48 pages (in Russian). https://scadsoft.com/download/GorKarpil1981.pdf
11. **Strang G., Fix G.** An Analysis of the Finite Element Method. Prentice Hall, Englewood Cliffs, N.J., 1973. 306p.
12. **Karpilovskyi V.S.** Finite Elements of the Plane Problem of the Theory of Elasticity with Drilling Degrees of Freedom. International Journal for Computational Civil and Structural Engineering, Vol. 16(1), 2020, pp. 48-72. DOI: 10.22337/2587-9618
13. **Macneal R.H., Harder, R.L.** A proposed standard set of problems to test finite element accuracy. // Finite elements in analysis and design, 1985, Vol. 1, pp. 3-20. DOI: 10.1016/0168-874X(85)90003-4

14. **Weinberg D.V.** Spravochnik po prochnosti. ustoychivosti i kolebaniyam plastin [Handbook of Strength. stability and vibration of plates]. Kyiv, Budivelnik, 1973, 488 pages (in Russian)
15. **Karpilovskyi V.S**. Tpeugolnyy shestiuzlovoy konechnyy element plity [Triangular six-node finite element of plate]. Izvestiya VUZov. Stpoitelstvo i apxitektupa [News of the Higher Educational Institutions. Construction and architecture], 1989, Vol. 6, pp. 35–39.
16. **Karpilovskyi V.S.** Chetyipexugolnyiy vosmiuzlovoy konechnyiy element plityi [Quadrangular eight-node finite element of plate]. Structural Mechanics and Analysis of Constructions], 1990, Vol. 2, pp. 13–17.

СПИСОК ЛИТЕРАТУРЫ

1. **Васидзу К.** Вариационные методы в теории упругости и пластичности. – М.: Мир, 1987. – 544с.
2. **Bathe K.J.** Finite Element Procedures. New Jersey, Prentice Hall, 1996, 1038p.
3. **Сливкер В.И.** Строительная механика. Вариационные основы. – М., ИАСВ, 2005. – 708с.
4. **Bathe K.J. Dvorkin, E.N.** A four-node plate bending element based on Mindlin/Reissner plate theory and a mixed interpolation. //Int. J. Num. Meth. Engrg., 1985, Vol. 21, pp. 367–383. DOI: doi.org/10.1002/nme.1620210213
5. **Bletzinger K.U, Bischoff M, Ramm E:** A unified approach for shear-locking-free triangular and rectangular shell finite elements. // Computers & Structures, 2000, Vol. 75, pp. 321-334. DOI:10.1016/S0045-7949(99)00140-6
6. **Zienkiewicz O.C., Taylor R.L.** The Finite Element Method. 3 volumes. Planta Tree, Butterworth-Heinemann, 2000, Vol. 1, pages 690, Vol. 2, pages 459, Vol. 3, pages 334.
7. **Карпиловский В.С.** Конструирование несовместных конечных элементов. Киев: Деп. в УкрНИИНТИ, 1980, 2153. – 49 с. – URL: https://scadsoft.com/download/Karpil1980.pdf
8. **Карпиловский В.С.** Исследование и конструирование некоторых типов конечных элементов для задач строительной механики. Диссертация на соискание ученой степени кандидата технических наук по специальности 01.02.03 – «Строительная механика». – Киев: Национальный транспортный университет (КАДИ), 1982, 179 с.
9. **Евзеров И.Д.** Оценки погрешности по перемещениям при использовании несовместных конечных элементов // Численные методы механики сплошной среды, Новосибирск, 1983, том 14, №5, с. 24-31.
10. **Городецкий А.С., Карпиловский В.С.** Методические рекомендации по исследованию и конструированию конечных элементов. Киев: NIIASS, 1981. – 48с. – URL: https://scadsoft.com/download/GorKarpil1981.pdf
11. **Стренг Г., Фикс Дж**. Теория метода конечных элементов – М.: Мир, 1977. – 349 с.
12. **Karpilovskyi V.S.** Finite Elements of the Plane Problem of the Theory of Elasticity with Drilling Degrees of Freedom. // International Journal for Computational Civil and Structural Engineering, 2020, Vol. 16(1), pp. 48–72. DOI: 10.22337/2587-9618
13. **Macneal R.H., Harder, R.L.** A proposed standard set of problems to test finite element accuracy. // Finite elements in analysis and design, 1985, Vol. 1, pp. 3-20. DOI: 10.1016/0168-874X(85)90003-4
14. **Вайнберг Д.В.** Справочник по прочности, устойчивости и колебаниям пластин. – Киев: Будівельник, 1973. – 488 с
15. **Карпиловский В.С.** Треугольный шестиузловой конечный элемент плиты. // Известия ВУЗов. Строительство и архитектура, 1989, №6. – С. 35–39.
16. **Карпиловский В.С.** Четырехугольный восьмиузловой конечный элемент плиты // Строительная механика и расчет сооружений, 1990, №2. – С. 13–17.

Viktor S. Karpilovskyi, PhD, Senior Researcher, director IT company ScadGroup Ltd.; 03037, 3A Osvity street, office 2, Kiev 03037, Ukraine. phone: +38(044)2497191(3); E-mail: kvs@scadsoft.com, http://www.scadsoft.com. orcid : 0000-0002-9437-0373

Карпиловский Виктор Семенович, к.т.н., ст.н.с., директор ООО ScadGroup; 03037, Украина, г.Киев, ул. Освіти (Просвещения), д.3а, оф. 2; тел: +38(044)2497191(3); E-mail: kvs@scadsoft.com, http://www.scadsoft.com. orcid : 0000-0002-9437-0373

DOI:10.22337/2587-9618-2021-17-3-63-82

CALCULATION SCHEME OF REINFORCED CONCRETE STRUCTURES OF CIRCULAR CROSS-SECTION UNDER BENDING WITH TORSION

Vladimir I. Kolchunov [1]***, Sergey A. Bulkin*** [2]

[1] South-West State University, Kursk, RUSSIA,

[2] Urban planning institute of residential and public buildings (GORPROJECT), Moscow, RUSSIA

Abstract. The developed design diagram of the ultimate resistance of reinforced concrete structures in bending with torsion of circular cross-sections most fully reflects the features of their actual exploitation. For a spatial crack of a diagonal large ellipse, sections are taken in the form of a swirling propeller with concave and convex spatial parabolas from the first and second blocks between vertical transverse circular sections from the beginning to the end of the crack. For practical calculations in compressed and tensioned concrete, a polyline section of three sections is considered: two longitudinal trapezoids and the third middle section of the radius curve of a small ellipse close to forty-five degrees. When calculating unknown forces, solutions of the equations of equilibrium and deformations of the sections are made up to the end of the crack passing through the moment points for the resultant moments and the projections of internal and external forces. Shear torsional stresses along the linear longitudinal sections of the trapezoid were presented, as well as normal and shear stresses located on the end cross-sections at a distance x from the support. The height of the compressed area of concrete decreases with an increase in bending moments in the spatial section between the first and third cross-sections. It is found in their relationships and connections. The dowel action of reinforcement is determined using a special model of the second level with discrete constants. The static loading scheme was considered from the standpoint of an additional proportional relationship between the torques along the length of the bar in the spatial section and the first and third transverse sections. For a dangerous spatial crack, when projected onto the horizontal axis, the length C was found from a diagonal large ellipse of a round bar.

Keywords: reinforced concrete, circular section, calculation scheme, bending moment, torsion, spatial crack, dangerous spatial crack, governing equations

РАСЧЕТНАЯ СХЕМА КРУГЛЫХ ЖЕЛЕЗОБЕТОННЫХ КОНСТРУКЦИЙ ПРИ СЛОЖНОМ ПРЕДЕЛЬНОМ СОПРОТИВЛЕНИИ-КРУЧЕНИИ С ИЗГИБОМ

Вл.И. Колчунов [1]***, С.А. Булкин*** [2]

[1] Юго-Западный государственный университет, г. Курск, РОССИЯ

[2] ЗАО «Городской проектный институт жилых и общественных зданий», г. Москва, РОССИЯ

Аннотация. Разработанная расчетная схема предельного сопротивления железобетонных конструкций при кручении с изгибом элементов с круглыми поперечными сечениями наиболее полно отражает особенности их действительной работы. Для пространственной трещины диагонального большого эллипса приняты сечения в виде закрученного пропеллера с вогнутой и выпуклой пространственными параболами из первого и второго блоков между вертикальными поперечными круглыми сечениями от начала до конца трещины. Для практических расчетов в сжатом и растянутом бетоне рассмотрено ломанное сечение из трех участков, – два продольных трапеции и третий средний близкий к сорока пяти градусам участок кривой радиуса малого эллипса. При расчете неизвестных усилий составлены разрешающие уравнения равновесия и деформаций поперечных сечений до конца трещины, проходящие через моментные точки для равнодействующих моментов и проекций внутренних и внешних сил. Были представлены касательные напряжения кручения по линейным продольным сечениям трапеции, а также нормальные и касательные напряжения, расположенные на концевых поперечных сечениях на расстоянии x от опоры. При этом с увеличением изгибающих моментов уменьшаются высоты сжатой области бетона в простран-

ственном сечении между первым и третьим поперечными сечениями, которые могут быть найдены из их отношений и связей. Учитывается «нагельный» эффект в растянутой продольной и поперечной арматуре, определяемый с привлечением специальной модели второго уровня с дискретными константами. Статическая схема нагружения рассматривалась с позиций дополнительного пропорционального соотношения между крутящими моментами по длине стержня в пространственном сечении и в поперечных первом и третьем сечениях. При этом для опасной пространственной трещины при проецировании на горизонтальную ось была найдена длина С из диагонального большого эллипса круглого стержня.

Ключевые слова: железобетонные конструкции, круглое сечение, расчетная схема, прочность, изгибающий момент, крутящий момент, опасная пространственная трещина, разрешающие уравнения

INTRODUCTION

In regard with the complication of the types of actions on building structures, the creation of calculated models and the construction of calculated diagrams of the complex resistance of reinforced concrete in torsion with bending becomes more and more urgent [1, 2, 3]. This is also due to the fact that, firstly, there are relatively few such studies [3–9], and secondly, with the noted actions, it is necessary to take into account the spatial work of the overwhelming majority of reinforced concrete structures with more and more original architectural and structural solutions of buildings and structures. The existing modern calculated models of reinforced concrete, the analysis of which is given, for example [6], does not fully take into account the features of the resistance of complexly stressed reinforced concrete elements after cracking, including the very scheme of cracks, taken in the calculation with different cross-section sizes and not always confirmed experimentally.

Therefore, the purpose of this research is to develop a calculated diagram of the ultimate resistance of reinforced concrete structures in torsion with bending for circular cross-sections, which most fully reflects the features of their resistance after cracking [2, 12, 17, 18].

METHODS

To determine the calculated forces, the resolving equations of equilibrium and deformations are drawn up. In this case, the projection of a dangerous spatial crack is determined through the diagonal (larger) ellipse of the round bar [13].

As a result, for a reinforced concrete structure of a beam in a circular cross-section, we obtain a spatial crack and, accordingly, a calculated scheme after its formation. In this case, there are cross-sections from sections 1-1 at the beginning to 3-3 at the end of the spatial crack - an ellipse for the first and second blocks (Figure 1). We obtain a calculated diagram of the resistance of a reinforced concrete beam of a circular cross-section from the action of combined bending with torsion, taking into account a spatial crack. In compressed concrete, there are three zones l_1, l_2, l_3, - longitudinal zones (and), as well as an ellipse in the zone l_2 (Figure 2). In tensioned concrete, the same three zones l_1, l_2, l_3, are located, but the ellipse is adopted for the zone l_2, as well as a parabola for the zones l_1 and l_3.

The equation of a small ellipse for a spatial section is:

$$\frac{y^2}{2R^2}+\frac{z^2}{R^2}=1. \qquad (1)$$

Here $b=R$; $a=\frac{R}{\cos\alpha}=\frac{R}{\cos 45^\circ}=R\sqrt{2}$.

Then, in stretched concrete in the first and second sections, we have spatial curves of the form $f_{par1,2,3}(x,y,z)$.

To construct the first spatial parabola

$f_{par1,2,3}(x,y,z)$, we find the coordinate T.1 (x, y, z) along the x-axis ($x = -l_1 - 0.5l_2$) belonging to the circle in section 1-1 in a plane parallel to the Ozy plane. Then, for the coordinate at the desired point, we can write:

$$y = \pm\sqrt{R^2 - (R - x_k)^2}\ . \qquad (2)$$

Now we find the ordinate of T.2 (x, y, z) along the x-axis ($x = -0.5l_2$) belonging to a small ellipse lying in the plane Ozy ($z = -R + x_k - \Delta x_1 - x_{b,k}$):

$$y = \pm\sqrt{R^2 - (-R + x_k - \Delta x_1 - x_{b,k})^2}\ . \qquad (3)$$

For a point lying in the plane of the coordinate axes Oyz we have the following coordinate values: x = 0; y = 0; z = -R.

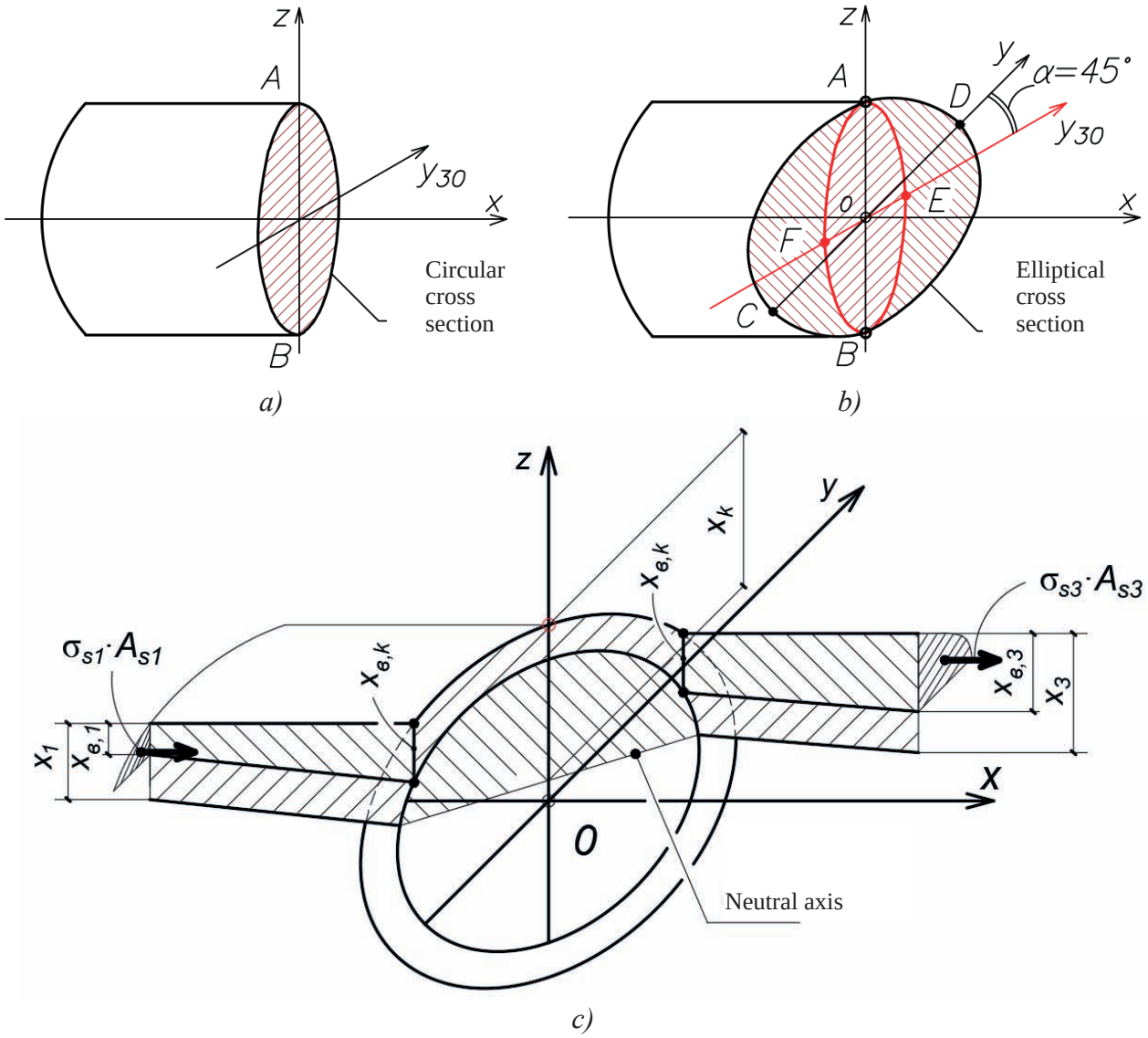

Figure 1. To the construction of an elliptical calculated scheme of a spatial crack in a reinforced concrete structure with a circular cross-section: a) a circular cross-section; b) elliptical section; c) the layout of the broken cross-section for compressed concrete

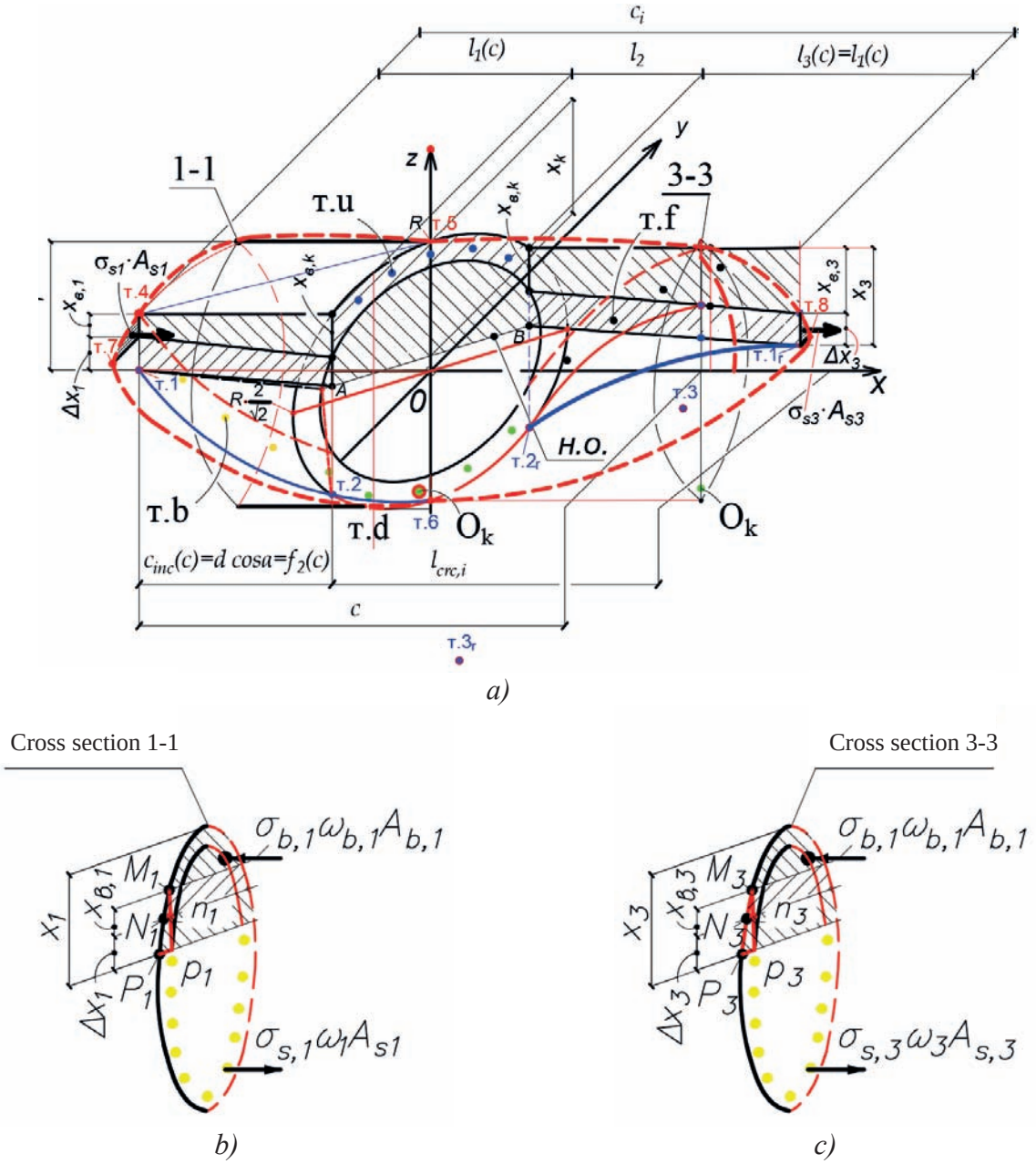

Figure 2. Calculated scheme for determining the ultimate resistance of a reinforced concrete structure in a complex stress state - torsion with bending: a spatial crack for a large ellipse with a swirling propeller in the direction of concave and convex spatial parabolas coming from the first and second blocks (a) and located between circular cross-sections I – I (b) and 3-3 (c)

Let's define the coefficients A_1, B_1, C_1 for the auxiliary curve $z_1(x) = A_1 \cdot x^2 + B_1 x + C_1$. To do this, we substitute the values of the coordinates at points 1, 2, 3 into the equation of this curve. After algebraic transformations, we get:

$$A_1 = \frac{2R - x_1 - x_k + \Delta x_1 + x_{b,k}}{(l_1 + 0.5l_2)^2 - (-0.5l_2)^2}; B_1 = 0; \quad (4)$$

$$C_1 = R - x_1 - \frac{2R - x_1 - x_k + \Delta x_1 + x_{b,k}}{(l_1 + 0.5l_2)^2 - (-0.5l_2)^2}(l_1 + 0.5l_2)^2. \quad (5)$$

Similarly, the values of the coefficients A_2, B_2, C_2 of the auxiliary plane curve are obtained, we obtain:

$$A_2 = \frac{\sqrt{R^2-(R-x_1)^2}-\sqrt{R^2-(-R+x_k-\Delta x_1-x_{b,k})^2}-\frac{\sqrt{R^2-(R-x_1)^2}}{(l_1+0.5l_2)}l_1}{(-0.5l_2)^2-(-l_1-0.5l_2)^2}; \quad (6)$$

$$B_2 = \frac{\sqrt{R^2-(R-x_1)^2}}{(l_1+0.5l_2)}; \quad (7)$$

$$C_2 = -\frac{\sqrt{R^2-(R-x_1)^2}-\sqrt{R^2-(-R+x_k-\Delta x_1-x_{b,k})^2}-\frac{\sqrt{R^2-(R-x_1)^2}}{(l_1+0.5l_2)}l_1}{\left((-0.5l_2)^2-(-l_1-0.5l_2)^2\right)\cdot(l_1+0.5l_2)^2}. \quad (8)$$

Let us write the equation of the first spatial parabola $f_{par1,2,3}(x,y,z)$:

$$f_{par1,2,3}(x,y,z) = \sqrt{z_1(x)^2+y_1(x)^2}. \quad (9)$$

To construct the second spatial parabola $f_{par1_r,2_r,3_r}(x,y,z)$ we define the coordinates of points 1r, 2r, and 3r (see Figure 2), which have coordinates similar to points 1,2 and 3:

$$m.1_r(0.5l_2+l_3;\sqrt{R^2-(R-x_3)^2};R-x_3); \quad (10)$$

$$m.2_r(0.5l_2;\sqrt{R^2-(-R+x_k-\Delta x_3-x_{b,k})^2};-R+x_k-\Delta x_3-x_{b,k}); \quad (11)$$

$$m.3_r(0.5l_2-l_3;\sqrt{R^2-(-R+x_3)^2};-R+x_3). \quad (12)$$

Then we can calculate the coefficients A_3, B_3, C_3 for the auxiliary curve $z_2(x) = A_3\cdot x^2 + B_3x + C_3$. To do this, substitute the values of coordinates at points 1r, 2r, 3r into the equation of this curve, and after algebraic transformations we obtain:

$$A_3 = \frac{\left(2R-x_3-x_k+\Delta x_3+x_{b,k}\right)2l_3}{(2l_3+0.5l_2)(0.5l_2+l_3)^2+(0.5l_2+l_3)^3-(0.5l_2-l_3)^2(l_3)-(0.5l_2)^2\cdot 2l_3}; \quad (13)$$

$$B_3 = \frac{-A_3\cdot(0.5l_2+l_3)^2+A_3\cdot(0.5l_2-l_3)^2}{2l_3}; \quad (14)$$

$$C_3 = \left(-R+x_k-\Delta x_3-x_{b,k}\right)-A_3\cdot\left(\frac{(0.5l_2)^2\cdot 2l_3-(0.5l_2+l_3)^2(0.5l_2)+(0.5l_2-l_3)^2(0.5l_2)}{2l_3}\right). \quad (15)$$

The coefficients A_4, B_4, C_4 for the auxiliary plane curve $y_2(x)$ are obtained in a similar way:

$$A_4 = \frac{B_4(2l_3)}{(0.5l_2-l_3)^2-(0.5l_2+l_3)^2}; \quad (16)$$

$$B_4 = \frac{\left((0.5l_2-l_3)^2-(0.5l_2+l_3)^2\right)\cdot\left(\sqrt{R^2-(R-x_3)^2}-\sqrt{R^2-(-R+x_k-\Delta x_3-x_{b,k})^2}\right)}{(2l_3-1)\cdot(0.5l_2+l_3)^2-(2l_3)\cdot(0.5l_2)^2+l_3\cdot(0.5l_2-l_3)^2}; \quad (17)$$

$$C_4 = \sqrt{R^2 - (-R + x_k - \Delta x_3 - x_{b,k})^2} - \frac{B_4 \cdot \left((2l_3)\cdot(0.5l_2)^2 + (0.5l_2)(0.5l_2 - l_3)^2 - (0.5l_2)(0.5l_2 + l_3)^2\right)}{(0.5l_2 - l_3)^2 - (0.5l_2 + l_3)^2}. \quad (18)$$

By analogy with Eq. (9), the equation of the second spatial parabola is also written:

$$f_{par1_r,2_r,3_r}(x,y,z) = \sqrt{z_2(x)^2 + y_2(x)^2}\ . \quad (19)$$

From the equilibrium equation of the moments of internal and external forces in section I – I relative to the y-axis passing through the point of application of the resultant forces O_I in the stretched reinforcement ($\sum M_{O,I}=0$), we obtain:

$$\begin{aligned} M_{bend,I} = R_{\text{sup},I,M}\cdot a_{m,I} = \varphi_{10,*}\cdot\sigma_{bu,x,I}A_{b,I}[h_0 - \varphi_{z,cir}\cdot x] + \\ +m\cdot R_{\text{sc,I,up}}\cdot\omega_{up,cir}\cdot A_{sc,up}\left(h_0 - a'_s\right) + \\ +\sum R_{\text{sc,I,i,lef}}\cdot\omega_{c,cir}\cdot A_{sc,I,i,\text{lef}}\left(\text{h}_0 - a'_{s,i,lef}\right) + \\ +\sum R_{\text{sc,I,i,rig}}\cdot\omega_{c,cir}\cdot A_{sc,I,i,\text{rig}}\left(\text{h}_0 - a'_{s,i,rig}\right) - \\ -\sum R_{\text{s,I,i,lef}}\cdot\omega_{cir}\cdot A_{s,I,i,\text{lef}}\left(a_{s,i,lef} - a_{s,d}\right) - \\ -\sum R_{\text{s,I,i,rig}}\cdot\omega_{cir}\cdot A_{s,I,i,\text{rig}}\left(a_{s,i,rig} - a_{s,d}\right) - \\ -\text{K}_\text{M}K_{pr,M}\cdot R_{\text{sup},I} - R_{\text{sup},I}\cdot a = 0\,. \end{aligned} \quad (20)$$

Here $\varphi_{10,*}$ is the parameter that takes into account the procedure for projecting the stress components in the *k* plane onto the I – I plane perpendicular to the longitudinal axis of the reinforced concrete element; sign * - means the reverse transition from section *k*, in the upper fiber of which the deformation criterion of strength is "triggered," to section I – I through the transition relations of projection of the diagram $\sigma_i - \varepsilon_i$ to the direction perpendicular to the plane k (see Figure 2); product $\varphi_{10,*}\sigma_{bu,x,I}A_b$ - the value for the considered section is known; $\sigma_{b,u} = \text{const}$; $A_b = R^2\arccos\left((R - x_1)/R\right) - -(R - x_1)\sqrt{2Rx_1 - x_1^2}$ - area of the compressed concrete zone in section 1-1; x_1 - the height of the compressed concrete zone in section 1-1; $h_0 - \varphi_{z,cir}\cdot x$ - shoulder of the inner pair to the center of the compressed zone of concrete; $\varphi_{z,*}$ - a static-geometric parameter that takes into account the location of the center of gravity of the compressed zone of concrete in section I – I (in the section x_B, the height of the compressive stress diagram is taken in the form of a pipe sector, in the section $x - x_B$ - in the form of an ellipse sector); K_M - a numerical coefficient that takes into account the static loading scheme from the standpoint of additional bending moments along the length of the bar. It is used when it is necessary to take into account the field of local stresses Δ_M and is found according to the proposals of S.P. Tymoshenko. Thus, it can be considered Δ_M a known quantity; $\text{K}_{\text{pr,M}}$ - coefficient, ratio (it is known and specified in the initial data is given) by the generalized support reaction R_{sup} and bending moment M; R_{sup} - generalized support reaction in the first block at the moment of exhaustion of the bearing capacity of the reinforced concrete structure of the beam; a - horizontal distance from the support of the beam to the section I – I; $\omega_{up,cir}$ - the filling factor of the diagram for the upper compressed reinforcement; ω_{cir} - coefficient of filling the diagram of a stretched right or left reinforcement; $\omega_{c,cir}$ - coefficient of filling the diagram of compressed right or left reinforcement.

The unknown $M_{bend,I}$ is found from this equation (20).

Next, we obtain an expression for the transverse force from internal forces:

$$Q_I = R_{\text{sup},I,M} = \frac{M_{bend,I}}{a_{m,I}}. \quad (21)$$

Here $M_{bend,I}$ is found from equation (20)

$$a_{m,I} = a + \mathrm{K_M} K_{pr,M}\,; \qquad (22)$$

From the equilibrium equation of the projections of all forces acting in section I – I on the x-axis, the area of the compressed concrete zone $A_{b,I}$ in this section is determined ($\sum X = 0$):

$$A_{b,I} = R^2 \arccos\left((R - x_1)/R\right) - (R - x_1)\sqrt{2Rx_1 - x_1^2} = \\ = \frac{1}{\varphi_{10,*}\sigma_{bu,x,I}\cdot\varphi_{y,*}} \cdot \left[m \cdot R_{s,I,d} \cdot \omega_{d,cir} \cdot A_{s,d} - \right. \\ - m \cdot R_{\mathrm{sc,I,up}} \cdot \omega_{up,cir} \cdot A_{sc,up} - \sum R_{\mathrm{sc,I,lef}} \cdot \omega_{c,cir} \cdot A_{sc,I,\mathrm{lef}} - \\ - \sum R_{\mathrm{sc,I,rig}} \cdot \omega_{c,cir} \cdot A_{sc,I,\mathrm{rig}} + \sum R_{\mathrm{s,I,lef}} \cdot \omega_{cir} \cdot A_{s,I,\mathrm{lef}} + \\ \left. + \sum R_{\mathrm{s,I,rig}} \cdot \omega_{cir} \cdot A_{s,I,\mathrm{rig}} \right]. \qquad (23)$$

From here, knowing the radius of the circle, you can calculate the height of the compressed zone of concrete x_1 in this section.

In equation (23) $\omega_{d,*}$ - the filling factor of the tensile reinforcement diagram; ω – the same, tensioned reinforcement right or left, ω_{up} – the same, compressed reinforcement, ω_{up} – the same, compressed reinforcement right or left; $R_{s,I,d}$, $R_{\mathrm{s,I,rig}}$, $R_{\mathrm{s,I,lef}}$ $R_{\mathrm{sc,I,up}}$, $R_{\mathrm{sc,I,rig}}$, $R_{\mathrm{sc,I,lef}}$, R_{sw} - respectively, calculated resistances of tensile reinforcement, tensile reinforcement of right or left, compressed reinforcement, compressed reinforcement of right or left, clamps.

Similarly, from the equilibrium equation of the projections of all forces acting in section III – III on the x axis, the area of the compressed concrete zone $A_{b,3}$ in this section is determined ($\sum X = 0$):

$$A_{b,3} = R^2 \arccos\left((R - x_3)/R\right) - (R - x_3)\sqrt{2Rx_3 - x_3^2} = \\ = \frac{1}{\varphi_{10,*}\sigma_{bu,x,3}\cdot\varphi_{y,*}} \cdot \left[m \cdot R_{s,3,d} \cdot \omega_{d,*} \cdot A_{s,d} - \right. \\ - m \cdot R_{\mathrm{sc,3,up}} \cdot \omega_{up} \cdot A_{sc,up} - \sum R_{\mathrm{sc,3,lef}} \cdot \omega_c \cdot A_{sc,3,\mathrm{lef}} - \\ - \sum R_{\mathrm{sc,3,rig}} \cdot \omega_c \cdot A_{sc,3,\mathrm{rig}} + \sum R_{\mathrm{s,3,lef}} \cdot \omega \cdot A_{s,3,\mathrm{lef}} + \\ \left. + \sum R_{\mathrm{s,3,rig}} \cdot \omega \cdot A_{s,3,\mathrm{rig}} \right]. \qquad (24)$$

From here, knowing the radius of the circle, you can calculate the height of the compressed zone of concrete x_3 in this section.

Now we obtain an expression for the torque from internal forces in section I-I (see Figure 3) from the equation of the sum of the torques relative to the point b_I ($\sum T_{b,I} = 0$):

$$M_{t,I} = \tau_{pl,u} \cdot \lambda x_1 \cdot b_{cir} \cdot \varphi_{cir,\tau} \cdot \left(z_1 - 0.5 \cdot \lambda x_1\right) + \\ + 0.5 \cdot \tau_{pl,u} \cdot \left(x_1 - \lambda x_1\right) \cdot b_{cir} \cdot \left[0.5 \cdot \lambda x_1 + \frac{1}{3} \cdot \left(x_1 - \lambda x_1\right) \right] + \\ + Q_s A_s \cdot \left(h_0 - z_1\right) \qquad (25)$$

Here $\varphi_{cir,\tau}$ is a parameter that takes into account the position of the center of gravity of the section; b_{cir} - the width of a segment of a circle in the section under consideration; $z_1 = R - \frac{S}{A}$ - distance from point b_I to the center of gravity of the section; S - the static moment of the section; A - area of a circle; λx_1 - the height of the plastic deformation zone, $b_{cir} = 2\sqrt{R^2 - (R - x_k)^2}$.

From the equilibrium equation of the projections of internal and external forces acting in section I – I on the Y axis ($\sum Y = 0$), it is possible to determine the parameter $k_{Q,m}$ that takes into account the presence of adjacent cracks:

$$-\tau_{pl,x} \cdot x \cdot b - \tau_{pl,x} \cdot k_{Q,m} \cdot \left(h_0 - x\right) \cdot b + K_M \cdot R_{\mathrm{sup}} = 0, \qquad (26)$$

Here $\mathrm{K_M}$ – the same as in the formula (20).

In formula (26), the thrust forces in the working reinforcement in the middle section I – I are taken equal to zero.

In this case, the transverse force perceived by the concrete in the compressed zone will be equal to:

$$\mathrm{Q_{I,b}} = \tau_{pl,x} \cdot x \cdot b\,. \qquad (27)$$

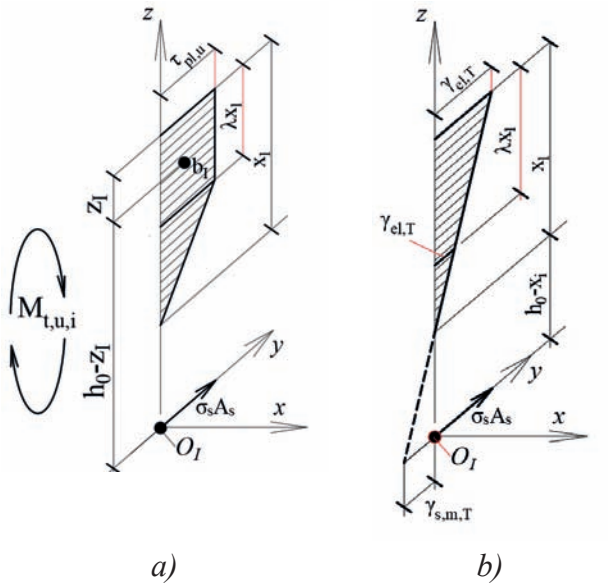

a) *b)*

Figure 3. Diagrams of forces in cross-section I-I (3-3) with torsion

In turn, the shear force perceived by the concrete in the tensile zone will be (Figure 4):

$$Q_{II,T} = \tau_{pl,x} \cdot k_{Q,m} \left(h_0 - x\right) \cdot b \,. \qquad (28)$$

On the other side:

$$Q_{II,T} = Q - Q_{I,b} \,. \qquad (29)$$

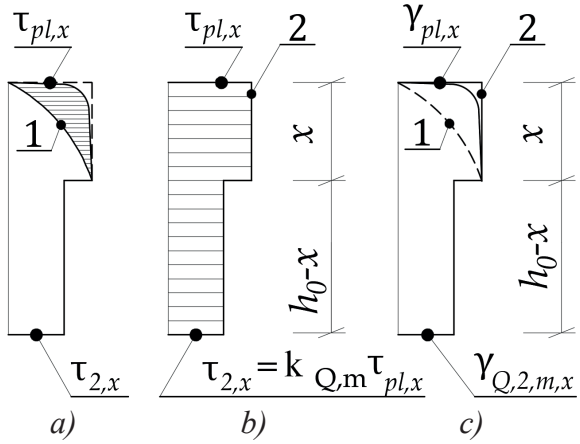

a) *b)* *c)*

Figure 4. Diagram of shear stresses τ_Q in the middle cross-sections I – I (3-3)

Equality (26) can be used to determine the parameter $k_{Q,m}$ that takes into account the presence of adjacent spatial cracks in the stress-strain state of the stretched zone of the middle cross-section I – I:

$$k_{Q,m} = \frac{K_M \cdot R_{\text{sup}} - \tau_{pl,x} \cdot x \cdot b}{\tau_{pl,x}\left(h_0 - x\right) \cdot b} \,. \qquad (30)$$

The formulation of the following equations requires some clarification. The upper, lower and lateral longitudinal reinforcement (in the presence of multi-tiered reinforcement) was conventionally not shown in Figure 2. Under equilibrium conditions, the stresses arising in the noted reinforcement are taken into account. The only exception is the equation of equilibrium of the moments of internal and external forces acting in section I – I relative to the axis x perpendicular to this section and passing through point b_k - the point of application of the resultant forces in the compressed zone ($T_{b,I} = 0$)

In the spatial section *k* for block 2, cut off by a complex section, passing along a spiral-shaped spatial crack and along a broken section of the compressed zone, all reinforcement [12] falling into this section is taken into account (see Figure 2). In this case, in the compressed upper longitudinal reinforcement, cut off by sections I – I and III – III (the dagger effect is not taken into account), and in the rest of the longitudinal and transverse reinforcement, the components of the dagger effect are taken into account. These components are determined using a special second-level model [1, 2, 13, 15].

The need to use a complex broken section of the compressed zone of concrete is due to the fact that its destruction occurs (as shown by experimental studies) in a certain volume located not along the entire length between points A and B (see Figure 2), but only in a certain volume located in the middle part of this volume. In this case, destruction occurs in the middle part not along the line AB, but at an angle close to 45^o to the upper surface of the reinforced concrete structure, which predetermined the direction of the middle part

of the broken section, where the ultimate stress-strain state is reached.

In the areas of the compressed zone located at the edges of the broken section, the stress-strain state changes from sections I – I and III – III to the middle zone according to linear dependences, respectively. In this case, the height of the compressed zone decreases with an increase in the bending moment (see Figure 2). Such a design scheme is most consistent with the actual resistance of structures in torsion with bending, the parameters of which are experimentally confirmed.

The lateral surfaces of the broken section in compressed concrete coincide with the planes of the axis (or "smeared" plane) of the longitudinal working reinforcement. In this case, the reinforcement located in the lateral zones of the section when crossing the broken section is considered to be located on the left for section I – I and on the right for section III – III. Thus, it is intersected by planes I – I, III – III, respectively, at the end sections of a complex broken section.

The equations for determining the shear stresses from torsion in a cross-section located at a distance x from the support are written in cylindrical and Cartesian coordinates.

It is also important to note that all geometric characteristics are considered relative to the geometric center of the section.

With regard to the average cross-section I – I, which is in conditions of complex resistance - torsion with bending, it is advisable to take into account the fact that a significant part of this section is subject to tension. It is known [1, 2, 15] that in tensile concrete there are a number of adjacent spatial cracks that affect the stress-strain state of the middle section I – I. We will take into account this effect of adjacent cracks using the parameter $k_{T,m}$.

If the torque along the longitudinal axis of the reinforced concrete structure is not constant, but changes, then an additional dependence is introduced into the calculation, the ratio between the torques in section *k* and in section I – I:

$$\frac{\mathrm{K_T}\cdot \mathrm{K_{pr,T}}\cdot M_{T,I}}{M_{T,k}}=\frac{a}{c-0{,}5b\cdot\sin\alpha},$$

$$M_{T,I}=\frac{a\cdot M_{T,k}}{\mathrm{K_T}\cdot \mathrm{K_{pr,T}}\cdot\left(c-0{,}5b\cdot\sin\alpha\right)}. \quad (31)$$

Here $\mathrm{K_T}$ is a numerical coefficient that takes into account the static loading scheme from the standpoint of additional torques along the length of the bar; $\mathrm{K_{pr,T}}$ - coefficient taking into account the ratio between $R_{\sup}$ and T; a is the horizontal distance from the structural support to the section I – I.

If the torque along the longitudinal axis of the reinforced concrete structure has a constant value, then the resulting stresses from torsion in stage III reach their limiting values equal to τ_u.

Knowing τ_u, we can determine the torque per *j*-th square of the compressed zone in section I – I by the formula:

$$T_c=M_{t,c}=\frac{\tau_{t,u}\cdot I_t}{\sqrt{\left(\zeta y\right)^2+z^2}}. \quad (32)$$

In the case when the torque along the longitudinal axis of the reinforced concrete structure changes and has a lower value than in section *k*, then instead of τ_u, should be inserted τ_{sum} into formula (32).

In turn, the torque received by the concrete in the tension zone will be equal to:

$$T_R=M_{t,R}=\frac{\tau_{t,u}\cdot k_{T,m}\cdot I_t}{\sqrt{\left(\zeta y\right)^2+z^2}}, \quad (33)$$

here $k_{T,m}$ is a parameter that takes into account the presence of adjacent spatial cracks in the stress-strain state caused by the torsion of the tensioned zone of the middle cross-section I – I.

On the other hand, again returning to the construction of general resolving equations (see Figure 3), for $M_{t,R}$, the equation of equilibrium

of the moments of internal and external forces acting in section I-I relative to the x axis, perpendicular to this section and passing through the point of application can be used resultant forces b_I in the compressed zone of concrete ($T_{b,I} = 0$):

$$M_{t,R} = M_t - M_{t,c}\,. \qquad (34)$$

The parameter can be found from this equation $k_{T,m}$:

$$k_{T,m} = \frac{\left(M_t - M_{t,c}\right)\sqrt{\left(\zeta y\right)^2 + z^2}}{\tau_{t,u} \cdot I_t}\,. \qquad (35)$$

Here $\tau_{t,u}$ is the shear torsional stress in compressed concrete, obtained in the third stage of stress-strain state by projecting the diagram "$\sigma_i - \varepsilon_i$" onto the section plane I – I for the dependence "$\tau - \gamma$", taking into account the ratio *Q:T* or *M: T*, one of which, as a rule, is given. If necessary, one should take into account the additional dependence arising from the ratio of the torques in section 1–1 and in section *k*.

It is also appropriate to note that the limiting stresses $\tau_{t,u}$, $\tau_{t,xy,ul}$, $\tau_{t,zx,ul}$, $\sigma_{b,ul}$ are known (they are located on the horizontal sections of the "strain-stress" relationship diagrams), since the plastic state occurs simultaneously for tangential and normal stresses.

From the hypothesis of proportionality of longitudinal deformations in the calculated section, we find stresses in longitudinal reinforcement:

$$\sigma_{s,I} = \frac{\phi_{10,*}\sigma_{bu,x,I} \cdot E_s(\lambda)}{E_b(\lambda)} \cdot \frac{h_0 - x}{x} + \sigma_0 \le \mathrm{R_{s,I}}\,. \qquad (36)$$

Here σ_0 – prestresses in the stressed reinforcement at the moment when the prestress value in concrete decreases to zero when the structure is loaded by external forces, taking into account the prestress losses corresponding to the considered stage of the structure operation. If the condition (36) is not met, then we assume $\sigma_{s,I}$ to be equal $R_{s,I}$. In equation (36), the notation $\phi_{10,*}$ is the same as in formula (20).

Normal shortening deformations along the *x*-axis in compressed concrete at various points of the *k-k* section and in the I-I section can be found from the same hypothesis of proportionality to the limiting deformations $\varepsilon_{bu,k,rig,x}$ at the rightmost point of the k-k section:–from the right point (rig) to the section I-I, –

$$\frac{\varepsilon_{b,I}}{\varepsilon_{bu,k,rig,x}} = \frac{a}{a - l_1}; \qquad (37)$$

$$\varepsilon_{b,I} = \frac{\varepsilon_{bu,k,rig,x} \cdot a}{a - l_1}\,. \qquad (38)$$

– rom the right point (rig) to the middle point (b_k):

$$\frac{\varepsilon_{bu,k,rig,x}}{\varepsilon_{b,k,x}} = \frac{a - l_1}{a - \left(l_1 + \frac{\sqrt{2}}{2} l_2 \cdot \frac{1}{2} - \eta_{hor,b} \cdot l_2\right)}; \qquad (39)$$

$$a_{m,b} = a - \left(l_1 + \frac{\sqrt{2}}{2} l_2 \cdot \frac{1}{2} - \eta_{hor,b} \cdot l_2\right); \qquad (40)$$

$$\varepsilon_{b,k,x} = \frac{\varepsilon_{bu,k,rig,x} \cdot a_{m,b}}{a - l_1} = \frac{\varepsilon_{bu,k,rig,x} \cdot \left[a - \left(l_1 + \frac{\sqrt{2}}{2} l_2 \cdot \frac{1}{2} - \eta_{hor,b} \cdot l_2\right)\right]}{a - l_1}; \qquad (41)$$

– from the right point (rig) to the left point (lef):

$$\frac{\varepsilon_{bu,k,rig,x}}{\varepsilon_{bu,k,lef,x}} = \frac{a - l_1}{a - (l_1 + l_2)}; \qquad (42)$$

$$\varepsilon_{bu,k,lef,x} = \frac{\varepsilon_{bu,k,rig,x} \cdot \left[a - (l_1 + l_2)\right]}{a - l_1}\,. \qquad (43)$$

Unknown deformations $\varepsilon_{s,k,rig,x}$ and $\varepsilon_{s,k,lef,x}$ we also determine from the proportionality conditions:

$$\varepsilon_{s,k,rig,x} = \frac{\varepsilon_{s,l} \cdot (a - l_1)}{a}; \quad (44)$$

$$\varepsilon_{s,k,lef,x} = \frac{\varepsilon_{s,k,rig,x} \cdot [a - (l_1 + l_2)]}{a - l_1}. \quad (45)$$

Then for the voltages, respectively, we can write

$$\sigma_{s,k,rig,x} = \varepsilon_{s,k,rig,x} \cdot E_s \cdot \nu_s(\lambda) \quad \text{and}$$
$$\sigma_{s,k,lef,x} = \varepsilon_{s,k,lef,x} \cdot E_s \cdot \nu_s(\lambda).$$

Next, we determine the unknown parameter $x_{B,k}$ from the condition that the sum of the projections of all forces acting in the spatial section ***k*** on the *x*-axis is equal to zero: $\sum X=0$, (see block II in Figure 2):

$$-\sigma_{\mathrm{s,k}} \cdot m_d \cdot A_{s,d} + \sum R_{\mathrm{sc,up,i}} \cdot \omega_{\mathrm{up}} \cdot A_{sc,\mathrm{up,i}} - $$
$$-\sum R_{\mathrm{s,i,rig}} \cdot \omega_{rig} \cdot A_{s,\mathrm{i,rig}} - \sum R_{\mathrm{s,i,lef}} \cdot \omega_{lef} \cdot A_{s,\mathrm{i,lef}} +$$
$$+\sum R_{\mathrm{sc,i,rig}} \cdot \omega_{c,rig} \cdot A_{sc,\mathrm{i,rig}} + \sum R_{\mathrm{sc,i,lef}} \cdot \omega_{c,lef} \cdot A_{sc,\mathrm{i,lef}} -$$
$$-\varphi_{10}\tau_{xy,u,Mt} \cdot A_{b,l_1} + \varphi_{10}\tau_{xy,u,Mt} \cdot A_{b,l_3} - \sigma_{b,1,rig} \cdot A_{b,*} -$$
$$-\sigma_{sc,1,rig} \cdot A_{sc,1,rig} - \sigma_{b,3,lef} \cdot A_{b,**} - \sigma_{sc,3,lef} \cdot A_{sc,3,lef} -$$
$$-X_{b,k} \cdot A_{b,k,x_B} - \varphi_{10}\tau_{xy,u,Mt} \cdot A_{b,l_1,ad} +$$
$$+\varphi_{10}\tau_{xy,u,Mt} \cdot A_{b,l_3,ad} - \sigma_{b,1,rig} \cdot A_{b,*,cir,ad} -$$
$$\sigma_{b,3,lef} \cdot A_{b,**,cir,ad} - X_{b,k} \cdot A_{b,k,core} = 0. \quad (46)$$

The following restrictions must be taken into account:

$$0.1h_0 \le x_{B,k} \le 0.3h_0; \quad (47)$$

$$x_{B,k} \le x_k; \quad (48)$$

In equation (46), $X_{b,k}$ – the projection of the components of the stresses on the axis of *x*; A_{b,l_1} – is the area of concrete on the zone l_1; A_{b,l_3} – the area of concrete on the zone l_3; $A_{b,*,cir}$ – the area of concrete of the right sector broken section (sector height $x_{B,1}$); $A_{b,**,cir}$ – the area of concrete left sector of the broken section (sector height $x_{B,3}$); $A_{b,l_1,ad}$ – the area of the concrete with a height Δx_1 of zone l_1; $A_{b,l_3,ad}$ – the area of the concrete with a height Δx_3 of zone l_3; $A_{b,*,cir,ad}$ – the area of the concrete part of the right sector altitude Δx_1; $A_{b,**,cir,ad}$ – square concrete of the left sector altitude Δx_3;

$A_{b,k,core} = \Big((R - x_B)^2 \arccos\big((R - x_k)/R - x_B\big) -$
$-(R - x_k)\sqrt{2(R - x_B)(x_k - x_B) - (x_k - x_B)^2}\Big)\sqrt{2}$ - the area of the core of the section of compressed concrete in the section k-k on the zone l_1;

$A_{b,k,x_B} = \Big(R^2 \arccos\big((R - x_k)/R\big) -$
$-(R - x_k)\sqrt{2Rx_k - x_k^{\,2}}\Big)\sqrt{2} - A_{b,k,core}$ – the area of the arc of the upper fibres of circular cross-section; $\sum_{k=1}^{n_{rig}} R_{\mathrm{s,i,rig}} \cdot \omega_{rig} \cdot A_{s,\mathrm{i,rig}}$ $(\sum_{k=1}^{m_{rig}} R_{\mathrm{sw,i,rig}} \cdot \omega_{rig} \cdot A_{sw,\mathrm{i,rig}})$ – stress is stretched in the transverse reinforcement (cross clamps) to the right of the contour of the first segment of a parabola spatial $f_{par1,2,3}(x,y,z)$ (zone l_1); $\sum_{k=1}^{m_{lef}} R_{\mathrm{sw,i,lef}} \cdot \omega_{lef} \cdot A_{sw,\mathrm{i,lef}}$ $(\sum_{k=1}^{n_{lef}} R_{\mathrm{s,i,lef}} \cdot \omega_{lef} \cdot A_{s,\mathrm{i,lef}})$ – stress is stretched in the longitudinal reinforcement (cross clamps) for the left loop of the second segment of a parabola spatial $f_{par1_r,2_r,3_r}(x,y,z)$ (zone l_3); h_0 – working height section.

$$A_{b,l_1} = \frac{(x_{B,k} + x_{B,1}) \cdot l_1}{2}; \quad (49)$$

$$A_{b,l_3} = \frac{(x_{B,k} + x_{B,3}) \cdot l_3}{2}. \quad (50)$$

The value $X_{b,k}$ for the midpoint (b_k) of the polyline section k (on the zone l_2) is:

$$X_{b,k}=\frac{\varphi_{z,1}\cdot\sigma_{bu,x,I}\cdot\varphi_{1,*}\cdot\left[a-\left(l_1+\frac{\sqrt{2}}{2}l_2\cdot\frac{1}{2}-\eta_{hor,b}\cdot l_2\right)\right]}{a}+$$
$$+\left(\pm\varphi_{10}\cdot\tau_{xy,u,Mt}\right)\cdot\varphi_{3,*}. \qquad (51)$$

Here $\varphi_{3,*}$ – is the transition coefficient from a cross-section to an oblique (oblique, – when the cross-section is located at an angle $\beta=45^\circ$, $\cos 45^\circ=\frac{\sqrt{2}}{2}$); $\sigma_{b,ad,x,k}-$ normal stresses in the cross-section k are taken instead of stresses $\sigma_{bu,x,k}$, and tangential stresses $\tau_{xy,ad,Mt}$ are taken instead of stresses $\tau_{xy,u,Mt}$, these stresses are calculated by the formulas:

$$\sigma_{b,ad,x,k}=\sigma_{bu,x,k}-\sigma_{b,crc,x,k};$$
$$\tau_{xy,ad,Mt}=\tau_{xy,u,Mt}-\tau_{xy,crc,Mt}. \qquad (52)$$

The second supporting block of section k-k is separated from the reinforced concrete element by a spatial section formed by a spiral crack and a vertical section passing through the compressed zone of concrete through the end of the spatial crack front.

The balance of this block is ensured by fulfilling the following conditions.

The sum of the moments of all internal and external forces acting in the vertical longitudinal plane relative *to* the *y*-axis passing through the point of application of the resultant forces b_k in the compressed zone is zero $\sum M_{b,k}=0$ (see block II, Figure 2):

$$M_{bend,k}=\frac{\sigma_{s,k}+\sigma_{s,rig}}{2}\cdot(h_0-0,5x_{B,k})\cdot\frac{m_d}{2}\cdot A_{s,d}+$$
$$+\frac{\sigma_{s,k}+\sigma_{s,lef}}{2}\cdot(h_0-0,5x_{B,k})\cdot\frac{m_d}{2}\cdot A_{s,d}+$$
$$+\varphi_{7,*}\cdot R_s\cdot\eta_{hor,s}\cdot c_{i-1}\sum\omega_{*,cir}A_s-\varphi_{5,*}\cdot R_s\cdot\sum\omega_{*,cir}A_s+$$
$$+\sum R_{s,i,rig}\cdot\omega_{rig,cir}\cdot A_{s,i,rig}\left[h_0-0,5x_{B,k}-a_{s,i,rig}\right]+$$
$$\sum R_{s,i,lef}\cdot\omega_{lef,cir}\cdot A_{s,i,lef}\left[h_0-0,5x_{B,k}-a_{s,i,lef}\right]+$$
$$+\varphi_{7,*,rig}R_{s,rig}\sum\omega_{r,*,cir}A_{s,rig}\cdot\left(0,5c_{inc,i-1}-0,5l_2-z_{sw}\right)-$$
$$-\varphi_{5,*,rig}R_{s,rig}\cdot\sum\omega_{r,*,cir}A_{s,rig}-$$
$$-\varphi_{7,*,lef}R_s\sum\omega_{l,*,cir}A_{s,l}\cdot\left[l_3(c_i)-0,5\cdot h\cdot\cos\alpha_0+\right.$$
$$\left.+0,5l_2-z_{sw}\right]+\varphi_{5,*,lef}R_{s,lef}\cdot\sum\omega_{l,*,cir}A_{s,lef}+$$
$$+q_{sw,rig}\cdot\frac{h}{2h+b}\cdot c\cdot\left(0,5\cdot\frac{h}{2h+b}\cdot c\cdot-0.5l_2-z_{sw}\right)-$$
$$-q_{sw,lef}\cdot\frac{h}{2h+b}\cdot c\cdot\left[c-(l_1+l_2)-0,5\cdot h\cdot\cos\alpha_0+0.5l_2-z_{sw}\right]+$$
$$+\left(\varphi_9\tau_{zy,u,Q}+\varphi_{11}\tau_{zy,u,Mt}\right)\cdot A_{b,l_1,ad}\cdot\left[\left(l_1-\frac{l_1}{3}\cdot\frac{2\cdot x_{B,k}+x_{B,1}}{x_{B,k}+x_{B,1}}\right)-\right.$$
$$\left.-(0.5\cdot l_2-\eta_{hor,b}\cdot l_2)\right]+\left(\varphi_9\tau_{zy,u,Q}-\varphi_{11}\tau_{zy,u,Mt}\right)\cdot A_{b,l_3}\cdot$$
$$\cdot\left[\left(\frac{l_3}{3}\cdot\frac{2\cdot x_{B,3}+x_{B,k}}{x_{B,3}+x_{B,k}}\right)+(0.5\cdot l_2+\eta_{hor,b}\cdot l_2)\right]+$$
$$+\left(\varphi_{12}\cdot\tau_{zx,u,Q}+\varphi_{14}\cdot\tau_{zx,u,Mt}\right)\cdot A_{b,*,cir}\cdot\left[l_1+\left(0.5\cdot l_2-\eta_{hor,b}\cdot l_2\right)\right]+$$
$$+\left(\varphi_{12}\cdot\tau_{zx,u,Q}-\varphi_{14}\cdot\tau_{zx,u,Mt}\right)\cdot A_{b,**,cir}\cdot\left[l_3+\left(0.5\cdot l_2+\eta_{hor,b}\cdot l_2\right)\right]+$$
$$+\left(\varphi_9\tau_{zy,u,Q}+\varphi_{11}\tau_{zy,u,Mt}\right)\cdot A_{b,l_1,ad}\cdot\left[\left(l_1-\frac{l_1}{3}\cdot\frac{2\cdot x_{B,k}+x_{B,1}}{x_{B,k}+x_{B,1}}\right)-\right.$$
$$\left.-(0.5\cdot l_2-\eta_{hor,b}\cdot l_2)\right]+\left(\varphi_9\tau_{zy,u,Q}-\varphi_{11}\tau_{zy,u,Mt}\right)\cdot$$
$$\cdot A_{b,l_3,ad}\cdot\left[\left(\frac{l_3}{3}\cdot\frac{2\cdot x_{B,3}+x_{B,k}}{x_{B,3}+x_{B,k}}\right)+(0.5\cdot l_2+\eta_{hor,b}\cdot l_2)\right]+$$
$$+\left(\varphi_{12}\cdot\tau_{zx,u,Q}+\varphi_{14}\cdot\tau_{zx,u,Mt}\right)\cdot A_{b,*,cir,ad}\cdot\left[l_1+\left(0.5\cdot l_2-\eta_{hor,b}\cdot l_2\right)\right]+$$
$$+\left(\varphi_{12}\cdot\tau_{zx,u,Q}-\varphi_{14}\cdot\tau_{zx,u,Mt}\right)\cdot A_{b,**,cir,ad}\cdot\left[l_3+\right.$$
$$\left.+\left(0.5\cdot l_2+\eta_{hor,b}\cdot l_2\right)\right]+X_{b,k}\cdot A_{b,k,x_B}\cdot l_{b,i}. \qquad (53)$$

Here K_M, $K_{pr,M}$ – numerical coefficients, the same as in the formula (20); $a_{m,b}(c)=a-c-l_1-\frac{1}{2}l_2$ – horizontal distance from the structural support to the center of gravity of the compressed concrete zone in section *k; (a –distance from section I-I to the structural support)*. The projection *c* is assumed to be constant at each step of the iterative

process. Concise valves on either side of the cross-section in this equation is not taken into account in view of the smallness of the shoulder relative to the point b_k (because of the smallness of the parameter x_B); ϕ_5, $\phi_{5,r}$, $\phi_{5,l}$, $\phi_{7,r}$, ϕ_8 - parameters, taking into account the components of the "pin" effect in the armature (at each step of the iteration are taken as constants and are determined based on the model of the second level); ω_1, ω_2 – filling ratio plots shear stresses; $\eta_{hor,b}$ – the distance between the center b_k (the longitudinal axis of the beam) and the point b (see figure 2); $l_{b,i}$ – shoulder from the point b_k to the center of gravity of the cross-section with an area of $(x_k - x_{B,k}) \cdot \sqrt{l_2^2 + b^2}$ on the zone l_2.

Equation (53) determines the bending moment $M_{bend,k}$.

Next, we determine the transverse force from internal forces:

$$Q_k = R_{\text{sup},k,M} = \frac{M_{bend,k}}{a_{m,k}}. \qquad (54)$$

Here, $M_{bend,k}$ is found from the equation (53).

$$a_{m,k} = a_{m,b}(c) + \text{K}_\text{M} K_{pr,M}. \qquad (55)$$

The height of the compressed zone x_k in cross-section k-k between cross-sections I-I and III-III (see Figure 2) can be found from the ratio:

$$x_k = \frac{x_1 + x_3}{2}. \qquad (56)$$

x_1 – height of the compressed zone in section I-I for the equation (23); x_3 – height of the compressed zone in section III-III for the equation (24).

Enter the notation:

$$\eta_1 = \frac{x_{B,k}}{x_{B,k} + \Delta x_1}. \qquad (57)$$

Here, the height of the compressed zone $x_{B,k}$ for the k-k section is determined from equations (46), including and x_k. Then, for the increment of the height of the compressed zone in sections k-k and 1-1, we can write:

$$\Delta x_1 = x_k - x_1. \qquad (58)$$

On the other hand, if the relation (57) holds for sections 1-1, we can write $\eta_1 = \frac{x_{B,1}}{x_{B,1} + \Delta x_1}$. From here $x_{B,1}$ we get:

$$x_{B,1} = \frac{\eta_1 \cdot \Delta x_1}{\eta_1 - 1}. \qquad (59)$$

In this equation, the value Δx_1 is known.

Similarly, by entering the notation η_3:

$$\eta_3 = \frac{x_{B,k}}{x_{B,k} - \Delta x_3}, \qquad (60)$$

Determine the height of the compressed zone in sections 3-3:

$$x_{B,3} = \frac{\eta_3 \cdot \Delta x_3}{(\eta_3 - 1)}. \qquad (61)$$

The sum of the projections of all forces acting in the spatial section ***k*** on the *z*-axis is zero ($\sum Z$=0, see block II, Figure 2):

$$\text{q}_{\text{sw,rig}} = \frac{tg\alpha}{h}\Big[\text{q}_{\text{sw,lef}} \cdot \eta_q \cdot \frac{h}{tg\alpha_0} - \\ -\varphi_{7,*} R_\text{s} \sum \omega_{*,cir} A_{s,*,cir} - \varphi_{7,*,rig} R_\text{s} \sum \omega_{rig,*,cir} A_{s,rig} + \\ +\varphi_{7,*,lef} R_\text{s} \sum \omega_{lef,*} A_{s,lef} - Q + R_{\text{sup}} \\ +\left(\varphi_{11}\tau_{zy,u,Mt} + \varphi_9 \tau_{zy,u,Q}\right) \cdot A_{b,l_1} +$$

$$+\left(\varphi_{11}\tau_{zy,u,Mt}-\varphi_{9}\tau_{zy,u,Q}\right)\cdot A_{b,l_3}+$$
$$\left(\varphi_{14}\cdot\tau_{zx,u,Mt}+\varphi_{12}\cdot\tau_{zx,u,Q}\right)\cdot A_{b,*,cir}+$$
$$\left(\varphi_{14}\cdot\tau_{zx,u,Mt}-\varphi_{12}\cdot\tau_{zx,u,Q}\right)\cdot A_{b,**,cir}+$$
$$Z_{b,k}\cdot A_{b,k,x_B}-\left(\varphi_{11}\tau_{zy,u,Mt}+\varphi_{9}\tau_{zy,u,Q}\right)\cdot A_{b,l_1,ad}+$$
$$\left(\varphi_{11}\tau_{zy,u,Mt}-\varphi_{9}\tau_{zy,u,Q}\right)\cdot A_{b,l_3,ad}+$$
$$\left(\varphi_{14}\cdot\tau_{zx,u,Mt}+\varphi_{12}\cdot\tau_{zx,u,Q}\right)\cdot A_{b,*,cir,ad}+$$
$$+\left(\varphi_{14}\cdot\tau_{zx,u,Mt}-\varphi_{12}\cdot\tau_{zx,u,Q}\right)\cdot A_{b,**,cir,ad}+Z_{b,k}\cdot A_{b,k,core}. \quad (62)$$

Here $Z_{b,k}$ – the projection of the components of stresses in the spatial section on the *z*-axis; $\varphi_{7,lef}$, $\varphi_{7,rig}$ – parameters that take into account the components of the "nagel" effect in the reinforcement (at each step they are taken as constants and determined based on the second – level model); Q – the transverse force in the section from the support to the k-k section.

For the midpoint (b_k) of a polyline spatial section k on the zone l_2 we can write:

$$Z_{b,k}=\left(\varphi_{12}\cdot\tau_{zx,u,Q}\pm\varphi_{14}\cdot\tau_{zx,u,Mt}\right)\cdot\frac{\sqrt{2}}{2}+$$
$$+\left(\varphi_{9}\cdot\tau_{zy,u,Q}\pm\varphi_{11}\cdot\tau_{zy,u,Mt}\right)\cdot\frac{\sqrt{2}}{2}. \quad (63)$$

Substituting in the formula (63) tangential stress $\tau_{zx,ad,Q}$ instead of $\tau_{zx,u,Q}$, $\tau_{zx,ad,Mt}$ instead of $\tau_{zx,u,Mt}$, $\tau_{zy,ad,Q}$ instead of $\tau_{zy,u,Q}$ and $\tau_{zy,ad,Mt}$ instead of $\tau_{zy,u,Mt}$ and using the dependencies $\tau_{zx,ad,Q}=\tau_{zx,u,Q}-\tau_{zx,crc,Q}$; $\tau_{zx,ad,Mt}=\tau_{zx,u,Mt}-\tau_{zx,crc,Mt}$; $\tau_{zy,ad,Q}=\tau_{zy,u,Q}-\tau_{zy,crc,Q}$; $\tau_{zy,ad,Mt}=\tau_{zy,u,Mt}-\tau_{zy,crc,Mt}$ the unknown $q_{sw,rig}$ - the linear force in the clamps on the right side of the section is determined from equation (62).

The linear force in the clamps on the left side of the section ($q_{sw,lef}$) can be found from the relation:

$$q_{sw,lef}=q_{sw,rig}-\bar{\eta}_{11,*}\cdot\tau_{Q}; \quad (64)$$

Here $\bar{\eta}_{11,*}=\bar{\eta}_{11}\cdot b$ – is a coefficient that takes into account the projection lengths of inclined cracks on the left and right faces are approximately the same, i.e. $c_1\approx c_2$, but $\pm\tau_Q$.

In this case, for the running force in the clamps, the condition must be met:

$$\frac{n\cdot R_{bt}\cdot A_{sw}}{u_s}\le q_{sw,lef}\le\frac{0.8\cdot R_{sw}\cdot A_{sw}}{u_s}-\bar{\eta}_{11}\cdot\tau_{Q}. \quad (65)$$

Here:

$$\sigma_{sw}=\frac{E_{sw}}{E_b}\cdot\sigma_{bt}=n\cdot R_{bt};\quad \frac{n\cdot R_{bt}\cdot A_{sw}}{u_s}=q_{sw,lef,\min}; \quad (66)$$
$$\eta_{11}\cdot\tau_{Q}=\bar{\psi}_{Q}\cdot\tau_{pl,u}=\bar{\psi}_{Q}\cdot R_{ch}\left(\frac{c}{h_0}\right);$$
$$\eta_{11}=\frac{\bar{\psi}_{Q}\cdot R_{ch}\left(\frac{c}{h_0}\right)}{\tau_{Q}}. \quad (67)$$

The sum of the moments of internal and external forces in the transverse plane relative to the *x*-axis passing through the point of application of the resultant forces b_k in the compressed zone is zero ($\sum T_{b,k}=0$, see block *II,* Figure 2):

$$M_t=\mathrm{R_{sup}}\cdot\eta_{hor,b}+\mathrm{K_T}\cdot\eta\cdot R_{\sup}\cdot a_m(c)=$$
$$=\mathrm{R_{sup}}\left(\eta_{hor,b}+\mathrm{K_T}\cdot\eta\cdot a_m(c)\right)=$$
$$=-q_{sw,\sigma}\sqrt{l_2^2+4R^2}\cdot\left(h_0-0{,}5x_{B,k}\right)-$$
$$-q_{sw,\mathrm{rig}}\cdot\frac{h}{tg\alpha}\cdot\left(0{,}5b-\eta_{hor,b}\cdot 2R\right)+$$
$$+q_{sw,lef}\,\eta_q\cdot\frac{h}{tg\alpha_0}\cdot\left(R+\eta_{hor,b}\cdot 2R\right)+$$
$$+\eta_{hor,b}\cdot b\cdot\varphi_{7,*}\mathrm{R}_s\sum\omega_{*,cir}A_s-$$
$$-\left(h_0-0{,}5x_{B,k}\right)\cdot\varphi_{8,*}R_s\sum\omega_{*,cir}A_s+$$
$$-\left(0{,}5b+\eta_{hor,b}\cdot b\right)\cdot\varphi_{7,*,\mathrm{lef}}R_s\cdot\sum\omega_{lef,*,cir}A_{s,lef}-$$
$$-\left(\mathrm{h}_0-x_{B,k}-a_{s,i,\mathrm{lef}}\right)\cdot\varphi_{8,*,\mathrm{lef}}R_s\sum\omega_{lef,*,cir}A_{s,lef}-$$

$$-\left(0,5b-\eta_{hor,b}\cdot b\right)\cdot\varphi_{7,*,\text{rig}}R_s\sum\omega_{rig,*,cir}A_{s,rig}$$
$$-\left(\text{h}_0-x_{B,k}-a_{s,i,rig}\right)\cdot\varphi_{8,*,\text{rig}}R_s\sum\omega_{rig,cir}A_{s,rig}-$$
$$-\text{R}_{\text{sup}}\cdot\eta_{hor,b}+\left(\varphi_{11}\tau_{yz,u,Mt}+\varphi_9\tau_{yz,u,Q}\right)$$
$$\cdot A_{b,l_1}\cdot\left[R-\eta_{hor,b}\cdot 2R-2a'_{sc}\right]+$$
$$+\left(\pm\varphi_{11}\tau_{yz,u,Mt}+\varphi_9\tau_{yz,u,Q}\right)\cdot A_{b,l_2}\cdot\left(R-2a'_{sc}\right)+$$
$$+\left(\varphi_{11}\tau_{yz,u,Mt}-\varphi_9\tau_{yz,u,Q}\right)\cdot A_{b,l_3}\cdot\left[R+\eta_{hor,b}\cdot 2R-2a'_{sc}\right]+$$
$$+\left(\varphi_{14}\cdot\tau_{yx,u,Mt}+\varphi_{12}\cdot\tau_{yx,u,Q}\right)\cdot A_{b,*,cir}\cdot\left[R-\right.$$
$$\left.-\eta_{hor,b}\cdot 2R-a'_{sc}\right]+\left(\varphi_{14}\cdot\tau_{yx,u,Mt}-\right.$$
$$\left.-\varphi_{12}\cdot\tau_{yx,u,Q}\right)\cdot A_{b,**,cir}\cdot\left[R+\eta_{hor,b}\cdot 2R-a'_{sc}\right]+$$
$$+\left(\varphi_{11}\tau_{yz,u,Mt}+\varphi_9\tau_{yz,u,Q}\right)\cdot A_{b,l_1,ad}\cdot\left[R-\right.$$
$$\left.-\eta_{hor,b}\cdot 2R-2a'_{sc}\right]+\left(\pm\varphi_{11}\tau_{yz,u,Mt}+\right.$$
$$\left.+\varphi_9\tau_{yz,u,Q}\right)\cdot A_{b,l_2,ad}\cdot\left(R-2a'_{sc}\right)+$$
$$+\left(\varphi_{11}\tau_{yz,u,Mt}-\varphi_9\tau_{yz,u,Q}\right)\cdot A_{b,l_3,ad}\cdot\left[R+\right.$$
$$\left.+\eta_{hor,b}\cdot 2R-2a'_{sc}\right]+\left[\varphi_{14}\cdot\tau_{yx,u,Mt}+\right.$$
$$\left.+\varphi_{12}\cdot\tau_{yx,u,Q}\right]\cdot A_{b,*,cir,ad}\cdot\left[R-\eta_{hor,b}\cdot 2R-a'_{sc}\right]+$$
$$+\left(\varphi_{14}\cdot\tau_{yx,u,Mt}-\varphi_{12}\cdot\tau_{yx,u,Q}\right)\cdot A_{b,**,cir,ad}\cdot\left[R+\right.$$
$$\left.+\eta_{hor,b}\cdot 2R-a'_{sc}\right]+Y_{b,k}\cdot A_{b,k,core}\cdot h_i=0\quad(68)$$

Here K_T,– is a numerical coefficient that takes into account the peculiarity of the static loading scheme in terms of additional torques along the length of the structure; $\text{K}_{\text{pr,T}}$ – a coefficient that takes into account the relations between R_{sup} and T; $\phi_{7,\text{lef}}$, $\phi_{7,rig}$, $\phi_{8,\text{lef}}$, $\phi_{8,rig}$, – parameters that take into account the components of the "nagel" effect in the reinforcement. At each iteration step, these parameters are taken into account as constants and determined using the second-level model; $\eta_{hor,b,lef}$ – the distance between the center b_k (the longitudinal axis of the beam) and the point b_{lef} (see Figure 2, left part of the plot); α_0 – the angle of inclination of the middle section of the compressed concrete zone to the horizontal plane. The value of this angle, based on experimental data, can be assumed to be 45^0 in the first approximation. The torque moment M_t can be expressed in terms of the bending moment using a relative parameter η taking into account the coefficient value K_T:

$$M_t=\eta\cdot M_{bend}.$$

The total torque moment M_t can be written as the sum of the torque moment expressed in terms of bending and the torque from the reaction of the support and the eccentricity of its application $\eta_{hor,b}$:

$$M_t=\text{R}_{\text{sup}}\cdot\eta_{hor,b}+\text{K}_\text{T}\cdot\eta\cdot R_{\text{sup}}\cdot a_m(c)=$$
$$=\text{R}_{\text{sup}}\left(\eta_{hor,b}+\text{K}_\text{T}\cdot\eta\cdot a_m(c)\right);$$

ω – filling ratio plot shear stresses in torsion in the compressed concrete in accounting for elastic-plastic work; $q_{sw,T}$ – linear stress to the clips that occur at the sides of the reinforced concrete element from the torque T (see figure 2); $q_{sw,\sigma}$ – linear stress to the clips that occurs on the bottom face of the concrete element from the torque T; h_i – shoulder from point b_k to the center of gravity of the cross-section area $(x_k-x_{B,k})\cdot\sqrt{l_2^2+b^2}$ at the zone l_2; $Y_{b,k}$ – projection components of the stresses in the broken section on the y-axis. For the midpoint (b_k) of the polyline section k on the section l_2, by analogy with (63), we can write:

$$Y_{b,k}=\varphi_9\cdot\tau_{zy,u,Q}\cdot\frac{\sqrt{2}}{2}\pm\varphi_{13}\cdot\tau_{yx,u,Mt}\cdot\frac{\sqrt{2}}{2}.\quad(69)$$

Substituting in (69) the tangent stress $\tau_{zy,ad,Q}$ instead of $\tau_{zy,u,Q}$, and $\tau_{yx,ad,Mt}$ instead of $\tau_{yx,u,Mt}$, and using the dependencies $\tau_{zy,ad,Q}=\tau_{zy,u,Q}-\tau_{zy,crc,Q}$;

$\tau_{yx,ad,Mt} = \tau_{yx,u,Mt} - \tau_{yx,crc,Mt}$ from the equation (68) the unknown M_t is found.

The sum of the projections of all forces acting in the spatial section ***k*** on the *y*-axis is zero ($\sum Y$=0, block *II,* see figure 2):

$$q_{sw,\sigma} = \frac{1}{\sqrt{l_2^2 + 4R^2}} \cdot \Big[-\varphi_{8,*,\text{rig}} R_s \sum \omega_{rig,cir} A_{s,rig} - \\ -\varphi_{8,*,\text{lef}} R_s \sum \omega_{lef,cir} A_{s,lef} - \varphi_{8,*} \cdot R_s \sum \omega_* A_s + \\ +\varphi_{13} \cdot \tau_{yx,u,Mt} \cdot A_{b,*} + \varphi_{13} \cdot \tau_{yx,u,Mt} \cdot A_{b,**} + \\ +Y_{b,k} \cdot x_{B,k} \cdot \sqrt{l_2^2 + b^2} + \varphi_{13} \cdot \tau_{yx,u,Mt} \cdot A_{b,*,ad} + \\ +\varphi_{13} \cdot \tau_{yx,u,Mt} \cdot A_{b,**,ad} + Y_{b,k} \cdot A_{b,k,x_B} + Y_{b,k} \cdot A_{b,k,core} \Big]. \quad (70)$$

Here ϕ_{8*} – is a parameter that takes into account the components of the "nagel" effect in the armature, which is taken as a constant at each iteration step and is determined using the second-level model [12,14,15].

From the equation (70) the unknown $q_{sw,\sigma}$ is found.

When composing a function of many variables, it is taken into account that $A_b = \phi(x)$, $a_{\text{m,S}} = \phi(c)$, $a_{\text{m,b}} = \phi(c)$, $a = const$, $c_\alpha = const$; $\sigma_{b,u} = \text{const}$; $\sigma_{b,\text{I}}$ is an unknown quantity, and the value $M_k = \text{const}$. The moment $M_I = f(c)$.

Transition coefficients ϕ_{10} etc. calculated iteratively, they are discrete constants at each step.

The functions $f(x,y,z)$ of the diagonal large ellipse of the considered construction of a circular cross-section (with a smaller diagonal $b = R$ and a larger diagonal $a = l_1(c) + l_2 + l_3(c)$ can be written:

$$\frac{y^2}{(2l(c) + R\sqrt{2})^2} + \frac{z^2}{R^2} = 1. \quad (71)$$

Here $l_2 = R\sqrt{2}$; $a = l(c) + R\sqrt{2} + l(c) = 2l(c) + R\sqrt{2}$.

From this equation we get:

$$l(c) = \frac{-R\sqrt{2}}{2} + \sqrt{\frac{R^2}{2} + \frac{y^2 R^2}{4(R^2 - z^2)}}. \quad (72)$$

Then the projection of the spatial crack on the horizontal axis is determined from the expression:

$$c = l_1(c) + l_2 + l_3(c) = 2\sqrt{\frac{R^2}{2} + \frac{y^2 R^2}{4(R^2 - z^2)}} \le R \cdot 3\sqrt{2}. \quad (73)$$

Here $l_1(c) = l_3(c) = d\cos\alpha = d \cdot \cos 45° = d\frac{\sqrt{2}}{2}$;

$a = d\frac{\sqrt{2}}{2} + R\sqrt{2} + d\frac{\sqrt{2}}{2} = R \cdot 3\sqrt{2}$.

CONCLUSION

1. A calculated model and a beam calculated scheme are proposed for analyzing the complex limiting resistance of a reinforced concrete structure from the action of bending with torsion, taking into account the spatial nature of cracks in reinforced concrete elements of circular cross-section.

2. For the calculated forces, the resolving equations of equilibrium and the equations of deformations are compiled. In the considered calculated sections I–I and III–III, unknown components of the torque, height, and area of the compressed zone of concrete for an element of a circular cross-section are obtained. Similarly, using the equilibrium equations and strain equations for the spatial section k passing along the surface of the spatial crack, the components of the torque, the height of the compressed concrete zone, deformations and stresses in the reinforcement for the left and right parts of the section under consideration, and the load intensity in the clamps are obtained.

3. In the spatial section k, cut off by a spiral-shaped spatial crack, all the reinforcement intersected by this section is taken into account. The use of a complex broken section of a compressed concrete zone for practical calculations was due to the fact that cracking and destruction occurred in a certain volume according to linear dependencies at an angle close to the middle part of the broken section, where the maximum stress-strain state is reached.
4. In the area of the stretched zone of the spatial crack of a reinforced concrete round rod, the right and left contours of the longitudinal stretched working reinforcement and clamps are highlighted. The calculation scheme also takes into account the "nagel" effect in the stretched longitudinal and transverse reinforcement falling into this spatial section, the parameters of which are determined using a special model of the second level.
5. The static scheme of loading of a reinforced concrete element during bending with torsion was considered from the positions of the proportional ratio between the torques (the coefficient from the reaction of the support R_{sup}) along the length of the rod in the spatial section k and in the cross-sections (first and third).

REFERENCES

1. **Bondarenko V.M.** Computational models of the strength resistance of reinforced concrete. / V.M. Bondarenko, V.I. Kolchunov. – M .: ACB, 2004. – 472 p.
2. **Golyshev A. B.** Resistance of reinforced concrete / A. B. Golyshev, V. I. Kolchunov. – K .: Osnova, 2009 .- 432 p.
3. **Travush V.I., Karpenko N.I., Kolchunov Vl. I., Kaprielov S.S., Demyanov A.I., Bulkin S.A., Moskovtseva V.S.** Results of experimental studies of high-strength fiber reinforced concrete beams with round cross-sections under combined bending and torsion// Structural Mechanics of Engineering Constructions and Buildings 2020 –Vol.16 (4). pp. 290-297.
4. **Adheena Thomas, Afia S Hameed.** An Experimental Study On Combined Flexural And Torsional Behaviour Of RC Beams. *International Research Journal of Engineering and Technology*. 2017. Vol. 04. Issue 05. Pp. 1367–1370.
5. **Khaldoun Rahal.** Combined Torsion and Bending in Reinforced and Prestressed Concrete beams Using Simplified Method for Combined Stress-Resultants. *ACI Structural Journal*. 2007. Vol. 104. No. 4. pp. 402–411.
6. **Kolchunov Vl.I., Fedorov V.S.** Conceptual hierarchy of models in the theory of resistance of building structures // Industrial and civil engineering. 2020 –№8 – P. 16-23.
7. **C. Kim, S. Kim, K.-H. Kim, D. Shin, M. Haroon, J.-Y. Lee**. Torsional Behavior of Reinforced Concrete Beams with High-Strength Steel Bars. 2019. Structural Journal. Vol. 116, pp. 251–233.
8. **Kandekar, S.B., Talikoti, R.S.** Study of torsional behavior of reinforced concrete beams strengthened with aramid fiber strips. International Journal of Advanced Structural Engineering. 2018. Vol. 10, pp. 465–474. doi: 10.1007/s40091-018-0208-y.
9. **Křístek, V., Průša, J., Vítek, J.L.**: Torsion of Reinforced Concrete Structural Members. Solid State Phenom. 2018. Vol. 272, pp. 178–184. doi:10.4028/www.scientific.net/SSP.272.178.
10. **Santhakumar R., Dhanaraj R., Chandrasekaran E.** Behaviour of retrofitted reinforced concrete beams under combined bending and torsion: A numerical study. Electronic Journal of Structural Engineering. 2007. No. 7. pp. 1–7.
11. **Ilker Kalkan, Saruhan Kartal.** Torsional Rigidities of Reinforced Concrete Beams Subjected to Elastic Lateral Torsional Buckling. International Journal of Civil and Environmental Engineering. 2017. Vol. 11. No.7. Pp. 969–972.

12. **Salnikov A., Kolchunov Vl., Yakovenko I.** The computational model of spatial formation of cracks in reinforced concrete constructions in torsion with bending (2015), Applied Mechanics and Materials Vols. 725-726 (2015) pp. 784–789.
13. **Iakovenko I., Kolchunov Vl.** (2017). The development of fracture mechanics hypotheses applicable to the calculation of reinforced concrete structures for the second group of limit states. Journal of Applied Engineering Science, Vol. 15(2017)3, article 455, pp. 366–375. (In English) doi:10.5937/jaes15-14662
14. **Demyanov A.I.** Development of a universal short two-console element to the resistance of reinforced concrete structures during torsion with bending / A.I. Demyanov Vl. I. Kolchunov, I. A. Yakovenko // Izvestiya VUZov. Textile industry technology. 2017. No. 4 (367). – pp. 258–263.
15 **Bernardo, L.** Modeling the Full Behavior of Reinforced Concrete Flanged Beams under Torsion. Applied Sciences. 2019. Vol. 9. doi:10.3390/app9132730.
16. **Pettersen J. S.** Non-Linear Finite Element Analyses of Reinforced Concrete with Large Scale Elements: Including a Case Study of a Structural Wall. Norwegian University of Science and Technology, 2014. 85 p.
17. **Nahvi H., Jabbari M.** Crack detection in beams using experimental modal data and finite element model. International Journal of Mechanical Sciences. 2005. Vol. 47. pp.1477–1497.
18. **Demyanov A., Kolchunov Vl.** The dynamic loading in longitudinal and transverse reinforcement at instant emergence of the spatial crack in reinforced concrete element under the action of a torsion with bending. Journal of Applied Engineering Science, vol. 15(2017)3, article 456, pp. 375–380. (In English) doi:10.5937/jaes15-14663
19. **Vishnu H. Jariwalaa, Paresh V. Patel, Sharadkumar P. Purohit.** Strengthening of RC Beams subjected to Combined Torsion and Bending with GFRP Composites. Procedia Engineering. 2013. Vol. 51. Pp. 282–289.
20. **Tsai H.-C., Liao M.-C.** Modeling Torsional Strength of Reinforced Concrete Beams using Genetic Programming Polynomials with Building Codes. 2019. KSCE Journal of Civil Engineering. Vol. 23, pp. 3464–3475 (2019). doi:/10.1007/s12205-019-1292-7.
21. **Arzamastsev S.A., Rodevich V.V.** To the calculation of reinforced concrete elements for bending with torsion. Izvestiya vysshikh uchebnykh zavod. Construction, 2015 –№9 - pp. 99-109.
22. **Karpyuk, V.M., Kostyuk, A.I., Semina, Y.A.** General Case of Nonlinear Deformation-Strength Model of Reinforced Concrete Structures. Strength Mater. 2018. Vol. 50, pp. 453–454. doi:10.1007/s11223-018-9990-9.
23. **Jan L. Vítek Jaroslav Průša, Vladimír Křístek, L.B.** Torsion of Rectangular Concrete Sections. ACI Symposium Publication. 2020. Vol. 344, pp. 111–130.
24 **Rahal, K.N.** Torsional strength of reinforced concrete beams. Canadian Journal of Civil Engineering. 2000. Vol. 27, pp. 445–453. doi:10.1139/cjce-27-3-445.
25. **Lin, W.** Experimental investigation on composite beams under combined negative bending and torsional moments. Advances in Structural Engineering. 2020. Vol. 24, pp. 1456–1465. doi:10.1177/1369433220981660.

СПИСОК ЛИТЕРАТУРЫ

1. **Бондаренко В.М.** Расчетные модели силового сопротивления железобетона. / В.М. Бондаренко, В.И. Колчунов. – М.: АСВ, 2004. – 472 с.

2. **Голышев А. Б.** Сопротивление железобетона / А. Б. Голышев, В. И. Колчунов. – К.: Основа, 2009. – 432 с.
3. **Травуш В.И., Карпенко Н.И, Колчунов Вл. И., Каприелов С.С., Демьянов А.И., Булкин С.А., Московцева В.С.** Результаты экспериментальных исследований сложно-напряженных балок круглого поперечного сечения из высокопрочного фиброжелезобетона // Строительная механика инженерных конструкций и сооружений. 2020 –т.16 – №4 – С. 290-297.
4. **Adheena Thomas, Afia S Hameed.** An Experimental Study On Combined Flexural And Torsional Behaviour Of RC Beams. *International Research Journal of Engineering and Technology*. 2017. Vol. 04. Issue 05. Pp. 1367–1370.
5. **Khaldoun Rahal.** Combined Torsion and Bending in Reinforced and Prestressed Concrete beams Using Simplified Method for Combined Stress-Resultants. *ACI Structural Journal*. 2007. Vol. 104. No. 4. pp. 402–411.
6. **Колчунов Вл.И., Федоров В.С.** Понятийная иерархия в теории сопротивления строительных конструкций // Промышленное и гражданское строительство. 2020 – №8 – с. 16-23.
7. **C. Kim, S. Kim, K.-H. Kim, D. Shin, M. Haroon, J.-Y. Lee**. Torsional Behavior of Reinforced Concrete Beams with High-Strength Steel Bars. 2019. Structural Journal. Vol. 116, pp. 251–233.
8. **Kandekar, S.B., Talikoti, R.S.** Study of torsional behavior of reinforced concrete beams strengthened with aramid fiber strips. International Journal of Advanced Structural Engineering. 2018. Vol. 10, pp. 465–474. doi: 10.1007/s40091-018-0208-y.
9. **Křístek, V., Průša, J., Vítek, J.L.**: Torsion of Reinforced Concrete Structural Members. Solid State Phenom. 2018. Vol. 272, pp. 178–184. doi:10.4028/www.scientific.net/SSP.272.178.
10. **Santhakumar R., Dhanaraj R., Chandrasekaran E.** Behaviour of retrofitted reinforced concrete beams under combined bending and torsion: A numerical study. Electronic Journal of Structural Engineering. 2007. No. 7. pp. 1–7.
11. **Ilker Kalkan, Saruhan Kartal.** Torsional Rigidities of Reinforced Concrete Beams Subjected to Elastic Lateral Torsional Buckling. International Journal of Civil and Environmental Engineering. 2017. Vol. 11. No.7. Pp. 969–972.
12. **Salnikov A., Kolchunov Vl., Yakovenko I.** The computational model of spatial formation of cracks in reinforced concrete constructions in torsion with bending (2015), Applied Mechanics and Materials Vols. 725-726 (2015) pp. 784–789.
13. **Iakovenko I., Kolchunov Vl.** (2017). The development of fracture mechanics hypotheses applicable to the calculation of reinforced concrete structures for the second group of limit states. Journal of Applied Engineering Science, Vol. 15(2017)3, article 455, pp. 366–375. (In English) doi:10.5937/jaes15-14662
14. **Демьянов А.И.** Разработка универсального короткого двух-консольного элемента к сопротивлению железобетонных конструкций при кручении с изгибом / А.И. Демьянов Вл. И. Колчунов, И. А. Яковенко // Известия ВУЗов. Технология текстильной промышленности. – 2017. №4(367). – С. 258–263.
15 **Bernardo, L.** Modeling the Full Behavior of Reinforced Concrete Flanged Beams under Torsion. Applied Sciences. 2019. Vol. 9. doi:10.3390/app9132730.
16. **Pettersen J. S.** Non-Linear Finite Element Analyses of Reinforced Concrete with Large Scale Elements : Including a Case Study of a Structural Wall. Norwegian University of Science and Technology, 2014. 85 p.

17. **Nahvi H., Jabbari M.** Crack detection in beams using experimental modal data and finite element model. International Journal of Mechanical Sciences. 2005. Vol. 47. pp.1477–1497.
18. **Demyanov A., Kolchunov Vl.** The dynamic loading in longitudinal and transverse reinforcement at instant emergence of the spatial crack in reinforced concrete element under the action of a torsion with bending. Journal of Applied Engineering Science, vol. 15(2017)3, article 456, pp. 375–380. (In English) doi:10.5937/jaes15-14663
19. **Vishnu H. Jariwalaa, Paresh V. Patel, Sharadkumar P. Purohit.** Strengthening of RC Beams subjected to Combined Torsion and Bending with GFRP Composites. Procedia Engineering. 2013. Vol. 51. Pp. 282–289.
20. **Tsai H.-C., Liao M.-C.** Modeling Torsional Strength of Reinforced Concrete Beams using Genetic Programming Polynomials with Building Codes. 2019. KSCE Journal of Civil Engineering. Vol. 23, pp. 3464–3475 (2019). doi:/10.1007/s12205-019-1292-7.
21. **Арзамасцев С.А., Родевич В.В.** К расчету железобетонных элементов на изгиб с кручением // Известия высших учебных заведений. Строительство, 2015 –№9 – с. 99-109.
22. **Karpyuk, V.M., Kostyuk, A.I., Semina, Y.A.** General Case of Nonlinear Deformation-Strength Model of Reinforced Concrete Structures. Strength Mater. 2018. Vol. 50, pp. 453–454. doi:10.1007/s11223-018-9990-9.
23. **Jan L. Vítek Jaroslav Průša, Vladimír Křístek, L.B.** Torsion of Rectangular Concrete Sections. ACI Symposium Publication. 2020. Vol. 344, pp. 111–130.
24 **Rahal, K.N.** Torsional strength of reinforced concrete beams. Canadian Journal of Civil Engineering. 2000. Vol. 27, pp. 445–453. doi:10.1139/cjce-27-3-445.
25. **Lin, W.** Experimental investigation on composite beams under combined negative bending and torsional moments. Advances in Structural Engineering. 2020. Vol. 24, pp. 1456–1465. doi:10.1177/1369433220981660.

Vladimir I. Kolchunov, Dr.Sc., Professor, Department of unique building and structures, South-Western State University, 94, 50 let Oktyabrya street, Kursk, 305040,Russia phone: +7 (910) 317-93-55; e-mail: vlik52@mail.ru

Bulkin S. Aleksandrovich, Chief Design Specialist of Urban planning institute of residential and public buildings (GORPROJECT), 105005, Russia, Moscow, Nizhny Susalny lane, 5, building 5A

Колчунов Владимир Иванович, доктор технических наук, профессор кафедры «Уникальные здания и сооружения», Юго-Западный государственный университет; 305040, Россия, г. Курск, ул. 50 лет Октября, дом 94; тел .: +7 (910) 317-93-55; e-mail: vlik52@mail.ru

Булкин Сергей Александрович, главный специалист-конструктор ЗАО «Городской проектный институт жилых и общественных зданий», Россия, 105005, Россия, г. Москва, Нижний Сусальный пер., 5, стр. 5А

International Journal for Computational Civil and Structural Engineering, 17(3) 83–93 (2021)

DOI:10.22337/2587-9618-2021-17-3-83-93

GEOMETRIC REPRESENTATIONS OF EQUILIBRIUM CURVES OF A COMPRESSED STIFFENED PLATE

Gaik A. Manuylov, Sergey B. Kosytsyn, Irina E. Grudtsyna

Russian University of Transport (RUT - MIIT), Moscow, RUSSIA

Abstract: The work is aimed at studying the solutions of the stability problem (subcritical and postcritical equilibrium) of an infinitely wide regular compressed reinforced plate, using a selected T-shaped fragment that is equally stable with others. The authors have given a classification of possible analytical solutions for these plates. The results of the work are presented in the form of variants of spatial bifurcation diagrams, values of critical loads, as well as coordinates of singular points for different cases of solutions.

Keywords: stability, stiffened plate, post-critical equilibrium, critical load, bifurcation curve

ГЕОМЕТРИЧЕСКИЕ ПРЕДСТАВЛЕНИЯ КРИВЫХ РАВНОВЕСИЯ СЖАТОЙ ПОДКРЕПЛЕННОЙ ПЛАСТИНЫ

Г.А. Мануйлов, С.Б. Косицын, И.Е. Грудцына

Российский университет транспорта (МИИТ), г. Москва, РОССИЯ

Аннотация: работа направлена на исследование решений задачи устойчивости (докритического и послекритического равновесия) бесконечно широкой регулярной сжатой подкрепленной пластины, при помощи выделенного, равноустойчивого с другими Т-образного фрагмента. Авторами дана классификация возможных аналитических решений для данных пластин. Результаты работы представлены в виде вариантов пространственных бифуркационных диаграмм, значений критических нагрузок, а также координат сингулярных точек для различных случаев решений.

Ключевые слова: устойчивость, подкрепленная пластина, послекритическое равновесие, критическая нагрузка, бифуркационная кривая

1. INTRODUCTION

Algorithms for solving the problem of stability of reinforced plates have been described by a fairly large number of authors, starting from the 50s of the twentieth century [1,3,5,7,10,11]. However, the main and extremely important research factor that unites all works on this topic is the interaction of its own forms (general and local forms of loss of stability). It is the interaction of forms that affects the bearing capacity of the reinforced plate, significantly reducing it in a number of cases. In this article, for the first time, a qualitative study of post-critical equilibria is presented, and a laconic classification of possible solutions presented in the form of spatial bifurcation diagrams is given.

2. PROBLEM FORMULATION

An infinitely wide reinforced plate is considered. Physical characteristics of the material:

$$E=2\cdot10^6 kg/cm^2,\ \mu = 0.3.$$

Boundary conditions: the plate is hinged-supported at the ends, the longitudinal edges are free. Figure 1 shows a cross-section of a reinforced plate with corresponding dimensions.

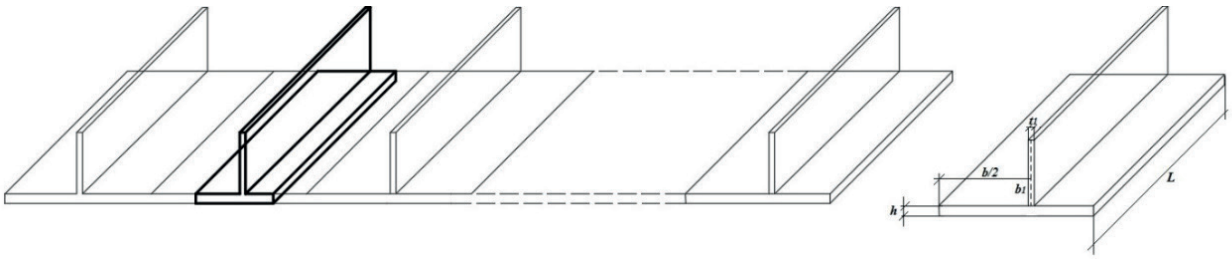

Figure 1. The plate cross section

Here b – is the distance between the ribs in the axes, h - is the thickness of the plate,
b_1 – is the height of the rib, t_1 – is the thickness of the rib, L – is the length of the reinforced plate.
Let us analyze the equilibrium of one T-shaped fragment of the reinforced plate, which is equally stable with the others. Boundary conditions for it: hinged support along the short sides, along the longitudinal edges, fastening of the movable termination type (Figure 2). A compressive force is applied at the center of gravity of the section.

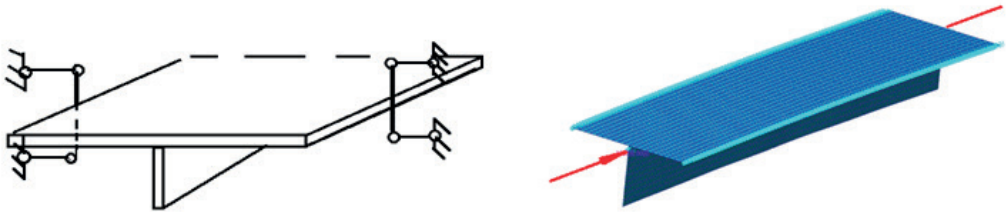

Figure 2. Conditions for fixing and finite-element model of the T-shaped fragment

3. CLASSIFICATION OF POSSIBLE SOLUTIONS

A reinforced plate is an example of an asymmetrical structure that consists of elements: a plate (sheathing) and reinforcing ribs. This design has several forms of buckling:

- the general shape, which is a half-wave of a sinusoid, which is close to the bulge shape of a wide Euler strut;
- local forms of wave formation.

Under central compression, a general deflection develops towards a more rigid element, i.e. if the reinforcing ribs are weaker in relation to the plate, then the deflection develops on the side of the plate, so that the ribs turn out to be on the concave side (Figure 3a). If the plate is conditionally "weak", then the edges turn out to be on the convex side (Figure 3b). Thus, the general form of buckling is characterized by the deflection direction.

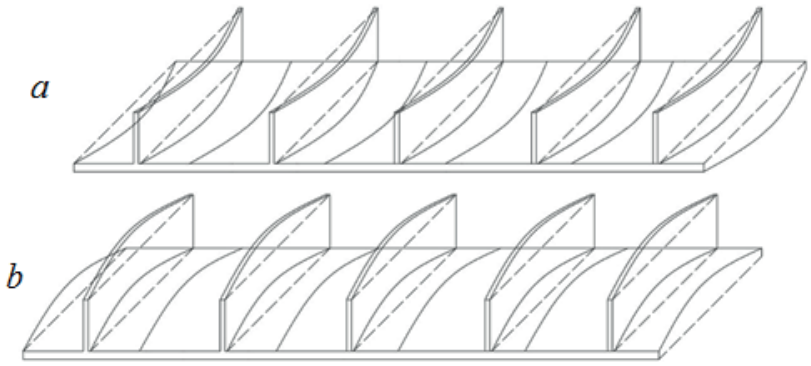

Figure 3. Two main types of general form of buckling

Considering the internal forces arising from the compression of the reinforced plate, it can be concluded that along with the compressive force, due to the inevitable small eccentricities, an internal bending moment also appears, and the more the deflection increases, the more the influence of this moment is manifested. In the usual understanding of the linear stability problem, any structure has linearly independent (orthogonal), and therefore independent from each other forms, they can be observed when solving buckling in any finite element complex. However, the nonlinear solution shows that the general shape with increasing deflection sooner or later generates a new one - wave formation in the plate or reinforcing ribs (Figure 4). Wave formation of the plate is possible when the ribs are in the stretched bending zone, and the plate is in the compressed one. Wave formation in the reinforcing ribs develops in the opposite direction of the general deflection.

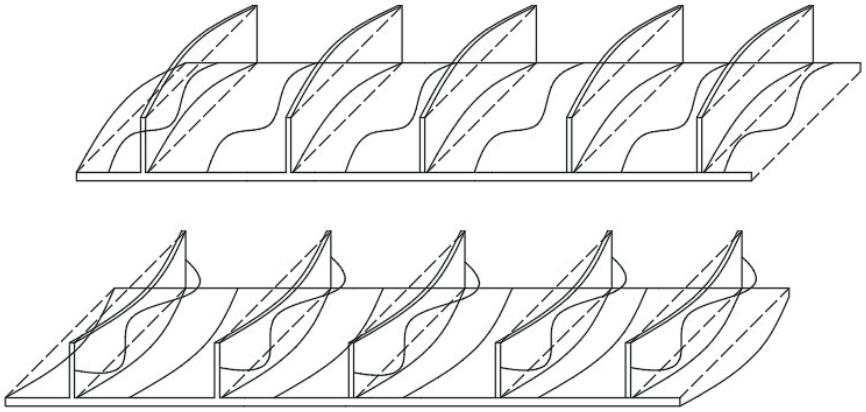

Figure 3. Local forms of buckling in the plate or in the stiffeners

The expression for the total potential energy of a compressed reinforced plate in the case of interaction of two forms of loss of stability (s = 2) has the form:

$$\Pi_э = a_0 + \frac{1}{2}a_1\left(1-\frac{\lambda}{\lambda_1}\right)\xi_1^2 + \frac{1}{2}a_2\left(1-\frac{\lambda}{\lambda_2}\right)\xi_2^2 + \frac{1}{3}a_{111}\xi_1^3 + a_{122}\xi_1\xi_2^2 + \frac{1}{4}a_{1111}\xi_1^4 + \\ + \frac{1}{4}a_{2222}\xi_2^4 + \frac{1}{2}a_{1122}\xi_1^2\xi_2^2 - \frac{\lambda}{\lambda_1}a_1\overline{\xi_1}\xi_1 - \frac{\lambda}{\lambda_2}a_2\overline{\xi_2}\xi_2 \quad (1)$$

where: ξ – are normalized eigenforms (the amplitude of the deviation of the eigenmode relative to the plate thickness;

λ – is the load parameter;

$\overline{\xi_s}$– are imperfections in the s-th form of buckling (s = 1, 2,… ..n).

Coefficients: a_{111} – characterizes the general form of buckling, a_{122} – interaction of forms.

The first variation of the total potential energy for each form gives the equilibrium equations:

$$\left(1-\frac{\lambda}{\lambda_1}\right)\xi_1 + d_1\xi_1^2 + d_2\xi_2^2 = \frac{\lambda}{\lambda_1}\overline{\xi_{1,}} \quad (2)$$

$$\left(1-\frac{\lambda}{\lambda_2}\right)\xi_2 + d_3\xi_1\xi_2 = \frac{\lambda}{\lambda_2}\overline{\xi_2} \quad (3)$$

where: $d_1 = \frac{a_{111}}{a_1}$, $d_2 = \frac{a_{122}}{a_1}$, $d_3 = \frac{2a_{122}}{a_2}$. $\mu_1 = \frac{\lambda}{\lambda_1}$ $\mu_2 = k\,\mu_1$

λ_1 – is the critical load of the linear calculation of the general form of buckling by the type of an Euler strut;
ξ_1 – relative amplitude corresponding to the general shape;
ξ_2 – relative amplitude corresponding to the local form of loss of stability of wave formation (plate or ribs);
λ_2 – waveform load.
The general form of buckling depends only on the direction of the deflection and the corresponding coordinate ξ_1; all solutions for a given form will be called unbound solutions. In this case, any wave formation (in the plate or reinforcing ribs) is absent ($\xi_2 = 0$).
The study of uncoupled solutions is based on considering the equilibrium equations (2) and (3). In the case of an ideal problem (without initial geometric imperfections), the right-hand sides of the equations are zeroed, and under the condition ($\xi_2 = 0$) from (2) we obtain the equation of the straight line of the general deflection:

$$\mu_1 = d_1\xi_1 + 1 \qquad (4)$$

and the expression for the coordinate of this straight line:

$$\xi_1 = -\frac{(1-\mu_1)}{d_1} \qquad (5)$$

The straight line of unbound equilibria is located in the plane $\lambda\xi_1$, the geometric meaning of the coefficient d_1 is expressed in the slope of this straight line. If the coordinate $\xi_1 > 0$, $d_1 < 0$ (always), then μ_1 decreases and vice versa (Figure 5). From equation (5) it follows that at a load $\mu_1 = 1$, (i.e., the compression load is equal to the critical load of the linear calculation), a bifurcation point appears, corresponding to the general form of buckling. The birth of bifurcation points is possible only if the system in subcritical equilibrium has an energy-orthogonal complement, i.e. there is a possibility of the emergence of new force factors, whose influence on the system forms a new form of equilibrium. In this case, the initial subcritical equilibrium is determined by the action of the compressive load. However, in any case, the development of the general deflection of the reinforced plate arises, and at the same time a new force factor appears - the bending moment. If the problem is considered taking into account the initial deflection ($\overline{\xi_1} \neq 0$), then the equation for μ_1 will take a slightly different form (the equation of imperfect curves-hyperbolas tending to a straight line of general deflection):

$$\mu_1 = \frac{\xi_1(d_1\xi_1 + 1)}{\xi_1 + \overline{\xi_1}} \qquad (6)$$

The local form of wave formation arises with the development of a bending moment and compressive stresses in the middle part of the reinforced plate, the action of which provokes a nonlinear system to self-organization (the definition is given by G.A. Manuylov [7]), this means to a change in the form of buckling, therefore the coordinate ξ_2 is a function total deflection, i.e. defines the associated strain.
The coupled solutions are divided into two types:

- bifurcation solutions with ($\overline{\xi_1} \neq 0$) or without the initial deflection ($\overline{\xi_1} = 0$);
- solutions with limit point ($\overline{\xi_1} \neq 0$ и $\overline{\xi_2} \neq 0$).

From equations (2) and (3) with $\xi_2 \neq 0$ and disregarding the initial imperfections ($\overline{\xi_1} = 0$ и $\overline{\xi_2} = 0$) we obtain that:

$$\xi_2 = \mp\xi_1 \sqrt{\frac{d_3\left(1-\frac{\lambda}{\lambda_1}\right)}{d_2\left(1-\frac{\lambda}{\lambda_2}\right)} - \frac{d_1}{d_2}} \qquad (7)$$

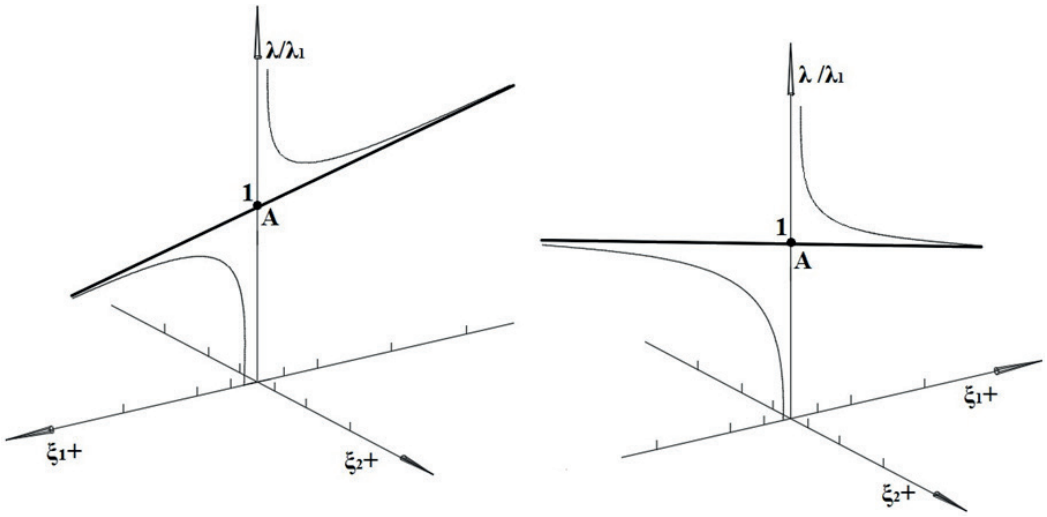

Figure 5. Bifurcation diagrams of unrelated solutions

Equation (7) defines post-bifurcation solutions of coupled equilibria. However, in order to obtain the bifurcation point itself, the condition of equality of the Hessian potential energy to zero is necessary. The Hesse matrix obtained from equations (2) and (3) has the form:

$$H_{\text{п}} = \begin{bmatrix} \left(1 - \frac{\lambda}{\lambda_1}\right) + 2d_1\xi_1 & 2d_2\xi_2 \\ d_3\xi_2 & \left(1 - \frac{\lambda}{\lambda_2}\right) + d_3\xi_1 \end{bmatrix}. \quad (8)$$

In the initial subcritical equilibrium, the waveform amplitude $\xi_2 = 0$, since pure compression is in effect. Equality to zero of determinant (8) is reduced to the condition of equality to zero h_{11} or h_{22}. Of greatest interest is the inversion of the h_{22} matrix (8), since it is related to the second equilibrium equation.

From the condition, $h_{22}(\lambda, d_3, \xi_1) = 0$ we obtain an expression for the coordinate of the deflection ξ_1 at the singular point:

$$\xi_1 = \frac{k\mu_1 - 1}{d_3} \quad (9)$$

Substituting this expression into equation (2), we obtain a quadratic equation to determine the relative bifurcation load:

$$\mu_1^2 (k^2 d_1 - d_3 k) + \mu_1 (d_3 + d_3 k - 2k d_1) + d_1 - d_3 = 0 \quad (10)$$

Equation (10) is common to any related solution; the main role in it is played by the coefficients d_i. The d_1 coefficient is always less than zero, the signs of the d_2 and d_3 coefficients indicate the nature of the wave formation. If $d_2 > 0$ and $d_3 > 0$, then wave formation should be expected in the reinforcing ribs.

Accordingly, if $d_2 < 0$, $d_3 < 0$, then wave formation will appear in the plate (skin). The values of the coefficients *di* (i = 1, 2, 3) are taken from the work of A.I. Manevich [11] for different cases of related solutions. For the case of wave formation in the reinforcing edges, the values of the coefficients are:

$d_1 = -0.009, d_2 = 1.024, d_3 = 0.975,$
$k = \frac{\lambda_1}{\lambda_2} = 1.4852.$

Then equation (10) will take the form:

$$\mu_1^2 - 1.6688\mu_1 + 0.67 = 0 \quad (11)$$

The roots of the equation are the values of the bifurcation load of wave formation in the edges:

$\mu_{1(1)} = 0.6733$ и $\mu_{1(2)} = 0.99558.$

For another plate, in which wave formation occurs in the skin, the values of the coefficients d_i are as follows:

$d_1 = -0.0069, d_2 = -0.503,$
$d_3 = -0.051, k = \frac{\lambda_1}{\lambda_2} = 1.287.$

Equation (10) will take the form:

$$\mu_1^2 - 1.8338\mu_1 + 0.81351 = 0 \quad (12)$$

The values of the bifurcation load of wave formation in the plate:

$\mu_{1(1)} = 1.0459$ и $\mu_{1(2)} = 0.777.$

Figure 6 shows a bifurcation diagram of coupled solutions (waving in reinforcing ribs). Figure 7 is a bifurcation diagram of coupled solutions (wave formation in a plate).

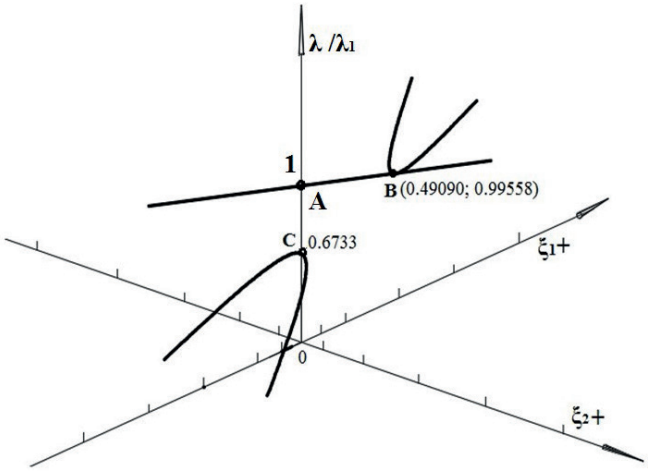

Figure 6. Bifurcation diagrams of related solutions (wave making of the stiffeners)

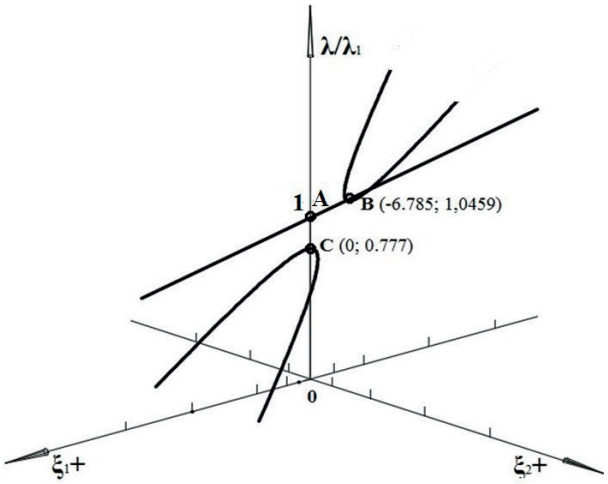

Figure 7. Bifurcation diagrams of related solutions (wave making of the plate)

In diagrams 6 and 7, point A is a bifurcation point in the general shape, B and C are wave formation bifurcations. As can be seen from the diagrams, the critical load of wave formation in both cases is lower than the load corresponding to the shape of the total deflection. This indicates a loss of bearing capacity near the critical waveform load. If the ribs are in the compressed zone and lose stability, then the difference between the critical load of nonlinear and linear calculations can reach up to 60% [7], [11]. If the plate loses its stability, the difference can be in the range of 15% - 30%. All new post-bifurcation coupled solutions are located in planes inclined to the plane $\xi_2 0\lambda$.. All of these solutions are unstable because the Hessian matrix is not positive definite, since $h_{22}(\lambda, d_3, \xi_1) = 0$ not only at the bifurcation point, but also along all curves ξ_2. The case of coupled buckling in the presence of initial deflection has a completely different form. Consider two options for the initial deflection:

- $\overline{\xi_1} = -0.5$ (wave formation in the edges);
- $\overline{\xi_1} = 0.5$ (wave formation in the plate);

$\overline{\xi_1}$ – is the amplitude related to the thickness of the plate (skin). Then the equilibrium equations (2) and (3):

Then the equilibrium equations (2) and (3):

$$\left(1 - \frac{\lambda}{\lambda_1}\right)\xi_1 + d_1\xi_1^2 + d_2\xi_2^2 = \frac{\lambda}{\lambda_1}\overline{\xi_1} \tag{13}$$

$$\left(1 - \frac{\lambda}{\lambda_2}\right)\xi_2 + d_3\xi_1\xi_2 = 0 \tag{14}$$

And equation (10), compiled taking into account the initial imperfections, will be written as follows:

$$\mu_1^2\,(k^2 d_1 - d_3\,k) + \mu_1\left(d_3 + d_3\,k - 2kd_1 - d_3^2\overline{\xi_1}\right) + d_1 - d_3 = 0 \tag{15}$$

The ξ_1 coordinate is calculated in the same way as in the previous cases; however, post-bifurcation solutions will depend on the imperfection amplitude $\overline{\xi_1}$:

$$\xi_2 = \mp\sqrt{\frac{\overline{\xi_1}\mu_1 - d_1\xi_1^2 - (1-\mu_1)\xi_1}{d_2}} \tag{16}$$

Equation (17) corresponding to the negative value of the deflection has the form:

$$\mu_1^2 - 1.9926\mu_1 + 0.67 = 0 \tag{17}$$

The critical loads of wave formation in the ribs have the following values:

$\mu_{1(1)} = 1.564$ и $\mu_{1(2)} = 0.428$

The bifurcation diagram is shown in Figure 8.

As can be seen from this graph, the values of bifurcation loads are lower than in the case of solutions without initial imperfections. The bifurcation points of wave formation B and C appear on unconnected curves of imperfect solutions constructed according to Eq. (6).

In a situation where the deflection of a positive sign (expected wave formation in the plate) develops, the bifurcation diagram turns out to be more complex, since the straight line of the total deflection is inclined with respect to the load axis at an angle less than 90 ° As a result, the curves of unconnected solutions with initial imperfections have two bifurcation points on each branch between which there is one limiting point. From equation (15) with the corresponding signs of the coefficients d_i, we obtain (18):

$$\mu_1^2 - 1.848\mu_1 + 0.81351 = 0 \tag{18}$$

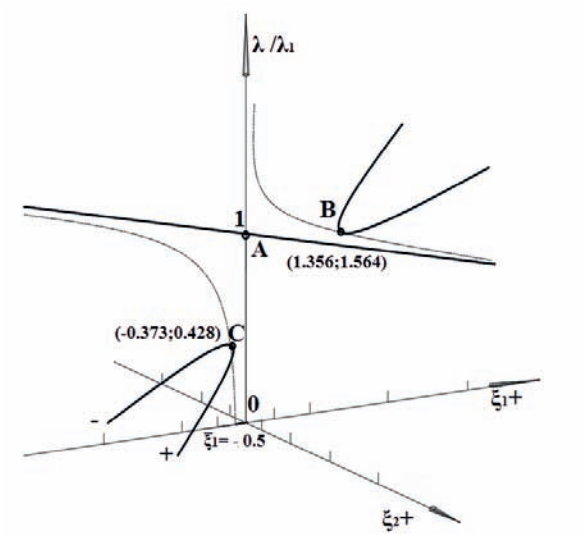

Figure 8. Bifurcation diagrams of related solutions (wave making of the stiffeners, $\overline{\xi_1} = -0.5$*)*

Values of bifurcation loads:

$\mu_{1(1)} = 1.125$ и $\mu_{1(2)} = 0.723$

The coordinates of the bifurcation points are calculated by the formula (19):

$$\xi_1 = -\frac{(1-\mu_1)}{2d_1} \mp \sqrt{\frac{(1-\mu_1)^2}{4d_1^2} + \frac{\mu_1 \overline{\xi_1}}{d_1}} \qquad (19)$$

Equating the discriminant of equation (19) to zero, we determine the load at the limiting points:

$$\mu_1^2 + \left(2 + \overline{\xi_1} 4d_1\right)\mu_1 + 1 = 0 \quad (20)$$

We get: $\mu_{1(1)} = 1.125$ и $\mu_{1(2)} = 0.889$

The coordinates of the limit points when two values of μ_1 are substituted:

$$\xi_{1(1,2)} = -\frac{(1-\mu_1)}{2d_1} \qquad (21)$$

The corresponding bifurcation diagram is shown in Figure 9.

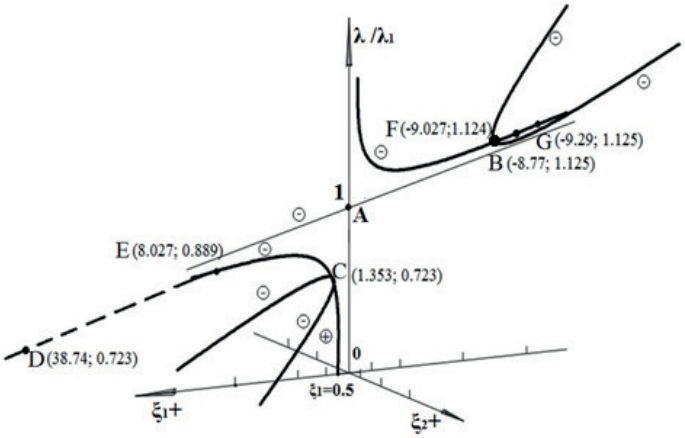

Figure 9. Bifurcation diagrams of related solutions (wave making of the plate, $\overline{\xi_1} = 0.5$*)*

Point B, C, D and G - points of wave formation bifurcation in the plate. Points F and E are limit points. Note that J. Hunt [2] previously predicted the constructed bifurcation diagrams using the example of concrete reinforced plates in general form based on energy considerations. The case of the appearance of limit points on the equilibrium curves is possible if in equations (2) and (3) the right-hand sides are not equal to zero ($\overline{\xi_1} \neq 0, \overline{\xi_2} \neq 0$). One of the options for determining the critical loads and the coordinates of the limit points is to solve the fourth-degree equation with respect to the coordinates of the limit point:

$$d_1 d_3 \xi_1^4 + [2d_1 d_3(1 - k\mu_1) + d_3^2(1 - \mu_1)]\xi_1^3 +$$
$$+\left[2d_3(1 - \mu_1)(1 - k\mu_1) + d_1(1 - k\mu_1)^2 - d_3^2\mu_1\overline{\xi_1}\right]\xi_1^2 +$$
$$+\left[(1 - \mu_1)(1 - k\mu_1)^2 - 2d_3(1 - k\mu_1)\mu_1\overline{\xi_1}\right]\xi_1 + (k\mu_1)^2 d_2\overline{\xi}_2^2 - (1 - k\mu_1)^2\mu_1\overline{\xi_1} = 0 \quad (22)$$

Some solution results are given in the article by the authors [6]. Typical bifurcation diagrams with limit points are shown in Figure 10.

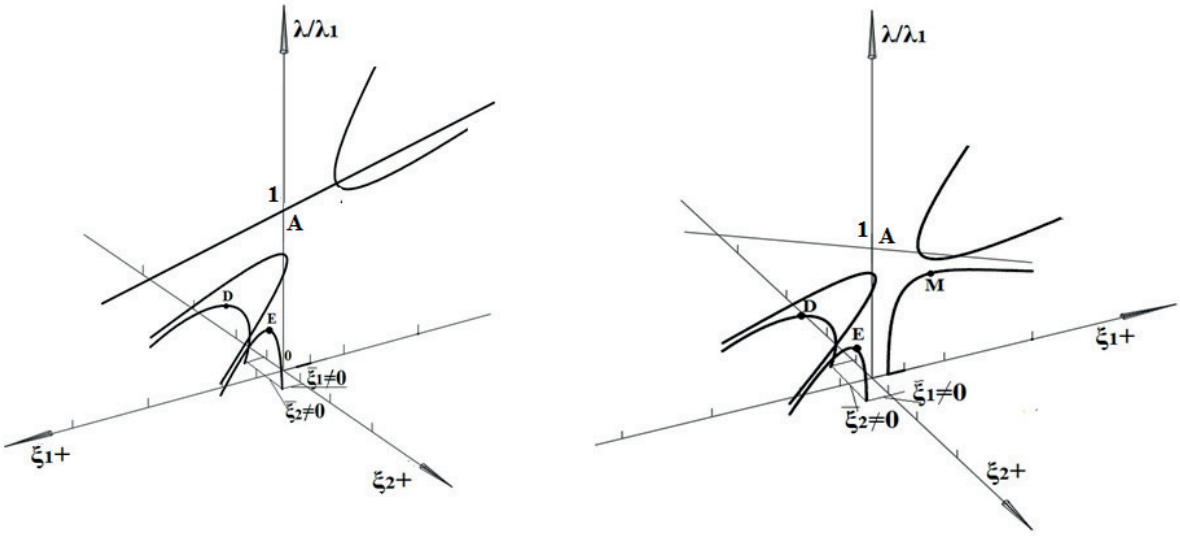

Figure 10. Bifurcation diagrams of related solutions with limit points, ($\overline{\xi_1} \neq 0, \overline{\xi_2} \neq 0$)

Note that the diagrams shown in Figures 6 and 7 correspond to the case when the critical loads of wave formation are less than the critical loads of the total deflection, since the post-bifurcation waveform is unstable, the bearing capacity of the reinforced plate is determined mainly by the sensitivity to initial imperfections by the type of waveforming.

If the geometry of the stiffened plate is changed so that the critical undulation load is greater than the critical load of the total deflection (Figure 11), then, in principle, it is possible to increase the bearing capacity of the reinforced plate by lifting it to a value close to the total deflection load. Bifurcation diagrams for cases where the critical load of wave formation exceeds the critical load of the total deflection (a - the case of wave formation in the ribs, b - the case of wave formation in the plate) are shown in Figure 11.

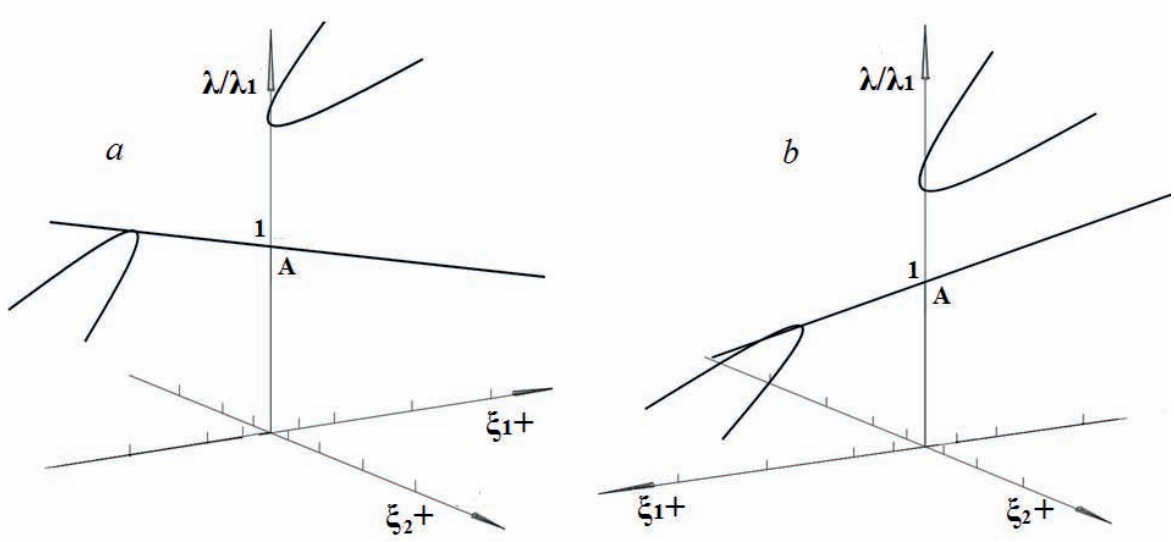

Figure 11. Bifurcation diagrams for the case of rational design of a stiffened plate

REFERENCES

1. **Hunt G.W.** (1977) // Imperfections and near-coincidence for semi-symmetric bifurcations (New York in Conference on Bifurcation Theory and Applications in Scientific Disciplines Ann. N. Y. Academy of Science 316) pp 572-589
2. **Hunt G.W.** (1981) // An algorithm for the nonlinear analysis of compound bifurcation (London Phil. Trans. R. Soc. Lond. A 1981 300) doi: 10.1098/rsta.1981.0075
3. **Hunt G.W.** (1977) // Imperfection-sensitivity of semi-symmetric branching (Proc. R. Soc. Lond. A 1977 357, 193-211) doi: 10.1098/rspa.1977.0163
4. **Thompson J.M.T, Tan J.K.Y., Lim K.C.** (1978) On the Topological Classification of Postbuckling Phenomena (Journal of Structural Mechanics Volume 6:4) pp. 383-414
5. **Tvergaard V.** (1973) // Imperfection sensitivity of a wide integrally stiffened panel under compression (Int. J. Solids Sructures 9) pp 177-192
6. **Manuylov G., Kositsyn S., Grudtsyna I.** (2021) // Geometrically nonlinear analysis of the stability of the stiffened plate taking into account the interaction of eigenforms of buckling Structural Mechanics And Analysis Of Constructions №17(1). c. 3-19
7. **Manuylov G., Kositsyn S., Grudtsyna I.** (2020) Influence of buckling forms interaction on stiffened plate bearing capacity International Journal for Computational Civil and Structural Engineering, 16(2), c. 83-93.
8. **Manuylov G., Kositsyn S., Begichev M.** (2016) // On stability loss of circular axially compressed cylindrical shell. part 1 // International Journal for Computational Civil and Structural Engineering, 12(3), 58–72
9. **Manevich A.I.** (1982) // On the theory of coupled loss of stability in stiffened thin-walled structures. Applicable mathematics and mechanics №2. p 337-345
10. **Manevich A.I.** (1981) // Interaction of forms of buckling failure of compressed stiffened panel. Structural Mechanics And Analysis Of Constructions №5. p 24-29
11. **Manevich A.I.** (1988) // Nonlinear theory of stability of stiffened plates and shells, with taking into account of buckling forms interaction. Dissertation abstract for procuring of the academic degree of Doctor of Engineering. p 8-25

СПИСОК ЛИТЕРАТУРЫ

1. **Hunt G.W.** (1977) // Imperfections and near-coincidence for semi-symmetric bifurcations (New York in Conference on Bifurcation Theory and Applications in Scientific Disciplines Ann. N. Y. Academy of Science 316) pp. 572-589.
2. **Hunt G.W.** (1981) // An algorithm for the nonlinear analysis of compound bifurcation (London Phil. Trans. R. Soc. Lond. A 1981 300) doi: 10.1098/rsta.1981.0075
3. **Hunt G.W.** (1977) // Imperfection-sensitivity of semi-symmetric branching (Proc. R. Soc. Lond. A 1977 357, 193-211) doi: 10.1098/rspa.1977.0163
4. **Thompson J.M.T., Tan J.K.Y., Lim K.C.** (1978) On the Topological Classification of Postbuckling Phenomena (Journal of Structural Mechanics Volume 6:4) pp. 383-414.
5. **Tvergaard V.** (1973) // Imperfection sensitivity of a wide integrally stiffened panel under compression (Int. J. Solids Sructures 9) pp 177-192
6. **Мануйлов Г.А., Косицын С.Б., Грудцына И.Е.** (2021) // Геометрически-нелинейный расчет на устойчивость подкрепленной пластины с учетом взаимодействия собственных форм выпучивания // Строительная механика и расчет сооружений №17(1). с.3-19
7. **Мануйлов Г.А., Косицын С.Б., Грудцына И.Е.** (2020) // Влияние взаимодействия форм выпучивания на несущую способность подкрепленной пластины // International Journal for Computational Civil and Structural Engineering, 16(2), с. 83-93.
8. **Мануйлов Г.А., Косицын С.Б., Бегичев М. (2016)** // О явлении потери устойчивости продольно сжатой круговой цилиндрической оболочки. часть 1: о послекритическом равновесии оболочки // International Journal for Computational Civil and Structural Engineering, 12(3), 58–72
9. **Маневич А.И.** (1982) // К теории связанной потери устойчивости подкрепленных тонкостенных конструкций. Прикладная математика и механика №2. р. 337-345.
10. **Маневич А.И.** (1981) // Взаимодействие форм потери устойчивости сжатой подкрепленной панели. Строительная механика и расчет сооружений №5. с 24-29.
11. **Маневич А.И.** (1988) // Нелинейная теория устойчивости подкрепленных пластин и оболочек с учетом взаимодействия форм выпучивания Автореферат на соискание ученой степени доктора технических наук. с 8-25

Gaik A. Manuylov, Ph.D., Associate Professor, Department of Structural Mechanics, Moscow State University of Railway Engineering (MIIT); 127994, Russia, Moscow, 9b9 Obrazcova Street; phone/fax +7(499)972-49-81.

Sergey B. Kosytsyn, Advisor of RAASN, Dr. Sc., Professor, Head of Department of Theoretical Mechanics, Russian University of Transport (MIIT); 127994, Russia, Moscow, 9b9 Obrazcova Street; phone/fax: +7(499) 978-16-73; E-mail: kositsyn-s@yandex.ru, kositsyn-s@mail.ru

Irina E. Grudtsyna, PhD student of Department of Theoretical Mechanics, Russian University of Transport (MIIT); 127994, Russia, Moscow, 9b9 Obrazcova Street; phone/fax: +7(915) 351-95-09; E-mail: Grudtsyna_ira90@mail.ru

Мануйлов Гайк Александрович, кандидат технических наук, доцент, доцент кафедры «Строительная механика» Российского Университета Транспорта (РУТ (МИИТ)); 127994, г. Москва, ул. Образцова, 9; тел./факс +7(499) 972-49-81

Косицын Сергей Борисович, доктор технических наук, профессор, заведующий кафедрой «Теоретическая механика» Российского Университета Транспорта (РУТ (МИИТ)); 127994, г. Москва, ул. Образцова, 9; тел./факс +7(499) 978-16-73; E-mail: kositsyn-s@yandex.ru, kositsyn-s@mail.ru

Грудцына Ирина Евгеньевна, ассистент кафедры «Теоретическая механика» Российского Университета Транспорта (РУТ (МИИТ)); 127994, г. Москва, ул. Образцова, 15; тел./факс +7(915) 351-95-09; E-mail: Grudtsyna_ira90@mail.ru

DOI:10.22337/2587-9618-2021-17-3-94-101

ANALYTICAL AND NUMERICAL METHODS FOR DETERMINING THE CARRYING CAPACITY OF A PILE BARETT ON WEAK SOILS IN DEEP PITS

Rashid A. Mangushev [1], ***Nadezhda S. Nikitina*** [2], ***Le Trung Hieu*** [3], ***Ivan Yu. Tereshchenko*** [4]

[1] Saint-Petersburg State University of Architecture and Civil Engineering, Saint-Petersburg, RUSSIA
[2,3] National Research Moscow State University of Civil Engineering, Moscow, RUSSIA
[4] LLC "GIPROATOM"; Moscow, Russia

Abstracts: The article provides an analysis of the bearing capacity of barrett piles in difficult geological conditions at a construction site in the city of Hanoi, Vietnam based on the results of analytical calculations according to Russian building codes, mathematical modeling and field full-scale tests. The paper describes a numerical test of a single barrette for Mohr-Coulomb and Hardening Soil models in the Midas GTS NX software package. The bearing capacity of a barrette in soft soils is also proposed to be determined by an analytical solution for calculating the settlement of a single pile, taking into account the unloading of the pit after soil excavation. The results of full-scale tests at the site of future construction, graphs of "load-settlement" of the barrette head from the applied vertical load and the general assessment of the bearing capacity of the barret pile by various methods are shown.

Keywords: pile-barrett, settlement-load dependence, bearing capacity, FEM, analytical solution, mathematical modeling

АНАЛИТИЧЕСКИЕ И ЧИСЛЕННЫЕ МЕТОДЫ ОПРЕДЕЛЕНИЯ НЕСУЩЕЙ СПОСОБНОСТИ СВАЙ-БАРЕТТ НА СЛАБЫХ ГРУНТАХ В ГЛУБОКИХ КОТЛОВАНАХ

Р.А. Мангушев [1], ***Н.С. Никитина*** [2], ***Ле Чунг Хиеу*** [3], ***И.Ю. Терещенко*** [4]

[1] Санкт-Петербургский государственный архитектурно-строительный университет (СПбГАСУ), г. Санкт-Петербург, РОССИЯ
[2,3] Национальный исследовательский Московский государственный строительный университет (НИУ МГСУ), г. Москва, РОССИЯ
[4] ООО "ГИПРОАТОМ", г. Москва, РОССИЯ

Аннотация: в статье приводится анализ несущей способности свай-баретт в сложных инженерно-геологических условиях на строительной площадке в городе Ханой, Вьетнам по результатам аналитических расчетов по Российским строительным нормам, математического моделирования и полевых натурных испытаний. Описывается проведение численного испытания одиночной баретты для моделей грунтов Mohr-Coulomb и Hardening Soil в программном комплексе Midas GTS NX. Несущую способность баретты в слабых грунтах также предлагается определять по аналитическому решению расчета осадки одиночной сваи с учетом разгрузки котлована после разработки. Показаны результаты натурных испытаний на площадке будущего строительства, графики «нагрузка-осадка» оголовка баретты от приложенной вертикальной нагрузки и общая оценка несущей способности сваи-барреты по различным методам.

Ключевые слова: свая-баретта, зависимость осадка-нагрузка, несущая способность, МКЭ, аналитическое решение, математическое моделирование

INTRODUCTION

Currently, the demand for the construction of high-rise buildings is very high in large metropolitan areas of the world [1]. Difficult geotechnical conditions dictate special requirements for the design of zero cycle structures for such facilities [2]. Therefore, piles-barrettas are gaining great

popularity as deep foundations, which can perceive significant longitudinal and transverse forces due to the increased bearing capacity both in material and in soil compared to alternative types of pile foundations [3]. At the preliminary design stage, when full-scale tests of piles have not yet been carried out, in order to assign the main structural parameters of foundations, a computational design method is used based on analytical and numerical calculations for limit states [1]. Taking into account the base formed by a layer of weak soils, the great depth of the excavation and the laying of barrett piles, a special approach to the calculation of the bearing capacity of the piles, taking into account the stress-strain state of the enclosing soil mass, is required [4,5,6]. On the construction site of a high-rise building with a developed underground part in the city of Hanoi, Vietnam, barrettas with a section of 800x2800 mm and a length of 37 meters were designed as foundations. In order to determine the bearing capacity of a single barrette on the ground, analytical calculations were carried out according to the method of Russian standards and mathematical modeling in the geotechnical software package. After assigning the parameters of the pile foundation, at the construction site, full-scale tests of a single barrette with a static indentation load were made and carried out.

GEOTECHNICAL CONDITIONS OF THE CONSTRUCTION SITE

According to the results of engineering and geological surveys, the geological zone under the well has a depth of 61 m, consists of 9 soil layers: IGE-1: compacted embankment; IGE-2: fluid clay, brownish-gray, mixed with organic inclusions; IGE-3: loose sand, ash-gray, medium brown of medium density, unimportant IGE-4: fluid-plastic clay, brownish-gray, mixed with organic inclusions; IGE-5: fine, gray and yellowish-gray sand, medium density, unimportant; IGE-6: soft-plastic loam, brownish-gray; IGE-7: fine sand, medium size, unimportant; IGE-8: fluid-plastic loam, brown-gray, dark gray, mixed organic; IGE-9: gravel and pebble soil. The engineering and geological conditions of the construction site are relatively difficult with layers of weak soils and a high level of groundwater at an elevation of -4.50 m from the earth's surface. The physical and mechanical properties of soils are shown in Table 1. A barrette with a section of 800x2800 mm and a length of 37 meters rests on a strong layer of IGE-9 – gravel-pebble soil (Figure 1).

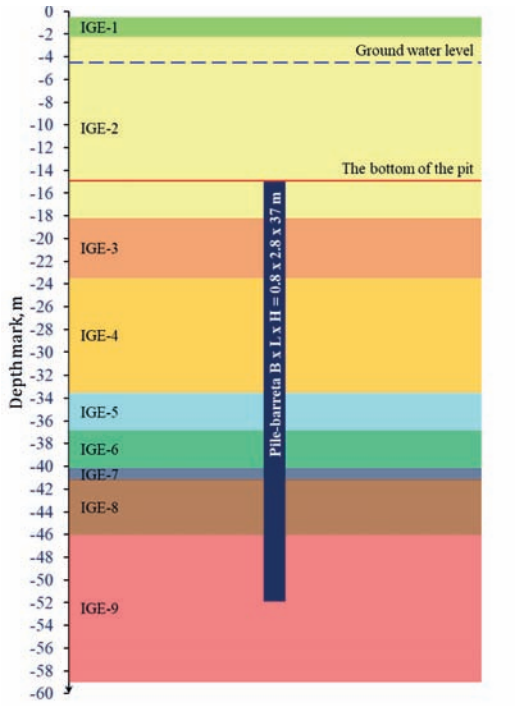

Figure 1. Layout of the pile-barrets in the ground

DETERMINATION OF THE BEARING CAPACITY OF PILES BY ANALYTICAL METHODS

In accordance with Russian standards [7], the bearing capacity of hanging piles is determined depending on the physical and mechanical properties of the foundation soil and the depth of the pile. Analytical calculations have shown the value of the total bearing capacity of this barrette equal to $F_{d,calc1}$ = 27285 kN. At the same time, 77% fell on the heel of the pile and only 23% on the side surface.

Table 1. Physical and mechanical properties of soils

No. layers	Soil	h, м (m)	γ, кН / м^3 (kN/m^3)	I_L	e	φ, град. (degree)	c, кПа (kPa)	E, МПа (MPa)
1	Compacted embankment	1.6	16.00	-	-	-	-	-
2	Fluid clay	16.1	17.00	1.408	1.246	6.30	7.00	1.5
3	Fine sand	5.1	19.00	0.350	0.771	30.00	-	13.5
4	Fluid-plastic clay	10.2	17.20	0.811	1.171	18.00	9.10	15.0
5	Fine sand	3.0	19.20	0.350	0.746	30.00	-	13.5
6	Soft-plastic loam	3.4	17.80	0.695	1.002	7.40	9.60	5.0
7	Fine sand	1.0	19.10	0.035	0.755	30.00	-	13.5
8	Fluid-plastic loam	4.8	17.50	0.930	1.082	8.00	9.50	3.0
9	Gravel and pebble soil	>15.8	20.10	0.300	0.524	38.00	2.00	50.0

Taking into account the significant thickness of soft soils with a low modulus of deformation within the barrette shaft, the deformability of the pile under load will play a significant role. Therefore, in the calculations, it was decided to limit the bearing capacity on the ground by the limiting settlement of a single pile, equal to 40 mm, similar to full-scale and numerical tests. The method for determining the settlement of a single pile depending on the average value of the soil shear modulus G within the pile and under its lower end is also described in the provisions of the Russian standard [7]. According to the results of the analytical calculation, it was found that the bearing capacity of the barrett from the condition of limiting the settlement to 40 mm was $F_{d,calc2}$ = 18450 kN. The depth of the projected pit is almost 15 meters. At depths of more than 5 meters, the effect of "unloading-reloading" becomes most pronounced for a certain thickness of the base as a result of excavation of the pit. This phenomenon will manifest itself especially in foundations composed of weak soils with a low modulus of deformation. Therefore, to calculate the settlement of barrett in deep pits, it was proposed to determine the shear modulus G taking into account the unloading of the base. For this purpos, a new term Hur is introduced, which means the depth of the unloading strata. The lower boundary of the unloading stratum is taken at a depth z = H_{ur}, where the condition is fulfilled:

$$\sigma_{zy} = 0{,}5\,\sigma_{zg}, \qquad (1)$$

where σ_{zy} is a vertical stress from the own weight of the soil, selected when cutting the excavation, at a depth z from the level of the bottom of the excavation, kPa. Determined according to the provisions of the Russian standard for geotechnical construction [8].

σ_{zg} is a vertical stress due to the own weight of the soil at a depth z from the level of the bottom of the excavation, kPa.

In this case, the depth of the unloading thickness H_{ur} should be no more than H_{max}, equal to (4 + 0.1b) at 10 <b ≤60 and 10 m at b> 60 m, where b is the width of the pit.

In the problem under consideration, H_{ur} = 10 m.

To calculate the settlement when determining the average value of the soil shear modulus, within the unloading thickness H_{ur} for soils, the elastic shear modulus Gur is taken, defined as

$$G_{ur}=\frac{1}{2(1+\upsilon_{ur})}E_{ur},$$

where E_{ur} is a modulus of soil deformation upon removal / reapplication of the load,
υ_{ur} is a coefficient of lateral deformation of the soil when removing / reapplying a load.
According to the results of the analytical calculation, taking into account the unloading of the soil in the excavation, it was found that the bearing capacity of the barrette from the condition of limiting the settlement of 40 mm was $F_{d,calc3}$ =24600 kN.

MODELING

Numerical modeling of changes in the stress-strain state of the soil mass in the process of virtual testing of the experimental barrette pile was carried out using the geotechnical software package Midas GTS NX in a spatial setting. A finite element model of the test barrette-surrounding soil mass system in Midas GTS NX is shown in Figure 2.
The dimensions of the computational area are taken in terms of 30.8 x 32.8 m and a depth of 66.2 m.
For the formation of finite elements, a hybrid mixed mesh, mainly hexahedral types of finite elements, was used. The grid step is condensed in the area where the barrets are located and is discharged to the boundaries of the computational domain. Consideration of the behavior of the soil at the contact between the barrett and the base mass was modeled using special interface contact elements. The stiffness parameters are assigned taking into account the reduction in contact strength, taking into account the reduction factors given in the Russian design standards [7].
Mathematical modeling of the test was carried out step by step in several stages:
1. Formation of the initial stress-strain state of the soil mass;
2. Development of the foundation pit;
3. Barretta device;
4. Loading the barrette (Figure 2). Gradual application of a vertical indentation load to the test barrette of 2500 kN at each stage.
To calculate the bearing capacity of a barrette in the Midas GTS NX program, two subgrade models were considered:
– Ideal-elastoplastic Mohr-Coulomb model.
– Elastoplastic model of the hardening soil "Hardening Soil".
The deformed model diagram and vertical displacements at an intermediate stage of testing (at P = 20,000 kN) for various soil models are shown in Figure 3.

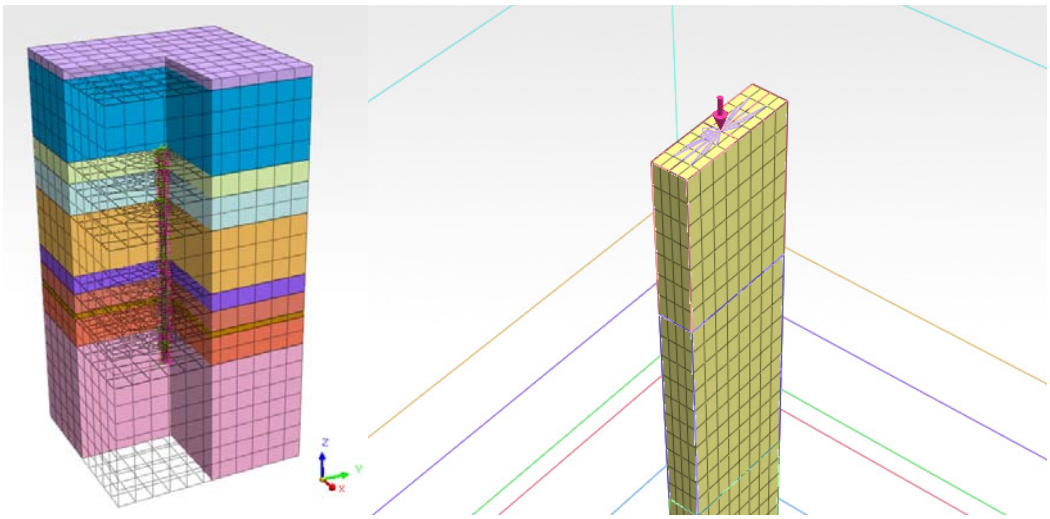

Figure 2. Mathematical FE-model

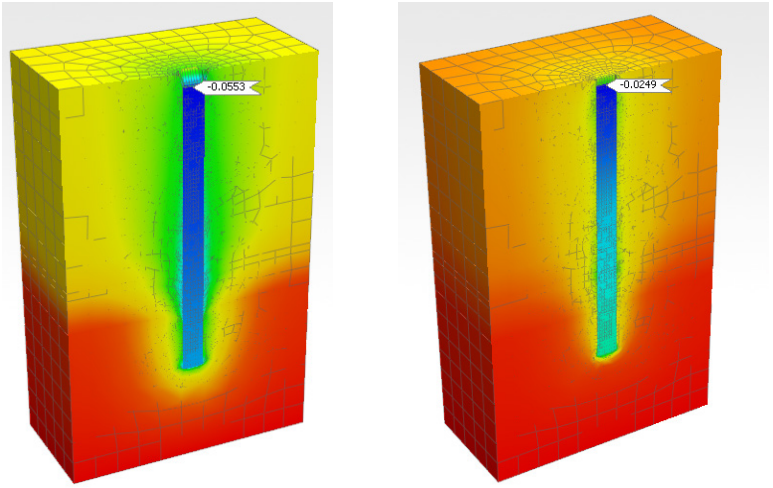

a) *b)*

Figure 3. Deformed diagram and vertical displacements of the model under a load of 20,000 kN: a) Mohr-Coulomb model, b) Hardening Soil model

The criterion for ensuring the bearing capacity of the pile on the ground is the vertical displacement of the barrette head, equal to 40 mm. This condition is met at the calculated vertical load equal to $F_{d,MC}$ = 16440 kN for the Mohr-Coulomb model and $F_{d,HS}$ = 23600 kN for the Hardening Soil model.

FULL-SCALE TESTS

Experimental barrette piles were made on the site for the construction of a high-rise building in the city of Hanoi. Tests of a single barrette with a section of 800x2800 mm and a length of 37 meters with a vertical static load were carried out using hydraulic jacks up to a maximum load of 30 MN using the Top-Down method.

The condition of the maximum settlement of the pile head under a load of 40 mm is achieved under a vertical load $F_{d,site}$ = 27500 kN (Figure 4). This value is taken as the bearing capacity of the barrette on the ground.

RESULTS

The results of determining the bearing capacity of a barrette on the ground by analytical and numerical methods, as well as the results of field tests, are presented in Table 2.

The combined load-settlement graph for various considered methods for determining the bearing capacity of a barrette is shown in Figure 5.

DISCUSSION

As it is well known, the ideal-elastoplastic soil Mohr-Coulomb model does not describe the behavior of the soil during unloading [9]. The same applies to the analytical method for determining the settlement of a single pile according to the Russian standard, where the soil is considered as a linearly deformed half-space, characterized by the shear modulus and Poisson's ratio. The results obtained by these methods are in good agreement with each other. The values of the bearing capacity differ by about 10% (Table 2), and at the initial stage of loading (at P <12500 kN) the graphs exactly coincide. However, the solutions based on these techniques do not agree well with the results of field tests and cannot be applied for practical purposes for conditions of soft soils and deep pits.

The proposed modification of the analytical method for calculating the settlement of a single pile in order to take into account the unloading of the base

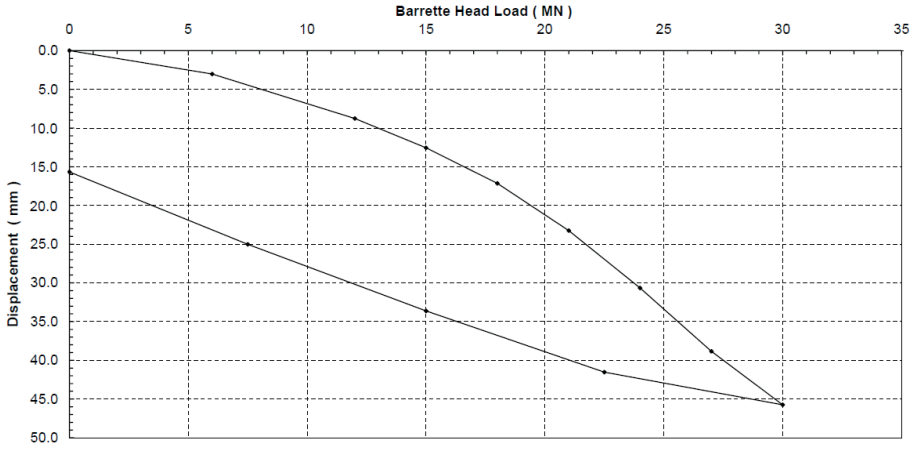

Figure 4. Results of full-scale static tests of barrette piles

Table 2. Bearing capacity of pile-barrets by different methods

	Methodology for calculating the bearing capacity of a pile on the ground	Bearing capacity of the pile on the ground, kN
	Field test results, $F_{d,site}$	27500
	Analytical classical method [7], $F_{d,calc1}$	27285 (-1%)
Taking into account unloading	Midas GTS NX software for *Hardening Soil* model, $F_{d,HS}$	23600 (-14%)
	Analytical method for settlement criterion (modified), $F_{d,calc3}$	24600 (-10%)
excluding unloading	Midas GTS NX software for *Mohr-Coulomb* model, $F_{d,MC}$	16440 (-40%)
	Analytical method according to the criterion of settlement [7] , $F_{d,calc2}$	18450 (-33%)

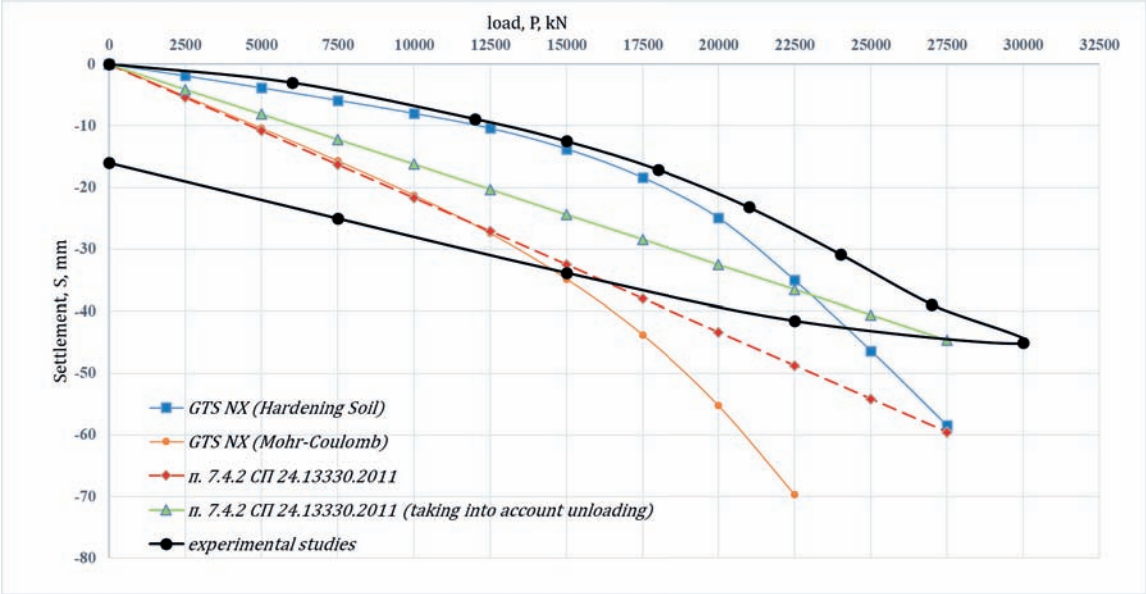

Figure 5. Combined load-settlement graph based on the results of analytical calculations, numerical modeling and field tests

during the development of a deep excavation made it possible to describe the behavior of a barrette under load with sufficient accuracy. The bearing capacity with a limiting settlement of 40 mm is in good agreement with the numerical solution (with the adopted Hardening Soil model), the analytical method for strength characteristics, and the results of full-scale static tests.

CONCLUSIONS

1) Complex design solutions of the zero cycle and difficult geological conditions of the construction site require a special approach to the design of deep foundations.
2) When using different soil models (MC and HS) in mathematical modeling of the test of a barrette in a deep pit, the graphs of barrett displacement under load are significantly different. For numerical calculations of piles in soft soils and deep pits, it is recommended to use the Hardening Soil model, which takes into account the work of the soil along the secondary loading branch. This solution, with sufficient accuracy for practical purposes, describes the results of field tests.
3) A good convergence of the value of the bearing capacity of the barrett on the soil is shown by the analytical solution for determining the settlement, where the reduced shear modulus G is determined taking into account the thickness of the base unloading, for which the soil deformation modulus is applied when removing / reapplying the load Eur. This technique is applicable for preliminary calculations of settlement and bearing capacity of piles.

REFERENCES

1. **Shulyat'yev O. A.** Osnovaniya i fundamenty vysotnykh zdaniy / O. A. Shulyat'yev [Soils and foundations of high-rise buildings]. – Moscow: ASV Publishing, 2020 – 442 p.
2. **Mangushev R.A., Osokin A.I., Konyushkov V.V.** et al. Proyektirovaniye osnovaniy, fundamentov i podzemnykh sooruzheniy [Design of foundations, foundations and underground structures]. Moscow: ASV Publishing, 2021. 632 p.
3. **Mangushev R.A., Gotman A.L., Znamenskiy V.V., Ponomarev A.B**. Svai i svaynyye fundamenty. Konstruktsii, proyektirovaniye i tekhnologii [Piles and pile foundations. Constructions, design and technology] / Under ed. Corr.-member of RAACS, Dr., prof. Mangushev R.A. Moscow: ASV Publishing, 2015. 320 p.
4. **Mangushev R.A., Nikitina N.S.** Evaluation and analysis of bearing capacity of bores piles and deep laid pile-barrette for a high-rise building on loose grounds based on calculations and field tests // International Journal for Computational Civil and Structural Engineering. 2018. Vol.14, Iss. 2. Pp. 109-116.
5. **Le Trung Hieu, Nikitina N.S.** Nekotoryye osobennosti vozvedeniya fundamenta na slabykh gruntakh pri stroitel'stve zdaniy [Some features of the construction of a foundation on soft soils during the construction of buildings]. Sbornik statey XXXVII mezhdunarodnoy nauchno-prakticheskoy konferentsii Moskva: «Nauchno-izdatel'skiy tsentr «Aktual'nost'. RF» [Collection of articles of the XXXVII International Scientific and Practical Conference Moscow: "Scientific Publishing Center" Actuality.RF "], 2021, Pp. 81-84.
6. **Van Thanh Tran.** Studying and calculating the bearing capacity of barrette piles based on comparison with O-cell test. Article: Tạp chí Xây dựng Việt Nam 59 (625), pp. 232-236.
7. Building Code of RF SP 24.13330.2011. Svod pravil. Svaynyye fundamenty. Aktualizirovannaya redaktsiya SNiP 2.02.03-85 [Pile foundations. Updated edition of SNiP 2.02.03-85].
8. SP 22.13330.2016. Svod pravil. Osnovaniya zdaniy i sooruzheniy. Aktualizirovannaya redaktsiya SNiP 2.02.01-83 [Foundations of buildings and structures. Updated edition of SNiP 2.02.01-83].
9. **Vermeer P.A., De Borst R.** Non-associated plasticity for soils, concrete and rock // Heron. 1984 Vol. 29 No. 3.

СПИСОК ЛИТЕРАТУРЫ

1. **Шулятьев О.А.** Основания и фундаменты высотных зданий / О. А. Шулятьев. — М.: АСВ, 2020 — 442 с.
2. **Мангушев Р.А., Осокин А.И., Конюшков В.В.** и др. Проектирование оснований, фундаментов и подземных сооружений / М: Изд-во АСВ, 2021. 632 с.
3. **Мангушев Р.А., Готман А.Л., Знаменский В.В., Пономарев А.Б.** Сваи и свайные фундаменты. Конструкции, проектирование и технологии / Под. ред.чл.корр. РААСН, д.т.н., проф. Мангушева Р.А. М.: Изд-во АСВ, 2015. 320 с.
4. **Мангушев Р.А., Никитина Н.С.** Оценка и анализ несущей способности буронабивных свай и свай-баррет глубокого заложения для высотного здания на слабых грунтах по результатам расчетов и полевых испытаний. Стаья: - М.: Международный журнал “International Journal for Computational Civil and Structural Engineering (Международный журнал по расчету гражданских и строительных конструкций)” (IJCCSE), 2018 г.
5. **Ле Чунг Хиеу, Никитина Н.С.** Некоторые особенности возведения фундамента на слабых грунтах при строительстве зданий. Сборник статей XXXVII международной научно-практической конференции Москва: «Научно-издательский центр «Актуальность.РФ», 2021, с 81-84.
6. **Van Thanh Tran**. Studying and calculating the bearing capacity of barrette piles based on comparison with O-cell test. Стаья: Tạp chí Xây dựng Việt Nam 59 (625), с 232-236.
7. СП 24.13330.2011. Свод правил. Свайные фундаменты. Актуализированная редакция СНиП 2.02.03-85.
8. СП 22.13330.2016. Свод правил. Основания зданий и сооружений. Актуализированная редакция СНиП 2.02.01-83.
9. **Vermeer P.A., De Borst R.** Non-associated plasticity for soils, concrete and rock // Heron. 1984 Vol. 29 № 3.

Rashid A. Mangushev. Corresponding Member of the RAACS, Professor, Doctor of Technical Sciences; Head of the Department of Geotechnics, St. Petersburg State University of Architecture and Civil Engineering (SPbGASU), Director of the Scientific and Production Consulting Center for Geotechnology, SPbGASU. Russia, St. Petersburg, 2nd Krasnoarmeiskaya 4; email: ramangushev@yandex.ru.

Nadezhda S. Nikitina. Candidate of Technical Sciences, Professor of the Department of Soil Mechanics and Geotechnics; National Research Moscow State University of Civil Engineering (NRU MSUCE); Moscow, Russia, 129337, Yaroslavskoe shosse, 26; tel./fax: +7 (495) 287-49-14; e-mail: nsnikitina@mail.ru;

Le Trung Hieu – Master's student of the Department of Soil Mechanics and Geotechnics; National Research Moscow State University of Civil Engineering (NRU MGSU); Moscow, Russia, 129337, Yaroslavskoe shosse, 26; tel./fax: +7 (995) 770-09-13; e-mail: hiuletrg@gmail.ru;

Ivan Yu. Tereshchenko – Chief Specialist of GIPROATOM LLC; Moscow, Nauchny proezd, house 8, building 1; e-mail: i.tereshchenko@giproatom.com.

Мангушев Рашид Абдуллович – член-корреспондент РААСН, профессор, доктор технических наук; заведующий кафедрой геотехники Санкт-Петербургского государственного архитектурно-строительного университета (СПбГАСУ), директор научно производственного консалтингового центра геотехнологий СПбГАСУ. Россия, Санкт-Петербург, 2-я Красноармейская 4; email: ramangushev@yandex.ru.

Никитина Надежда Сергеевна – к.т.н., профессор кафедры «Механики грунтов и геотехники»; Национальный исследовательский Московский государственный строительный университет (НИУ МГСУ); г. Москва, Россия, 129337, Ярославское шоссе, д.26; тел./факс: +7(495) 287-49-14; e-mail: nsnikitina@mail.ru;

Ле Чунг Хиеу – магистрант кафедры «Механики грунтов и геотехники»; Национальный исследовательский Московский государственный строительный университет (НИУ МГСУ); г. Москва, Россия, 129337, Ярославское шоссе, д.26; тел./факс: +7(995) 770-09-13; e-mail: hiuletrg@gmail.ru;

Терещенко Иван Юрьевич – главный специалист ООО "ГИПРОАТОМ"; г. Москва, Научный проезд, дом 8, строение 1; e-mail: i.tereshchenko@giproatom.com.

International Journal for Computational Civil and Structural Engineering, 17(3) 102–113 (2021)

DOI:10.22337/2587-9618-2021-17-3-102-113

STATIC BENDING STRENGTH OF SANDWICH COMPOSITE PLATES WITH TETRACHIRAL HONEYCOMBS

Alexey V. Mazaev, Marina V. Shitikova

Voronezh State Technical University, Voronezh, RUSSIA
Research Institute of Building Physics of Russian Academy of Architecture and Construction Sciences, Moscow, RUSSIA

Abstract: The article presents a numerical strength analysis of sandwich plates with solid face layers and tetrachiral honeycomb core layer under static bending conditions. An aluminum alloy was chosen as the material of plates. For honeycomb core layers, the discretization (number of unit cells) and the relative density were varied with a constant thickness. Calculations were performed for the case of bending with rigidly clamped ends and three-point bending within the framework of the theory of elasticity by the finite element method. The strength analysis enables one to determine the load values, at which the maximal stresses according to the von Mises criterion were equal to the conventional yield stress of the material. The aim of this work is to study the effect of discretization and relative density of honeycomb core layers of tetrachiral type on the strength of sandwich plates.

Keywords: composite plates, tetrachiral honeycombs, multilayer plates, strength analysis, static bending, finite element method

ПРОЧНОСТЬ СЛОИСТЫХ КОМПОЗИТНЫХ ПЛАСТИН С ТЕТРАКИРАЛЬНЫМИ СОТАМИ ПРИ СТАТИЧЕСКОМ ИЗГИБЕ

А.В. Мазаев, М.В. Шитикова

Воронежский государственный технический университет, г. Воронеж, РОССИЯ
Научно-исследовательский институт строительной физики РААСН, г. Москва, РОССИЯ

Аннотация: В работе производился численный анализ прочности слоистых композитных пластин со сплошными внешними слоями и сотовой прослойкой тетракирального типа в условиях статического изгиба. В качестве материала пластин выбран алюминиевый сплав. У сотовых прослоек варьировалась дискретизация (количество элементарных ячеек) и относительная плотность при постоянной толщине. Расчеты производились при жестком защемлении с торцов и трехточечном изгибе в рамках теории упругости методом конечных элементов. В процессе анализа прочности определялись значения нагрузки, при которых максимальные напряжения по критерию Мизеса приравнивались к условному пределу текучести материала. Целью работы является изучение влияния дискретизации и относительной плотности сотовых прослоек тетракирального типа на прочность композитных пластин.

Ключевые слова: композитные пластины, тетракиральные соты, многослойные пластины, анализ прочности, статический изгиб, метод конечных элементов

1. INTRODUCTION

In the last three decades, much attention has been paid to materials with negative Poisson's ratio, which are called auxetics [1-3]. These materials have a non-standard deformation mechanism, namely: they expand with tension and contract with compression. Despite the recent special attitude to auxetic materials, the theoretical admissibility of the existence of such materials was first shown by Love more than 120 years ago [4]. Later, Landau came to the similar conclusion [5]. Based on the well-known expression for the shear modulus for an isotropic material, it follows that when Poisson's ratio tends to -1, the shear resistance increases significantly, which is an important property for many applications. Currently, it is known about many advantages of auxetics over materials with classical behavior [6], for example: increased resistance to indentation, resistance to the process of initiation and opening of cracks, increased energy absorption, etc. Such properties of auxetics remarkably complement the properties of classical materials in composite structures, in particular, layered plates.

Honeycomb structures of certain geometry are most often used as auxetic in sandwich composites. Prall and Lakes [7] theoretically and experimentally determined negative Poisson's ratio in trichiral honeycomb structures. They also showed that Young moduli of chiral honeycombs depend on the ratio of the length of tangentially attached ribs and the radius of the cylinders, as well as on the ratio of the distance between the centers of adjacent cylinders (connected by ribs) and the radius of the cylinders. Scarpa and Tomlinson [8] theoretically assumed that re-entrant honeycomb core layers with negative Poisson's ratio increase the flexural stiffness of composite plates. They also suggested using honeycomb core layers to design composites with pre-tuned mechanical properties by changing the geometric parameters of the unit cells.

Alderson et al. [9] numerically and experimentally determined Poisson's ratios for chiral honeycombs of various types (hexa-, tetra-, antitetra-, tri- and antitri- chiral cells) under plane uniaxial compression. Honeycombs differ in the number of tangentially attached ribs, and in antichiral structures, adjacent unit cells have mirror symmetry. Alderson et al. [9] used finite element modeling and ambient experiments, in so doing prototypes were made from nylon using additive technologies. It is shown that the chiral honeycombs family has a negative Poisson's ratio. However, the trichiral structure showed a positive Poisson's ratio, and the antitrichiral structure showed auxetic behavior with short tangentially attached ribs and classic behavior with long ribs. It was showed that chiral structures, in comparison with antichiral structures, have a higher Young modulus under plane uniaxial compression for any number of ribs.

Lira et al. [10] have shown numerically and experimentally that an auxetic honeycomb structure of the re-entrant type has an increased specific flexural stiffness relative to hexagonal honeycombs. Such a structure with a reduced mass also allows one to obtain the same first natural frequency in comparison with hexagonal cells. Li and Wang [11] made sandwich composites with various honeycomb core layers: truss type, conventional honeycombs, and re-entrant honeycombs. It has been shown [11] that under the three-point bending, sandwich composites with a re-entrant type auxetic honeycombs exhibit high energy absorption and more efficient stress distribution before failure.

Alomarah et al. [12] numerically and experimentally investigated popular auxetic honeycomb structures under plane uniaxial compression: re-entrant, tetrachiral and antitetrachiral. They also investigated a new honeycomb structure, namely: re-entrant chiral. The prototypes were made of polyamide using additive technologies. Alomarah et al. [12] obtained the stress-strain curves, showed the strain modes of the investigated structures,

investigated energy absorption, and determined the magnitudes of the negative Poisson's ratio.

Xiao et al. [13] numerically and experimentally investigated the behavior of a rigidly fixed sandwich beam with re-entrant honeycombs under conditions of a local shock pulse. The deformation of the facial sheets and the auxetic core layer was also analyzed. The composites were made of an aluminum alloy using additive manufacturing. It has been experimentally shown [13] that re-entrant honeycombs with thin walls exhibit local densification in composites due to the negative Poisson's ratio. Re-entrant honeycombs with thick walls showed only global deformation without auxetic behavior.

Essassi et al. [14] experimentally and numerically investigated sandwich composites with re-entrant honeycomb core layers under three-point bending conditions. The composites were made of biological material using additive technologies. During manufacturing, the relative density of the honeycomb structure was varied. Flexural stiffness, shear stiffness and shear modulus for the sandwich composites under investigation were determined, and the effect of the relative density of the core layers on these values was evaluated.

Composite panels with auxetic honeycombs under three-point bending have been investigated in [15, 16]. The composites were made of wood-based materials. The authors determined the stiffness, strength and energy absorption capacity of the composite panels. It has been shown that sandwich panels with auxetic honeycombs have advantages over those with classical honeycombs, in so doing the plane of honeycomb core layers with auxetic behavior is oriented parallel and perpendicular to the plane of composite panels, respectively, in [10, 15-16] and [11, 13].

In the present paper, three-layer sandwich plates with solid face layers and tetrachiral honeycomb core layer under static bending are investigated numerically.

2. FORMULATION OF THE PROBLEM

Let us consider a honeycomb structure consisting of ordered cylinders arranged in a square grid pattern, which are connected to each other by tangentially attached ribs, where each of the cylinders contains four attached ribs (Fig. 1). It has been shown experimentally [9, 12] that tetrachiral honeycombs exhibit auxetic behavior in the plane. In the sandwich plates under consideration, the plane of honeycomb core layers with auxetic behavior is oriented parallel to the plane of the plates.

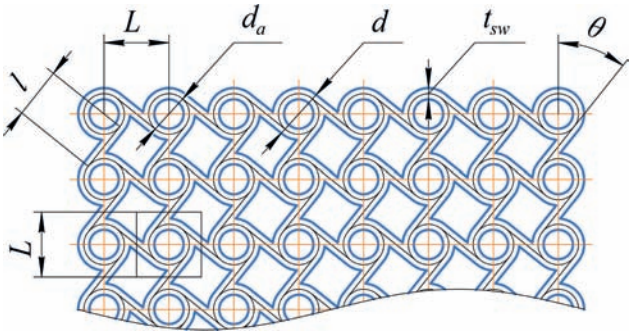

Figure 1. Parameters of the honeycomb structure of tetrachiral type

For numerical experiments, tetrachiral honeycombs have been designed with different discretization (number of unit cells) and equal relative density ρ_r, which is defined as the ratio of the volume of solid body of the honeycombs to the volume of the central layer of composites along the outer faces. The honeycombs have been considered with four values of the size of elementary cells $L = 1.6 d_a$, where $d_a \in$ 1, 1.3, 1.6, and 1.9. The volume of a solid body of the honeycomb structures could be varied by changing the thickness of their walls t_{sw}. For each discretization of the structure, 9 honeycomb models have been constructed with the equal step of increasing volume. At each of the four values of *L*, the tetrachiral honeycombs uniformly fill the central layer of the composites. For the obtained honeycombs, the following geometric parameters have been used:

$r_a/l = \text{const}$ $(r_a = d_a/2)$, $\theta = \text{const}$; at $\rho_r = \text{const}$, $\alpha = l/r \approx \text{const}$ $(r = d/2)$, and $\beta = t_{sw}/r \approx \text{const}$. The total thickness of the sandwich plates is 2 mm, the thickness of the face layers is 0.5 mm, and the thickness of the honeycomb core layers is 1 mm. For comparative analysis, 11 models of solid plates have been considered with an equal step of increasing volume by changing the thickness of plates from 1 to 2 mm with a step of 0.1 mm. Strength calculations for composite and solid plates have been carried out within the framework of elasticity theory by the finite element method using the «Structural Mechanics» module [17] from the «COMSOL Multiphysics 5.6» numerical simulation system.

A linear elastic body model is used to describe the behavior of the plate's material. Under the conditions of bending of composite and solid plates with rigid fixation, the displacements of nodes (Fig. 2) have been subjected to the following boundary conditions:

$$\begin{aligned} &u_{x,y,z}\left(0 \le x \le x_1, y = 0, 0 \le z \le h\right) = 0, \\ &u_{x,y,z}\left(x_2 \le x \le a, y = 0, 0 \le z \le h\right) = 0, \\ &u_{x,y,z}\left(0 \le x \le x_1, y = b, 0 \le z \le h\right) = 0, \\ &u_{x,y,z}\left(x_2 \le x \le a, y = b, 0 \le z \le h\right) = 0. \end{aligned} \quad (1)$$

Under the conditions of three-point bending of the plates, the displacements of nodes on straight line segments have been supposed as

$$\begin{aligned} &u_{x,y,z}\left(x = x_1, y = 0, 0 \le z \le h\right) = 0, \\ &u_{x,y,z}\left(x = x_2, y = 0, 0 \le z \le h\right) = 0. \end{aligned} \quad (2)$$

The plate is subjected to the external load F_y uniformly distributed over a straight line segment (Fig. 2):

$$F_y = F_y\left(x = l_1, y = b, 0 \le z \le h\right), \quad (3)$$

where $a = 54$ mm and $h = 13$ mm are plate dimensions, $b = 2$ mm is its thickness, $l_1 = a/2$ mm, $x_1 = 12$ mm, and $x_2 = 42$ mm. To exclude the deflection in the *zy*-plane, the displacements of nodes in the face layers of composites and solid plates have been considered as $u_z = 0$.

The finite element mesh of the composite plates is constructed separately for each layer:

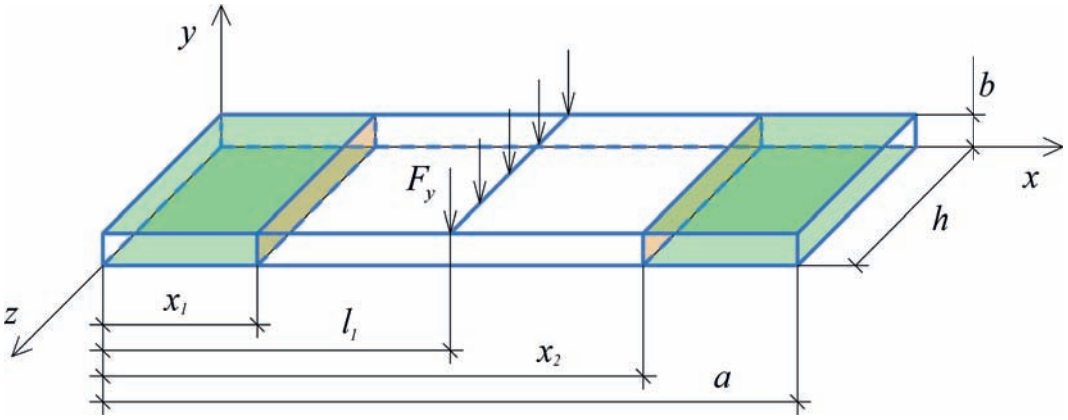

Figure 2. Boundary conditions of composite and solid plates

quadrangular prisms and triangular prisms are used for solid layers and honeycomb core layers, respectively (Fig. 3). The condition of continuity of field variables is established at the layer interfaces of composite plates. Figure 4 shows a finite element mesh of unit cells of tetrachiral structures at each step of increasing relative density. For constructing the mesh for solid plates, quadrilateral prisms have been

used. Finite elements of the serendipity family of the second order are used in all models.

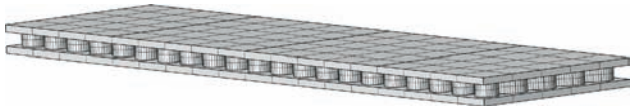

Figure 3. Mesh of finite elements of composite plates

The properties of the D16 aluminum alloy [18] are used as the material properties of composite and solid plates, namely: Poisson's ratio $\mu = 0.33$, elastic modulus $E = 72$ GPa, density $\rho = 2780$ kg/m^3, and the conventional yield point $\sigma_{0.2} = 290$ MPa.

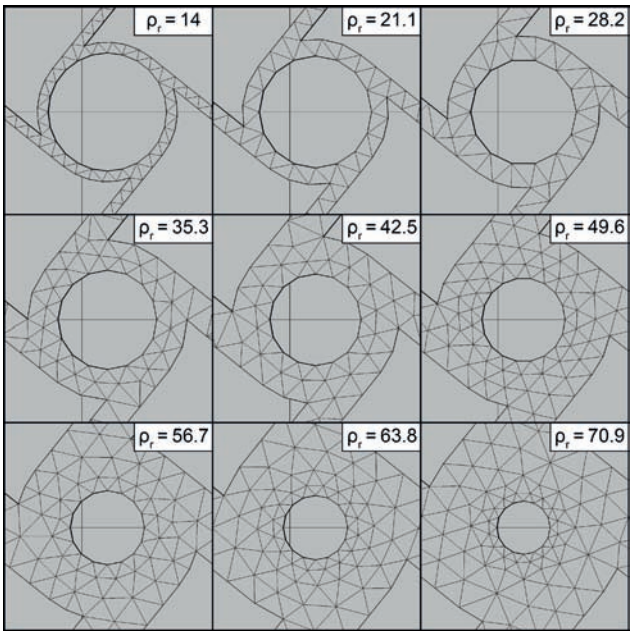

Figure 4. Finite element mesh of unit cells of tetrachiral structures

During static bending of composite and solid plates, the load values F_y (N) have been determined, at which the maximum stresses according to the von Mises criterion are equal to the conventional yield stress of the material $\sigma_{max} = \sigma_{0.2}$.

In order to verify the results of calculations via the «COMSOL» system, additional calculations of solid plates have been performed by the finite element method in displacements using the algorithm for solving the plane problem based on the known equations of theory of elasticity [19-20], adopting the following boundary conditions (Fig. 2):

$$\begin{aligned} u_{x,y,z}\left(x = x_1, 0 \le y \le b, 0 \le z \le h\right) = 0, \\ u_{x,y,z}\left(x = x_2, 0 \le y \le b, 0 \le z \le h\right) = 0. \end{aligned} \tag{4}$$

In the case of the three-point bending of the plates, the boundary conditions (2) and (3) have been used.

The algorithm for solving the plane problem was adapted for plate calculations, in so doing the stiffness matrix of the finite element k^e is determined by the expression

$$k^e_{r,s} = k^E_{r,s} + k^G_{r,s}, \tag{5}$$

where the submatrix of normal deformations k^E and the submatrix of shear deformations k^G have the following form:

$$k^E_{r,s} = \frac{Eh}{4(1+\mu)(1-2\mu)} \cdot (1-\mu) \cdot \begin{bmatrix} \gamma\xi_r\xi_s\left(1+\frac{\eta_r\eta_s}{3}\right) & \frac{\mu\xi_r\eta_s}{(1-\mu)} \\ \frac{\mu\eta_r\xi_s}{(1-\mu)} & \frac{\eta_r\eta_s}{\gamma}\left(1+\frac{\xi_r\xi_s}{3}\right) \end{bmatrix}, \tag{6}$$

$$k^G_{r,s} = \frac{Gh}{4} \cdot \begin{bmatrix} \frac{\eta_r\eta_s}{\gamma}\left(1+\frac{\xi_r\xi_s}{3}\right) & \eta_r\xi_s \\ \xi_r\eta_s & \gamma\xi_r\xi_s\left(1+\frac{\eta_r\eta_s}{3}\right) \end{bmatrix}, \tag{7}$$

$G = E/2(1+\mu)$ is the shear modulus, r and s are numbers of matrix blocks ($r = 1, 2 \ldots 4$,

$s = 1,2\ldots 4$), a_{fe} and b_{fe} are dimensions of the sides of the rectangular finite element along the *x*- and *y*-axes, respectively, *h* is the size of the finite element along *z* axis, $\gamma = b_{fe}/a_{fe}$ is the dimensionless parameter, ξ_r, ξ_s and η_r, η_s are dimensionless coordinates of the rectangular element, which take on the following magnitudes: $\xi_1 = -1$, $\eta_1 = -1$, $\xi_2 = 1$, $\eta_2 = -1$, $\xi_3 = 1$, $\eta_3 = 1$, $\xi_4 = -1$, $\eta_4 = 1$.

The matrix *N* matching the global numbers of nodes to the local numbers is constructed according to the rule $N_{m,i} = q$ with $m \in 1,2\ldots m_f$, $i \in 1,2\ldots i_f$, and $q \in 1,2\ldots 4$, where *m* is the global node number (Fig. 5, a), m_f is the quantity of global nodes, *i* is the finite element number (Fig. 5, b), i_f is the quantity of finite elements, and *q* is the local number of the node of the *i*-th finite element (Fig. 6), in so doing if $N_{m,i} \notin q$, then $N_{m,i} = 0$.

$r = N_{m,i}$, $s = N_{n,i}$, $m,n \in 1,2\ldots m_f$, if $r \vee s = 0$ then $k^e_{r,s} = \begin{pmatrix} 0 & 0 \\ 0 & 0 \end{pmatrix}$.

The stiffness matrix of the finite element model *K* is determined by summing the extended stiffness matrices $K = \sum_i k^{exp}(i)$. To consider the external fixation of the finite element model node, it is necessary to delete the rows $i_1 = 2m_p - 1$, $i_2 = 2m_p$ and columns $j_1 = 2m_p - 1$, $j_2 = 2m_p$ of the stiffness matrix *K*, where m_p is the number of the fixed node.

The displacements of nodes are determined by the expression

$$u_a = K_a^{-1} \cdot P_a, \tag{8}$$

where K_a^{-1} is the inverse stiffness matrix with due account for the fixed nodes, $P_a = \left\{ P^x_{a_1} \quad P^y_{a_2} \quad \cdots \quad P^x_{a_{c-1}} \quad P^y_{a_c} \right\}$ is the vector of nodal forces (hereinafter, the row matrix in

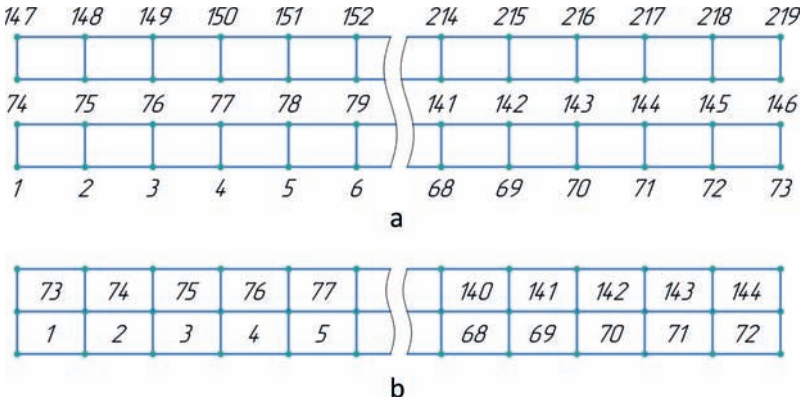

Figure 5. Scheme of finite elements of the plate: (a) global numbering of nodes, (b) numbering of finite elements

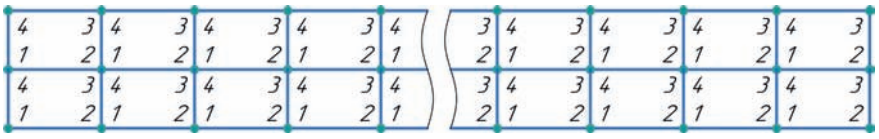

Figure 6. Scheme of local numbering of nodes of finite elements

The extended stiffness matrix k^{exp} is constructed according to the $k^{exp}_{m,n}(i) = k^e_{r,s}$ principle, where curly braces means the column matrix), $c = 2\left(m_f - p\right)$, $P^x_{a_{c-1}}$ and $P^y_{a_c}$ are nodal forces

along *x*- and *y*-axes, respectively, and *p* is the quantity of the fixed nodes.

The full vector of displacements $u=\left\{u_1^x \quad u_2^y \quad \cdots \quad u_{e-1}^x \quad u_e^y\right\}$ $(e=2m_f)$ includes zero displacements $u_{k_o}=0$, $o\in 1,2$, where $k_1=2m_p-1$, $k_2=2m_p$, and the matrix $u_a=\left\{u_{a_1}^x \quad u_{a_2}^y \quad \cdots \quad u_{a_{c-1}}^x \quad u_{a_c}^y\right\}$ is a submatrix of *u*, where $u_{a_c}\neq 0$.

The vectors of displacements along *x*- and *y*-axes are determined by the expressions $u_m^x=u_{m_x}$ and $u_m^y=u_{m_y}$ respectively, where $m_x=2m-1$, $m_y=2m$.

The displacement vector *v* of the nodes of the *i*-th finite element is constructed as $v_i=\left\{u_{m^1}^x \quad u_{m^1}^y \quad u_{m^2}^x \quad u_{m^2}^y \quad u_{m^3}^x \quad u_{m^3}^y \quad u_{m^4}^x \quad u_{m^4}^y\right\}$, where $N_{m^1,i}=1$, $N_{m^2,i}=2$, $N_{m^3,i}=3$, $N_{m^4,i}=4$, $u_{m^q}^x$ and $u_{m^q}^y$ are the nodal displacements along *x*- and *y*-axes, respectively.

The strain vector ε of the *i*-th finite element is determined from the expression

$$\varepsilon\left(i,\xi,\eta\right)=\beta\left(\xi,\eta\right)\cdot v_i, \tag{9}$$

where $\beta(\xi,\eta)$ is the matrix of the relationship between nodal displacements and deformations,

$$\beta(\xi,\eta)=\frac{1}{2}\begin{pmatrix} b_a\left(1,\eta\right) & 0 \\ 0 & a_a\left(1,\xi\right) \\ b_a\left(2,\eta\right) & 0 \\ 0 & a_a\left(2,\xi\right) \\ b_a\left(3,\eta\right) & 0 \\ 0 & a_a\left(3,\xi\right) \\ b_a\left(4,\eta\right) & 0 \\ 0 & a_a\left(4,\xi\right) \end{pmatrix}^T, \tag{10}$$

with $a_a(q,\xi)=\eta_q\left(1+\xi_q\xi\right)\big/b_{fe}$,

$b_a(q,\eta)=\xi_q\left(1+\eta_q\eta\right)\big/a_{fe}$, and $q=1,2\ldots 4$.

The vector of nodal stresses σ of the *i*-th finite element is determined as

$$\sigma\left(i,\xi,\eta\right)=\chi\varepsilon\left(i,\xi,\eta\right), \tag{11}$$

where χ is the matrix of elastic constants, $\xi=\xi_q$, $\eta=\eta_q$, and

$$\chi=\frac{E}{\left(1+\mu\right)\left(1-2\mu\right)}\begin{pmatrix} 1-\mu & \mu \\ \mu & 1-\mu \end{pmatrix}, \tag{12}$$

The equivalent stresses σ_e at nodes of the finite element are determined by the von Mises criterion [21]

$$\sigma_e=\sqrt{\sigma_1^{\,2}+\sigma_2^{\,2}-\sigma_1\cdot\sigma_2}, \tag{13}$$

where σ_1 and σ_2 are the principal stresses.

3. RESULTS

Diagrams of the stress distribution in solid plates obtained in the «Structural Mechanics» module of the «COMSOL» package have been verified using the algorithm for solving the plane problem. Based on the calculated results for the solid plate with the thickness $t=1.5$ mm using the constructed algorithm and boundary conditions (4), a graph of isolines with the stress distribution is shown in Fig. 7, a. A similar stress distribution diagram obtained in the COMSOL software with the boundary conditions (1) is presented in Fig. 7, b. The load magnitudes according to the constructed algorithm at $\sigma_{max}=\sigma_{0.2}$ for plates with the thickness $t=1.5$ and $t=2$ mm are 435 and 785.5 N, respectively, and those obtained via the COMSOL software for the same plates are 425.7 and 755.9 N, respectively. The solutions according to the two approaches are in good agreement.

The stress distribution diagrams under the condition of the three-point bending (2) for a plate with the thickness $t=1.5$ mm obtained via the algorithm for solving the plane problem and

the «COMSOL» system are presented, respectively, in Fig. 8, a and Fig. 8, b. The load magnitudes calculated via the constructed algorithm for plates with the thickness $t = 1.5$ and $t = 2$ mm at $\sigma_{max} = \sigma_{0.2}$ are 282.4 and 505.8 N, respectively, and for the same plates via the COMSOL package are 307.7 and 558.2 N, respectively. The solutions obtained using the two approaches are in good agreement.

Based on the results of the strength analysis, graphs of the sandwich plate honeycomb core relative density dependence of the load F_y are shown in Fig. 9 and Fig. 10, respectively, for the boundary conditions (1) and (2). The solid body volume of composite and solid plates dependence of the load F_y at bending with rigid fixation (Fig. 11) and three-point bending (Fig. 12) are also presented.

Reference to Fig. 9 shows that under the conditions of bending with rigid fixation (1), within the range of values of the honeycomb core relative density from 20 to 35 %, there is a significant difference in the strength of sandwich plates with different discretization of tetrachiral structures at the same relative density. From Fig. 10 it is seen that under the conditions of three-point bending (2), sandwich plates with different discretization and equal relative density of tetrachiral honeycombs demonstrate a small difference in the strength over the entire range of values of the relative density. Composite plates with tetrachiral honeycombs (Figs. 11-12) could significantly reduce the volume of a solid body relative to solid plates with equal strength.

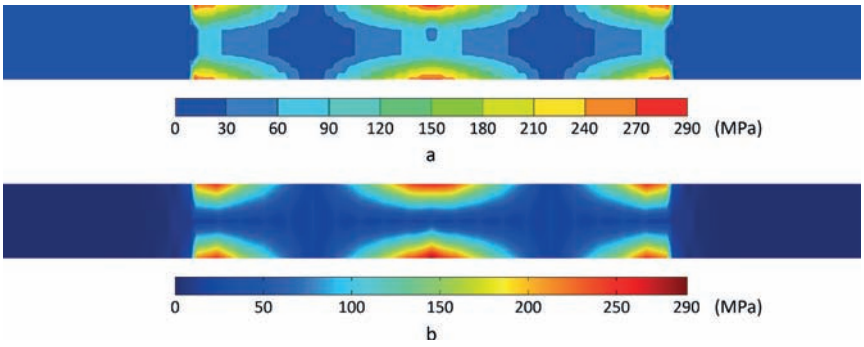

Figure 7. The stress distribution diagrams for a solid plate with thickness $t = 1.5$ mm under the bending with rigid fixation conditions at $\sigma_{max} = \sigma_{0.2}$ obtained using (a) the algorithm for solving the plane problem, and (b) the «COMSOL» software

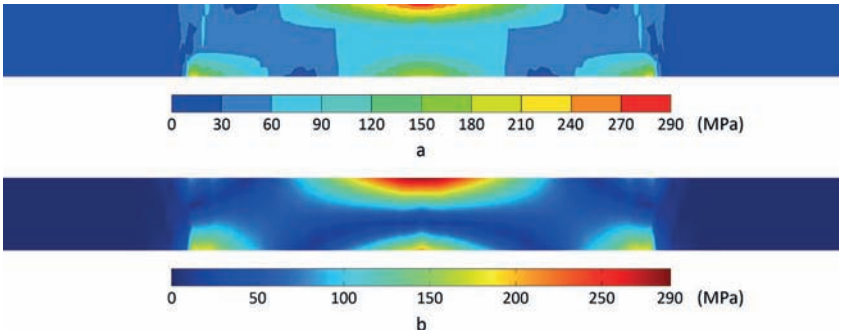

Figure 8. The stress distribution diagrams for a solid plate with thickness $t = 1.5$ mm under the three-point bending conditions (2) at $\sigma_{max} = \sigma_{0.2}$ obtained using (a) the algorithm for solving the plane problem, and (b) the «COMSOL» software

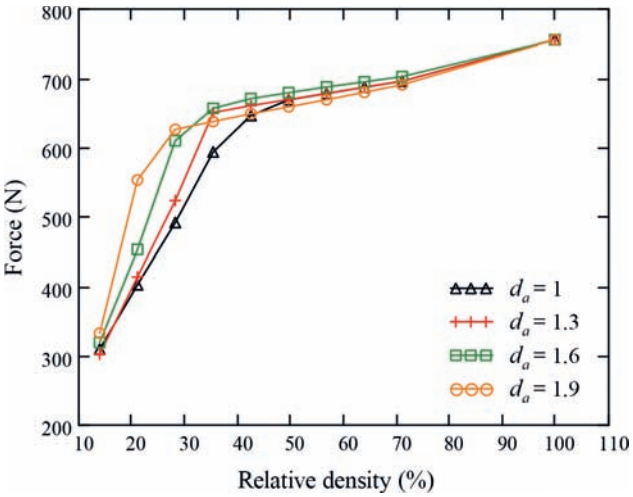

Figure 9. Diagram of the sandwich plate honeycomb core relative density dependence of the load F_y (at $\sigma_{max} = \sigma_{0.2}$) at bending with rigid fixation (1)

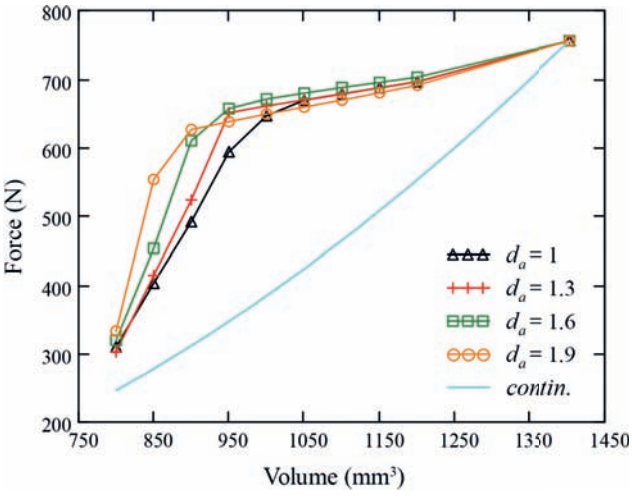

Figure 11. Diagram of the solid body volume of composite and solid plates dependence of the load F_y (at $\sigma_{max} = \sigma_{0.2}$) under bending with rigid fixation (1)

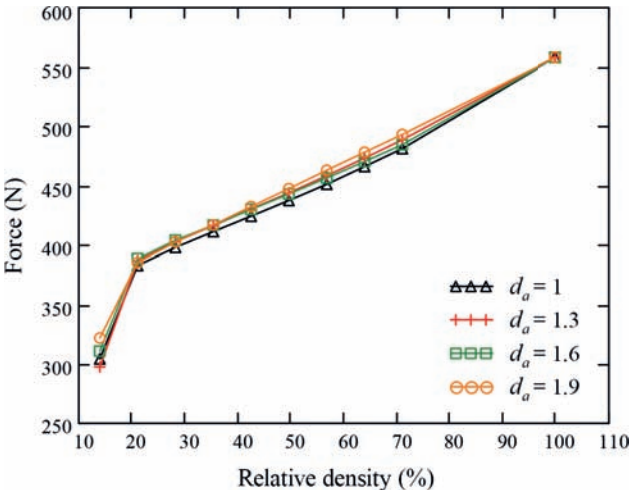

Figure 10. Diagram of the sandwich plate honeycomb core relative density dependence of the load F_y (at $\sigma_{max} = \sigma_{0.2}$) at three-point bending (2)

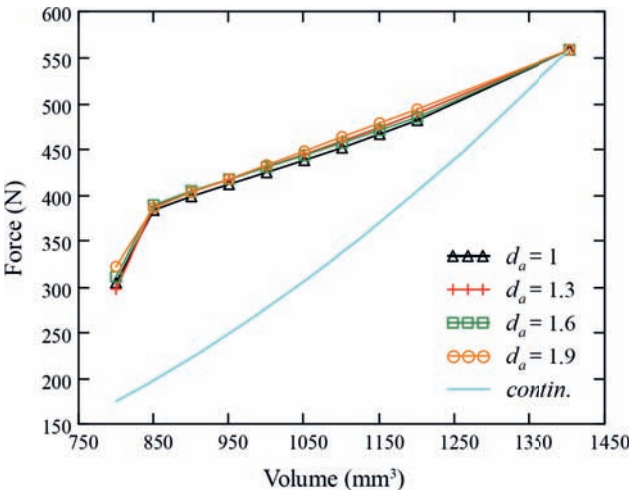

Figure 12. Diagram of the solid body volume of composite and solid plates dependence of the load F_y (at $\sigma_{max} = \sigma_{0.2}$) under three-point bending (2)

CONCLUSIONS

Based on the results of the numerical analysis, it has been shown that composite plates with tetrachiral honeycombs with a relative density of honeycomb cores from 20 to 70% have a significantly higher strength relative to solid plates with an equal volume of a solid body. At

bending with rigid fixation, the discretization of tetrachiral structures effects the strength of composite plates at relative density values from 20 to 35%. Honeycombs with large unit cell size are stronger relative to those with smaller unit cell size at the same relative density. The use of tetrachiral honeycomb cores in the design of composite plates is a promising approach for improving the mechanical properties of composite plates.

FUNDING

This research has been supported by the Project #3.1.1.2 within the 2021 Plan of Fundamental Research of the Russian Academy of Architecture and Civil Engineering and Ministry of Civil Engineering and Public Utilities of the Russian Federation. The studies have been carried out using the facilities of the Collective Research Center named after Professor Yu. M. Borisov, Voronezh State Technical University, which is partly supported by the Ministry of Science and Education of the Russian Federation, Contract No 075- 15-2021-662.

REFERENCES

1. **Saxena K.K., Das R., Calius E.P.** Three decades of auxetics research – materials with negative Poisson's ratio: a review // Advanced Engineering Materials, 2016, Vol. 18, pp. 1847-1870. DOI:10.1002/adem.201600053
2. **Lakes R.S.** Negative-Poisson's-ratio materials: auxetic solids // Annual review of materials research, 2017, Vol. 47, pp. 63-81. DOI:10.1146/annurev-matsci-070616-124118
3. **Wang Z., Luan C., Liao G., Liu J., Yao X., Fu J.** Progress in auxetic mechanical metamaterials: structures, characteristics, manufacturing methods, and applications // Advanced Engineering Materials, 2020, Vol. 22, Article ID 2000312. DOI:10.1002/adem.202000312
4. **Love A.E.H.** A treatise on the mathematical theory of elasticity // Cambridge University Press, Cambridge, 1892. https://hal.archives-ouvertes.fr/hal-01307751
5. **Landau L.D., Lifshitz E.M.** Course of Theoretical Physics Vol 7: Theory and Elasticity // Pergamon Press, Oxford, 1959**.**
6. **Mazaev A.V., Ajeneza O., Shitikova M.V.** Auxetics materials: classification, mechanical properties and applications // IOP Conference Series: Materials Science and Engineering, 2020, Vol. 747, p. 012008. DOI:10.1088/1757-899X/747/1/012008
7. **Prall D., Lakes R.S.** Properties of a chiral honeycomb with a Poisson's ratio of -1 // International Journal of Mechanical Sciences, 1997, Vol. 39, pp. 305-314. DOI:10.1016/S0020-7403(96)00025-2
8. **Scarpa F.L., Tomlinson G.R.** Vibroacoustics and damping analysis of negative Poisson's ratio honeycombs // Proceedings of SPIE, Smart Structures and Materials: Passive Damping and Isolation, 1998, Vol. 3327, pp. 339-348. DOI:10.1117/12.310695
9. **Alderson A., Alderson K.L., Attard D., Evans K.E., Gatt R., Grima J.N., Miller W., Ravirala N., Smith C.W., Zied K.** Elastic constants of 3-, 4-and 6-connected chiral and anti-chiral honeycombs subject to uniaxial in-plane loading // Composites Science and Technology, 2010, Vol. 70, pp. 1042-1048. DOI:10.1016/j.compscitech.2009.07.009
10. **Lira C., Scarpa F., Rajasekaran R.** A gradient cellular core for aeroengine fan blades based on auxetic configurations // Journal of Intelligent Material Systems and Structures, 2011, Vol. 22, pp. 907-917. DOI:10.1177/1045389X11414226
11. **Li T., Wang L.** Bending behavior of sandwich composite structures with tunable 3D-printed core materials // Composite Structures, 2017, Vol. 175, pp. 46-57. DOI:10.1016/j.compstruct.2017.05.001
12. **Alomarah A., Masood S.H., Sbarski I., Faisal B., Gao Z., Ruan D.** Compressive

properties of 3D printed auxetic structures: experimental and numerical studies // Virtual and Physical Prototyping, 2020, Vol. 15, pp. 1-21. DOI:10.1080/17452759.2019.1644184

13. **Xiao D., Chen X., Li Y., Wu W., Fang D.** The structure response of sandwich beams with metallic auxetic honeycomb cores under localized impulsive loading-experiments and finite element analysis // Materials & Design, 2019, Vol. 176, p. 107840. DOI:10.1016/j.matdes.2019.107840
14. **Essassi K., Rebiere J.L., El Mahi A., Ben Souf M.A., Bouguecha A., Haddar M.** Investigation of the static behavior and failure mechanisms of a 3D printed bio-based sandwich with auxetic core // International Journal of Applied Mechanics, 2020, Vol. 12, p. 2050051. DOI:10.1142/S1758825120500519
15. **Smardzewski J.** Experimental and numerical analysis of wooden sandwich panels with an auxetic core and oval cells // Materials & Design, 2019, Vol. 183, p. 108159. DOI:10.1016/j.matdes.2019.108159
16. **Peliński K., Smardzewski J.** Bending behavior of lightweight wood-based sandwich beams with auxetic cellular core // Polymers, 2020, Vol. 12, p. 1723. DOI:10.3390/polym12081723
17. COMSOL AB. Structural Mechanics Module User's Guide // COMSOL AB, Stockholm, 2020
18. **Shalin R.E.** Aviation materials: reference book. Aluminum and beryllium alloys. Deformable aluminum alloys and beryllium-based alloys (in Russian) // VIAM, Moscow, 1982.
19. **Obraztsov I.F., Savel'ev L.M., Khazanov K.S.** Finite element method in problems of structural mechanics of aircraft (in Russian) // Vysshaya Shkola, Moscow, 1985.
20. **Zienkiewicz O.C., Morice P.B.** The finite element method in engineering science // McGraw-Hill, London, 1971.
21. **Rabotnov Yu.N.** Resistance of materials (in Russian) // Fizmatgiz, Moscow, 1962.

СПИСОК ЛИТЕРАТУРЫ

1. **Saxena K.K., Das R., Calius E.P.** Three decades of auxetics research – materials with negative Poisson's ratio: a review // Advanced Engineering Materials, 2016, Vol. 18, pp. 1847-1870. DOI:10.1002/adem.201600053
2. **Lakes R.S.** Negative-Poisson's-ratio materials: auxetic solids // Annual review of materials research, 2017, Vol. 47, pp. 63-81. DOI:10.1146/annurev-matsci-070616-124118
3. **Wang Z., Luan C., Liao G., Liu J., Yao X., Fu J.** Progress in auxetic mechanical metamaterials: structures, characteristics, manufacturing methods, and applications // Advanced Engineering Materials, 2020, Vol. 22, Article ID. 2000312. DOI:10.1002/adem.202000312
4. **Ляв А.** Математическая теория упругости // М.-Л.: ОНТИ, 1935.
5. **Ландау Л.Д., Лифшиц Е.М.** Механика сплошных сред. Гидродинамика и теория упругости // М.-Л.: Гостехиздат, 1944.
6. **Mazaev A.V., Ajeneza O., Shitikova M.V.** Auxetics materials: classification, mechanical properties and applications // IOP Conference Series: Materials Science and Engineering, 2020, Vol. 747, p. 012008. DOI:10.1088/1757-899X/747/1/012008
7. **Prall D., Lakes R.S.** Properties of a chiral honeycomb with a Poisson's ratio of -1 // International Journal of Mechanical Sciences, 1997, Vol. 39, pp. 305-314. DOI:10.1016/S0020-7403(96)00025-2
8. **Scarpa F.L., Tomlinson G.R.** Vibroacoustics and damping analysis of negative Poisson's ratio honeycombs // Proceedings of SPIE, Smart Structures and Materials: Passive Damping and Isolation, 1998, Vol. 3327, pp. 339-348. DOI:10.1117/12.310695
9. **Alderson A., Alderson K.L., Attard D., Evans K.E., Gatt R., Grima J.N., Miller W., Ravirala N., Smith C.W., Zied K.** Elastic constants of 3-, 4-and 6-connected chiral and

anti-chiral honeycombs subject to uniaxial in-plane loading // Composites Science and Technology, 2010, Vol. 70, pp. 1042-1048. DOI:10.1016/j.compscitech.2009.07.009
10. **Lira C., Scarpa F., Rajasekaran R.** A gradient cellular core for aeroengine fan blades based on auxetic configurations // Journal of Intelligent Material Systems and Structures, 2011, Vol. 22, pp. 907-917. DOI:10.1177/1045389X11414226
11. **Li T., Wang L.** Bending behavior of sandwich composite structures with tunable 3D-printed core materials // Composite Structures, 2017, Vol. 175, pp. 46-57. DOI:10.1016/j.compstruct.2017.05.001
12. **Alomarah A., Masood S.H., Sbarski I., Faisal B., Gao Z., Ruan D.** Compressive properties of 3D printed auxetic structures: experimental and numerical studies // Virtual and Physical Prototyping, 2020, Vol. 15, pp. 1–21. DOI:10.1080/17452759.2019.1644184
13. **Xiao D., Chen X., Li Y., Wu W., Fang D.** The structure response of sandwich beams with metallic auxetic honeycomb cores under localized impulsive loading-experiments and finite element analysis // Materials & Design, 2019, Vol. 176, p. 107840. DOI:10.1016/j.matdes.2019.107840
14. **Essassi K., Rebiere J.L., El Mahi A., Ben Souf M.A., Bouguecha A., Haddar M.** Investigation of the static behavior and failure mechanisms of a 3D printed bio-based sandwich with auxetic core // International Journal of Applied Mechanics, 2020, Vol. 12, p. 2050051. DOI:10.1142/S1758825120500519
15. Smardzewski J. Experimental and numerical analysis of wooden sandwich panels with an auxetic core and oval cells // Materials & Design, 2019, Vol. 183, Article ID 108159. DOI:10.1016/j.matdes.2019.108159
16. **Peliński K., Smardzewski J.** Bending behavior of lightweight wood-based sandwich beams with auxetic cellular core // Polymers, 2020, Vol. 12, p. 1723. DOI:10.3390/polym12081723
17. COMSOL AB. Structural Mechanics Module User's Guide // COMSOL AB, Stockholm, 2020
18. **Шалин Р.Е.** Авиационные материалы. Алюминиевые и бериллиевые сплавы. Деформируемые алюминиевые сплавы и сплавы на основе бериллия // М.: ОНТИ, 1982.
19. **Образцов И.Ф., Савельев Л.М., Хазанов Х.С.** Метод конечных элементов в задачах строительной механики летательных аппаратов // М.: Высшая школа, 1985.
20. **Зенкевич О.** Метод конечных элементов в технике. М.: Мир, 1975.
21. **Работнов Ю.Н.** Сопротивление материалов // М.: Физматгиз, 1962.

Alexey V. Mazaev, PhD Student, Junior Researcher, Research Center on Dynamics of Solids and Structures; Voronezh State Technical University; 84, 20-letija Oktyabrya, Voronezh, 394006, Russia; Reserach Engineer, RAASN Research Institute of Structural Physics, Moscow, Russia. E-mail: mazaevonline@gmail.com.

Marina V. Shitikova, Advisor of the Russian Academy of Architecture and Construction Sciences, Prof., Dr. Sc., Research Center on Dynamics of Solids and Structures; Voronezh State Technical University; 84, 20-letija Oktyabrya, Voronezh, 394006, Russia; phone +7 (473) 271-52-68; fax +7 (473) 271-52-68; Senior Researcher, RAASN Research Institute of Structural Physics, Moscow, Russia. E-mail: mvs@vgasu.vrn.ru.

Мазаев Алексей Вячеславович, аспирант; младший научный сотрудник научного Центра по фундаментальным исследованиям в области естественных и строительных наук; Воронежский государственный технический университет; 394006, Россия, г. Воронеж, ул. 20 лет Октября, д. 84; инженер-исследователь, Научно-исследовательский институт строительной физики РААСН, Москва, Россия. E-mail: mazaevonline@gmail.com.

Шитикова Марина Вячеславовна, советник РААСН, профессор, доктор физико-математических наук; руководитель международного научного Центра по фундаментальным исследованиям в области естественных и строительных наук; Воронежский государственный технический университет; 394006, Россия, г. Воронеж, ул. 20 лет Октября, д. 84, тел. +7 (473) 271-52-68; факс +7 (473) 271-52-68; Главный научный сотрудник, Научно-исследовательский институт строительной физики РААСН, Москва, Россия. E-mail: mvs@vgasu.vrn.ru.

International Journal for Computational Civil and Structural Engineering, 17(3) 114–119 (2021)

DOI:10.22337/2587-9618-2021-17-3-114-119

ON THE CHOICE OF PRESTRESSING PARAMETERS

Anatolii V. Perelmuter

SCAD Soft, Ltd, Kiev, UKRAINE

Abstract: This paper focuses on the regulation of forces in a statically indeterminate system under the action of many loads. This regulation is realized by prestressing. The paper compares two proposed methods for selecting rational values of the prestressing parameters: maximizing the minimum bearing capacity margin for the elements of the system (1) and equalizing the margins for all elements (2). An illustrative example is provided.

Keywords: prestressing, bearing capacity margins, Chebyshev solution, margin equalization

О ВЫБОРЕ ПАРАМЕТРОВ ПРЕДНАПРЯЖЕНИЯ

А.В. Перельмутер

НПО «СКАД Софт», г. Киев, УКРАИНА

Аннотация: Рассматривается задача о регулировании усилий в статически неопределимой системе находящейся под воздействием многих нагружений. Регулирование выполняется путем создания предварительного напряжения. Сопоставляются два предлагаемых метода для выбора рациональных значений параметров преднапряжения: максимизация минимального по элементам системы запаса несущей способности (1) и выравнивание запасов по всем элементам (2). Приведен иллюстративный пример.

Ключевые слова: преднапряжение, запасы несущей способности, чебышевское решение, выравнивание запасов

1. INTRODUCTION

One of the effective ways to improve a design is prestressing, which regulates the internal forces in the system. Many works on structural optimization consider prestressing forces as design parameters, along with the cross-sectional dimensions of the structural members [6, 7, 8].

However, such a problem formulation is not the only possible one; there is often a problem of choosing prestressing parameters for a structure with known dimensions, which will not be changed unless absolutely necessary. For example, this situation is typical when analyzing existing structures under changed loading conditions (e.g. during reconstruction). There are many other cases when it is necessary to adjust internal forces in a structure (equalizing moments in continuous beams and stiffening girders of cable-stayed bridges [3, 6], adjustment of cable-stayed structures [9] and others [4]).

2. PROBLEM FORMULATION

We will assume that an internal force envelope diagram is obtained as a result of the analysis of an unstressed system for all the load cases.

With a known internal force envelope diagram we will determine the prestressing parameters, which make it possible, in a way, to improve the distribution of internal forces in the system (e.g. to expand the elastic deformation area, or to reveal the bearing capacity margins, improve the operating mode of the structure, etc.).

Let us show that this problem can be solved using optimization methods. To do this, consider the

expressions for true extreme forces (stresses) in an element (section) of the elastic system

$$\begin{aligned} S_i^+ &= S_i^{prest} + S_i^{max}; \\ S_i^- &= S_i^{prest} + S_i^{min} \quad (i = 1,2,...,m) \end{aligned} \tag{1}$$

Here S_i^{max}, S_i^{min} are the maximum and minimum internal forces in the *i*-th element, obtained as a result of a standard analysis of an elastic *n*-times statically indeterminate system, taking into account the deformation compatibility conditions and possible unfavorable load combinations. The calculated values $S_{i,0}^{max}$ and $S_{i,0}^{min}$ are corrected as follows (Fig. 1).

$$\begin{aligned} S_i^{\max} &= \max\left(0, S_{i,0}^{\max}\right), \\ S_i^{\min} &= \min\left(0, S_{i,0}^{\min}\right). \end{aligned} \tag{2}$$

This ensures that values S_i^{max} are positive and S_i^{min}. are negative.

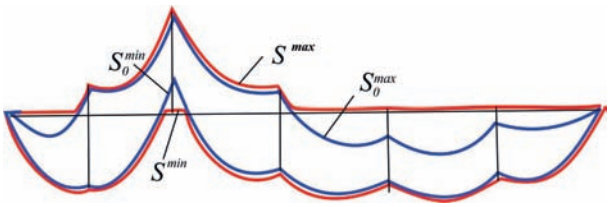

Figure 1.

The prestressing force is determined by the following expression

$$S_i^{prestr} = \sum_{j=1}^{n} s_{ij} x_j \quad (i = 1,2,...,m) \tag{3}$$

where s_{ij} is the force in the *i*-th element of the system from the action $x_j = 1$ of the *j*-th prestressing parameter (unknown of the force method).

If the values of tensile R_i^+ and compressive R_i^- bearing capacity are known, then the bearing capacity conditions are written as

$$S_i^+ \le R_i^+, S_i^- \ge -R_i^+ \quad (i = 1,...,m), \tag{4}$$

or as system of two-sided inequalities

$$\begin{aligned} -R_i^- - S_i^{min} \le \sum_{j=1}^{n} s_{ij} x_j \le R_i^+ - S_i^{max} \\ (i = 1,2,...,m). \end{aligned} \tag{5}$$

System (5) determines the feasibility of the design. If it is consistent, i.e. there are values $x_j \left(j = 1,2,...,n\right)$ which satisfy inequalities (5), then they can be selected as prestressing parameters. If it is inconsistent, we have to set other values of R_i^+ and R_i^-.

It should be noted that if a system is made of an ideal elastoplastic material, and the inequalities (5) are consistent, it will exhibit purely elastic behavior after a certain number of plastic deformation cycles for all possible changes in the live load, i.e. the system will be adaptable. This conclusion follows directly from the Bleich-Melan adaptability theorem.

It means that in cases where the physical realization of an optimal elastic system can be achieved with the help of prestressing, it is always possible to design an optimal elastoplastic system that adapts to a given load program, and there is no need for the artificial regulation of forces.

Not to be bounded by the values of the bearing capacity of the truss members, assuming that the bearing capacity of each member is equal to the extreme force possible for it, i.e. consider the so-called fully stressed structure [5, p. 78], where every part is stressed to the maximum permissible stress at least under one of the possible load combinations, we will consider the following conditions instead of (5)

$$-S_i^{min} \le \sum_{j=1}^{n} s_{ij} x_j \le S_i^{max} \quad (i = 1,2,...,m), \tag{6}$$

that is, our goal is to find the prestress that should reduce the internal force variation range calculated without its effect.

When the system (6) is consistent, there is an infinite set of solutions which forms a domain Ω in the space of values $\mathbf{x}=(x_1,...,x_n)$. You can choose from this set the values of the prestressing parameters which satisfy some predetermined conditions. Let us consider some of the possible options.

3. OPTIONS

Bearing capacity margin maximization.
We will assume that, all other things being equal, prestressing ensuring the maximum bearing capacity margin of the system will be the best. Since the values

$$\begin{aligned} f_i(\mathbf{x}) &= S_i^{max} - \sum_{j=1}^{n} s_{ij}x_j \quad (i=1,2,...,m); \\ f_i(\mathbf{x}) &= S_i^{min} + \sum_{j=1}^{n} s_{ij}x_j \quad (i=m+1,...,2m) \end{aligned} \tag{7}$$

characterize these margins for all elements (sections) of the system, it is advisable to look for such a vector $\mathbf{x}^*=(x_1^*,...,x_n^*)$, for which the following condition is satisfied

$$L(\mathbf{x}^*)=\max_x \min_{1\le i\le 2m} f_i(\mathbf{x}), \tag{8}$$

i.e. the minimum bearing capacity margin for the elements of the system is maximized. Determining the value $L(\mathbf{x})$ from the condition (8) with limitations (6) is the problem of finding the Chebyshev point of a system of linear inequalities. This problem can also be solved as the following linear programming problem [2]:

find the maximum of a linear form

$$z = x_{n+1} \tag{9}$$

with limitations

$$\begin{aligned} f_i(\mathbf{x}) &= S_i^{max} - \sum_{j=1}^{n} s_{ij}x_j + x_{n+1} \\ &\quad (i=1,2,...,m); \\ f_i(\mathbf{x}) &= S_i^{min} + \sum_{j=1}^{n} s_{ij}x_j + x_{n+1} \\ &\quad (i=m+1,...,2m) \end{aligned} \tag{10}$$

If we denote the Chebyshev solution of the inconsistent system as $X^*=(x_1^*,...,x_n^*)$ then by creating the corresponding prestress in the system, we can obtain the following values of the required bearing capacity parameters:

$$\begin{aligned} R_i^{\%} &= S_i^{max} - \sum_{j=1}^{n} s_{ij}x_j^*, \\ R_i^{\%} &= S_i^{min} + \sum_{j=1}^{n} s_{ij}x_j^* \quad (i=1,2,...,m) \end{aligned} \tag{11}$$

Strength margin equalization.
Strength margin of a complex multi-element system is often determined by forces in only a few design members, while other members have much larger bearing capacity margins. Therefore, you might want to use prestressing to obtain a system with uniform margins [1].
The consistency condition for the system of inequalities (3), which can be written as follows

$$f_i(x_1,...,x_n)\ge 0 \quad (i=1,...,2m), \tag{12}$$

indicates that there are interior points in the domain Ω defined by the inequalities (10) if at least one of these inequalities is strict. We will further proceed from this assumption.
Following [1], we consider an auxiliary function in the form of the product of the bearing capacity margins

$$P = f_1 \cdot f_2 ... f_{2m}. \tag{13}$$

The function P is smooth and takes positive values at all interior points of the domain Ω, and vanishes at the boundary of this domain, since here at least one of the functions (7) is equal to

zero. Hence the smooth function P reaches its maximum at an interior point of the domain Ω.
To show that this maximum is realized at a single point M^* and, therefore, the local maximum coincides with the global one, consider the logarithm of P.

$$L = \ln P = \sum_{i=1}^{2m} \ln f_i. \tag{14}$$

The function L is negatively defined and concave in the domain Ω, as evidenced by the analysis of a matrix of the second partial derivatives

$$\frac{\partial^2 L}{\partial x_i \partial x_k} = \sum_{j=1}^{2m} \frac{1}{f_j} \cdot \frac{\partial^2 f_j}{\partial x_i \partial x_k} - \sum_{j=1}^{2m} \frac{\partial f_j}{\partial x_i} \cdot \frac{1}{f_j^2} \cdot \frac{\partial f_j}{\partial x_k} \quad (i,k = 1,\ldots,n) \tag{15}$$

Taking into account that

$$f_j = \left(\sum_{s=1}^{n} a_{js} x_s + b_j \right), \tag{16}$$

we obtain

$$\frac{\partial^2 L}{\partial x_i \partial x_k} = -\sum_{j=1}^{2m} \cdot \frac{a_{ji} a_{jk}}{\left(\sum_{s=1}^{n} a_{js} x_s + b_j \right)^2} \quad (i,k = 1,\ldots,n) \tag{17}$$

The negative definiteness of a matrix with such coefficients follows from the conditions of linear independence of functions (10).

The solution corresponding to the point M^*, located as far as possible from the boundaries of the permissible domain, and its deviations from the boundaries determine a balanced system of strength margins.

4. NUMERICAL EXAMPLE

As an illustrative example, consider a simple system of four bars with the same tension-compression stiffness shown in Fig. 2. It can be subjected to one of the three independent loads at a time: P_1=10 t, P_2=10 t and P_3=10 t.

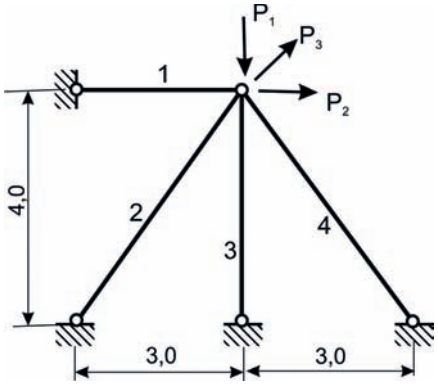

Figure 2.

Forces in the 1st and 3rd bars are used as the prestressing parameters of this twice statically indeterminate system. Force values obtained as a result of the static analysis are given in Table 1

Table 1

Bar	Forces from loads:			Extreme		Prestressing	
J	P_1	P_2	P_3	S^{max}	S^{min}	x_1=1	x_2=1
1	0.000	6.983	5.382	6.983	0.000	1.000	0.000
2	-3.162	2.514	4.375	4.375	3.808	-0.707	-0.707
3	-4.941	0.000	3.808	-3.162	-4.941	0.000	1.000
4	-3.162	-2.514	0.499	0.499	-3.162	0.707	-0.707

Inequalities of type (5) for this system have the form

$$0 \le x_1 \le 6.983,$$

$$3.808 \le -0.707x_1 - 0.707x_2 \le 4.375,$$
$$-4.941 \le x_2 \le -3.162,$$
$$-3.162 \le 0.707x_1 - 0.707x_2 \le 0.499.$$

Their graphical representation is shown in Fig. 3. As can be seen from Fig. 3, only four limitations shown with a bold line are active.

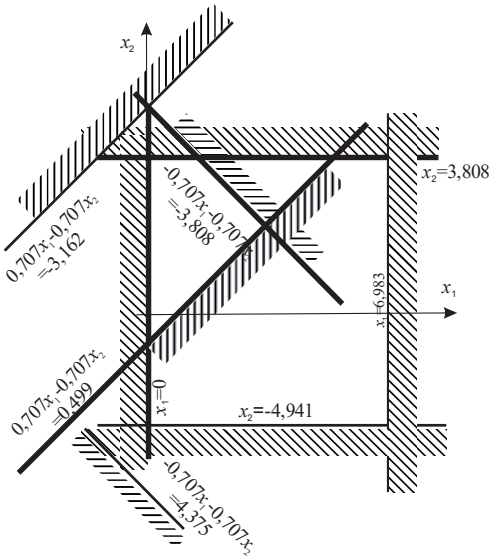

Figure 3

These limitations can be expressed in the form of the following inequalities:

$$x_1 \geq 0$$
$$-3.162 \leq -0.707x_1 - 0.707x_2$$
$$x_2 \leq 3.808$$
$$0.707x_1 - 0.707x_2 \leq 0.499$$

We will further consider only these limitations, although it should be noted that in practical problems it is impossible to discard inactive limitations in advance and, as a result, the amount of computation increases significantly.

It should also be noted, however, that using only active limitations has no effect on the calculation results, since the unaccounted values of the bearing capacity margins $f_j(\mathbf{x})$ a priori exceed the considered values.

Both solutions can be illustrated graphically for the considered problem with two unknowns. The solution to the Chebyshev point problem is shown in Fig. 4.*a*, where the lines of the function level are shown by the dotted line

$$L(\mathbf{x}) = \min[f_1(\mathbf{x}), f_2(\mathbf{x}), f_3(\mathbf{x}), f_3(\mathbf{x})].$$

The solution to the equal margin problem is shown in Fig. 4.*b*, where the lines of the function level are shown by the dotted line

$$P(\mathbf{x}) = f_1(\mathbf{x}) \times f_2(\mathbf{x}) \times f_3(\mathbf{x}) \times f_4(\mathbf{x}).$$

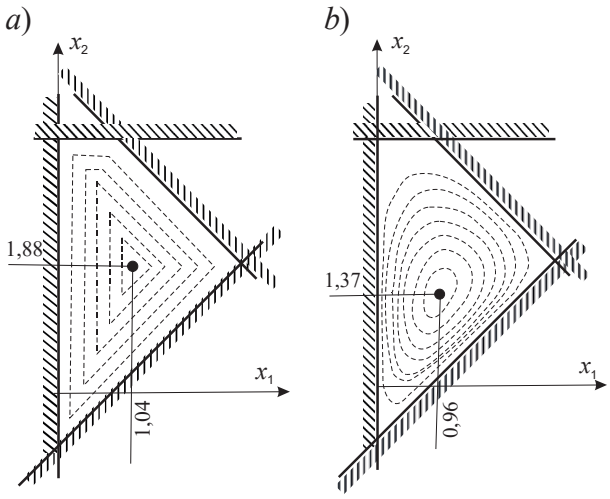

Figure 4

Table 2 provides forces in the bars adjusted by prestressing for the Chebyshev point problem. And while for a system without prestressing with bars of the same cross-section it was necessary at least to ensure the following values $R^+ = 6.983$ and $R^- = 4.941$, for a prestressed system we have $R^+ = 6.44$ and $R^- = 6.82$.

Table 2

j	P_1	P_2	P_3	S^{max}	S^{min}
1	-1.04	5.94	4.34	5.94	-1.04
2	-1.10	4.58	6.44	6.44	-1.10
3	-6.82	-1.88	1.93	1.93	-6.82
4	-2.57	-1.92	1.09	1.09	-2.57

Table 3 provides the adjusted force values for the equal margin problem. Here we have the minimum possible values of the bearing capacity parameters R+ = 6.02 and R– = 2.87.

Table 3

j	P_1	P_2	P_3	S^{max}	S^{min}
1	-0.96	6.02	4.42	6.02	-0.96
2	-1.51	4.16	6.02	6.02	-1.51
3	-6.31	-1.37	2.44	2.44	-1.37
4	-2.87	-2.22	0.79	0.79	-2.87

As you can see, in this example ensuring uniform bearing capacity margins is more advantageous in terms of the weight of the structure.

There can be other relationships between the considered solutions as well. The choice between them depends on many factors and is informal.

REFERENCES

1. **Gordeev V.N**. A method of solution of a convex programming problem // Cybernetics and Systems Analysis, 1971, No.2, p.70-73.
2. **Zukhovitsky S.I., Avdeeva L.I.** Linear and convex programming – M.: Nauka, 1967 –460 p.
3. Korneev M.M. Steel Bridges: Theoretical and Practical Guide to the Design of Bridges. In 3 volumes – K.: Ultradruk, 2018 – 390+445+541 p.
4. **Perelmuter A.V.** Prestressed steel structures: A historical overview // The collection of proceedings of the V.N. Shimanovsky Ukrainian Institute of Steel Construction. Issue 20 – K.: Publishing house “Steel”, 2017 – p. 4-38.
5. **Reitman M.I., Shapiro G.S.** Methods of optimal design of deformable bodies – M.: Nauka, 1976 – 268 p.
6. **Trofimovich V.V., Permyakov V.A.** Optimal design of steel structures – K.: Budivelnyk, 1981 – 136 p.
7. **Felton L.P., Dobbs M.W.** On optimized prestressed trusses // AIAA Journal, 1977, Vol. 15 – P.1037-1039.
8. **Hoffmeister L.D., Felton L.P.** Prestressing in structural synthesis // A1AA Journal, 1970, Vol., – P. 363-366.
9. **Quagliaroli M., Malerba G., Albertin A., Pollini N.** The role of prestress and its optimization in cable domes design // Computers & Structures, 2015, vol. 161 – P. 17–30.

СПИСОК ЛИТЕРАТУРЫ

1. **Гордеев В.Н.** Об одном методе решения задачи выпуклого программирования // Кибернетика, 1971, 2№ С.70-73.
2. **Зуховицкий С.И., Авдеева Л.И.** Линейное и выпуклое рограммирование – М.: Наука, 1967 – 460 с.
3. **Корнеев М.М.** Стальные мосты: Теоретическое и практическое пособие по проектированию. В 3 томах – К.: Ультрадрук, 2018 – 390+445+541 с.
4. **Перельмутер А.В.** Преднапряженные металлические конструкции: исторический обзор // Збірник наукових праць Українського інституту сталевих конструкцій імені В.М. Шимановського. Вип. 20 – К.: Видавництво «Сталь», 2017 – С. 4-38.
5. **Рейтман М.И., Шапиро Г.С.** Методы оптимального проектирования деформируемых тел – М.: Наука, 1976 – 268 с.
6. **Трофимович В.В., Пермяков В.А.** Оптимальное проектирование металлических конструкций – К.: Будівельник, 1981 – 136 с.
7. **Felton L.P., Dobbs M.W.** On optimized prestressed trusses // AIAA Journal, 1977, Vol. 15 – P.1037-1039.
8. **Hoffmeister L.D., Felton L.P.** Prestressing in structural synthesis // A1AA Journal, 1970, Vol., – P. 363-366.
9. **Quagliaroli M., Malerba G., Albertin A., Pollini N.** The role of prestress and its optimization in cable domes design // Computers & Structures, 2015, vol. – P. 17–30.

Anatolii V. Perelmuter, Foreign member of Russian Academy of Architecture and Construction Sciences, Doctor of Science, SCAD Soft, Ltd, Kiev, Ukraine
e-mail: AnatolyPerelmuter@gmail.com.

Перельмутер Анатолий Викторович, иностранный член РААСН, доктор технических наук, НПО СКАД Софт, 03037, Украина, г.Киев, ул. Просвящения, дом 3а, офис 2, e-mail: AnatolyPerelmuter@gmail.com.

DOI:10.22337/2587-9618-2021-17-3-120-131

DYNAMIC BEHAVIOR OF REINFORCED CONCRETE COLUMN UNDER ACCIDENTAL IMPACT

Sergey Yu. Savin [1], ***Vitaly I. Kolchunov*** [1,2]
[1] National Research Moscow State University of Civil Engineering, Moscow, RUSSIA
[2] Southwest state university, Kursk, RUSSIA

Abstract: The analysis of scientific literature shows that to date, the physical parameters of the deformation of reinforced concrete bar structures during their dynamic buckling and the influence of the dissipative properties of the structural system on this process remain insufficiently studied. In this regard, the paper proposes an analytical solution to the problem of dynamic buckling of a reinforced concrete column when it is loaded with an impact load, taking into account the presence of initial geometric and (or) physical imperfections and damping properties of the system, as well as an analysis and assessment of the column deformation parameters based on the obtained analytical solution. An expression for the dynamic deflection of a bar element under its axial loading with a high-speed shock load, taking into account damping, is obtained in an analytical form. For practical calculations in a quasi-static formulation, the paper proposes an expression for the dynamic factor kd of bar structures under axial shock load. A numerical example of calculating a reinforced concrete column using the obtained analytical expressions with and without damping is considered. It was found that the maximum deflection of the elastic axis of the column under high-speed loading was achieved at t = 0.04 s. In this case, the total dynamic deflection taking into account damping was 4.8% less than the deviation without taking into account damping and 1.18 times more than the corresponding static value.

Keywords: reinforced concrete, column, buckling, accidental impact, progressive collapse, deflection, velocity, acceleration

ДЕФОРМИРОВАНИЕ ЖЕЛЕЗОБЕТОННОЙ ВНЕЦЕНТРЕННО СЖАТОЙ КОЛОННЫ ПРИ ДОГРУЖЕНИИ УДАРНОЙ НАГРУЗКОЙ

С.Ю. Савин [1], ***В.И. Колчунов*** [1,2]
[1] Национальный исследовательский Московский государственный строительный университет, г. Москва, РОССИЯ
[2] Юго-Западный государственный университет, г. Курск, РОССИЯ

Аннотация: Анализ научной литературы показывает, что к настоящему времени остаются недостаточно исследованными физические параметры деформирования железобетонных стержневых конструкций при их динамическом продольном изгибе и влияние на этот процесс диссипативных свойств конструктивной системы. В связи с этим, в рассматриваемой работе предложено аналитическое решение задачи о динамическом продольном изгибе железобетонной колонны при ее догружении ударной нагрузкой с учетом наличия начальных геометрических и (или) физических несовершенств и демпфирующих свойств системы, а также дан анализ и оценка параметров деформирования колонны на основе полученного аналитического решения. В аналитической форме получено выражение динамического отклонения упругой оси стержневого элемента при его продольном нагружении высокоскоростной ударной нагрузкой с учетом демпфирования. Для практических расчетов в квазистатической постановке предложено выражение коэффициента динамичности kd стержневых конструкций на продольную ударную нагрузку. Рассмотрен численный пример расчета железобетонной колонны с использованием полученных аналитических выражений при учете демпфирования и без него. Установлено, что наибольшее отклонение упругой оси рассматриваемой колонны при высокоскоростном нагружении было достигнуто при t = 0.04 s. При этом полное динамическое отклонение с учетом демпфирования на 4,8 % меньше отклонения без учета демпфирования и в 1,18 раз больше соответствующей статической величины.

Ключевые слова: железобетон, колонна, продольный изгиб, ударная нагрузка, прогрессирующее обрушение, отклонение, скорость, ускорение

INTRODUCTION

During the entire service life, the buildings and structures are subject to power and environmental influences of various nature and intensity. In some cases, such influences can lead to a loss of the bearing capacity of the structural elements of a building, which in turn can lead to a disproportionate failure of the entire structural system that got name of progressive collapse. Major accidents such as the collapse of a section of the Ronan Point high-rise residential building (London, 1968) [1], the Sampoong Department Store (Seoul, 1995) [2], the Transvaal Park (Moscow, 2004) [3], the WTC building (New York, 2011) [4], the federal buildings of Alfred Murray (Oklahoma City, USA, 1995) [5], the residential building Champlain Towers South (Florida, USA, 2021), etc., clearly demonstrated the relevance of this problem.

In the event that the removal time of the bearing element is counted in fractions of a second, then this process is accompanied by the emergence of significant inertial forces, which leads to dynamic loading of the remaining elements of the bearing system of the building. This is confirmed by the results of field tests carried out by Sasani and Sagiroglu [6] during the demolition of buildings, as well as by testing scale models of flat and spatial frames of buildings made by V.I. Kolchunov, N.V. Fedorova, P.A. Korenkov, N.T. Vu et al. [7–10], A.I. Demyanov and Alcadi S.A. [11] and others. According to the results of the aforementioned studies, the elements of coatings (floors) over the structure to be removed are the first to be included in the dynamic process of redistribution of power flows through the alternate load paths.

However, a scenario is possible in which the removal of the structural element of the building frame can lead to the buckling of the eccentrically compressed elements of the deformed structural system. Such a scenario for the development of progressive collapse can be associated with the accumulation of environmental damage (corrosion, high temperatures) [12-14], a change in the nature of the stress-strain state of eccentrically compressed elements due to an increase in the span of the floor structure or an increase in the eccentricity of the application of a longitudinal force, an increase in the effective length of the considered eccentrically compressed element, due to removal of vertical ties or degradation of the fastening [15,16].

V.A. Gordon and V.I. Kolchunov [17] investigated the stability of the columns of the reinforced concrete building frames under the degradation of the conditions of fastening in the nodes. V.I. Kolchunov, N.O. Prasolov and Kozharinova L.V. [16] carried out numerical and experimental studies of the stability of reinforced concrete frames with a sudden change in the effective lengths of the elements. V.M. Bondarenko [18] investigated the issues of survivability exposure of reinforced concrete corrosively damaged eccentrically compressed bar elements. Investigations of the dynamic stability of reinforced concrete compressed bar elements taking into account the partial absence of adhesion of reinforcement to concrete were carried out by A.G. Tamrazyan, D.S. Popov. and Ubysz A. [19]. D.G. Utkin [20] carried out the study of the bearing capacity and methods of strengthening reinforced concrete columns subjected to transverse impact. In the work of Alekseytsev A.V. [21], it was carried out a numerical study of the mechanical safety of reinforced concrete frames of buildings under transverse impact using NX Nastran, in which, among other things, the bearing capacity of eccentrically compressed elements was assessed according to the strength and stability criteria.

A brief analysis of the mentioned above and other scientific publications on the issue of buckling and stability of columns of reinforced concrete frames of buildings during structural alterations caused by the occurrence of local damage or destruction of load-bearing structures allows us to conclude that by now the parameters of dynamic deformation of reinforced concrete bar structures remain insufficiently studied. during their buckling and the influence on this process of the dissipative

properties of the bearing structural system of a building or structure.

In this regard, the purpose of the presented study was to obtain an analytical solution to the problem of dynamic buckling of a reinforced concrete column when it is loaded with a shock load, taking into account the presence of initial geometric and (or) physical imperfections and damping properties of the system, as well as to estimate the column deformation parameters based on the obtained analytical solution

MATERIALS AND METHODS

Let us consider a reinforced concrete frame of a multi-storey civil building. Figure 1 shows a variant of its secondary design scheme for the analysis of resistance to progressive collapse. The column of the first floor in the axes "A" - "2" of such a frame with a sudden removal of the column of the first floor in the axes "A" - "1" can be considered as an eccentrically compressed element, loaded with a rapidly increasing load. As shown by the results of experimental studies [6], the redistribution of power flows along alternative paths can occur in tenths, and in some cases hundredths parts of a second.

Material parameters adopted in the study are the follows: concrete B25, reinforcement bars A400. The axial force in the column from the operating load P = 5000 kN. After a sudden failure of the outermost column of the frame, the considered column is loaded with an axial force of 2000 kN during 0.01 s.

It's should be noted that the issue of assessing the time of redistribution of efforts during a sudden failure of the structural member is not considered in this study. Therefore, we have assumed that the magnitude of the force and the time of its application to the considered eccentrically compressed bar element of the column are known preliminary. The problem is solved under the assumption that there are no longitudinal inertial forces in the bar when it is dynamically loaded.

The differential equation of motion of an eccentrically compressed bar (Figure 2, a) when it is loaded with a high-speed shock load, taking into account the damping properties of the system, can be written in the following form:

$$EJ\frac{\partial^4\left(w_1-w_0\right)}{\partial x^4}+P\frac{\partial^2 w_1}{\partial x^2}+\frac{\gamma\cdot A}{g}\frac{\partial^2 w}{\partial t^2}+k\frac{\partial w}{\partial t}=0, \quad (1)$$

where $w_0 = w_0(x)$ is the initial deviation of the elastic axis of the rod from the vertical axis passing through the center of gravity of one of the end sections. The appearance of the initial deviation is due to the geometric and (or) physical imperfections of the column sections, acquired during manufacture and operation, as well as buckling from a statically applied operational load.

$w_1 = w_1(x, t)$ is the total deflection of the elastic axis of the bar at time t;

$w = w_1 - w_0$ - additional deflection of the elastic axis of the rod at time t;

E is the initial modulus of elasticity of concrete;

J is the moment of inertia of the reduced section of a reinforced concrete bar element, taken constant along the length of the bar along the section with the lowest bending stiffness;

$P = P(t)$ - the law of variation in time of the longitudinal force (Figure 2, b), adopted in the form:

$$P=\begin{cases}P_0+\Omega\cdot t, & for \quad 0\le t\le t_1;\\ P_0+\Omega\cdot t_1, & for \quad t>t_1,\end{cases} \quad (2)$$

where P_0 is a statically attached axial force;

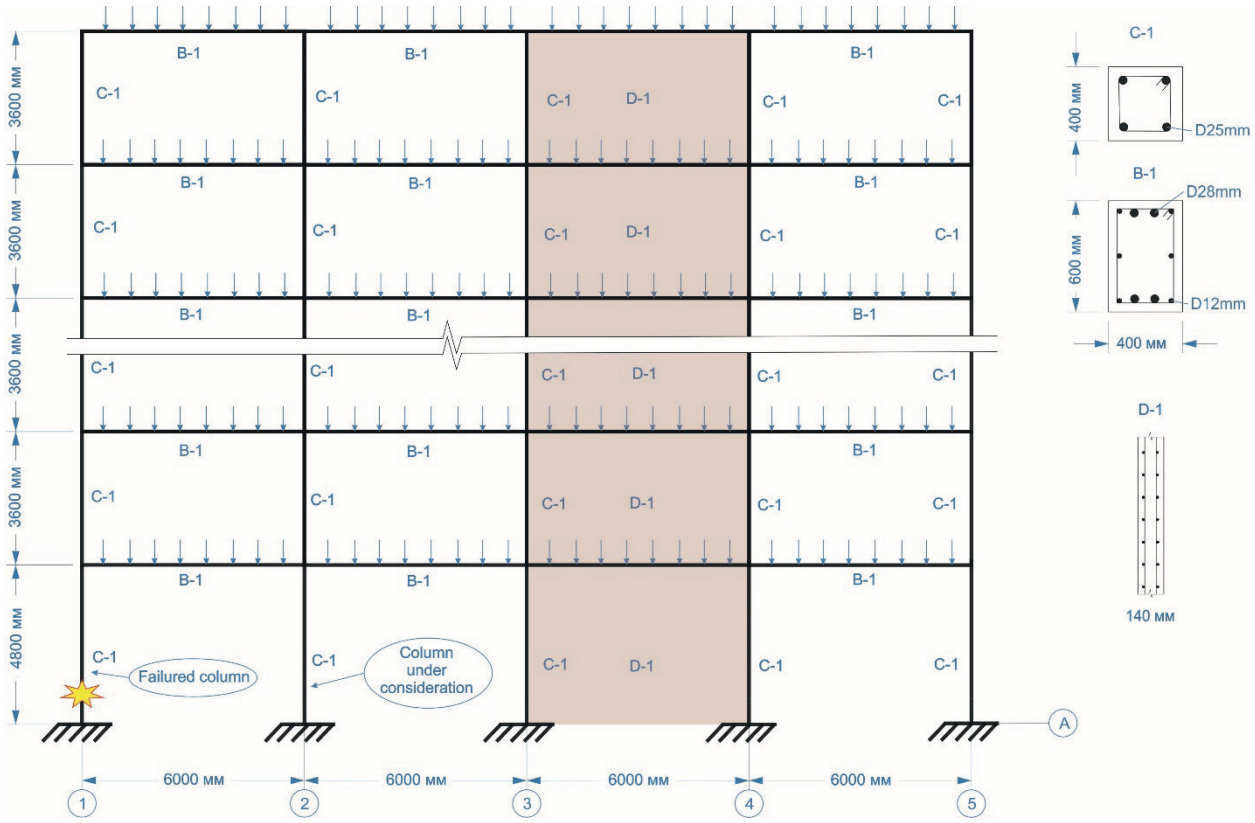

Figure 1. Secondary design scheme of a reinforced concrete frame of a building for analysis of resistance to progressive collapse

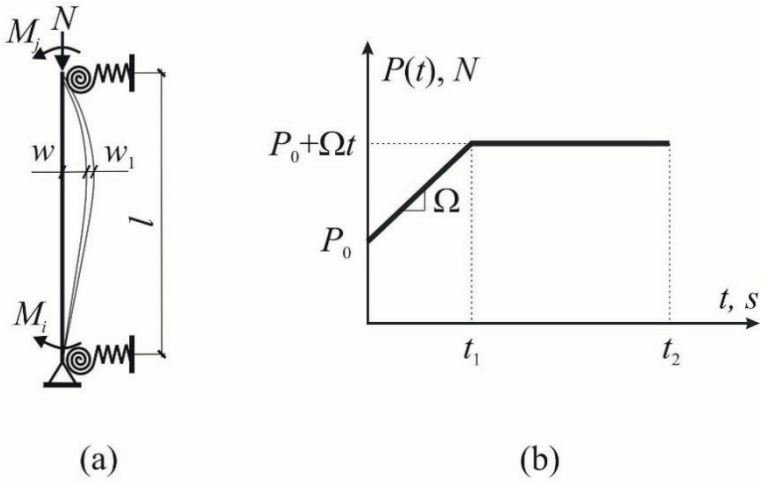

Figure 2. Design scheme of an eccentrically compressed bar member (a) and the law of variation of the axial compressive force in time (b)

Ω is a velocity of the bar member dynamic loading, N/s;
t_1 is a time of dynamic loading of the bar member by shock load;
γ is a specific gravity of the material;
A is an area of reduced cross section;
g is the acceleration of gravity;
k is proportionality factor accounting damping properties, taken as a first approximation

$$k = \frac{\delta \cdot \omega \cdot \gamma \cdot A}{\pi \cdot g}.$$

Here $\delta = 0.31$ is – vibration decrement for reinforced concrete structures, adopted according to [22], ω is the circular vibration frequency.

In order to solve equation (1), we used the separation of variables, setting the shape of the elastic line of the deformed column bar, as well as the shape of the initial deviation in the form of a half-wave of a sinusoid:

$$w_0 = f_0 \cdot sin\left(\frac{m \cdot \pi \cdot x}{l}\right);$$

$$w_1 = f_1(t) \cdot sin\left(\frac{m \cdot \pi \cdot x}{l}\right), \quad (3)$$

where f_0 is amplitude value of the initial deviation along the length of the rod;

$f_1(t)$ is amplitude value of total deflection along the length of the rod at time t;

m is the number of half-waves of a sinusoid along the length of the bar;

l is an effective length of the bar.

Substituting (3) into equation (1) and excluding the variable x, we obtain:

$$\frac{df_1^2}{dt^2} + \frac{k \cdot l^2 \cdot \omega^2}{\pi^2 \cdot P_E}\frac{df_1}{dt} + \omega^2 m^2\left(m^2 - \frac{P}{P_E}\right)f_1 = \omega^2 m^4 f_0. \quad (4)$$

In equation (4), the following designations are adopted:

$$\omega = \frac{\pi^2}{l^2}\sqrt{\frac{E \cdot g}{\gamma} \cdot \frac{J}{A}}; \quad P_E = \frac{\pi^2 \cdot E \cdot J}{l^2}.$$

Here ω is the frequency of the first vibration tone,

P_E is Euler critical force.

We solved equation (4) during two stages. At the first stage, accepting the law of variation of the axial force in time $P(t) = P_0 + \Omega t$, we obtain a solution to equation (4) for the time interval $0 \le t \le t_1$. At the second stage, taking the longitudinal force $P = P_0 + \Omega t_1 = \text{const}$, we obtain a solution to equation (4) for the time interval $t > t_1$. In this case, the initial conditions at the second stage are the deviation of the elastic axis and the velocity of transverse displacement at time $t = t_1$, obtained from the solution of the differential equation at the first stage. When performing operations of differentiation, integration and search for numerical values of variables, we used the MathCAD software package.

RESULTS

Solution to the problem of dynamic buckling with a load increasing in time and damping. In order to simplify the form of writing the differential equation (4), taking into account the law of variation of the longitudinal force in time $P(t) = P_0 + \Omega t$, we introduce the change of the variable $t_\omega = t$

$$f_1 = y \cdot e^{-\frac{\alpha \cdot t_\omega}{2}}, \text{ where } \alpha = \frac{k \cdot \omega \cdot l^4}{\pi^4 \cdot E \cdot J}.$$

Then, taking into account the adopted law of the change in the longitudinal force in time, we obtain:

$$y'' + \left(m^4 - \frac{P_0}{P_E} m^2 - \frac{\alpha^2}{4} - \frac{\Omega \cdot m^2}{\omega \cdot P_E} t_\omega \right) y = m^4 \cdot f_0 \cdot e^{\frac{\alpha \cdot t_\omega}{2}}. \quad (5)$$

Let us the following substitute into the equation (5):

$$y(t_\omega) = \eta(\zeta); \quad t_\omega = b - a^{\frac{1}{2}} \cdot \zeta,$$

$$b = \frac{\omega}{\Omega}\left(P_E \cdot m^2 - P_0 - \frac{\alpha^2 \cdot P_E}{4 \cdot m^4} \right); \quad a = \left(\frac{\omega}{\Omega} \frac{P_E}{m^2} \right)^2,$$

taking into account which we get:

$$\frac{d^2\eta}{d\zeta^2} + a \cdot \zeta \cdot \eta = m^4 \cdot f_0 \cdot e^{\frac{\alpha}{2}\left(b - a^{\frac{1}{2}} \cdot \zeta \right)}. \quad (6)$$

We exclude the parameter a from the left-hand side of Eq. (6) by performing an additional substitution $\psi(z) = \eta(\zeta)$, $z = a^{1/3}\zeta$, as a result of which we obtain the inhomogeneous equation:

$$\frac{d^2\psi}{dz^2} + z \cdot \psi = a^{\frac{1}{3}} \cdot m^4 \cdot f_0 \cdot e^{\frac{\alpha}{2}\left(b - a^{\frac{1}{6}} \cdot z \right)}, \quad (7)$$

the solution of which we found in the form of the sum of the solution of the homogeneous equation known in the scientific literature [23] and the particular solution, selected according to the form of the right-hand side:

$$\psi = C_1 \cdot z^{\frac{1}{2}} \cdot J_{1/3}\left(\frac{2}{3} z^{\frac{3}{2}} \right) + C_2 \cdot z^{\frac{1}{2}} \cdot J_{-1/3}\left(\frac{2}{3} z^{\frac{3}{2}} \right) + \frac{4 \cdot a^{\frac{1}{3}} \cdot m^4 \cdot f_0}{\alpha^2 \cdot a^{\frac{1}{3}} + 4 \cdot z} \cdot e^{\frac{\alpha}{2}\left(b - a^{\frac{1}{6}} \cdot z \right)}. \quad (8)$$

In the expression (8), $J_{1/3}\left(\frac{2}{3} z^{\frac{3}{2}} \right)$, $J_{-1/3}\left(\frac{2}{3} z^{\frac{3}{2}} \right)$ are Bessel functions;

C_1, C_2 are the arbitrary constants determined from the initial conditions of the problem:

$$\psi = f_0, \quad \frac{d\psi}{dz} = 0 \quad for \quad t = 0 \quad or \quad z = b \cdot a^{-\frac{1}{6}}.$$

It should be noted that the parameter z decreases with increasing time t. Therefore, when it goes into the negative range of values in expression (8), the Bessel functions $J_{1/3}\left(\frac{2}{3} z^{\frac{3}{2}} \right)$, $J_{-1/3}\left(\frac{2}{3} z^{\frac{3}{2}} \right)$ must be replaced by modified Bessel functions $I_{1/3}\left(\frac{2}{3} z^{\frac{3}{2}} \right)$, $I_{-1/3}\left(\frac{2}{3} z^{\frac{3}{2}} \right)$, and the arbitrary constants C_1, C_2 must be redefined under the initial conditions for $z = 0$ obtained by solving the original equation (8).

For the reinforced concrete column under consideration, the graphs of the change in the parameter z, lateral deviation f_1, velocity and acceleration for the time interval $0 \le t \le t_1$ with and without damping are shown in Figure 3.

Solution to the problem of dynamic buckling of a bar with a constant axial force and damping. At the second stage of the study, taking the longitudinal force constant $P = P_0 + \Omega t_1 = \text{const}$, for $P < P_E$ we obtain a solution to equation (4) for the time interval $t > t_1$:

$$f_1 = e^{-\frac{\beta \cdot t_2}{2}} \cdot \left(D_1 \cdot cos\left(\frac{\lambda \cdot t_2}{2}\right) + D_2 \cdot sin\left(\frac{\lambda \cdot t_2}{2}\right)\right) + \frac{f_0}{1 - \frac{P}{m^2 \cdot P_E}}, \quad (9)$$

in which a particular solution (the last term) is a static deflection of an eccentrically compressed rod with an initial deflection f_0;
D_1, D_2 - arbitrary constants determined from the initial conditions, which are the deviation of the elastic axis and the speed of transverse displacement at time $t = t_1$, obtained from expression (8) and its first derivative, respectively;

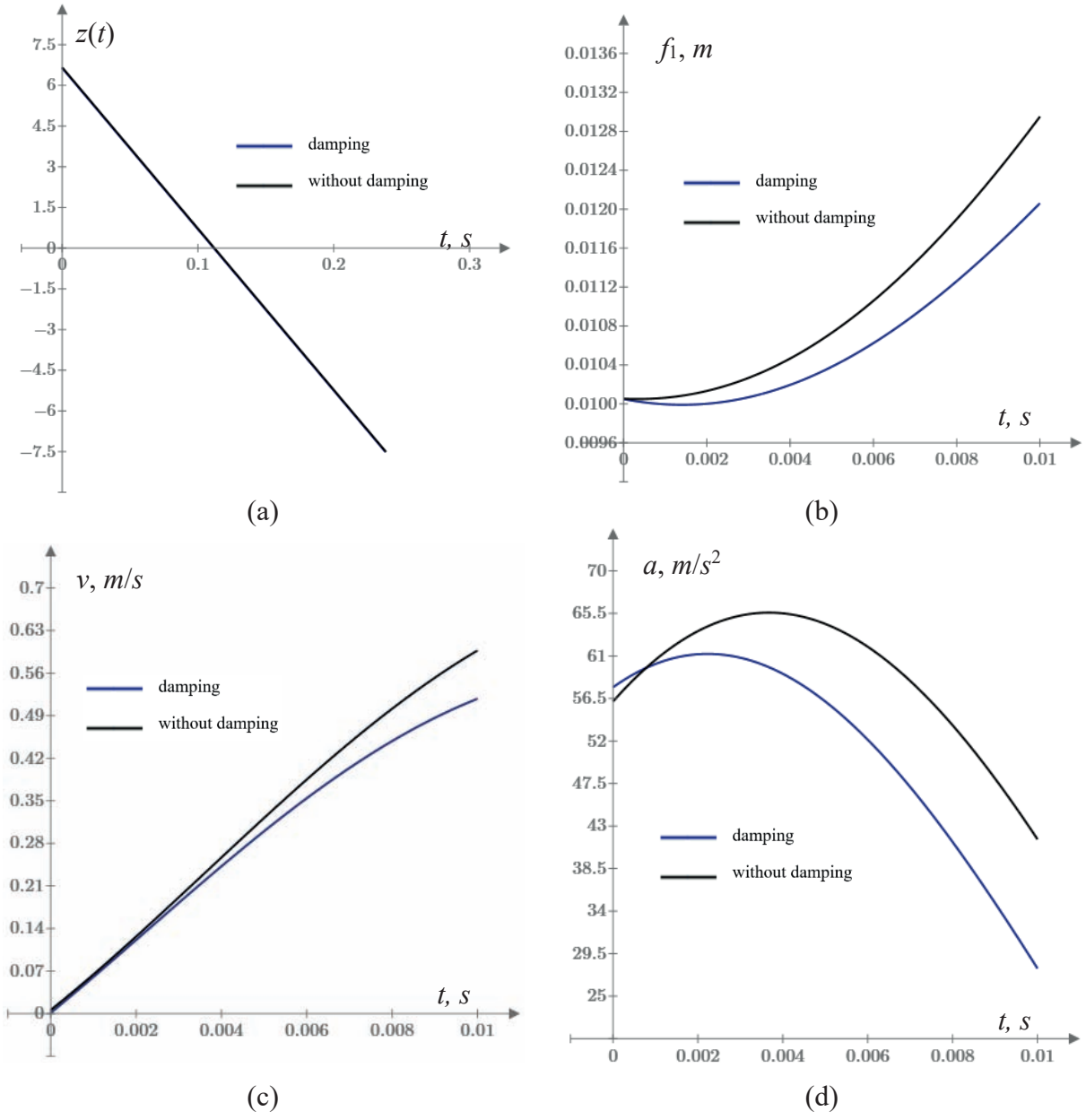

Figure 3. Parameters of reinforced concrete column deformation for the time interval $0 \le t \le t_1$: dimensionless time parameter z (a), deflection of the elastic axis of the bar element (b), lateral displacement rate (c), acceleration of the lateral displacement (d)

$$\beta = \frac{k \cdot l^2 \cdot \omega^2}{P_E \cdot \pi^2}, \quad t_2 = t - t_1 \quad for \quad t > t_1,$$

$$\lambda^2 = \beta^2 - 4\omega^2 \cdot m^4 \left(1 - \frac{P}{m^2 \cdot P_E}\right).$$

It should be noted that the above assumption $P < P_E$ corresponds to the case $\lambda^2 < 0$. Analysis of the expression for the parameter λ^2 shows that if the value of the longitudinal force approaches P_E, then λ^2 changes its sign, and the first term in expression (9) must be written in hyperbolic functions.

For the reinforced concrete column under consideration, the graphs of changes in the lateral deflection f_1, speed, acceleration and the ratio of dynamic to static deflection for the time interval $t > t_1$ (in the presence and absence of damping are shown in Figure 4.

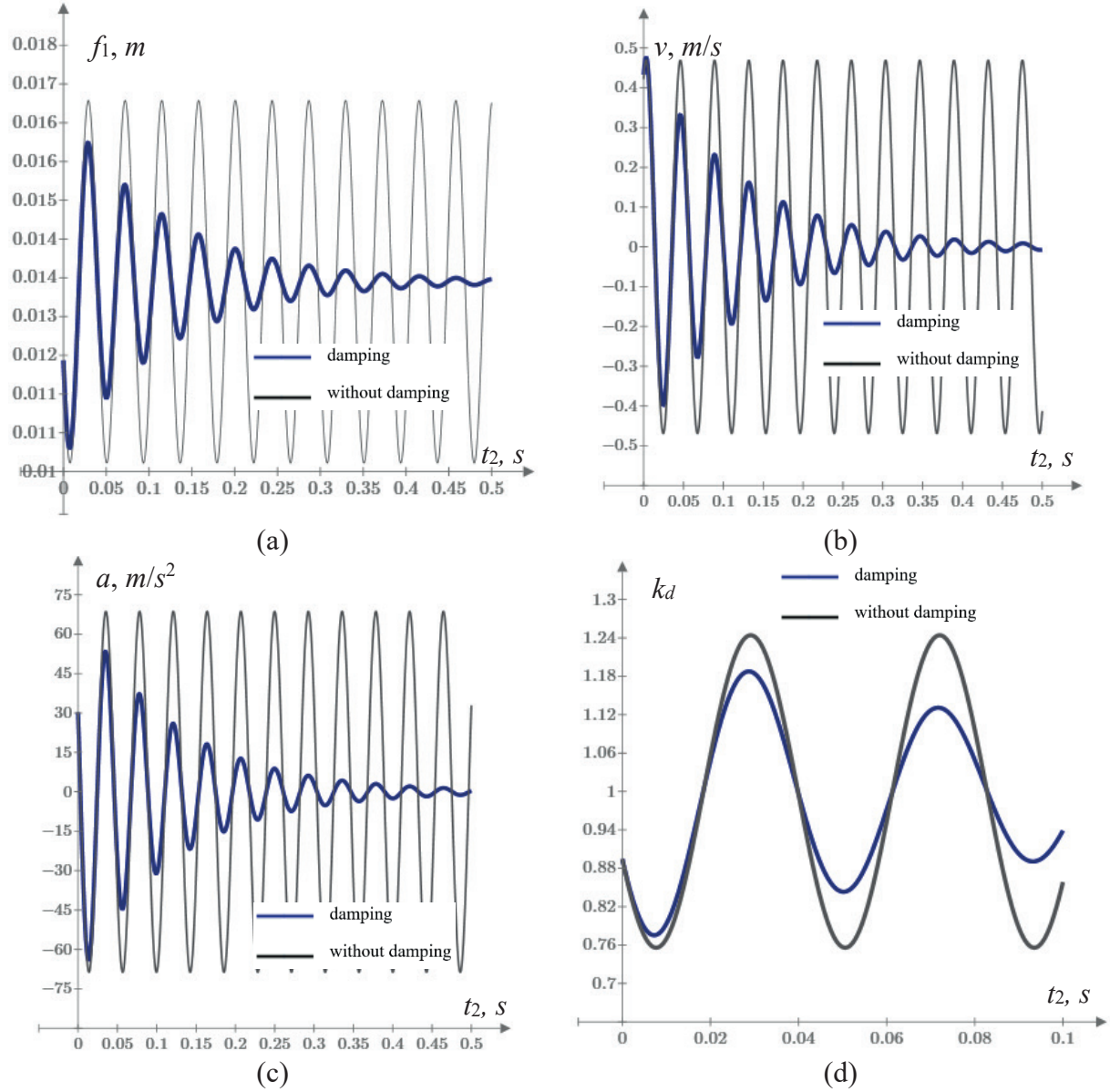

Figure 4. Parameters of deformation of a reinforced concrete column for the time interval $t > t_1$: deviation of the elastic axis of the bar element (a), the rate of lateral displacement (b), acceleration of the lateral displacement (c); the ratio of the dynamic deflection of an eccentrically compressed bar element to the static one (d)

Considering that on the first wave of transverse vibrations in the time interval $t > t_1$, the decrease in the value of dynamic deflection when taking into account damping compared to dynamic deflection without taking into account damping is within 5% (see Figure 4, d), then for practical calculations of bar structures in a quasi-static formulation, the dynamic factor k_d can be calculated by the formula:

$$k_d = 1 + \left(D_1 \cdot cos\left(\frac{\lambda \cdot t_2}{2} \right) + D_2 \cdot sin\left(\frac{\lambda \cdot t_2}{2} \right) \right) \frac{1 - \frac{P}{m^2 \cdot P_E}}{f_0}. \quad (10)$$

DISCUSSION

Analysis of the plots presented in the previous section shows that the maximum deviation of the elastic axis of the column under the considered shock impact was achieved at $t = t_1 + t_2 = 0.04$ s. In this case, the total dynamic deflection taking into account damping was 16 mm, which is 4.8% less than the deviation without taking into account damping and 1.18 times more than the corresponding static value.

Attention should be paid to the fact that the time to reach the maximum deflection of the elastic axis of the column is comparable to the time the elastic wave running the length of the bar. Therefore, in further studies, it is advisable to take into account the forces of longitudinal inertia.

Based on the results obtained in the previous section, the amplitude values of the dynamic transverse deflections of the elastic axis of the bar, it can be assumed that the transverse vibrations of the bar have practically no effect on the magnitude of the longitudinal forces due to the small deviations compared to the dimensions of the cross-section of the bar. Thus, a possible way to solve the problem can be the search for the function $P(t)$ from the solution of the wave equation with substitution this one into the differential equation of dynamic buckling.

CONCLUSION

Summarizing the results of the study, the following conclusions can be drawn:

1. In an analytical form, an expression was obtained for the dynamic deflection of the elastic axis of a bar element under its longitudinal loading with a high-speed shock load, taking into account damping.
2. For practical calculations in a quasi-static formulation, an expression is proposed for the dynamic factor k_d of bar structures under axial shock load.
3. It was found that for the reinforced concrete column under consideration, the maximum deviation of its elastic axis under impact action was achieved at t = 0.04 s. In this case, the total dynamic deflection taking into account damping was 16 mm, which is 4.8% less than the deviation without taking into account damping and 1.18 times more than the corresponding static value.
4. In the considered example, the time to reach the maximum dynamic deflection of the elastic axis of the column is comparable to the time the elastic wave running the length of the bar. Therefore, when studying the dynamic buckling from the shock load, it is advisable to take into account the forces of longitudinal inertia.

REFERENCES

1. **Pearson C., Delatte N.** Ronan Point Apartment Tower Collapse and its Effect on Building Codes. J. Perform. Constr. Facil. 2005. Vol. 19, No 2. P. 172–177.
2. **Fedorova N.V., Savin S.Y.** Progressive collapse resistance of facilities experienced to localized structural damage - an

analytical review. Build. Reconstr. 2021. Vol. 95, No 3. P. 76–108.
3. **Belostotsky A.M., Pavlov A.S.** Long span buildings analysys under phisical, geometic and structural nonlinearities consideration. Int. J. Comput. Civ. Struct. Eng. 2010. Vol. 6, No 1-2. P. 80–86.
4. **Adam J.M. et al.** Research and practice on progressive collapse and robustness of building structures in the 21st century. Eng. Struct. Elsevier, 2018. Vol. 173, March. P. 122–149.
5. **Byfield M., Paramasivam S.** Murrah Building Collapse: Reassessment of the Transfer Girder. J. Perform. Constr. Facil. 2012. Vol. 26, № 4. P. 371–376.
6. **Sasani M., Sagiroglu S.** Progressive collapse resistance of hotel San Diego. J. Struct. Eng. 2008.
7. **Fedorova N. V., Korenkov P.A.** Static and dynamic deformation of monolithic reinforced concrete frame building in ultimate limit and beyond limits states. Stroit. i rekonstruktsiya. 2016. Vol. 6, No 68. P. 90–100.
8. **Fedorova N. V., Ngoc V.T.** Deformation and failure of monolithic reinforced concrete frames under special actions. J. Phys. Conf. Ser. 2019. Vol. 1425, No 1. P. 012033.
9. **Fedorova N. V, Vu N.T., Iliushchenko T.A.** The effect of energy dissipation on the dynamic response of reinforced concrete structure // IOP Conf. Ser. Mater. Sci. Eng. 2020. Vol. 962. P. 022063.
10. **Fedorova N. et al.** The dynamic effect in a structural adjustment of reinforced concrete structural system. IOP Conf. Ser. Mater. Sci. Eng. 2020. Vol. 869. P. 052078.
11. **Dem'yanov A.I., Alkadi S.A.** Experimental-Theoretical Studies of Static-Dynamic Deformation of a Spatial Reinforced Concrete Frame with Complex-Stressed Beams of Solid and Composite Cross-Sections. Promyshlennoe i grazhdanskoe stroitelstvo. 2018. No 6. P. 68–75.
12. **Tamrazyan A.G., Avetisyan L.A.** Behavior of compressed reinforced concrete columns under thermodynamic influences taking into account increased concrete deformability. IOP Conf. Ser. Mater. Sci. Eng. 2018. Vol. 365, № 5. P. 052034.
13. **Tamrazyan A.G., Fedorov V.S., Kharun M.** The effect of increased deformability of columns on the resistance to progressive collapse of buildings. IOP Conf. Ser. Mater. Sci. Eng. 2019. Vol. 675. P. 012004.
14. **Kolchunov V.I., Savin S.Y.** Survivability criteria for reinforced concrete frame at loss of stability. Mag. Civ. Eng. 2018. Vol. 80, № 4. P. 73–80.
15. **Savin S.Y., Kolchunov V.I., Korenkov P.A.** Experimental research methodology for the deformation of RC frame under instantaneous loss of column. IOP Conf. Ser. Mater. Sci. Eng. 2020. Vol. 962. P. 022054.
16. **Kolchunov V.I., Prasolov N.O., Kozharinova L. V.** Experimental and theoretical research on survivability of reinforced concrete frames in the moment of individual element buckling. Vestn. MGSU. 2011. No 3–2. P. 109–115.
17. **Gordon V.A., Kolchunov V.I.** To the calculation for the stability of an evolutionarily damaged reinforced concrete element with "degrading" support conditions. Struct. Mech. Anal. Constr. 2006. No 4. P. 33–38.
18. **Bondarenko V.M.** Accounting for energy and corrosion dissipation of power resistance when assessing the stability of building structures. Struct. Mech. Anal. Constr. 2011. Vol. 235, No 2. P. 51–57.
19. **Tamrazyan A.G., Popov D.S., Ubysz A.** To the dynamically loaded reinforced-concrete elements' calculation in the absence of adhesion between concrete and reinforcement. IOP Conf. Ser. Mater. Sci. Eng. 2020. Vol. 913. P. 022012.
20. **Utkin D.G.** Strength of bent reinforced concrete elements with zone reinforcement made of steel fiber. Build. Reconstr. 2021. Vol. 93, No 1. P. 85–95.

21. **Alekseytsev A. V.** Mechanical safety of reinforced concrete frames under complex emergency actions. Mag. Civ. Eng. 2021. Vol. 103, No 3.
22. **Nazarov Yu.P., Simbirkin V.N.** Analysis and limitation of vibrations of structures under the influence of people. Vestnik TsNIISK im. V.A. Kucherenko. 2009. Vol. 1, No XXVI. P. 1–11.
23. **Kamke E.** Handbook of Ordinary Differential Equations. Moscow: Publishing house "Science,"1971. 576 p.

СПИСОК ЛИТЕРАТУРЫ

1. **Pearson C., Delatte N.** Ronan Point Apartment Tower Collapse and its Effect on Building Codes // J. Perform. Constr. Facil. 2005. Vol. 19, № 2. P. 172–177.
2. **Fedorova N.V., Savin S.Y.** Progressive collapse resistance of facilities experienced to localized structural damage - an analytical review // Build. Reconstr. 2021. Vol. 95, № 3. P. 76–108.
3. **Belostotsky A.M., Pavlov A.S.** Long span buildings analysys under phisical, geometic and structural nonlinearities consideration // Int. J. Comput. Civ. Struct. Eng. 2010. Vol. 6, № 1&2. P. 80–86.
4. **Adam J.M. et al.** Research and practice on progressive collapse and robustness of building structures in the 21st century // Eng. Struct. Elsevier, 2018. Vol. 173, № March. P. 122–149.
5. **Byfield M., Paramasivam S.** Murrah Building Collapse: Reassessment of the Transfer Girder // J. Perform. Constr. Facil. 2012. Vol. 26, № 4. P. 371–376.
6. **Sasani M., Sagiroglu S.** Progressive collapse resistance of hotel San Diego // J. Struct. Eng. 2008.
7. **Fedorova N. V., Korenkov P.A.** Static and dynamic deformation of monolithic reinforced concrete frame building in ultimate limit and beyond limits states // Stroit. i rekonstruktsiya. 2016. Vol. 6, № 68. P. 90–100.
8. **Fedorova N. V., Ngoc V.T.** Deformation and failure of monolithic reinforced concrete frames under special actions // J. Phys. Conf. Ser. 2019. Vol. 1425, № 1. P. 012033.
9. **Fedorova N. V, Vu N.T., Iliushchenko T.A.** The effect of energy dissipation on the dynamic response of reinforced concrete structure // IOP Conf. Ser. Mater. Sci. Eng. 2020. Vol. 962. P. 022063.
10. **Fedorova N. et al.** The dynamic effect in a structural adjustment of reinforced concrete structural system // IOP Conf. Ser. Mater. Sci. Eng. 2020. Vol. 869. P. 052078.
11. **Демьянов А.И., Алькади С.А.** Экспериментально-теоретические исследования статико-динамического деформирования пространственной железобетонной рамы со сложнонапряженными ригелями сплошного и составного сечения // Промышленное и гражданское строительство. 2018. № 6. P. 68–75.
12. **Tamrazyan A.G., Avetisyan L.A.** Behavior of compressed reinforced concrete columns under thermodynamic influences taking into account increased concrete deformability // IOP Conf. Ser. Mater. Sci. Eng. 2018. Vol. 365, № 5. P. 052034.
13. **Tamrazyan A.G., Fedorov V.S., Kharun M.** The effect of increased deformability of columns on the resistance to progressive collapse of buildings // IOP Conf. Ser. Mater. Sci. Eng. 2019. Vol. 675. P. 012004.
14. **Kolchunov V.I., Savin S.Y.** Survivability criteria for reinforced concrete frame at loss of stability // Mag. Civ. Eng. 2018. Vol. 80, № 4. P. 73–80.
15. **Savin S.Y., Kolchunov V.I., Korenkov P.A.** Experimental research methodology for the deformation of RC frame under instantaneous loss of column // IOP Conf. Ser. Mater. Sci. Eng. 2020. Vol. 962. P. 022054.
16. **Kolchunov V.I., Prasolov N.O., Kozharinova L. V.** Experimental and theoretical research on survivability of reinforced concrete frames in the moment

of individual element buckling // Vestn. MGSU. 2011. № 3–2. P. 109–115.
17. **Gordon V.A., Kolchunov V.I.** To the calculation for the stability of an evolutionarily damaged reinforced concrete element with "degrading" support conditions // Struct. Mech. Anal. Constr. 2006. № 4. P. 33–38.
18. **Bondarenko V.M.** Accounting for energy and corrosion dissipation of power resistance when assessing the stability of building structures // Struct. Mech. Anal. Constr. 2011. Vol. 235, № 2. P. 51–57.
19. **Tamrazyan A.G., Popov D.S., Ubysz A.** To the dynamically loaded reinforced-concrete elements' calculation in the absence of adhesion between concrete and reinforcement // IOP Conf. Ser. Mater. Sci. Eng. 2020. Vol. 913. P. 022012.
20. **Utkin D.G.** Strength of bent reinforced concrete elements with zone reinforcement made of steel fiber // Build. Reconstr. 2021. Vol. 93, № 1. P. 85–95.
21. **Alekseytsev A. V.** Mechanical safety of reinforced concrete frames under complex emergency actions // Mag. Civ. Eng. 2021. Vol. 103, № 3.
22. **Назаров Ю.П., Симбиркин В.Н.** Анализ и ограничение колебаний конструкций при воздействии людей // Вестник ЦНИИСК им. В.А. Кучеренко. 2009. Vol. 1, № XXVI. P. 1–11.
23. **Камке Э.** Справочник по обыкновенным дифференциальным уравнениям. М.: Издательство "Наука," 1971. 576 p.

Sergey Yu. Savin, Candidate of Technical Sciences, Docent, Associated Professor of the Department of Reinforced Concrete and Masonry Structures of Moscow State University of Civil Engineering (National Research University) (MGSU); 26 Yaroslavskoe shosse, Moscow, 129337, Russian Federation; Scopus ID: 57052453700, ResearcerID: M-8375-2016, ORCID: 0000-0002-6697-3388; phone +7(495)287-49-14, e-mail: savinsyu@mgsu.ru.

Vitaly I. Kolchunov, Full Member of RAACS, Professor, Doctor of Technical Sciences, Professor of the Department of Reinforced Concrete and Masonry Structures; Moscow State University of Civil Engineering (National Research University) (MGSU), head of the department of Southwest State University; 26 Yaroslavskoe shosse, Moscow, 129337, Russian Federation; Scopus ID: 55534147800, ResearcerID: J-9152-2013, ORCID: 0000-0001-5290-3429; phone +7(495)287-49-14, e-mail: asiorel@mail.ru.

Савин Сергей Юрьевич, кандидат технических наук, доцент, доцент кафедры железобетонных и каменных конструкций; Национальный исследовательский Московский государственный строительный университет (НИУ МГСУ); 129337, г. Москва, Ярославское шоссе, д. 26; Scopus ID: 57052453700, ResearcerID: M-8375-2016, ORCID: 0000-0002-6697-3388; тел. +7(495)287-49-14, e-mail: savinsyu@mgsu.ru.

Колчунов Виталий Иванович, академик РААСН, профессор, доктор технических наук, профессор кафедры железобетонных и каменных конструкций Национального исследовательского Московского государственного строительного университета (НИУ МГСУ), заведующий кафедрой уникальных зданий и сооружений Юго-Западного государственного университета; 129337, г. Москва, Ярославское шоссе, д. 26; Scopus ID: 55534147800, ResearcerID: J-9152-2013, ORCID: 0000-0001-5290-3429; тел. +7(495)287-49-14, e-mail: asiorel@mail.ru.

International Journal for Computational Civil and Structural Engineering, 17(3) 132–156 (2021)

DOI:10.22337/2587-9618-2021-17-3-132-156

APPLICATION OF GRADIENT PROJECTION METHOD TO PARAMETRIC OPTIMIZATION OF STEEL LATTICE PORTAL FRAME

Vitalina V. Yurchenko [1]***, Ivan D. Peleshko*** [2]***, Nikita A. Biliaiev*** [3]

[1] Kyiv National University of Civil Engineering and Architecture, Kyiv, UKRAINE
[2] Lviv Polytechnic National University, Lviv, UKRAINE
[3] BM Prefab Engineering, Kyiv, UKRAINE

Abstract. The paper has proposed a mathematical model for parametric optimization problem of the steel lattice portal frame. The design variable vector includes geometrical parameters of the structure (node coordinates), as well as cross-sectional dimensions of the structural members. The system of constraints covers load-carrying capacities constraints formulated for all design sections of structural members of the steel structure subjected to all ultimate load case combinations. The displacements constraints formulated for the specified nodes of the steel structure subjected to all serviceability load case combinations have been also included into the system of constraints. Additional requirements in the form of constraints on lower and upper values of the design variables, constraints on permissible minimal thicknesses, constraints on permissible maximum diameter-to-thickness ratio for the structural members with circle hollow sections, as well as the conditions for designing gusset-less welded joints between structural members with circle hollow sections have been also considered in the scope of the mathematical model. The method of the objective function gradient projection onto the active constraints surface with simultaneous correction of the constraints violations has been used to solve the formulated parametric optimization problem. New optimal layouts of the steel lattice portal frame by the criterion of the minimum weight, as well as minimum costs on manufacturing and erection have been presented.

Keywords: optimization, steel lattice frame, nonlinear programming, strength, buckling, stiffness, gradient projection method, finite element method, numerical algorithm

ПРИМЕНЕНИЕ МЕТОДА ПРОЕКЦИИ ГРАДИЕНТА ДЛЯ ПАРАМЕТРИЧЕСКОЙ ОПТИМИЗАЦИИ СТАЛЬНОЙ РЕШЕТЧАСТОЙ РАМЫ

В.В. Юрченко [1]***, И.Д. Пелешко*** [2]***, Н.А. Биляев*** [3]

[1] Киевский национальный университет строительства и архитектуры, Киев, УКРАИНА
[2] Национальный университет «Львовская политехника», Львов, УКРАИНА
[3] BM Prefab Engineering, Киев, УКРАИНА

Аннотация. В статье предложена математическая модель для задачи параметрической оптимизации стальной решетчатой поперечной рамы каркаса здания, несущие элементы которой выполнены из круглых труб. Вектор переменных проектирования содержит геометрические параметры конструкции (координаты узлов), а также размеры поперечных сечений несущих элементов конструкции. Система ограничений включает ограничения несущей способности, сформулированные для всех расчетных сечений элементов конструкции, подлежащей действию всех комбинаций нагрузок первой группы предельных состояний. В систему ограничений также включены ограничения перемещений узлов, сформулированные для определенных узлов конструкции, подлежащей действию всех комбинаций нагрузок второй группы предельных состояний. Дополнительные ограничения в форме ограничений на верхнюю и нижнюю границы варьирования переменных проектирования, ограничения на допустимую минимальную толщину сечения, ограничения на допустимое максимальное отношение диаметра к толщине трубы, а также условия конструирования бесфасоночных узлов решетчатой конструкции с элементами их круглых труб также были рассмотрены в составе системы ограничений математической модели. Для решения сформулированной задачи параметрической оптимизации использовался метод проекции градиента функции цели на поверхность активных ограничений при одновременной ликвидации невязок в нарушенных

ограничениях. В результате получены новые оптимальные проектные решения стальной решетчатой поперечной рамы по критерию минимума массы конструкции, а также по критерию минимума сметной стоимости на ее изготовление и возведение.

Ключевые слова: оптимизация, стальная решетчатая рама, нелинейное программирование, прочность, устойчивость, жесткость, градиентный метод, метод конечных элементов, численный алгоритм.

INTRODUCTION

Over the past 50 years, numerical optimization and the finite element method have individually made significant advances and have together been developed to make possible the emergence of structural optimization as a potential design tool. In recent years, great efforts have been also devoted to integrate optimization procedures into the CAD facilities. With these new developments, lots of computer packages are now able to solve relatively complicated industrial design problems using different structural optimization techniques.

Applied optimum design problems for bar structures in some cases are formulated as parametric optimization problems, namely as searching problems for unknown structural parameters, which provide an extreme value of the specified purpose function in the feasible region defined by the specified constraints [1]. In this case, structural optimization is performed by variation of the structural parameters when the structural topology, cross-section types and node type connections of the bars, the support conditions of the bar system, as well as loading patterns and load design values are prescribed and constants.

Kibkalo et al. in the paper [2] formulated a parametric optimization problem for thin-walled bar structures and considered methods to solve them. The searching for the optimum solution has been performed by varying the structural parameters providing the required load-carrying capacity of structural members and the minimum value of manufacturing costs.

Alekseytsev has described the process of developing a parametrical-optimization algorithm for steel trusses in the paper [3]. Parametric optimization has been performed taking into account strength, stability and stiffness constraints formulated for all truss members.

Serpik et al. in the paper [4] developed an algorithm for parametric optimization of steel flat rod systems. The optimization problem has been formulated as a structural weight minimization problem taking into account strength and displacement constraints, as well as overall stability constraints. The cross-sectional dimensions of the truss members and the coordinates of the truss panel joints have been considered as design variables. The structural analysis of internal forces and displacements for considered structures has been performed using the finite element method. An iterative procedure for searching for optimum solution has been proposed in [5].

Sergeyev et al. in the paper [6] formulated a parametric optimization problem with constraints on faultless operation probability of bar structures with random defects. The weight of the bar structures has been considered as the objective function. Initial global imperfections have been considered as small independent random variables distributed according to normal distribution law, as well as buckling load value has been also considered as a random variable.

The mathematical model of the parametric optimization problem of structures includes a set of design variables, an objective function, as well as constraints, which reflect generally non-linear dependences between them [7]. If the purpose function and constraints of the mathematical model are continuously differentiable functions, as well as the search space is smooth, then the parametric

optimization problems are successfully solved using gradient projection non-linear methods [8]. The gradient projection methods operate with the first derivatives or gradients only both of the objective function and constraints. The methods are based on the iterative construction of such a sequence of the approximations of design variables that provides convergence to the optimum solution (optimum values of the structural parameters) [9].

Additionally, a sensitivity analysis is a useful optional feature that could be used in scope of the numerical algorithms developed based on the gradients methods [10]. Thus, in the paper [11] Sergeyev et al. formulated a parametric optimization problem of linearly elastic space frame structures taking into account the stress and multiple natural frequency constraints. The cross-sectional parameters of structural members as well as node positions of the considered bar structures has been considered as design variables. The sensitivity analysis of multiple frequencies has been performed using analytic differentiation with respect to the design variables. The optimal design of the structure has been obtained by solving a sequence of quadratic programming problems.

In this paper, steel lattice portal frame is considered as research object, which investigated for the searching for optimum parameters of the structural form. The following research tasks are formulated: to develop a mathematical model for parametric optimization of the considered steel structures taking into account load-carrying capacities and stiffness constraints; to propose a numerical algorithm for parametric optimization of the steel structures based on the gradient projection method; to confirm the validity of the optimum solutions obtained using the proposed methodology based on numerical examples.

1. PROBLEM FORMULATION FOR PARAMETRIC OPTIMIZATION OF STEEL STRUCTURES

Let us consider a parametric optimization problem of a structure consisting of bar members. The problem statement can be performed taking into account the following assumptions widely used in structural mechanic problems: the material of the structure is ideal elastic; the bar structure is deformable linearly; external loadings applied to the structure are quasi-static.

Let us also formulate the following pre-conditions for calculation: cross-section types and dimensions of structural members are constant along member lengths; external loadings are applied to the structural members without eccentricities relating to the center of mass and shear center of its cross-sections; an additional restraining by stiffeners are provided in the design sections where point loads (reactions) applied with the exception of cross-section warping and local buckling of the cross-section elements; load-carrying capacity of the structural joints, splices and connections are provided by additional structural parameters do not covered by the considered parametric optimization problem.

A parametric optimization problem of the structure can be formulated as presented below: *to find optimum values for geometrical parameters of the structure, member's cross-section dimensions and initial pre-stressing forces introduced into the specified redundant members of the bar system, which provide the extreme value of the determined optimality criterion and satisfy all load-carrying capacities and stiffness requirements.* We assume, that the structural topology, cross-section types and node type connections of the bars, the support conditions of the bar system, as well as loading and pre-stressing patterns are prescribed and constants.

The formulated parametric optimization problem can be considered integrally using the mathematical model in the form of the non-

linear programming task including an objective function, a set of independent design variables and constraints, which reflect generally non-linear dependences between them. The validity of the mathematical model can be estimated by the compliance of its structure with the design code requirements.

The parametric optimization problem of steel structures can be stated in the following mathematical terms: to find unknown structural parameters $\vec{X} = \{X_\iota\}^T$, $\iota = \overline{1, N_X}$ (N_X is the total number of the design variables), providing the least value of the determined objective function:

$$f^* = f(\vec{X}^*) = \min_{\vec{X} \in \Im} f(\vec{X}), \qquad (1.1)$$

in a feasible region (search space) $\Im$ defined by the following system of constraints:

$$\boldsymbol{\psi}(\vec{X}) = \{\psi_\kappa(\vec{X}) = 0 \mid \kappa = \overline{1, N_{EC}}\}; \qquad (1.2)$$

$$\boldsymbol{\varphi}(\vec{X}) = \{\phi_\eta(\vec{X}) \le 0 \mid \eta = \overline{N_{EC}+1, N_{IC}}\}; \qquad (1.3)$$

where $\vec{X}$ is the vector of the design variables (unknown structural parameters); f, ψ_κ, φ_η are the continuous functions of the vector argument; $\vec{X}^*$ is the optimum solution or optimum point (the vector of optimum values of the structural parameters); f^* is the optimum value of the optimum criterion (objective function); N_{EC} is the number of constraints-equalities $\psi_\kappa(\vec{X})$, which define hyperplanes of the feasible solutions; N_{IC} is the number of constraints-inequalities $\varphi_\eta(\vec{X})$, which define a feasible region in the design space $\Im$.

The vector of the design variables comprises of unknown geometrical parameters of the structure $\vec{X}_G = \{X_{G,\chi}\}^T$, $\chi = \overline{1, N_{X,G}}$, and unknown cross-sectional dimensions of the structural members $\vec{X}_{CS} = \{X_{CS,\alpha}\}^T$, $\alpha = \overline{1, N_{X,CS}}$:

$$\vec{X} = \{\vec{X}_G, \vec{X}_{CS}\}^T = \{\{X_{G,\chi}\}, \{X_{CS,\alpha}\}\}^T; \qquad (1.4)$$

where $N_{X,G}$ is the total number of unknown node coordinates of the steel structure; $N_{X,CS}$ is the total number of unknown cross-sectional dimensions of the structural members, $N_{X,G} + N_{X,CS} = N_X$.

The specific technical-and-economic index (material weight, material cost, construction cost etc.) or another determined indicator can be considered as the objective function Eq. (1.1) taking into account the ability to formulate its analytical expression as a function of design variables $\vec{X}$.

Load-carrying capacities constraints (strength and stability inequalities) formulated based on the design code requirements [12] for all design sections of the structural members subjected to all design load combinations at the ultimate limit state as well as displacements constraints (stiffness inequalities) for the specified nodes of the bar system subjected to all design load combinations at the serviceability limit state should be included into the system of constraints Eqs. (1.2) – (1.3). Additional requirements, which describe structural, technological and serviceability particularities of the considered structure can be also included into the system Eqs. (1.2) – (1.3).

The design internal forces in the structural members used in the strength and stability inequalities of the system Eqs. (1.2) – (1.3) are considered as state variables depending on design variables $\vec{X}$ and can be calculated from the following linear equations system of the finite element method [13], $k = \overline{1, N_{LC}^{ULS}}$:

$$\mathbf{K}(\vec{X}_G, \vec{X}_{CS}) \times \vec{z}_{ULS,k} = \vec{p}_{ULS,k}(\vec{X}_G); \qquad (1.5)$$

where $\mathbf{K}\left(\vec{X}_G, \vec{X}_{CS}\right)$ is the stiffness matrix of the finite element model of the bar system, which should be formed depending on the unknown (variable) cross-sectional dimensions of the structural members $\vec{X}_{CS}$, as well as unknown (variable) node coordinates of the structure $\vec{X}_G$; $\vec{p}_{ULS,k}\left(\vec{X}_G\right)$ is the column-vector of the node's loads for k th design load combination of the ultimate limit state, which should be formed depending on unknown (variable) node coordinates of the structure $\vec{X}_G$; $\vec{z}_{ULS,k}$ is the result column-vector of the node displacements for k th design load combination of the ultimate limit state, $\vec{z}_{ULS,k} = \mathbf{Z}^{ULS}_{\mathbf{FEM},k}\left(\vec{X}_G, \vec{X}_{CS}\right) = \mathbf{Z}^{ULS}_{\mathbf{FEM},k}\left(\vec{X}\right)$; N^{ULS}_{LC} is the number of the design ultimate load combinations. For each i th design section of j th structural member subjected to k th ultimate design load combination the design internal forces (axial force, bending moments and shear forces) can be calculated depending on node displacement column-vector $\vec{z}_{ULS,k}$.

The node displacement of the bar system used in stiffness inequalities of the system Eqs. (1.2) – (1.3) are also considered as state variables depending on design variables $\vec{X}$ and can be calculated from the following linear equations system of the finite element method [13], $k = \overline{1, N^{SLS}_{LC}}$:

$$\mathbf{K}\left(\vec{X}_G, \vec{X}_{CS}\right) \times \vec{z}_{SLS,k} = \vec{p}_{SLS,k}\left(\vec{X}_G\right); \quad (1.6)$$

where $\vec{p}_{SLS,k}\left(\vec{X}_G\right)$ is the column-vector of the node's loads for k th design load combination of the serviceability limit state, which should be formed depending on unknown (variable) node coordinates of the structure $\vec{X}_G$; $\vec{z}_{ULS,k}$ is the result column-vector of the node displacements for k th design load combination of the serviceability limit state, $\vec{z}_{SLS,k} = \mathbf{Z}^{SLS}_{\mathbf{FEM},k}\left(\vec{X}_G, \vec{X}_{CS}\right) = \mathbf{Z}^{SLS}_{\mathbf{FEM},k}\left(\vec{X}\right)$; N^{SLS}_{LC} is the number of the design serviceability load combinations. For each m th node of the finite element model subjected to k th serviceability design load combination the design vertical and horizontal displacements can be calculated depending on node displacement column-vector $\vec{z}_{SLS,k}$.

2. IMPROVED GRADIENT PROJECTION METHOD TO SOLVE THE FORMULATED PARAMETRIC OPTIMIZATION PROBLEM

The parametric optimization problem stated as non-linear programming task by Eqs. (1.1) – (1.3) can be solved using a gradient projection method. The method of objective function gradient projection onto the active constraints surface with simultaneous correction of the constraints violations ensures effective searching for solution of the non-linear programming tasks occurred when optimum designing of the building structures [14, 15].

The gradient projection method operates with the first derivatives or gradients only of both the objective function Eq. (1.1) and constraints Eqs. (1.2) – (1.3). The method is based on the iterative construction of such sequence Eq. (2.1) of the approximations of the design variables $\vec{X} = \{X_\iota\}^T$, $\iota = \overline{1, N_X}$, that provides the convergence to the optimum solution (optimum values of the structural parameters):

$$\vec{X}_{t+1} = \vec{X}_t + \Delta\vec{X}_t, \quad (2.1)$$

where $\vec{X}_t = \{X_\iota\}^T$, $\iota = \overline{1, N_X}$ is the current approximation to the optimum solution $\vec{X}^*$ that satisfies both constraints-equalities Eq. (1.2) and constraints-inequalities Eq. (1.3) with the extreme value of the objective function Eq. (1.1); $\Delta\vec{X}_t = \{\Delta X_\iota\}^T$, $\iota = \overline{1, N_X}$, is the increment vector for the current values of the

design variables $\vec{X}_t$; t is the iteration's index. The start point of the iterative searching process $\vec{X}_{t=0}$ can be assigned as engineering estimation of the admissible design of the structure.

The active constraints only of constraints system Eqs. (1.2) – (1.3) should be considered at each iteration. A set of active constraints numbers $\mathbf{A}$ calculated for the current approximation $\vec{X}_t$ to the optimum solution (current design of the structure) is determined as:

$$\begin{aligned} &\mathbf{A} = \boldsymbol{\kappa} \cup \boldsymbol{\eta}, \\ &\boldsymbol{\kappa} = \left\{ \kappa \,\middle|\, \left| \psi_\kappa \left(\vec{X}_t \right) \right| \geq -\varepsilon \right\}, \\ &\boldsymbol{\eta} = \left\{ N_{EC} + \eta \,\middle|\, \phi_\eta \left(\vec{X}_t \right) \geq -\varepsilon \right\}, \end{aligned} \tag{2.2}$$

where ε is a small positive number introduced here in order to diminish the oscillations on movement alongside of the active constraints surface.

The increment vector $\Delta\vec{X}_t$ for the current values of the design variables $\vec{X}_t$ can be determined by the following equation:

$$\Delta\vec{X}_t = \Delta\vec{X}^t_\perp + \Delta\vec{X}^t_\square, \tag{2.3}$$

where $\Delta\vec{X}^t_\perp$ is the vector calculated subject to the condition of elimination the constraint's violations; $\Delta\vec{X}^t_\square$ is the vector determined taking into consideration the improvement of the objective function value. Vectors $\Delta\vec{X}^t_\square$ and $\Delta\vec{X}^t_\perp$ are directed parallel and perpendicularly accordingly to the subspace with the vectors basis of the linear-independent constraint's gradients, such that:

$$\left(\Delta\vec{X}^t_\perp \right)^T \Delta\vec{X}^t_\square = 0. \tag{2.4}$$

The values of the constraint's violations for the current approximation $\vec{X}_t$ of the design variables are accumulated into the following vector:

$$\mathbf{V} = \left(\psi_\kappa \left(\vec{X} \right) \forall \kappa \in \boldsymbol{\kappa};\ \phi_\eta \left(\vec{X} \right) \forall \eta \in \boldsymbol{\eta} \right).$$

Let us introduce a set $\mathbf{L}$, $\mathbf{L} \subseteq \mathbf{A}$, of the constraint's numbers, such that the gradients of the constraints at the current approximation $\vec{X}_t$ to the optimum solution are linear-independent.

Component $\Delta\vec{X}^t_\perp$ is calculated from the equation presented below:

$$\Delta\vec{X}^t_\perp = \left[\nabla\varphi \right] \vec{\mu}_\perp, \tag{2.5}$$

where $\left[\nabla\varphi \right]$ is the matrix that consists of components $\dfrac{\partial\psi_\kappa}{\partial X_\iota}$ and $\dfrac{\partial\phi_\eta}{\partial X_\iota}$, here $\iota = \overline{1, N_X}$, $\kappa \in \mathbf{L}$, $\eta \in \mathbf{L}$; $\vec{\mu}_\perp$ is the column-vector that defines the design variables increment subject to the condition of elimination the constraint's violations. Vector $\vec{\mu}_\perp$ can be calculated as presented below.

In order to correct constraint's violations $\mathbf{V}$, vector $\Delta\vec{X}^t_\perp$ to a first approximation should also satisfy Taylor's theorem for the continuously differentiable multivariable function in the vicinity of point $\vec{X}_t$ for each constraint from set $\mathbf{L}$, namely:

$$-\mathbf{V} = \left[\nabla\varphi \right]^T \Delta\vec{X}^t_\perp. \tag{2.6}$$

With substitution of Eq. (2.5) into Eq. (2.6) we obtain the system of equations to determine column-vector $\vec{\mu}_\perp$:

$$\left[\nabla\varphi \right]^T \left[\nabla\varphi \right] \vec{\mu}_\perp = -\mathbf{V}. \tag{2.7}$$

Component $\Delta\vec{X}^t_\square$ is determined using the following equation:

$$\Delta\vec{X}_{\square}^{t} = \xi \times \vec{p}_{\nabla f} = \xi\left(\nabla\vec{f} - [\nabla\varphi]\vec{\mu}_{\square}\right), \quad (2.8)$$

where $\nabla\vec{f}$ is the vector of the objective function gradient in the current point (current approximation of the design variables) $\vec{X}_t$; $\vec{p}_{\nabla f}$ is the projection of the objective function gradient vector onto the active constraints surface in the current point $\vec{X}_t$; $\vec{\mu}_{\square}$ is the column-vector that defines the design variable's increment subject to the improvement of the objective function value. Column-vector $\vec{\mu}_{\square}$ can be calculated approximately using the least-square method by the following equation:

$$[\nabla\varphi]\vec{\mu}_{\square} \approx \nabla\vec{f}, \quad (2.9)$$

or from the equation presented below:

$$[\nabla\varphi]^T [\nabla\varphi]\vec{\mu}_{\square} = [\nabla\varphi]^T \nabla\vec{f}; \quad (2.10)$$

where ξ is the step parameter, which can be calculated subject to the desired increment Δf of the purpose function on movement along the direction of the purpose function anti-gradient. The increment Δf can be assign as 5...25% from the current value of the objective function $f\left(\vec{X}_t\right)$:

$$\Delta f = \xi\left(\nabla\vec{f}\right)^T \nabla\vec{f}, \; \xi = \frac{\Delta f}{\left(\nabla\vec{f}\right)^T \nabla\vec{f}}, \quad (2.11)$$

where in case of minimization Eq. (1.1) Δf and ξ accordingly have negative values. The parameter ξ can be also calculated using the dependency presented below:

$$\xi = \frac{\Delta f}{\left(\vec{p}_{\nabla f}\right)^T \nabla\vec{f}}, \quad (2.12)$$

that follows from the condition of attainment the desired increment of the objective function Δf on the movement along the direction of the objective function anti-gradient projection onto the active constraints surface. Step parameter ξ can be also selected as a result of numerical experiments performed for each type of the structure individually [16, 17].

Using Eqs. (2.5) and (2.8), Eq. (2.3) can be rewritten as presented below:

$$\Delta\vec{X}_t = [\nabla\varphi]\ \vec{\mu}_{\perp} + \xi\left(\nabla\vec{f} - [\nabla\varphi]\ \vec{\mu}_{\square}\right), \quad (2.13)$$

Or

$$\Delta\vec{X}_t = \xi\ \nabla\vec{f} + [\nabla\varphi]\left(\vec{\mu}_{\perp} - \xi\ \vec{\mu}_{\square}\right), \quad (2.14)$$

where column-vectors $\vec{\mu}_{\perp}$ and $\vec{\mu}_{\square}$ are calculated using Eq. (2.7) and Eq. (2.9) or Eq. (2.10), respectively.

The linear-independent constraints of the system Eqs. (1.2) – (1.3) should be detected when constructing the matrix of the active constraints gradients $[\nabla\varphi]$ used by Eq. (2.7) and Eq. (2.9) or Eq. (2.10). Selection of the linear-independent constraints can be performed based on the equivalent transformations of the resolving equations of the gradient projection method using the non-degenerate transformation matrix $\mathbf{H}$, such that the sub-diagonal elements of the matrix $\mathbf{H}[\nabla\varphi]$ equal to zero. An orthogonal matrix of the elementary mapping (Householder's transformation) [18] has been used to select linear-independent constraints of the system Eqs. (1.2) – (1.3) as well as to form triangular structure of the nonzero elements of matrix $\mathbf{H}[\nabla\varphi]$ [14].

Using Householder's transformations described above triangular structure of the nonzero elements of matrix $\mathbf{H}[\nabla\varphi]$ is formed step-by-step. Besides, Eq. (2.7) and Eq. (2.9) can be rewritten as follow:

$$\left([\nabla\varphi]^T \mathbf{H}^T\right)\left(\mathbf{H}[\nabla\varphi]\right)\vec{\mu}_{\perp} = -\mathbf{V}; \quad (2.15)$$

$$\mathbf{H}\left[\nabla\varphi\right]\vec{\mu}_{\square} \approx \mathbf{H}\nabla\vec{f}\,. \tag{2.16}$$

Equivalent Householder transformations of the resolving equations Eqs. (2.15), (2.16) have been proposed by the paper [14]. They increase numerical efficiency of the algorithm developed based on the considered method.

In order to calculate column-vectors $\vec{\mu}_{\perp}$ and $\vec{\mu}_{\square}$, it is required only to perform forward and backward substitutions in Eq. (2.15) and Eq. (2.16).

To accelerate the convergence of the minimization algorithm presented above, h th columns should be excluded from matrix $\mathbf{H}\left[\nabla\varphi\right]$. These columns correspond to those constraints from Eq. (1.3), for which the following inequality satisfies:

$$\mu_{\perp h} - \xi \times \mu_{\square h} > 0\,. \tag{2.17}$$

As presented by the papers [14, 15], when $\mu_{\perp h} - \xi \times \mu_{\square h} > 0$, then the return onto the active constraints surface from the feasible region $\Im$ is performed with simultaneous degradation of the objective function value. At the same time, in case of $\mu_{\perp h} - \xi \times \mu_{\square h} < 0$, both the improvement of the objective function value and the return from the inadmissible region onto the active constraints surface are performed.

When excluding h th columns from matrix $\mathbf{H}\left[\nabla\varphi\right]$ corresponded to those constraints for which Eq. (2.17) is satisfied, the matrix $\left(\mathbf{H}\left[\nabla\varphi\right]\right)_{red}$ with a broken (non-triangular) structure of the non-zero elements is obtained. The set $\mathbf{L}$ of the linear-independent active constraints numbers transforms into the set $\mathbf{L}_{red}$ respectively. At the same time, the vector of the constraint's violations $\mathbf{V}$ reduced into the vector $\mathbf{V}_{red}$ accordingly. In order to restore the triangular structure of the matrix $\left(\mathbf{H}\left[\nabla\varphi\right]\right)_{red}$ with zero sub-diagonal elements, Givens transformations (Givens rotations) [18] can be used.

Considering Givens transformations, Eq. (2.15) and Eq. (2.16) for column-vectors $\left(\vec{\mu}_{\perp}\right)_{red}$ and $\left(\vec{\mu}_{\square}\right)_{red}$ can be rewritten as:

$$\begin{aligned}&\left(\left[\nabla\varphi\right]^{T}\mathbf{H}^{T}\right)_{red}\mathbf{G}^{T}\times\\ &\times\mathbf{G}\left(\mathbf{H}\left[\nabla\varphi\right]\right)_{red}\left(\vec{\mu}_{\perp}\right)_{red} = -\mathbf{V}_{red};\end{aligned} \tag{2.18}$$

$$\mathbf{G}\left(\mathbf{H}\left[\nabla\varphi\right]\right)_{red}\left(\vec{\mu}_{\square}\right)_{red} \approx \mathbf{GH}\nabla\vec{f}\,. \tag{2.19}$$

Equivalent transformations of the resolving equations Eqs. (2.18), (2.19) using Givens rotations (transformations with matrix $\mathbf{G}$) ensure acceleration of the iterative searching process Eq. (2.1) in those cases when Eq. (2.17) takes into account due to decreasing the amount of calculations [14].

The main resolving equation of the gradient method Eq. (2.13) and Eq. (2.14) can be rewritten as presented below:

$$\begin{aligned}\Delta\vec{X}_{t} &= \left(\mathbf{H}\left[\nabla\varphi\right]\right)_{red}\left(\vec{\mu}_{\perp}\right)_{red} +\\ &+\xi\left(\nabla\vec{f} - \left(\mathbf{H}\left[\nabla\varphi\right]\right)_{red}\left(\vec{\mu}_{\square}\right)_{red}\right);\end{aligned} \tag{2.20}$$

Or

$$\begin{aligned}\Delta\vec{X}_{t} &= \xi\ \nabla\vec{f} +\\ &+\left(\mathbf{H}\left[\nabla\varphi\right]\right)_{red}\left(\left(\vec{\mu}_{\perp}\right)_{red} - \xi\left(\vec{\mu}_{\square}\right)_{red}\right).\end{aligned} \tag{2.21}$$

It should be noted that the lengths of the gradient vectors for the objective function Eq. (1.1), as well as for constraints Eqs. (1.2) – (1.3), remain as they were in scope of the proposed equivalent transformations ensuring the dependability of the optimization algorithm [14].

The determination the convergence criterion is the final question when using the iterative searching for the optimum point Eq. (2.1) described above. Considering the geometrical content of the gradient steepest descent method, we can assume that at the permissible point $\vec{X}_{t}$ the component of the increment vector $\Delta\vec{X}_{\square}^{t}$ for the design variables

should be vanish, $\Delta\vec{X}_{\square}^{t} \to 0$, in case of approximation to the optimum solution of the non-linear programming task presented by Eqs. (1.1) – (1.5). So, the following convergence criterion of the iterative procedure Eq. (2.1) can be assigned:

$$\left\|\Delta\vec{X}_{\square}^{k}\right\| = \sqrt{\sum_{\iota=1}^{N_X}\left(\Delta X_{\square,\iota}^{k}\right)^2} < \varepsilon_1, \qquad (2.22)$$

where ε_1 is a small positive number. In the paper [14] the convergence criteria for the iterative procedure Eq. (2.1) has been presented in detail.

3. MATHEMATICAL MODEL FOR PARAMETRIC OPTIMIZATION OF THE LATTICE PORTAL FRAME

A parametric optimization task for lattice portal frame of the steel warehouse framework designed as repository for the granulated sulfur has been considered. Building object locates in seaport Ust-Luga of Russian Federation The general building sizes are length 247.25 m and width 69.0 m. Steel framework of the building consists of portal frames with span 69.0 m positioned along building length with bay 7.5 m. Steel portal frames consist of the lattice structural members fabricated from pipes with steel grade St20 according to design code [12]. Joints in the lattice structural members were designed using welded connections without gussets.

There is a service platform at the level +28.25 m provided for supporting the crane-loader and conveyor (see Fig. 3.1). The load-bearing structures of the platform are suspended to the structural members of the portal frames. Welded I-beams of this platform were manufactured from the universal steel sheets of grade S245.

Design scheme of the steel lattice portal frame was assumed as a hinged-bar structure with hinged column bases. Geometrical scheme of the portal frame was described using the set of nodes and bars with orientation on implementation of the finite element method for linear static analysis. Node coordinates of the design scheme were determined in Cartesian coordinate system and presented as expressions in dependence of geometrical design variables of the optimization task.

Figure 3.1. Assembling process on job site (Photo has been provided by V. Shymanovsky Ukrainian Research and Design Institute of Steel Construction)

Dead loads included self weight of the portal frame, roof purlins, roof bracings, fire escape staircase and mezzanines, profiled panels which is used as non-warmth-keeping walling as well as service loads on fire escape staircase and mezzanines. Safety factors for the design loads

and effects as well as safety factor for the building responsibility were defined according to [12]. Live loads (or technological loads) were accepted according to the target specification. Calculation the design values for climate loadings has been performed according to the requirements [12]. So, tree types of snow loads and two types of wind load have been considered when optimum designing of the steel portal frames.

Design loads and effects have been combined in 16 design load case combinations taken into account the combination factors according to requirements of design code [12]. All loads and effects on the structure were presented as concentrated loads at the nodes and were determined analytically depending on the variable parameters of the geometrical scheme.

Mathematical model of the parametric optimization task for the steel portal frame with lattice structural members has been formulated as nonlinear programming task including the set of design variables, system of constraints as well as specified purpose function.

3.1. Design variables

Parameters of the geometric scheme of the portal frames have been considered as design variables. Variable parameters of the geometrical scheme were building height at the eave node H_{zdk} and at the ridge H_{zd}, distance between upper and lower chords of the lattice rafter at the eave node hop and at the erection joints h_2, h_4, h_6 i h_7, distance between chords of the lattice column at the eave node bop and parameter b_7 (see Fig. 3.2). Start values for the design variables were accepted according to the design decision of the steel framework developed by Open Join-Stock Company "V. Shymanovsky Ukrainian Research and Design Institute of Steel Construction", namely: $H_{zd} = 39.58\,\text{m}$, $H_{zdk} = 10.63\,\text{m}$, $h_2 = h_4 = h_6 = h_7 = h_{op} = b_{op} = 2.6\,\text{m}$, $b_7 = 0.56\,\text{m}$. Additionally, cross-sectional sizes of the structural members with circle hollow sections (CHS) for each stiffness type were considered as design variables (see Table 3.1).

Table 3.1. Variable cross-sectional sizes for the CHS structural members of the portal frame

Destination and location of structural member	Stiffness type number	Design variables name, diameter× thickness	Start values, mm×mm	Stiffness type number	Design variables name, diameter× thickness	Start values, mm×mm
Chords of the lattice structural members	1	$d_1 \times t_1$	299×25	7	$d_6 \times t_7$	299×16
	2	$d_1 \times t_2$	299×14	8	$d_8 \times t_8$	299×10
	3	$d_1 \times t_3$	299×10	9	$d_9 \times t_9$	299×10
	4	$d_1 \times t_4$	299×14	10	$d_{10} \times t_{10}$	299×14
	5	$d_1 \times t_5$	299×14	11	$d_{11} \times t_{11}$	180×12
	6	$d_6 \times t_6$	299×10	–	–	–
Elements of the lattice rafters	12	$d_{12} \times t_{12}$	152×8	14	$d_{14} \times t_{14}$	102×5
	13	$d_{13} \times t_{13}$	121×8	–	–	–
Frame ridge	15	$d_{15} \times t_{15}$	152×8	17	$d_{17} \times t_{17}$	180×12
	16	$d_{16} \times t_{16}$	102×5	18	$d_{18} \times t_{18}$	180×12
Elements of the lattice columns	19	$d_{19} \times t_{19}$	299×10	21	$d_{21} \times t_{21}$	299×25
	20	$d_{19} \times t_{20}$	299×25	22	$d_{22} \times t_{22}$	102×5
Suspension arm of the service platform	23	$d_{23} \times t_{23}$	180×12	–	–	–

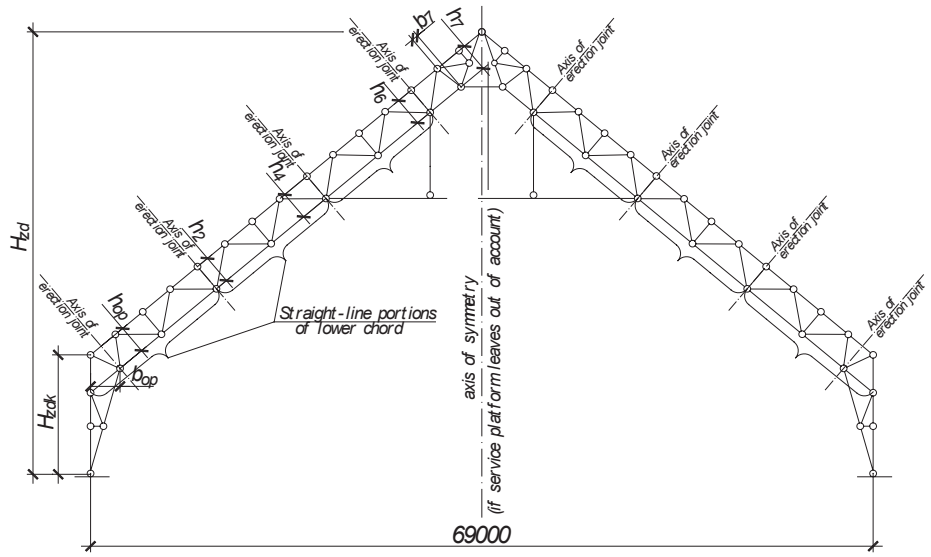

Figure 3.2. The design scheme of the portal frame with specification of the variable geometrical parameters

3.2. System of constraints

The system of constraints Eqs.(1.2) – (1.3) should cover strength and stability constraints formulated for all design sections of all structural members of the considered steel structure subjected to all design load combinations at the ultimate limit state. The following strength constraints have been included in the system of constraints Eqs. (1.2) – (1.3), formulated for all design sections, $\forall i = \overline{1, N_{DS}}$ (N_{DS} is the total number of the design sections in structural members), of all structural members, $\forall j = \overline{1, N_B}$ (N_B is the total number of the structural members), subjected to all ultimate load case combination, $\forall k = \overline{1, N_{LC}^{ULS}}$, namely normal stresses verifications:

$$\frac{N_{ijk}\left(\vec{X}\right)}{A_{n,j}\left(\vec{X}_{CS}\right)R_{y,j}\gamma_c} - 1 \le 0; \qquad (3.1)$$

where $\sigma_{ijk}\left(\vec{X}\right) = \dfrac{N_{ijk}\left(\vec{X}\right)}{A_{n,j}\left(\vec{X}_{CS}\right)}$ is the value of the normal stresses caused by axial force $N_{ijk}\left(\vec{X}\right)$ acting in i th design section of j th structural member subjected to k th ultimate load case combination calculated from the linear equations system of the finite element method presented by Eq.(1.5); $A_{n,j}\left(\vec{X}_{CS}\right)$ is the net cross-sectional area of j th structural member calculated depending on the variable cross-sectional dimensions of the structural members $\vec{X}_{CS}$; γ_c is the safety factor [12]; $R_{y.j}$ is the design strength for steel member subjected to tension, bending and compression; $R_y\gamma_c$ are allowable value for normal stresses [12]; $\sigma_{x,ijk}\left(\vec{X}\right)$ are normal stresses at the specified cross-section point caused by internal forces acting in i th design section of j th structural member subjected to k th ultimate load case combination calculated from the linear equations system of the finite element method presented by Eq. (1.5). The value of the normal stresses $\sigma_{x,ijk}\left(\vec{X}\right)$ at the specified cross-section point has been calculated depending on the variable geometrical parameters of the structure

$\vec{X}_G$ and variable cross-sectional dimensions of the structural members $\vec{X}_{CS}$.

The following constraints on slenderness of the structural members have been included in the system of constraints Eqs. (1.2) – (1.3), $\forall j = \overline{1, N_B}$:

$$\frac{l_{ef,y,j}\left(\vec{X}_G\right)}{i_{y,j}\left(\vec{X}_{CS}\right)\lambda_{uy,j}} - 1 \le 0; \quad (3.2)$$

$$\frac{l_{ef,z,j}\left(\vec{X}_G\right)}{i_{z,j}\left(\vec{X}_{CS}\right)\lambda_{uz,j}} - 1,0 \le 0; \quad (3.3)$$

where $i_{y,j}\left(\vec{X}_{CS}\right)$ and $i_{z,j}\left(\vec{X}_{CS}\right)$ are radiuses of inertia for j th structural member's design cross-section relative to the main axis of inertia and calculated depending on the variable cross-sectional dimensions of the structural members $\vec{X}_{CS}$; $l_{ef,y,j}\left(\vec{X}_G\right)$ and $l_{ef,z,j}\left(\vec{X}_G\right)$ are design lengths for j th structural member in the main planes of inertia calculated depending on the variable geometrical parameters of the structure $\vec{X}_G$; $\lambda_{uy,j}$ and $\lambda_{uz,j}$ are the ultimate slenderness for j th structural member. Design lengths of the structural members $l_{ef,y,j}\left(\vec{X}_G\right)$ and $l_{ef,z,j}\left(\vec{X}_G\right)$ were defined according to [12] as: for chords, support diagonals and support columns of the lattice structural members – $l_{ef,y,j}\left(\vec{X}_G\right) = l_j\left(\vec{X}_G\right)$; $l_{ef,z,j}\left(\vec{X}_G\right) = l_{1,j}$; for other elements of the lattice structural members – $l_{ef,y,j}\left(\vec{X}_G\right) = 0.85 l_j\left(\vec{X}_G\right)$; $l_{ef,z,j}\left(\vec{X}_G\right) = 0.85 l_{1,j}$; here l_j is the geometrical length for j th bar of lattice structural member; $l_{1,j}$ is the distance between out-of-plane restraints of the member from the horizontal displacements in out-of-plane direction. Ultimate values for the slenderness of the lattice structural members were specified according to [12] as: $\lambda_{uy,j} = \lambda_{uz,j} = 400$ for all tensioned members; $\lambda_{uy,j} = \lambda_{uz,j} = 150$ for all compressed members.

The following stability constraints have been included in the system of constraints Eqs. (1.2) – (1.3), formulated for all design sections, $\forall i = \overline{1, N_{DS}}$, of the structural members subjected to all ultimate load case combination, $\forall k = \overline{1, N_{LC}^{ULS}}$, namely flexural buckling verifications for all structural members subjected to axial compression force $N_{ijk}\left(\vec{X}\right)$, $\forall j = \overline{1, N_B}$:

$$\frac{N_{ijk}\left(\vec{X}\right)}{\varphi_{y,j}\left(\vec{X}_G, \vec{X}_{CS}\right) A_j\left(\vec{X}_{CS}\right) R_{y,j}\gamma_c} - 1 \le 0; \quad (3.4)$$

$$\frac{N_{ijk}\left(\vec{X}\right)}{\varphi_{z,j}\left(\vec{X}_G, \vec{X}_{CS}\right) A_j\left(\vec{X}_{CS}\right) R_{y,j}\gamma_c} - 1 \le 0; \quad (3.5)$$

where $A_j\left(\vec{X}_{CS}\right)$ is the gross cross-sectional area of j th structural member calculated depending on the variable cross-sectional dimensions of the structural members $\vec{X}_{CS}$; $\varphi_{y,j}\left(\vec{X}_G, \vec{X}_{CS}\right)$ and $\varphi_{z,j}\left(\vec{X}_G, \vec{X}_{CS}\right)$ are column's stability factors corresponded to flexural buckling relative to the main axes of inertia and calculated depending on the design lengths $l_{ef,y,j}\left(\vec{X}_G\right)$, $l_{ef,z,j}\left(\vec{X}_G\right)$, cross-section type and cross-section geometrical properties for the j th structural member [12]. The flexural buckling factors $\varphi_{y,j}\left(\vec{X}_G, \vec{X}_{CS}\right)$ and $\varphi_{z,j}\left(\vec{X}_G, \vec{X}_{CS}\right)$ calculated depending on the variable geometrical parameters of the structure $\vec{X}_G$ and variable cross-sectional dimensions of the structural members $\vec{X}_{CS}$.

The following local buckling constraints have been also included into the system of constraints:

$$\frac{\overline{\lambda}_{w,j}\left(\vec{X}_{CS}\right)}{\overline{\lambda}_{uw,j}\left(\vec{X}\right)}-1\le 0; \tag{3.6}$$

$$\frac{\overline{\lambda}_{f,j}\left(\vec{X}_{CS}\right)}{\overline{\lambda}_{uf,j}\left(\vec{X}\right)}-1\le 0 \tag{3.7}$$

where $\overline{\lambda}_{w,j}\left(\vec{X}_{CS}\right)$ and $\overline{\lambda}_{f,j}\left(\vec{X}_{CS}\right)$ are the non-dimensional slenderness of the web and flange respectively of the cross-section for j th structural member; $\overline{\lambda}_{uw,j}\left(\vec{X}\right)$ and $\overline{\lambda}_{uf,j}\left(\vec{X}\right)$ are the maximum values for corresponded non-dimensional slenderness for column structural members calculated depending on the internal forces (ration of the bending moment to the axial force), as well as depending on the design lengths $l_{ef,y,j}$, $l_{ef,z,j}$, cross-section type and cross-section geometrical properties for the j th structural member [12]. The non-dimensional slenderness $\overline{\lambda}_{w,j}\left(\vec{X}_{CS}\right)$ and $\overline{\lambda}_{f,j}\left(\vec{X}_{CS}\right)$ calculated depending on the variable cross-sectional dimensions of the structural members $\vec{X}_{CS}$ only. At the same time, the maximum values for corresponded non-dimensional slenderness $\overline{\lambda}_{uw,j}\left(\vec{X}\right)$ and $\overline{\lambda}_{uf,j}\left(\vec{X}\right)$ calculated depending on the variable geometrical parameters of the structure $\vec{X}_G$ and variable cross-sectional dimensions of the structural members $\vec{X}_{CS}$.

The system of constraints Eqs. (1.2) – (1.3) has been also covered the displacements constraints (stiffness inequalities) for the specified nodes of the considered steel structure subjected to all design load combinations at the serviceability limit state. The following horizontal and vertical displacements constraints have been included into the system of constraints Eqs. (1.2) – (1.3), formulated for all nodes, $\forall m=\overline{1,N_N}$ (N_N is the total number of nodes in the considered steel structure), of the steel structure subjected to all serviceability load case combination, $\forall k=\overline{1,N_{LC}^{SLS}}$, namely:

$$\frac{\delta_{x,mk}\left(\vec{X}\right)}{\delta_{ux,m}}-1\le 0; \tag{3.8}$$

$$\frac{\delta_{z,mk}\left(\vec{X}\right)}{\delta_{uz,m}}-1\le 0; \tag{3.9}$$

where $\delta_{x,mk}\left(\vec{X}\right)$ and $\delta_{z,mk}\left(\vec{X}\right)$ are the horizontal and vertical displacements respectively for l th node of the steel structure subjected to k th serviceability load case combination calculated from the linear equations system of the finite element method presented by Eq. (1.6); $\delta_{ux,m}$ and $\delta_{uz,m}$ are the allowable horizontal and vertical displacements for m th structural node. Ultimate values for linear node displacements of the steel lattice portal frame were calculated according to [12] as $\delta_{ux,m}=H_{zd}/210$ and $\delta_{uz,m}=L/300=230$ mm.

Additional requirements that describe structural, technological and serviceability particularities of the considered structure, as well as constraints on the building functional volume (see Fig. 3.3) can be also included into the system Eqs. (1.2) – (1.3). In particular these requirements can be presented in the form of constraints on lower and upper values of the design variables, $\forall \imath=\overline{1,N_X}$:

$$1-\frac{X_\imath}{X_\imath^L}\le 0; \tag{3.10}$$

$$\frac{X_\imath}{X_\imath^U}-1\le 0; \tag{3.11}$$

where $X_\imath^L$ and $X_\imath^U$ are the lower and upper bounds for the design variable $X_\imath$; N_X is the total number of the design variables.

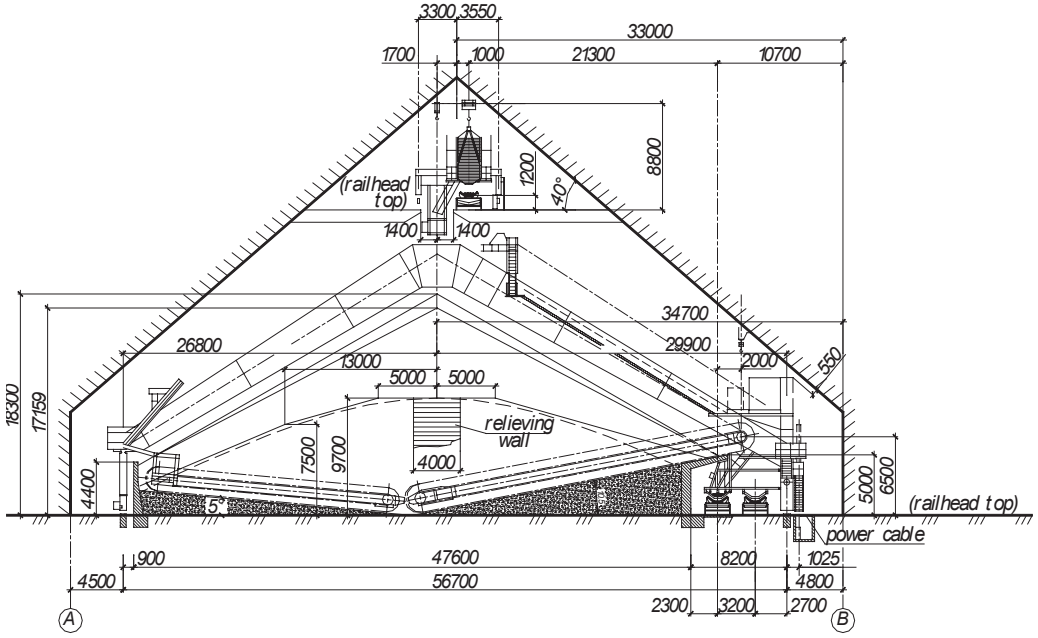

Figure 3.3. Technological equipments and constraints that describe useful space in the building

Additional constraints on cross-sectional sizes of the structural members with circle hollow sections type have been formulated according to the requirements of [12]. There were constraints of permissible minimal thickness and permissible maximum diameter-to-thickness ratio for the structural members, namely, $\forall l = \overline{1, N_{ST}}$:

$$1,0 - \frac{t_l}{t_{\min,l}} \le 0; \qquad (3.12)$$

$$\frac{D_l}{t_l \delta_{\max,l}} - 1,0 \le 0; \qquad (3.13)$$

where l is the number of the stiffness type; N_{ST} is the overall quantity of the stiffness types in the considered steel lattice portal frame; t_l and D_l are thickness and diameter of the circle hollow section for lth stiffness type (see Table 3.1) respectively; $t_{\min,l}$ is the minimum thickness of the circle hollow section in accordance with design code [12] as $t_{\min,l} = 3\,\text{mm}$ for chords, support diagonals and support columns of lattice structural members and $t_{\min,l} = 2.5\,\text{mm}$ for other lattice elements; $\delta_{\max,l}$ is the maximum diameter-to-thickness ratio for the structural member with circle hollow section in accordance with design code [12] depending on the yield stress value $R_{yn} = 245\,\text{MPa} < 295\,\text{MPa}$ as $\delta_{\max,l} = 30$ for chords elements of the lattice structural members and $\delta_{\max,l} = 90$ for other lattice elements.

The following constraints that describe conditions for designing gusset-less welded joints between CHS structural members formulated according to the requirements [12] have been also included in the system Eqs. (1.2) – (1.3), $q, p = 1...N_{ST}$:

$$0,3 d_p \le d_q \le d_p; \qquad (3.14)$$

where p and q are the numbers of the stiffness types of structural members connected in the joint, here p is the number of the chord's stiffness type; q is the number of the lattice stiffness type.

3.3. Objective function

Minimum weight as well as minimum construction budget has been considered as purpose function. Analytical expression for the structural weight depending on the variable cross-sectional sizes of the members can be written by the following formula:

$$\begin{aligned}\mathbf{M}\left(\vec{X}_G,\vec{X}_{CS}\right)&=\varphi\rho\sum_{j=1}^{N_E}A_j l_j=\\&=4\pi\varphi\rho\sum_{j=1}^{N_E}t_j\left(D_j-t_j\right)l_j\rightarrow\min;\end{aligned}\tag{3.15}$$

where A_j and l_j are gross cross-sectional area and geometrical length for j th structural member respectively; ρ – steel density, $\rho=7850$ kg/m3; φ is the factor that takes into account the increment of structural weight due to the present of the adjunct elements in the structural members and joints (stiffeners, ribs, end-plates, gussets etc.), φ was defined according to the steel specification mentioned in the source project for the warehouse framework, φ 1,1.

Construction budget of the steel portal frame with lattice structural members taken into account construction budget of mezzanines erected at the level +28,25 can be presented as follow:

$$\begin{aligned}\mathbf{K}&=C_{mnf}^{lt}+C_{mnf}^{sl}+C_{asm}+C_{asm}^{wl}+\\&+C_{c.p.}+C_{q.c.}+C_{mat};\end{aligned}$$

where C_{mnf}^{lt} is the manufacturing cost of lattice structural members; C_{mnf}^{sl} is the manufacturing cost of mezzanine's structural members; C_{asm} is the assembly cost for steel portal frame; C_{asm}^{wl} is the assembly cost for walling; $C_{c.p.}$ is the cost on the work package for corrosion protection of the steel framework; $C_{q.c.}$ is the cost for the quality control of welded connections; C_{mat} is the material cost for structural members of the steel portal frame. Analytical expression of the construction budget for manufacturing and erection of the steel lattice portal frame depending on the design variables have been presented by the following, UAH:

$$\begin{aligned}K&=20670\mathbf{M}\left(\vec{X}_G,\vec{X}_{CS}\right)+1525D_{ov}\left(\vec{X}_G\right)+\\&+1300H_{zdk}+110\mathbf{A_s}\left(\vec{X}_G,\vec{X}_{CS}\right)+\\&+21120\rightarrow\min;\end{aligned}\tag{3.16}$$

where D_{ov} is the half-rafter length, $D_{ov}=\left((0,5L)^2+\left(H_{zd}-H_{zdk}\right)^2\right)^{\frac{1}{2}}$; L is the portal frame span, $L=69$ m; $\mathbf{A_s}\left(\vec{X}_G,\vec{X}_{CS}\right)$ is the total surface area of the steel lattice portal frame to be subjected to anti-corrosion treatment.

4. PARAMETRIC OPTIMIZATION ALGORITHM BASED ON THE GRADIENT PROJECTION METHOD

Let present the following numerical algorithm to solve the parametric optimization problem for steel structures formulated above.

Step 1. Describing an initial design (a set of design variables) and initial data for structural optimization.

The design variable vector $\vec{X}_k=\left(\vec{X}_G,\vec{X}_{CS}\right)_k^T$ has been specified, where k is the iteration index, $k=0$. The structural topology, cross-section types and node type connections of the bars, the support conditions of the bar system, as well as loading patterns, load case combinations and load design values are prescribed and constants.

Initial data for optimization of the considered steel structure are design strength for steel member R_y, safety factor γ_c, factors to define flexural design lengths $l_{ef,y,j}$, $l_{ef,z,j}$ for all column structural members; allowable values

for horizontal and vertical displacements $\delta_{ux,l}$ and $\delta_{uz,l}$ of the specified nodes of the considered steel structure; lower $\vec{X}^L$ and upper $\vec{X}^U$ bounds for the design variables; as well as specified objective function $f(\vec{X}_k)$.

Step 2. Calculation of the geometrical and design lengths for all structural members.

The geometrical lengths l_j of all structural members are calculated based on the node coordinates of the considered steel structure. The latter depend on the unknown (variable) geometrical parameters of the structure $\vec{X}_G$. The design lengths $l_{ef,y,j}$, $l_{ef,z,j}$ of all column structural members are calculated using calculated geometrical lengths l_j and initial data relating to the design length factors. The latter are constant during the iteration process presented below. Variation of the geometrical lengths l_j and corresponded design lengths $l_{ef,y,j}$, $l_{ef,z,j}$ on the further iterations has been performed based on the current values of the variable (unknown) parameters $\vec{X}_G$ of the geometrical scheme.

Step 3. Calculation of the cross-section dimensions and geometrical properties for all design cross-sections.

Geometrical properties of the design cross-sections (areas, moments of inertia, elastic section moments, radiuses of inertia, etc.), as well as non-dimensional slenderness for cross-section elements (webs and flanges) $\overline{\lambda}_{w,j}\left(\vec{X}_{CS}\right)$ and $\overline{\lambda}_{f,j}\left(\vec{X}_{CS}\right)$ have been calculated depending on the current values of the unknown (variable) cross-section dimensions $\vec{X}_{CS}$.

Step 4. Linear structural analysis of the considered steel structure.

For each m th node of the finite element model subjected to k th serviceability load case combination the displacements and rotations, as well as the design horizontal $\delta_{x,mk}\left(\vec{X}\right)$ and vertical $\delta_{z,lk}\left(\vec{X}\right)$ displacements can be calculated using the linear equations system of the finite element method presented by Eq. (1.6).

For each i th design section of j th structural member subjected to k th ultimate load case combination the design internal forces can be calculated using the linear equations system of the finite element method presented by Eq. (1.5).

Step 5. Calculation of the state variables (stresses, buckling factors, allowable non-dimensional slenderness etc.).

The value of the normal $\sigma_{x,ijk}\left(\vec{X}\right)$ stresses at the specified cross-section point has been calculated depending on the axial force acting in i th design section of j th structural member subjected to k th ultimate load case combination as presented by the design code.

The flexural buckling factors $\varphi_{y,j}\left(\vec{X}_G,\vec{X}_{CS}\right)$, $\varphi_{z,j}\left(\vec{X}_G,\vec{X}_{CS}\right)$ have been calculated depending on the corresponded design lengths, cross-section type and cross-section geometrical properties for the structural members according to the design code [12].

The maximum values for corresponded non-dimensional slenderness $\overline{\lambda}_{uw,j}\left(\vec{X}\right)$ and $\overline{\lambda}_{uf,j}\left(\vec{X}\right)$ for column structural members have been calculated depending on the design lengths $l_{ef,y,j}$, $l_{ef,z,j}$, cross-section type and cross-section geometrical properties for the j th structural member [12].

Step 6. Verifications of the constraints and construction the set of active constraints numbers $\mathbf{A}$.

Verification of the constraints Eqs. (3.1), (3.4), (3.5) has been performed for all ultimate load case combinations and all design cross-sections of all structural members. Verification of the constraints Eqs. (3.8), (3.9) have been also conducted for all serviceability load case combinations and all design structural nodes.

Additional requirements in the form of constraints Eqs. (3.10), (3.11) on lower and upper values of the design variables, local buckling constraints Eqs. (3.6), (3.7), constraints on the member's slenderness Eqs. (3.2), (3.3), constraint Eq. (3.12) on permissible minimal thickness, constraint Eq. (3.13) on permissible maximum diameter-to-thickness ratio for the structural members, as well as the conditions Eq. (3.14) for designing gusset-less welded joints between structural members with circle hollow sections have been also verified. Set of the active constraints numbers $\mathbf{A}$ calculated for the current approximation $\vec{X}_k$ has been constructed according to Eq. (2.2).

Step 7. Calculation of the current objective function value $f(\vec{X}_k)$, objective function gradient $\nabla f(\vec{X}_k)$ and determination of the desired decrement of the objective function value $\Delta f(\vec{X}_k)$.

The objective function gradient $\nabla f(\vec{X}_k)$ can be calculated by the numerical differentiation with respect to the design variables using the finite difference approximation. The desired decrement of the objective function value $\Delta f(\vec{X}_k)$ can be assigned as 5…25% from the current objective function value $f(\vec{X}_k)$.

Step 8. Construction of the constraint's violations vector $\mathbf{V}$ and the matrix of the active constraint's gradients $[\nabla\varphi]$. The vector of the values of the constraint's violations $\mathbf{V}$ and the matrix of the constraint's gradients $[\nabla\varphi]$ are constructed for active constraints only according to the set of active constraints numbers $\mathbf{A}$.

Step 9. Construction the matrix of active linear-independent constraint's gradients with triangular structure. The set of linear-independent constraint's numbers $\mathbf{L}$ and the matrix of active linear-independent constraint's gradients $\mathbf{H}[\nabla\varphi]$ with triangular structure are constructed according to the algorithm presented by the paper [14].

Step 10. Step parameter ξ calculation. Step parameter ξ has been calculated according to Eq. (2.11) or Eq. (2.12) and can be modified on the further iterations depending on convergence of the iterative process presented by Eq. (2.1).

Step 11. Calculation the column-vectors $\vec{\mu}_\perp$ and $\vec{\mu}_\square$ which define the design variables increment subject to the condition of elimination the constraint's violations and subject to the improvement of the objective function value.

The vectors $\vec{\mu}_\perp$ and $\vec{\mu}_\square$ can be calculated using Eq. (2.18) and Eq. (2.19) respectively.

If some h th component of the column-vectors $\vec{\mu}_\perp$ and $\vec{\mu}_\square$ satisfies Eq. (2.17), the corresponded constraint gradient $\nabla\varphi_h$ has been excluded from the matrix $[\nabla\varphi]$, and corresponded violations V_h has been excluded from the vector $\mathbf{V}$, as well as the return to step 9 has to be conducted. In contrary case transition to the step 11 has been performed.

Step 12. Calculation the increment vector for the current design variables and determination the improved approximation to the optimum solution. The increment vector $\Delta\vec{X}_k$ for the current design variables values $\vec{X}_k$ has been calculated according to Eq. (2.20) or Eq. (2.21). The improved approximation $\vec{X}_{k+1}$ to the optimum solution has been determined according to Eq. (2.1).

Step 13. Stop criteria verification of iterative searching for the optimum solution. If all constraints Eqs. (3.1) – (3.14) are satisfied with appropriate accuracy, as well as inequality Eq. (2.22) or one of the stop criteria described by the paper [14] is also satisfied, then transition to the step 13 has been performed. In contrary case return to the step 1 has been conducted with $k \leftarrow k+1$.

Step 14. Discretization the optimum solution $\vec{X}_k$ obtained in the continuum space of the design variables.

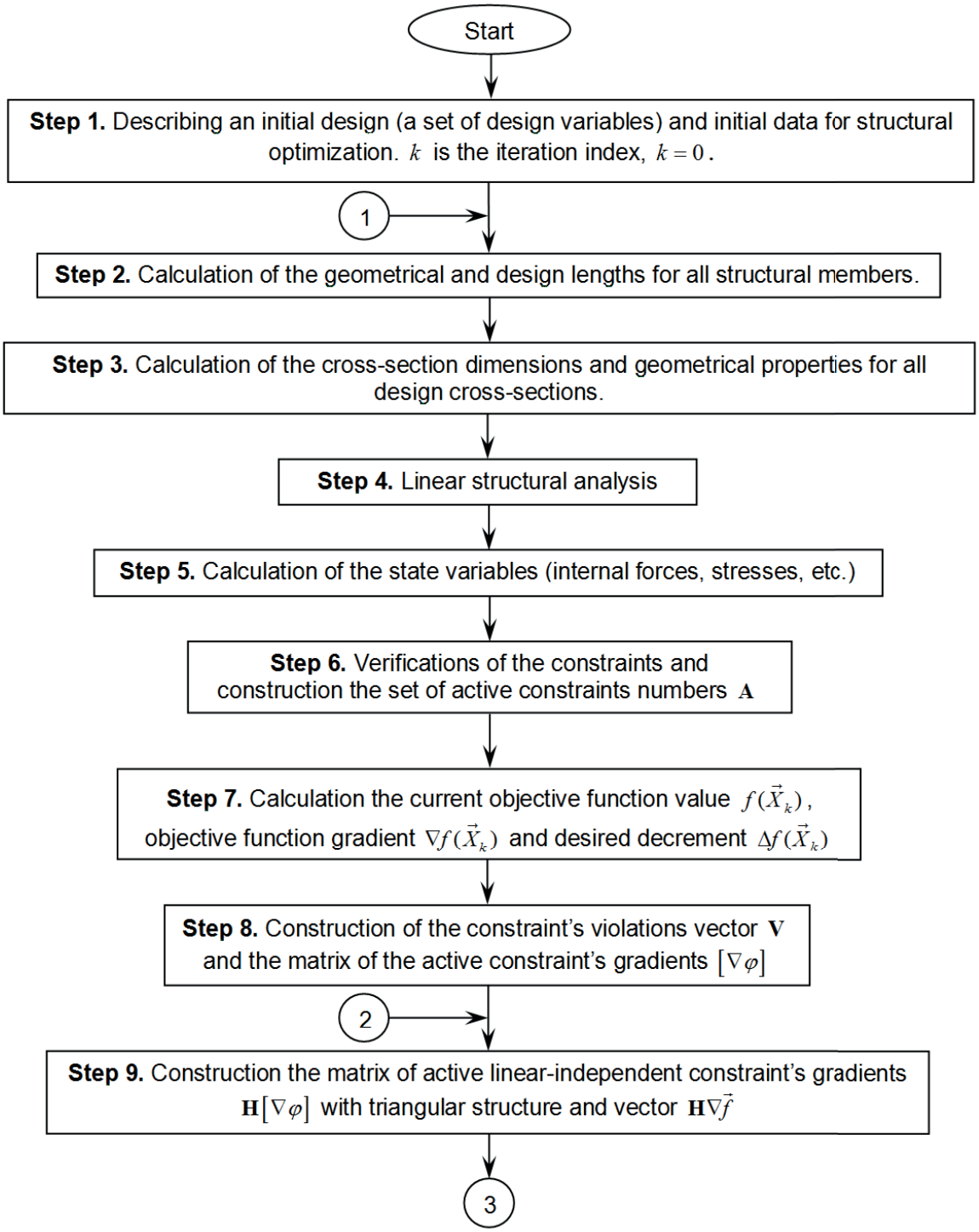

Figure 4.1. The flow chart for structural optimization according to the searching technique based on the gradient projection method

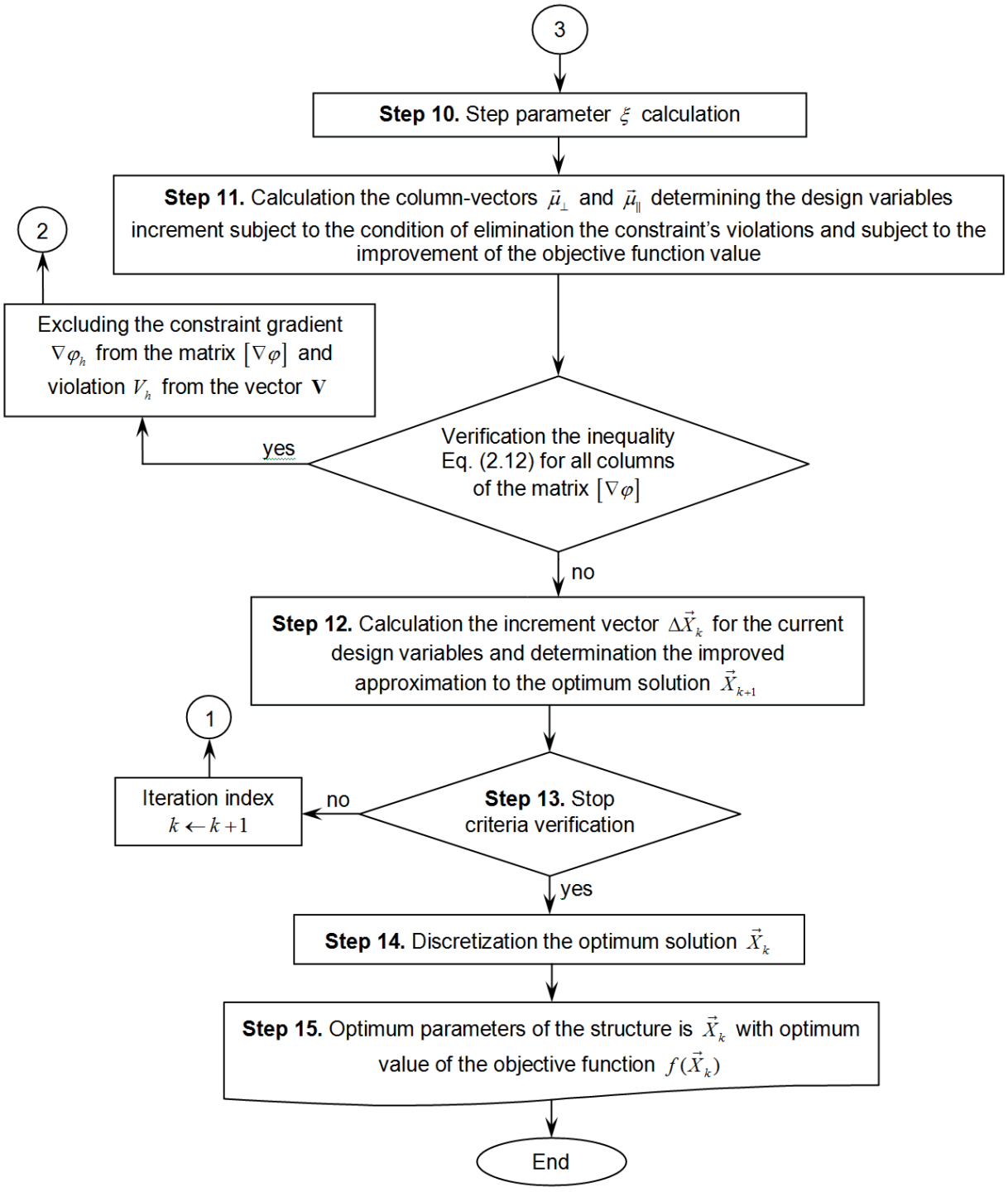

Figure 4.1. (continuation). The flow chart for structural optimization according to the searching technique based on the gradient projection method

Step 15. Optimum parameters of the structure is $\vec{X}_k$ with optimum value of the objective function $f(\vec{X}_k)$.

Figure 4.1 presents the flow chart for structural optimization according to the searching

technique describing by the gradient projection method considered above.

5. OPTIMIZATION RESULTS

A parametric optimization methodology presented above has been realized in software OptCAD [19]. This software provides solutions to a wide range of problems, namely: (i) linear static analysis of bar structures; (ii) verification of the load-bearing capacity of the structural members according to specified design code; (iii) searching for values of the structural parameters when structure complies with design code requirements and designer's criterions; (iv) parametric optimization of the steel bar structures by the determined criterion. Mathematical apparatus of the software combines the finite element method to perform linear static analysis of the bar system, as well as improved gradient projection method to solve parametric optimization problems formulated as non-linear programming tasks [19].

Table 5.1. Optimal values for variable geometrical parameters of the portal frame's design scheme

Design variable	Start value, m	Optimum values, m, by the criterion of minimum			
		weight		costs on fabrication and erection	
		when lower chord of lattice rafter is			
		straight-line	polygonal	straight-line	polygonal
H_{zd}	39.58	38.82	39.55	38.74	39.44
H_{zdk}	10.63	11.92	11.84	12.08	12.03
h_2	2.60	–	3.23	–	3.31
h_4	2.60	–	3.21	–	3.23
h_6	2.60	–	2.68	–	2.70
h_7	2.60	2.18	2.68	2.13	2.61
b_7	0.55773	1.00	0.56	1.05	0.63
h_{op}	2.60	3.61	3.72	3.73	3.87
b_{op}	2.60	3.08	3.02	3.02	2.95
Weight, $\times 10^3$,kg	**30.78**	**18.98**	**18.45**		
Costs, UAH	**786681**			**534647**	**524257**

Table 5.2. Optimal values for variable cross-sectional sizes of the lattice structural members of the portal frame

Design variable	Start value, m	Optimum values, mm×mm, by the criterion of minimum					
		weight			costs on fabrication and erection		
		when lower chord of the lattice rafter is					
		straight-line	polygonal		straight-line	polygonal	
		in the search space					
		continuous		discrete	continuous		discrete
$d_1 \times t_1$	299×25	183.4×8.4	192.3×8.6	194×9.0	173.9×9.3	172.9×8.6	168×11.0
$d_1 \times t_2$	299×14	183.4×6.1	192.3×6.4	194×7.0	173.9×6.9	172.9×6.3	168×8.0
$d_1 \times t_3$	299×10	183.4×6.9	192.3×6.5	194×6.5	173.9×7.3	172.9×7.4	168×8.5
$d_1 \times t_4$	299×14	183.4×8.5	192.3×9.3	194×9.0	173.9×10.7	172.9×9.3	168×11.0
$d_1 \times t_5$	299×14	183.4×6.1	192.3×6.4	194×6.5	173.9×5.8	172.9×5.8	168×6.0
$d_6 \times t_6$	299×10	297.4×9.9	303.1×10.1	299×10.0	298.1×9.9	292.3×9.7	299×10.0
$d_6 \times t_7$	299×16	297.4×11.3	303.1×11.4	299×12.0	298.1×11.6	292.3×11.5	299×12.0
$d_8 \times t_8$	299×10	264.4×8.8	269.4×9.0	299×10.0	269.0×9.0	263.6×8.8	273×9.5
$d_9 \times t_9$	299×10	203.0×6.8	210.7×7.0	194×8.5	211.5×7.0	202.8×6.8	219×7.5
$d_{10} \times t_{10}$	299×14	143.5×4.8	147.1×4.9	152×5.5	148.1×4.9	143.3×4.8	146×5.5
$d_{11} \times t_{11}$	180×12	183.4×9.7	192.3×9.6	194×9.5	173.9×11.5	172.9×11.1	168×13.0
$d_{12} \times t_{12}$	152×8	161.2×4.5	165.6×4.6	152×5.5	164.9×4.6	160.8×4.5	168×5.0
$d_{13} \times t_{13}$	121×8	110.3×3.9	107.4×3.6	108×4.0	80.7×4.9	79.1×5.6	83×5.0
$d_{14} \times t_{14}$	102×5	89.2×3.5	90.9×3.5	95×3.5	89.4×3.5	87.7×3.5	95×3.5
$d_{15} \times t_{15}$	152×8	143.5×5.2	147.1×5.1	152×5.0	133.5×5.9	135.1×5.6	133×6.0
$d_{16} \times t_{16}$	102×5	55.0×3.5	57.9×3.5	60×3.5	52.2×3.5	51.9×3.5	54×3.5
$d_{17} \times t_{17}$	180×12	112.8×4.9	116.3×4.7	108×5.0	90.4×6.1	101.8×5.4	95×6.0
$d_{18} \times t_{18}$	180×12	143.5×6.3	147.1×6.6	152×6.5	148.1×6.6	143.3×6.4	146×7.5
$d_{19} \times t_{19}$	299×10	297.4×9.9	303.2×10.1	299×10.0	298.1×9.9	292.3×9.7	299×10.0
$d_{19} \times t_{20}$	299×25	297.4×9.9	303.2×10.1	299×10.0	298.1×9.9	292.3×9.7	299×10.0
$d_{21} \times t_{21}$	299×25	297.4×21.0	303.2×21.1	299×22.0	298.1×22.3	292.3×22.3	299×24.0
$d_{22} \times t_{22}$	102×5	89.2×3.5	90.9×3.5	95×3.5	89.4×3.5	87.7×3.5	95×3.5
$d_{23} \times t_{23}$	180×12	148.9×5.3	151.6×5.3	152×5.5	79.7×11.4	81.8×10.6	83×1.2
Weight, $\times 10^3$,kg	**30.78**	**18.45**	**18.98**	**19.70**	–	–	–
Costs, UAH	**786681**	–	–	–	**534647**	**524257**	**552368**

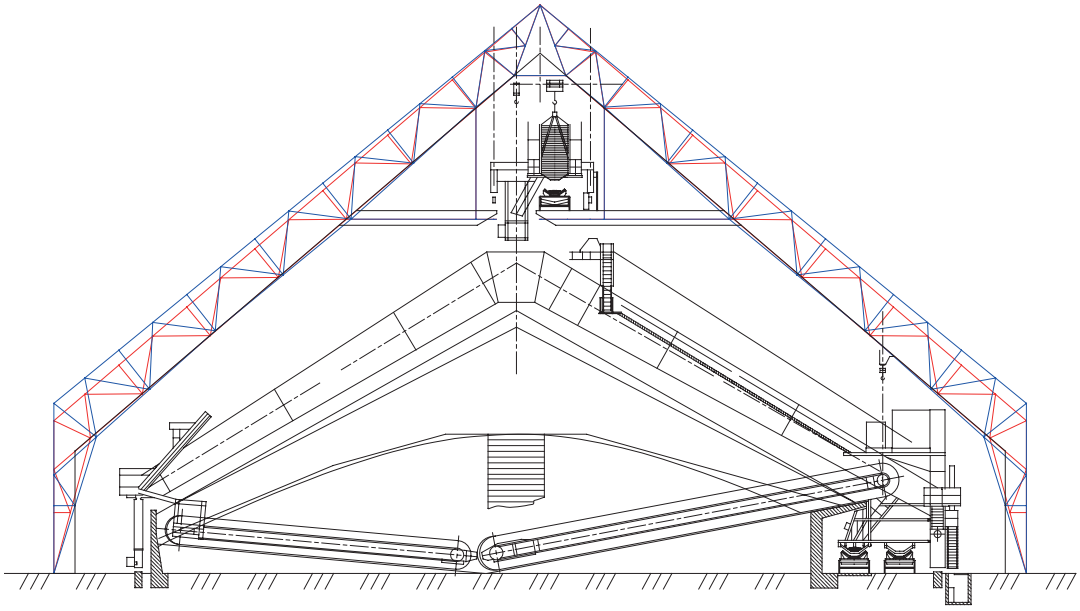

Figure 5.1. The optimum design decision by the criterion of minimum structural weight when lower chord of the lattice rafter is straight-line

Formulated parametric optimization problem for the steel lattice portal frame has been solved using software OptCAD. Task dimensions are: account of design variables is 50, account of problem constraints is 14000.

Optimization results received using software OptCAD are presented by the Tables 5.1 and 5.2. Figure 5.1 show optimal design decision by the criterion of minimum structural weight of the steel lattice portal frame (project with start values of the design variables is indicated by the red color, optimum project is indicated by the blue color).

CONCLUSIONS

The results of the presented study can be formulated as follow:

1. The paper has proposed a mathematical model for parametric optimization problem of the steel lattice portal frame with CHS structural members. The design variable vector includes geometrical parameters of the structure (node coordinates), as well as cross-sectional dimensions of the structural members. The system of constraints covers load-carrying capacities constraints formulated for all design sections of structural members of the steel structure subjected to all ultimate load case combinations. The displacements constraints formulated for the specified nodes of the steel structure subjected to all serviceability load case combinations have been also included into the system of constraints. Additional requirements in the form of constraints on lower and upper values of the design variables, constraints on permissible minimal thicknesses, constraints on permissible maximum diameter-to-thickness ratio for the structural members with circle hollow sections, as well as the conditions for designing gusset-less welded joints between structural members with circle hollow sections have been also considered in the scope of the mathematical model.
2. The method of the objective function gradient projection onto the active constraints surface with simultaneous correction of the constraints violations has been applied to solve the formulated parametric optimization problem.

3. A numerical algorithm for solving the parametric optimization problems of steel lattice portal frames with CHS structural members has been presented in the paper.
4. New optimal layouts of the steel lattice portal frame by the criterion of the minimum weight, as well as minimum costs on manufacturing and erection have been shown.

REFERENCES

1. **Alpatov V.** The task of multi-criteria optimization of metal frame structures // MATEC Web of Conferences. – 2017. – No. 117. – Article 00007. DOI: 10.1051/matecconf/201711700007
2. **Kibkalo A., Lebedeva M., Volkov M.** Methods of parametric optimization of thin-walled structures and parameters which influence on it // MATEC Web of Conferences. – 2016. – No. 53. – Article 01051. DOI: 10.1051/matecconf/20165301051
3. **Alekseytsev A. V.** Evolutionary optimization of steel trusses with the nodal joints of rods // Magazine of Civil Engineering. – 2013. – No. 40(5). – P. 28–37. (rus). DOI: 10.5862/MCE.40.3.
4. **Serpik I. N., Alekseytsev A. V., Balabin P. Yu., Kurchenko N. S.** Flat rod systems: optimization with overall stability control // Magazine of Civil Engineering. – 2017. – No. 76(8). – P. 181–192. DOI: 10.18720/MCE.76.16.
5. **Serpik I. N., Alekseytsev A. V.** Optimization of frame structures with possibility of emergency actions // Magazine of Civil Engineering. – 2013. – No. 44(9). – P. 23–29. (rus). DOI: 10.5862/MCE.44.3.
6. **Sergeyev O. A., Kiselev V. G., Sergeyeva S. A.** Overall instability and optimization of bar structures with random defects in case of constraints on faultless operation probability // Magazine of Civil Engineering. – 2013. – No. 44(9). – P. 30–41. (rus). DOI: 10.5862/MCE.44.4.
7. **Permyakov V. O., Yurchenko V. V., Peleshko I. D.** An optimum structural computer-aided design using hybrid genetic algorithm // Proceeding of the International Conference “Progress in Steel, Composite and Aluminium Structures”. – Taylor & Francis Group. London, 2006. – P. 819–826.
8. **Peleshko I., Yurchenko V.** Parametric optimization of steel structures based on gradient projection method // Strength of Materials and Theory of Structures: Scientific-and-technical collected articles. – Kyiv: KNUBA, 2020. – Issue 105. – P. 192-220. DOI: 10.32347/2410-2547.2020.105.192-220.
9. **Yurchenko V.V., Peleshko I. D.** Searching for optimal pre-stressing of steel bar structures based on sensitivity analysis // Archives of Civil Engineering. 2020. – Vol. 66. – No. 3. – P. 525-540. DOI: 10.24425/ACE.2020.134411
10. **Kuci E., Henrotte F., Duysinx P., Geuzaine C.** Design sensitivity analysis for shape optimization based on the Lie derivative // Computer methods in applied mechanics and engineering. – 2017. – Vol. 317. – P. 702–722. DOI: 10.1016/j.cma.2016.12.036
11. **Sergeyev O. A., Kiselev V. G., Sergeyeva S. A.** Optimal design of 3D frame structures taking into account the stress and multiple natural frequency constraints // Magazine of Civil Engineering. – 2016. – No. 61(1). – P. 74–81. (rus). DOI: 10.5862/MCE.61.7
12. **Huebner K. H., Dewhirst D. L., Smith D. E., Byrom T. G.** The finite element method for engineers. – 4th ed. John Wiley & Sons, 2001. – 744 p.
13. **SP 16.13330.2017.** Steel structures. Moscow: Minstroy, 2017. – 140 p. (rus)
14. **Peleshko I. D., Yurchenko V. V.** Improved gradient projection method for parametric optimization of bar structures // Magazine of Civil Engineering. – 2020. – No. 98(6). – Article No. 9812. DOI: 10.18720/MCE.98.12.

15. **Peleshko I., Yurchenko V.** An improved gradient-based method to solve parametric optimisation problems of the bar structures // Strength of Materials and Theory of Structures: Scientific-and-technical collected articles. – Kyiv: KNUBA, 2020. – Issue 104. – P. 265–288. DOI: 10.32347/2410-2547.2020.104.265-288.
16. **Haug E. J., Arora J. S.** Applied optimal design: mechanical and structural systems. – John Wiley & Sons, 1979. – 520 p.
17. **Reklaitis G. V., Ravindran A., Ragsdell K. M.** Engineering optimization. Methods and applications. – Wiley, 2006. – 688 p.
18. **Wilkinson J. H., Reinsch C.** Handbook for Automatic Computation. Volume II: Linear Algebra. – Heidelberg New York Springer-Verlag Berlin, 1971. – 441 p. DOI: 10.1137/1014116
19. **Peleshko I., Yurchenko V.** An optimum structural computer-aided design using update gradient method // Proceedings of the 8th International Conference "Modern Building Materials, Structures and Techniques", VGTU, 2004. – P. 860–865.

СПИСОК ЛИТЕРАТУРЫ

1. **Alpatov V.** The task of multi-criteria optimization of metal frame structures // MATEC Web of Conferences. – 2017. – No. 117. – Article 00007. DOI: 10.1051/matecconf/201711700007
2. **Kibkalo A., Lebedeva M., Volkov M.** Methods of parametric optimization of thin-walled structures and parameters which influence on it // MATEC Web of Conferences. – 2016. – No. 53. – Article 01051. DOI: 10.1051/matecconf/20165301051
3. **Алексейцев А. В.** Эволюционная оптимизация стальных ферм с учетом узловых соединений стержней // Инженерно-строительный журнал. – 2013. – №. 40(5). – С. 28–37. DOI: 10.5862/MCE.40.3.
4. **Serpik I. N., Alekseytsev A. V., Balabin P. Yu., Kurchenko N. S.** Flat rod systems: optimization with overall stability control // Magazine of Civil Engineering. – 2017. – No. 76(8). – P. 181–192. DOI: 10.18720/MCE.76.16.
5. **Серпик И. Н., Алексейцев А. В.** Оптимизация рамных конструкций с учетом возможности запроектных воздействий // Инженерно-строительный журнал. – 2013. – №. 44(9). – С. 23–29. DOI: 10.5862/MCE.44.3.
6. **Сергеев О. А., Киселев В. Г., Сергеева С. А.** Общая потеря устойчивости и оптимизация стержневых конструкций со случайными несовершенствами при ограничениях на вероятность безотказной работы // Инженерно-строительный журнал. – 2013. – №. 44(9). – С. 30–41. DOI: 10.5862/MCE.44.4.
7. **Permyakov V. O., Yurchenko V. V., Peleshko I. D.** An optimum structural computer-aided design using hybrid genetic algorithm // Proceeding of the International Conference "Progress in Steel, Composite and Aluminium Structures". – Taylor & Francis Group. London, 2006. – P. 819–826.
8. **Peleshko I., Yurchenko V.** Parametric optimization of steel structures based on gradient projection method // Strength of Materials and Theory of Structures: Scientific-and-technical collected articles. – Kyiv: KNUBA, 2020. – Issue 105. – P. 192-220. DOI: 10.32347/2410-2547.2020.105.192-220.
9. **Yurchenko V.V., Peleshko I. D.** Searching for optimal pre-stressing of steel bar structures based on sensitivity analysis // Archives of Civil Engineering. 2020. – Vol. 66. – No. 3. – P. 525-540. DOI: 10.24425/ACE.2020.134411
10. **Kuci E., Henrotte F., Duysinx P., Geuzaine C.** Design sensitivity analysis for shape optimization based on the Lie derivative // Computer methods in applied mechanics and engineering. – 2017. –

Vol. 317. – P. 702–722. DOI: 10.1016/j.cma.2016.12.036
11. **Сергеев О. А., Киселев В. Г., Сергеева С. А.** Оптимальное проектирование рам с учетом ограничений по прочности и кратным частотам собственных колебаний // Инженерно-строительный журнал. – 2016. – №. 61(1). – С. 74–81. DOI: 10.5862/MCE.61.7
12. **Huebner K. H., Dewhirst D. L., Smith D. E., Byrom T. G.** The finite element method for engineers. – 4th ed. John Wiley & Sons, 2001. – 744 p.
13. **СП 16.13330.2017.** Металлические конструкции. Москва: Минстрой, 2017. – 140 с.
14. **Peleshko I. D., Yurchenko V. V.** Improved gradient projection method for parametric optimization of bar structures // Magazine of Civil Engineering. – 2020. – No. 98(6). – Article No. 9812. DOI: 10.18720/MCE.98.12.
15. **Peleshko I., Yurchenko V.** An improved gradient-based method to solve parametric optimisation problems of the bar structures // Strength of Materials and Theory of Structures: Scientific-and-technical collected articles. – Kyiv: KNUBA, 2020. – Issue 104. – P. 265–288. DOI: 10.32347/2410-2547.2020.104.265-288.
16. **Haug E. J., Arora J. S.** Applied optimal design: mechanical and structural systems. – John Wiley & Sons, 1979. – 520 p.
17. **Reklaitis G. V., Ravindran A., Ragsdell K. M.** Engineering optimization. Methods and applications. – Wiley, 2006. – 688 p.
18. **Wilkinson J. H., Reinsch C.** Handbook for Automatic Computation. Volume II: Linear Algebra. – Heidelberg New York Springer-Verlag Berlin, 1971. – 441 p. DOI: 10.1137/1014116
19. **Peleshko I., Yurchenko V.** An optimum structural computer-aided design using update gradient method // Proceedings of the 8th International Conference "Modern Building Materials, Structures and Techniques", VGTU, 2004. – P. 860–865.

Vitalina V. Yurchenko, Doctor of Science, Professor; Kyiv National University of Construction and Architecture; Kyiv 03680, Ukraine, 32 Povitroflotskyj av.; phone: +38 063 89 26 491; e-mail: vitalina@scadsoft.com.

Ivan D. Peleshko, Candidate of Science, Associate Professor; Lviv Polytechnic National University; Lviv, 79013, Ukraine, 6, Karpins'kogo str., ap. 419; phone: +38 098 415 75 17; e-mail: ipeleshko@hotmail.com.

Nikita A. Biliaiev, Master of Science; BM Prefab Engineering; Kyiv 03179, Ukraine, 14a, Nikolya Ushakova str.; phone: +38 093 22 33 768; e-mail: info@prefab.com.ua.

Юрченко Виталина Витальевна, доктор технических наук, профессор; Киевский национальный университет строительства и архитектуры, 03680, Украина, г. Киев, просп. Воздухофлотский, 32; тел. +38 063 89 26 491; E-mail: vitalina@scadsoft.com.

Пелешко Иван Дмитриевич, кандидат технических наук, доцент; Национальный университе «Львовская политехника», 79013, Украина, г. Львов, ул. Карпинського, 6, км. 419; тел. +38 098 415 75 17; E-mail: ipeleshko@hotmail.com.

Биляев Никита Аркадиевич, магистр; BM Prefab Engineering; 03179, Украина, г. Киев, ул. Ушинского, 14а; тел. +38 093 22 33 768; E-mail: info@prefab.com.ua.

International Journal for Computational Civil and Structural Engineering, 17(3) 157–172 (2021)

DOI:10.22337/2587-9618-2021-17-3-157-172

LOCALIZATION OF SOLUTION OF THE PROBLEM FOR POISSON'S EQUATION WITH THE USE OF B-SPLINE DISCRETE-CONTINUAL FINITE ELEMENT METHOD

Marina L. Mozgaleva, Pavel A. Akimov

National Research Moscow State University of Civil Engineering, Moscow, RUSSIA

Abstract: Localization of solution of the problem for Poisson's equation with the use of B-spline discrete-continual finite element method (specific version of wavelet-based discrete-continual finite element method) is under consideration in the distinctive paper. The original operational continual and discrete-continual formulations of the problem are given, some actual aspects of construction of normalized basis functions of a B-spline are considered, the corresponding local constructions for an arbitrary discrete-continual finite element are described, some information about the numerical implementation and an example of analysis are presented.

Keywords: localization, wavelet-based discrete-continual finite element method, B-spline discrete-continual finite element method, discrete-continual finite element method, finite element method, B-spline, numerical solution, Poisson's equation

ЛОКАЛИЗАЦИЯ РЕШЕНИЯ ЗАДАЧИ ДЛЯ УРАВНЕНИЯ ПУАССОНА НА ОСНОВЕ ВЕЙВЛЕТ-РЕАЛИЗАЦИИ ДИСКРЕТНО-КОНТИНУАЛЬНОГО МЕТОДА КОНЕЧНЫХ ЭЛЕМЕНТОВ С ИСПОЛЬЗОВАНИЕМ B-СПЛАЙНОВ

М.Л. Мозгалева, П.А. Акимов

Национальный исследовательский Московский государственный строительный университет, г. Москва, РОССИЯ

Аннотация: В настоящей статье рассматривается локализация решения задачи для уравнения Пуассона на основе вейвлет-реализации дискретно-континуального метода конечных элементов с использованием B-сплайнов. Приведены исходные операторные континуальная и дискретно-континуальная постановки задачи, рассмотрены некоторые актуальные вопросы построения нормализованных базисных функций B-сплайна, описаны соответствующие локальные построения для произвольного дискретно-континуального конечного элемента, представлены некоторые сведения о численной реализации и пример расчета.

Ключевые слова: локализация, вейвлет-реализация метода конечных элементов, дискретно-континуальный метод конечных элементов, метод конечных элементов, B-сплайны, численное решение, уравнение Пуассона

INTRODUCTION

Various problems of continuum mechanics are reduced to the Poisson equation and other similar equations of elliptic type [1-6]. As is known, boundary value problems with the Poisson equation describe, in particular, a stationary temperature field, a stress state during torsion of a rod, membrane deflection, etc. In addition, the operator of the corresponding problem (the Laplace operator) is part of other problems that determine the state of structures under stationary and non-stationary actions. From a mathematical point of view, it is the simplest qualita-

tive analogue of other problems and an equivalent operator in iterative processes [7]. In many numerical models, at different time steps, it becomes necessary to solve (numerically) one or several boundary value problems for the Poisson equation, and in some applications the number of time steps during one analysis of the model can be of the order of thousands to millions or more [8]. In this regard, the objective of the distinctive paper is devoted to the semi-analytical method of analysis of corresponding structures with constant physical and geometric parameters in one of the directions (the so-called "basic direction") [7, 9, 10]. This objective seems to be very relevant. The considering method is semi-analytical in the sense that along the basic direction of the structure the problem remains continual and its exact analytical solution is constructed, while in another, non-basic direction, a numerical approximation is performed. In general, this paper continues a series of papers devoted to the research and development of various wavelet-based versions of the discrete-continuous finite element method.

In the theory of boundary value problems for the Poisson and Laplace equations, several classical well-tested solution methods are normally used [1, 11-13], which, in particular, include method of separation of variables or Fourier method, Green's function method and a method of reducing boundary value problems for the Laplace equation to integral equations using potential theory.

Besides, numerical methods (finite element method, boundary element method, finite difference method, variational-difference method, finite volume method, method of point field sources, fast Fourier transform method using parallel computations (with the implementation on the cores of the central processor and on graphic processors (GPU), etc.) for solving the Poisson equation are normally used [8, 14, 15].

1. FORMULATIONS OF THE PROBLEM

Formulation of the problem has the form:

$$L\,u = F\,, \quad 0 \le x_1 \le \ell_1\,, \quad 0 \le x_2 \le \ell_2\,; \quad (1.1)$$

$$\ell u\big|_{\Gamma} = g\,, \quad (1.2)$$

where L is the operator of the problem within the initial domain;

$$L = -\partial_1^2 - \partial_2^2; \quad \partial_1 = \partial / \partial x_1; \quad \partial_2 = \partial / \partial x_2\,; \quad (1.3)$$

ℓ is the operator of boundary conditions.

Let x_2 be direction along which parameters of the problem are constant (so-called "main direction"). Let us introduce the following notations

$$\bar{v} = \partial_2 \bar{u} = \bar{u}'; \quad \bar{v}' = \partial_2 \bar{v}\,. \quad (1.4)$$

Then we can rewrite (1.1) in the following form:

$$L_{uu}u - L_{vv}v' = F \;\text{ or }\; L_{vv}v' = L_{uu}u - F\,, \quad (1.5)$$

where we have

$$L_{uu} = -\partial_1^2 = \partial_1^* \partial_1; \quad L_{vv} = 1\,. \quad (1.6)$$

Finally we obtain system of differential equations with operational coefficients:

$$\bar{U}' = A\bar{U} + \bar{F}\,, \quad (1.7)$$

where

$$A = \begin{bmatrix} 0 & 1 \\ L_{vv}^{-1}L_{uu} & 0 \end{bmatrix}; \quad \bar{F} = \begin{bmatrix} 0 \\ -L_{vv}^{-1}F \end{bmatrix}; \quad \bar{U} = \begin{bmatrix} u \\ v \end{bmatrix}. \quad (1.8)$$

The system of equations (1.7) is supplemented by boundary conditions, which are set in sections with coordinates $x_2^1 = 0$ and $x_2^2 = \ell_2$.

2. SOME ASPECTS OF THE CONSTRUCTION OF NORMALIZED BASIS FUNCTIONS OF THE B-SPLINE

The construction of B-spline basic functions is determined by the recursive Cox-de Boer formulas [16-21]:

$$k=1: \quad \varphi_{i,1}(t)=\begin{cases}1, & x_i \le t < x_{i+1}\\ 0, & t < x_i \vee t \ge x_{i+1}\end{cases}, \tag{2.1}$$

$$k \ge 2: \quad \varphi_{i,k}(t)=\frac{(t-x_i)\varphi_{i,k-1}(t)}{x_{i+k-1}-x_i}+\frac{(x_{i+k}-t)\varphi_{i+1,k-1}(t)}{x_{i+k}-x_{i+1}}. \tag{2.2}$$

We will consider such a construction for the case $x_i = i$ are integers. Let us note that,

$$\varphi_{i,k}(t)=\varphi_{0,k}(t-i)$$

and therefore, recursive formulas (2.1)-(2.2) can be represented in the form

$$k=1: \quad \varphi_{0,1}(t)=\begin{cases}1, & 0 \le t < 1\\ 0, & t < 0 \vee t \ge 1;\end{cases} \tag{2.3}$$

$$k \ge 2: \quad \varphi_{0,k}(t)=\frac{1}{k-1}[t\cdot\varphi_{0,k-1}(t)+(k-t)\varphi_{0,k-1}(t-1)]. \tag{2.4}$$

The function $\varphi_{0,1}(t)$ can be represented by formula

$$\varphi_{0,1}(t)=\frac{1}{2}[\mathrm{sign}(t)-\mathrm{sign}(t-1)]. \tag{2.5}$$

Let us denote by Δ_1 the operator of the first difference. Then we have

$$\varphi_{0,1}(t)=-\frac{1}{2}\Delta_1\,\mathrm{sign}(t). \tag{2.6}$$

We can substitute formula (2.5) into (2.4) in order to determine $\varphi_{0,2}(t)$:

$$\begin{aligned}\varphi_{0,2}(t)&=1\cdot[t\cdot\varphi_{0,1}(t)+(2-t)\varphi_{0,1}(t-1)]=\\&=\frac{1}{2}\{t\cdot[\mathrm{sign}(t)-\mathrm{sign}(t-1)]+\\&(2-t)[\mathrm{sign}(t-1)-\mathrm{sign}(t-2)]\}=\\&=\frac{1}{2}[t\,\mathrm{sign}(t)-2(t-1)\mathrm{sign}(t-1)+\\&(t-2)\,\mathrm{sign}(t-2)]=\frac{1}{2}[|t|-2|t-1|+|t-2|.\end{aligned}$$

Let us denote by Δ_2 the operator of the second difference. Then we have

$$\varphi_{0,2}(t)=\frac{1}{2}[|t|-2|t-1|+|t-2|=\frac{1}{2}\Delta_2\,|t-1|. \tag{2.7}$$

We can define function $\varphi_{0,3}(t)$:

$$\varphi_{0,3}(t)=\frac{1}{2}[t\cdot\varphi_{0,2}(t)+(3-t)\varphi_{0,2}(t-1)].$$

Omitting intermediate calculations, we get

$$\begin{aligned}\varphi_{0,3}(t)&=\frac{1}{4}[t\cdot|t|-3(t-1)|t-1|+\\&+3(t-2)|t-2|-(t-3)|t-3|]=\\&=-\frac{1}{2!}\frac{1}{2}\Delta_1\Delta_2((t-1)|t-1|).\end{aligned} \tag{2.8}$$

Based on formulas (2.8) and (2.4), we can define the function

$$\varphi_{0,4}(t)=\frac{1}{3}[t\cdot\varphi_{0,3}(t)+(4-t)\varphi_{0,3}(t-1)].$$

Omitting intermediate calculations, as a result we get

$$\begin{aligned}\varphi_{0,4}(t)&=\\&=\frac{1}{2\cdot 3}\cdot\frac{1}{2}[t^2\cdot|t|-4(t-1)^2|t-1|+\\&+6(t-2)^2|t-2|-4(t-3)^2|t-3|+\\&+(t-4)^2|t-4|]=\\&=\frac{1}{3!}\frac{1}{2}(\Delta_2)^2((t-2)^2|t-2|).\end{aligned} \tag{2.9}$$

It can be proved that for even $k=2m$ we have

$$\varphi_{0,k}(t)=\frac{1}{(2m-1)!}\frac{1}{2}(\Delta_2)^m((t-m)^{2m-2}|t-m|) \tag{2.10}$$

and for odd (uneven) $k=2m+1$ we have

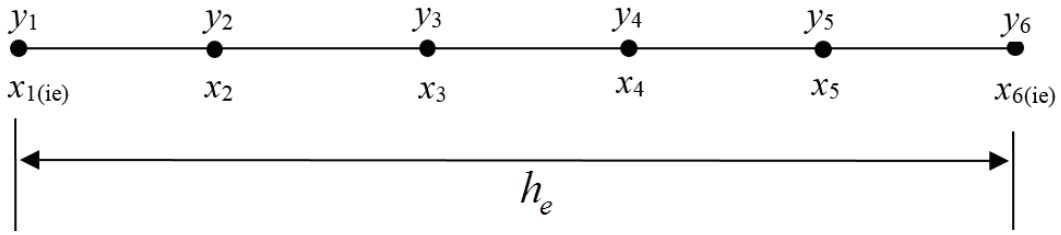

Figure 3.1. Finite element discretication for $N_k = 5$ *(sample).*

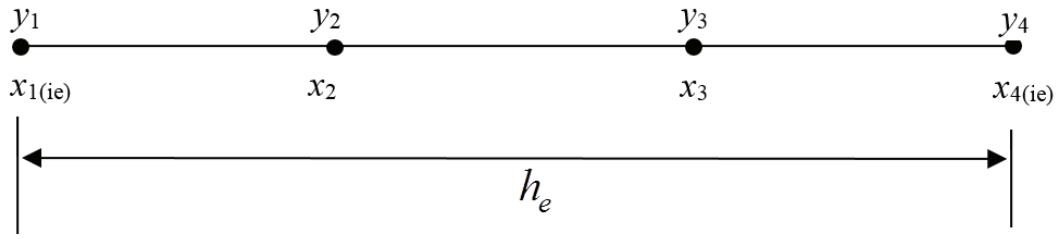

Figure 3.2. Finite element discretication for $N_k = 3$ *(sample).*

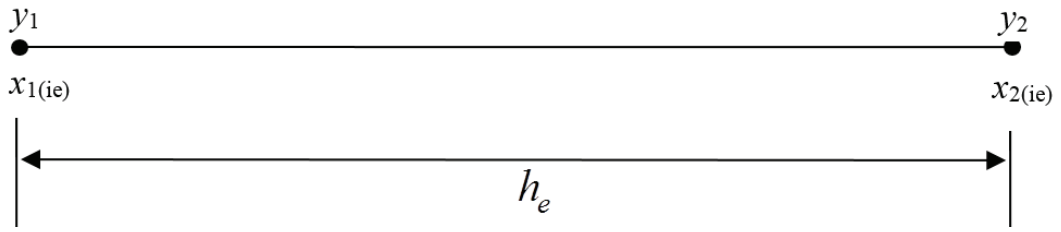

Figure 3.3. Finite element discretication for $N_k = 1$ *(sample).*

$$\varphi_{0,k}(t) = -\frac{1}{(2m)!}\frac{1}{2}\Delta_1(\Delta_2)^m((t-m)^{2m-1}\,|\,t-1|)\,. \tag{2.11}$$

Note that $\varphi_{0,k}(t)$ is a polynomial of degree $k-1$ with bounded support and, as follows from the difference operator, this support is equal to the interval $[0,\ k]$.

In addition, we should note the following property of B-spline basis functions:

$$\sum_i \varphi_{0,k}(t-i) \equiv 1 \text{ for arbitrary } t\,. \tag{2.12}$$

3. SOME GENERAL ASPECTS OF FINITE ELEMENT APPROXIMATION

The discrete component of the numerical solution is represented by the direction along the axis corresponding to x_1. The fulfillment within an element (interval) for all components of a vector functions $\bar{u}$ and $\bar{v}$ (see (1.8)) is the same. Therefore, let us use the following notation for simplicity:

$$x = x_1,\ \ell = \ell_1,\ y = y(x)\,, \tag{3.1}$$

where $y = y(x)$ is unknown function (component of vector function).

Let us divide the interval $(0, \ell)$ segment into N_e parts (elements). Therefore $h_e = \ell / N_e$ is the length of the element. Besides, let us also divide each element into N_k parts. It should be noted that on the elements of the localization of the solution, parameter N_k is of greater importance than on the other elements. For example, on localization elements, we can set $N_k = 5$, i.e. unknown functions will be represented by polynomials (B-splines) of the 5th degree (Figure 3.1).

Let us use the following notation system: i_e is the element number; $N_p = N_k + 1 = 6$ is the number of nodes within the element; $x_1(i_e)$ is the coordinate of the starting point of the i_e-th element; $x_6(i_e)$ is the coordinate of the end point of the i_e-th element. Thus, the number of unknowns per element with such approximation is equal to

$$N_{ie} = N_p = 6.$$

For the elements of localization we can take reduced number of N_k. For instance, if we take $N_k = 3$ (Figure 3.2) we get $N_p = N_k + 1 = 4$ and the number of unknowns per element with such approximation is equal to

$$N_{ie} = N_p = 4;$$

$x_1(i_e)$ is the coordinate of the starting point of the i_e-th element; $x_4(i_e)$ is the coordinate of the end point of the i_e-th element.

Besides, let us consider the case with $N_k = 1$ (Figure 3.3). Therefor we have $N_p = N_k + 1 = 2$ and the number of unknowns per element with such approximation is equal to

$$N_{ie} = N_p = 2,$$

where $x_1(i_e)$ is the coordinate of the starting point of the i_e-th element; $x_2(i_e)$ is the coordinate of the end point of the i_e-th element.

4. LOCAL CONSTRUCTIONS FOR ARBITRARY FINITE ELEMENT

Let us introduce local coordinates:

$$t = (x - x_{1(ie)})/h_e, \quad x_{1(ie)} \le x \le x_{N_p(ie)}, \ 0 \le t \le 1. \tag{4.1}$$

In this case, we have the following relations:

$$x = x_i \Rightarrow t_i = (x_i - x_{1(ie)})/h_e, \quad i = 1,..., N_p; \tag{4.2}$$

$$\frac{d^p}{dx^p} = \frac{1}{h_e^p}\frac{d^p}{dt^p}; \quad dx = h_e \cdot dt. \tag{4.3}$$

Since the number of unknowns on the element is equal to $N_{ie} = 6$, we use a B-spline of the fifth degree in order to represent the unknown deflection function.

Let us use the following notation:

$$\varphi(t) = \varphi_{0,6}(t+3);$$

$$\varphi(t) = \frac{1}{5!}\frac{1}{2}(\Delta_2)^3(t^4 \mid t \mid) =$$
$$= \frac{1}{5!\cdot 2}[(t+3)^4 \mid t+3 \mid -6(t+2)^4 \mid t+2 \mid +$$
$$+15(t+1)^4 \mid t+1 \mid -20t^4 \mid t \mid +$$
$$+15(t-1)^4 \mid t-1 \mid -6(t-2)^4 \mid t-2 \mid +$$
$$+(t-3)^4 \mid t-3 \mid]. \tag{4.4}$$

This function is a B-spline, symmetric with respect to $t = 0$ and its support is defined by an interval $[-3,3]$ (Figure 4.1).

We take the following six functions as basis functions on the unit interval (Figures 4.2, 4.3):

$$\varphi_1(t) = \varphi(t+2), \quad \varphi_2(t) = \varphi(t+1),$$
$$\varphi_3(t) = \varphi(t), \quad \varphi_4(t) = \varphi(t-1),$$
$$\varphi_5(t) = \varphi(t-2), \quad \varphi_6(t) = \varphi(t-3),$$
$$0 \le t \le 1. \tag{4.5}$$

Since the number of unknowns on the element is equal to $N_{ie} = 4$, we use a B-spline of the third degree in order to represent the unknown deflection function.

Let us use the following notation:

$$\varphi(t) = \varphi_{0,4}(t+4);$$

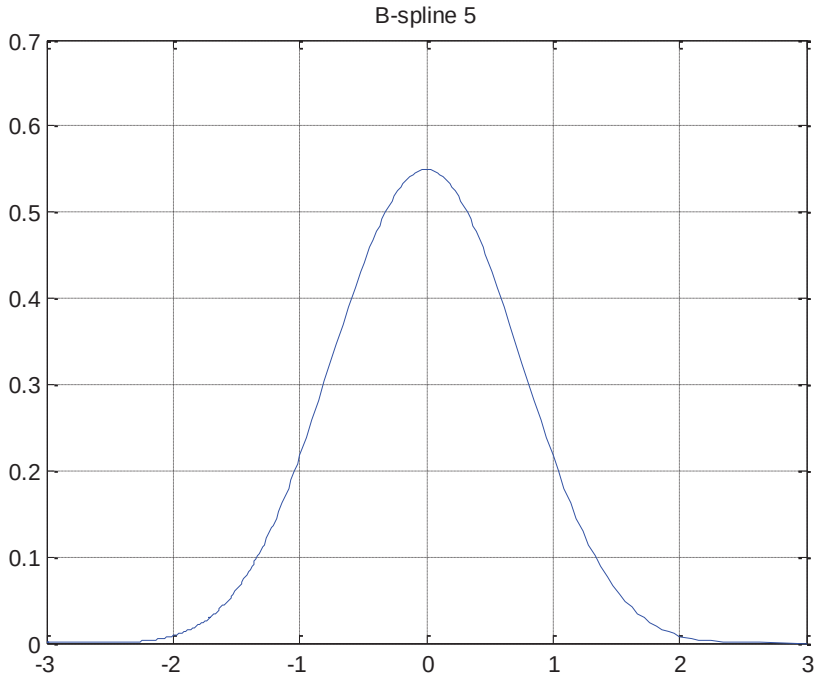

Figure 4.1. *B-spline of the fifth order* $\varphi(t) = \varphi_{0,6}(t+3)$.

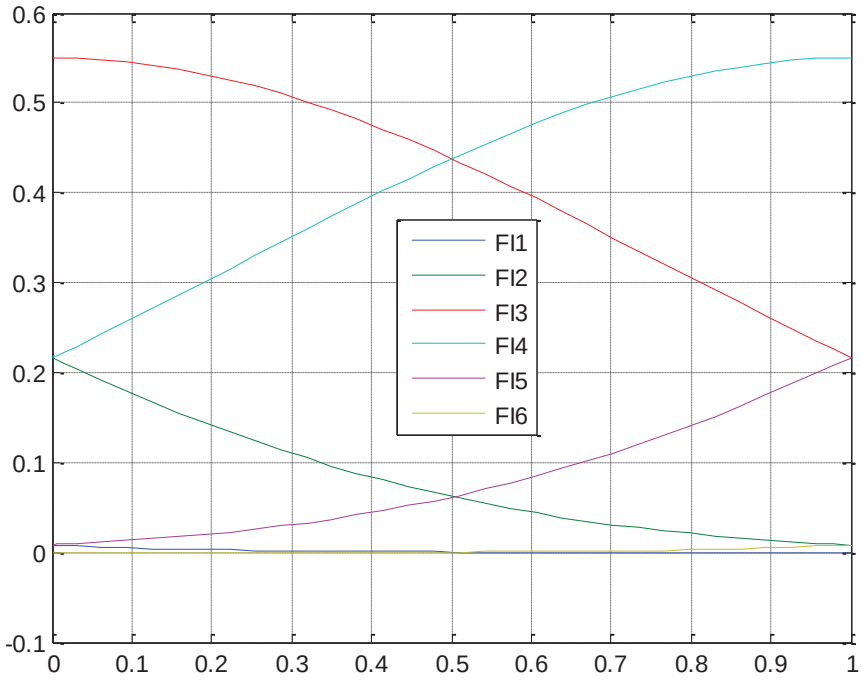

Figure 4.2. *Basis functions* $\varphi_k(t)$, $k = 1,2,...,6$.

$$\varphi(t) = \frac{1}{3!}\frac{1}{2}(\Delta_2)^2(t^2\,|\,t\,|) =$$
$$= \frac{1}{3!\cdot 2}[(t+2)^2\,|\,t+2\,| - 4(t+1)^2\,|\,t+1\,| +$$
$$+ 6t^2\,|\,t\,| - 4(t-1)^2\,|\,t-1\,| +$$
$$+ (t-2)^2\,|\,t-2\,|]. \qquad (4.6)$$

This function is a B-spline, symmetric with respect to $t = 0$ and its support is defined by an interval $[-2,2]$ (Figure 4.4).

We take the following four functions as basis functions on the unit interval (Figures 4.5):

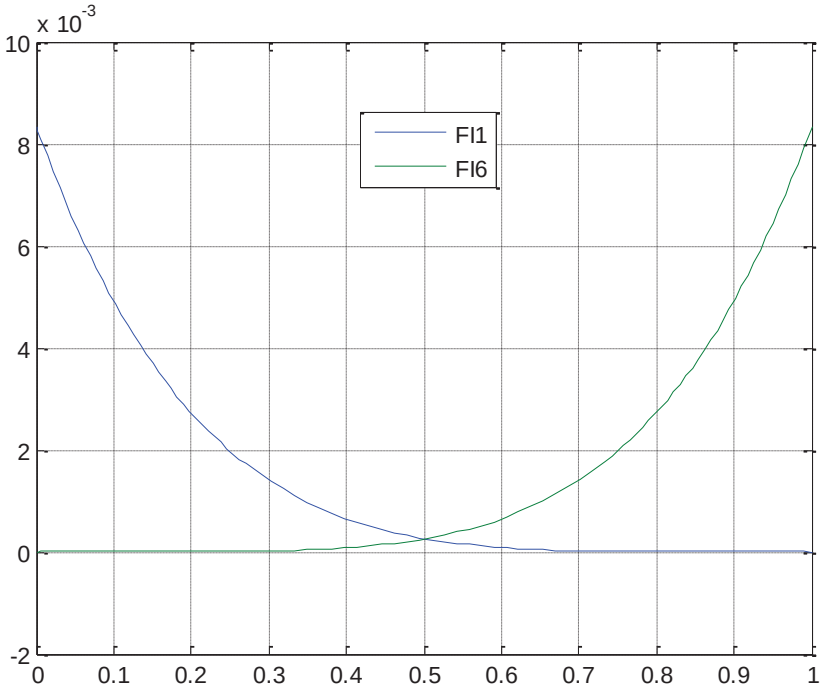

Figure 4.3. Basis functions $\varphi_1(t)$ *and* $\varphi_6(t)$.

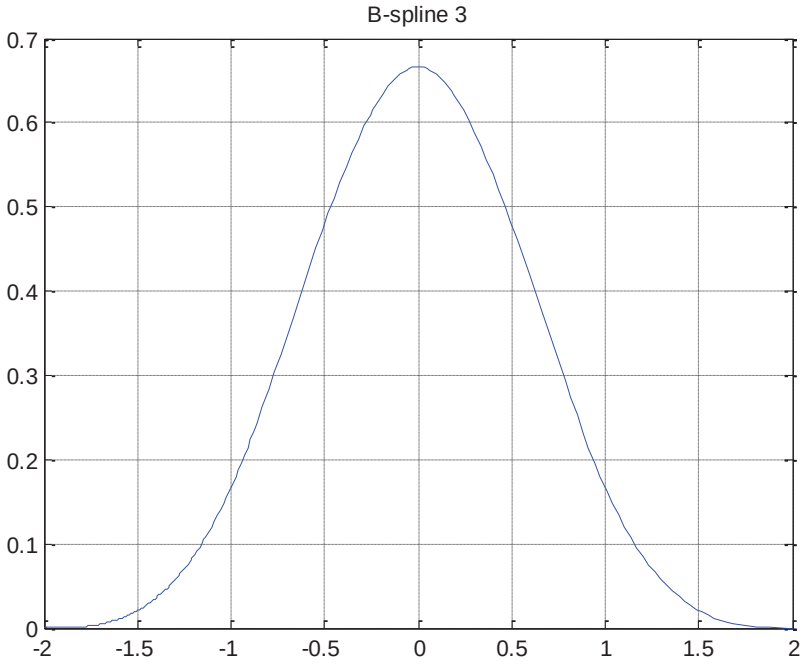

Figure 4.4. B-spline of the third order $\varphi(t) = \varphi_{0,4}(t+2)$.

$$\varphi_1(t) = \varphi(t+1), \quad \varphi_2(t) = \varphi(t),$$
$$\varphi_3(t) = \varphi(t-1), \quad \varphi_4(t) = \varphi(t-2),$$
$$0 \le t \le 1. \quad (4.7)$$

Since the number of unknowns on the element is equal to $N_{ie} = 2$, we use a B-spline of the first degree in order to represent the unknown deflection function.

Let us use the following notation:

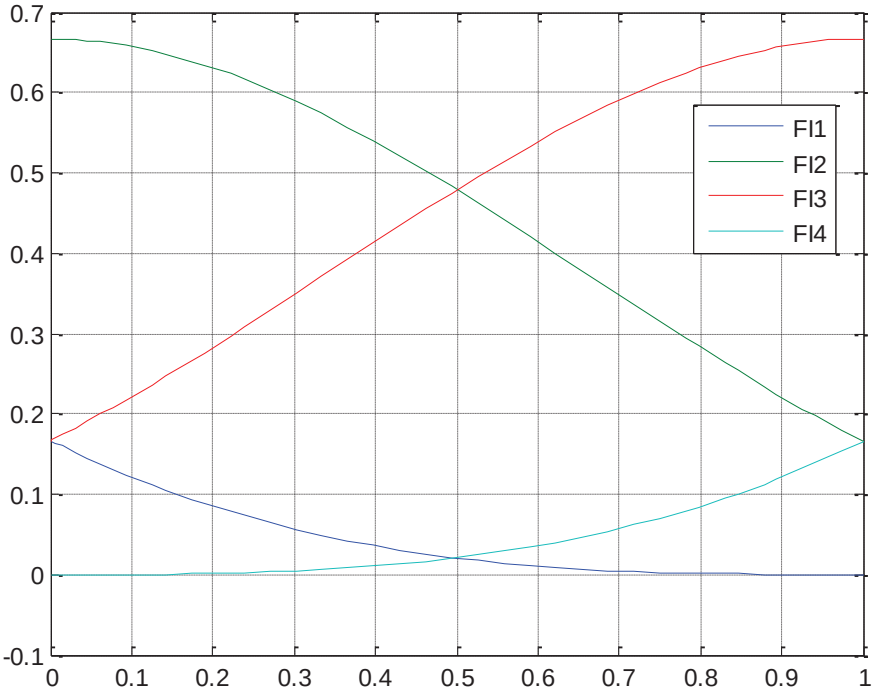

Figure 4.5. Basis functions $\varphi_k(t)$, $k = 1,2,3,4$.

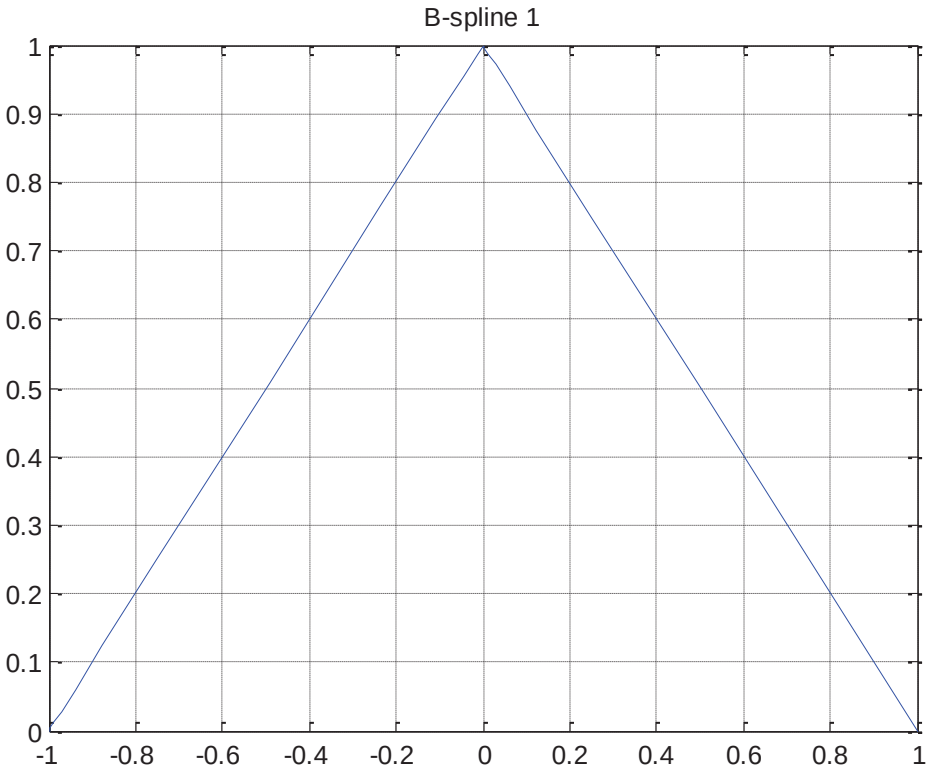

Figure 4.6. B-spline of the first order $\varphi(t) = \varphi_{0,2}(t+1)$.

$$\varphi(t) = \varphi_{0,2}(t+1);$$

$$\varphi(t) = \frac{1}{2}\Delta_2 \mid t \mid = \frac{1}{2}[\mid t+1 \mid -2 \mid t \mid + \mid t-1 \mid]. \quad (4.8)$$

This function is a B-spline, symmetric with respect to $t = 0$ and its support is defined by an interval $[-1,1]$ (Figure 4.6).

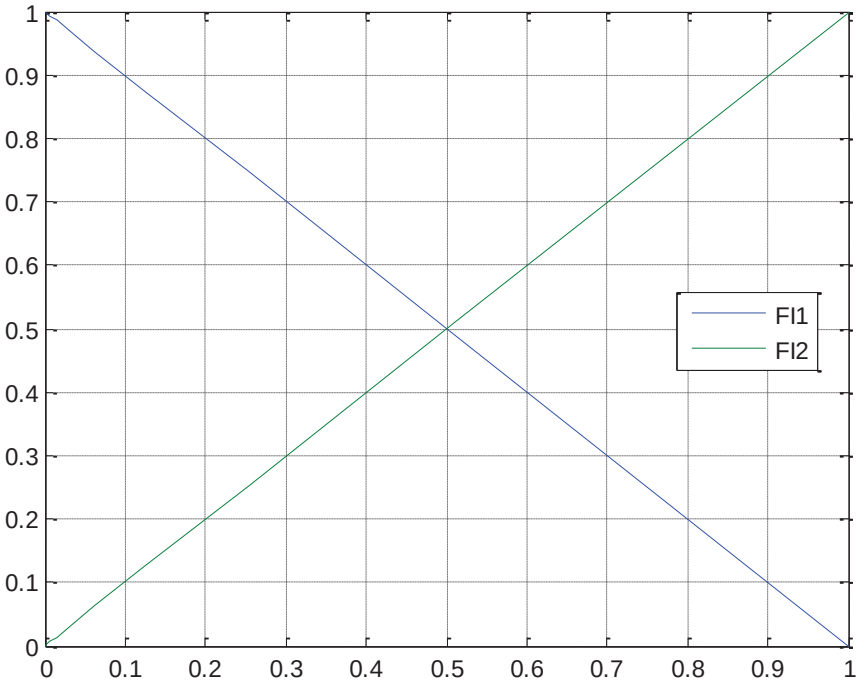

Figure 4.7. Basis functions $\varphi_k(t)$, $k=1,2$.

We take the following two functions as basis functions on the unit interval (Figures 4.7):

$$\varphi_1(t)=\varphi(t), \quad \varphi_2(t)=\varphi(t-1), \quad 0\le t\le 1. \quad (4.9)$$

We represent the unknown function $y(x)$ within the element number i_e in the form

$$y(x)=w(t)=\sum_{k=1}^{N_p}\alpha_k\varphi_k(t), \quad x_{1(i_e)}\le x\le x_{N_p(i_e)}, \quad 0\le t\le 1. \quad (4.10)$$

We have to consider bilinear forms with allowance for relations (4.2)-(4.3) in order to construct local stiffness matrices corresponding to the operators L_{uu}, L_{vv} (see (1.6)):

$$B_{uu}(y,z)=<L_{uu}y,z>=-\int_{x_{1(ie)}}^{x_{N_p(ie)}}\frac{d^2y}{dx^2}\cdot z\,dx=$$
$$=\int_{x_{1(ie)}}^{x_{N_p(ie)}}\frac{dy}{dx}\cdot\frac{dz}{dx}dx=\frac{1}{h_e}\int_0^1\frac{dw}{dt}\cdot\frac{dq}{dt}dt=B_{vv}(w,q); \quad (4.10)$$

$$B_{vv}(y,z)=<L_{vv}y,z>=\int_{x_{1(ie)}}^{x_{N_p(ie)}}y\cdot z\,dx=$$
$$=h_e\int_0^1 w\cdot q\,dt=B_{vv}(w,q). \quad (4.11)$$

for the following type of functions

$$y(x)=w(t)=\sum_{k=1}^{N_{ie}}\alpha_k\varphi_k(t),$$
$$z(x)=q(t)=\sum_{k=1}^{N_{ie}}\beta_k\varphi_k(t), \quad (4.12)$$

where we have $x_{1(ie)}\le x\le x_{N_p(ie)}$, $0\le t\le 1$.
Let us substitute (4.12) into (4.9)-(4.10):

$$B_{uu}(w,q)=\frac{1}{h_e}\int_0^1\frac{dw}{dt}\cdot\frac{dq}{dt}dt=$$
$$=\frac{1}{h_e}\sum_{i=1}^{N_{ie}}\sum_{j=1}^{N_{ie}}\alpha_i\beta_j\int_0^1\varphi_i'(t)\varphi_j'(t)\,dt=\frac{1}{h_e}(K_{\alpha\beta}^{uu}\overline{\alpha},\overline{\beta}), \quad (4.16)$$

where

where

$$K^{uu}_{\alpha\beta}(i,j)=\int_0^1 \varphi_i'(t)\varphi_j'(t)\,dt;\quad \varphi'=\frac{d\varphi}{dt};\quad (4.17)$$

$$B_{vv}(w,q)=h_e\int_0^1 w\cdot q\,dt=$$

$$=h_e\sum_{i=1}^{N_{ie}}\sum_{j=1}^{N_{ie}}\alpha_i\beta_j\int_0^1\varphi_i(t)\varphi_j(t)\,dt=h_e(K^{vv}_{\alpha\beta}\overline{\alpha},\overline{\beta}),\quad (4.18)$$

where

$$K^{vv}_{\alpha\beta}(i,j)=\int_0^1\varphi_i(t)\varphi_j(t)\,dt;\quad (4.19)$$

Let us define the parameters α_k and β_k through the nodal unknowns on the element:

$$y_i=w(t_i)=\sum_{k=1}^{N_{ie}}\alpha_k\varphi_k(t_i),$$

$$t_i=(x_i-x_{1(ie)})/h_e,\quad i=1,...,\ N_p.\quad (4.20)$$

For the case $N_{ie}=6$ we have

$$\overline{y}^{ie}=T_6\overline{\alpha},\quad (4.21)$$

where

$$\overline{y}^{i_e}=[y_1\ \ y_2\ \ y_3\ \ y_4\ \ y_5\ \ y_6]^T;\quad (4.22)$$

$$\overline{\alpha}=[\alpha_1\ \ \alpha_2\ \ \alpha_3\ \ \alpha_4\ \ \alpha_5\ \ \alpha_6]^T.\quad (4.23)$$

$$T_6=\begin{bmatrix}\varphi_1(0) & \varphi_2(0) & \varphi_3(0) & \varphi_4(0) & \varphi_5(0) & \varphi_6(0)\\ \varphi_1(0.2) & \varphi_2(0.2) & \varphi_3(0.2) & \varphi_4(0.2) & \varphi_5(0.2) & \varphi_6(0.2)\\ \varphi_1(0.4) & \varphi_2(0.4) & \varphi_3(0.4) & \varphi_4(0.4) & \varphi_5(0.4) & \varphi_6(0.4)\\ \varphi_1(0.6) & \varphi_2(0.6) & \varphi_3(0.6) & \varphi_4(0.6) & \varphi_5(0.6) & \varphi_6(0.6)\\ \varphi_1(0.8) & \varphi_2(0.8) & \varphi_3(0.8) & \varphi_4(0.8) & \varphi_5(0.8) & \varphi_6(0.8)\\ \varphi_1(1) & \varphi_2(1) & \varphi_3(1) & \varphi_4(1) & \varphi_5(1) & \varphi_6(1)\end{bmatrix},\quad (4.24)$$

For the case $N_{ie}=4$ we have

$$\overline{y}^{ie}=T_4\overline{\alpha},\quad (4.25)$$

$$\overline{y}^{i_e}=[y_1\ \ y_2\ \ y_3\ \ y_4]^T;\quad (4.26)$$

$$\overline{\alpha}=[\alpha_1\ \ \alpha_2\ \ \alpha_3\ \ \alpha_4]^T;\quad (4.27)$$

where

$$T_4=\begin{bmatrix}\varphi_1(0) & \varphi_2(0) & \varphi_3(0) & \varphi_4(0)\\ \varphi_1(1/3) & \varphi_2(1/3) & \varphi_3(1/3) & \varphi_4(1/3)\\ \varphi_1(2/3) & \varphi_2(2/3) & \varphi_3(2/3) & \varphi_4(2/3)\\ \varphi_1(1) & \varphi_2(1) & \varphi_3(1) & \varphi_4(1)\end{bmatrix};\quad (4.28)$$

For the case $N_{ie}=2$ we have

$$\overline{y}^{ie}=T_2\overline{\alpha},\quad (4.29)$$

where

$$\overline{y}^{i_e}=[y_1\ \ y_2]^T;\quad (4.30)$$

$$\overline{\alpha}=[\alpha_1\ \ \alpha_2]^T;\quad (4.31)$$

$$T_2=\begin{bmatrix}\varphi_1(0) & \varphi_2(0)\\ \varphi_1(1) & \varphi_2(1)\end{bmatrix}.\quad (4.32)$$

Similarly, we get

$$\overline{z}^{ie}=T_{N_{ie}}\overline{\beta}\quad (4.33)$$

for $N_{ie}=6$, $N_{ie}=4$, $N_{ie}=2$.

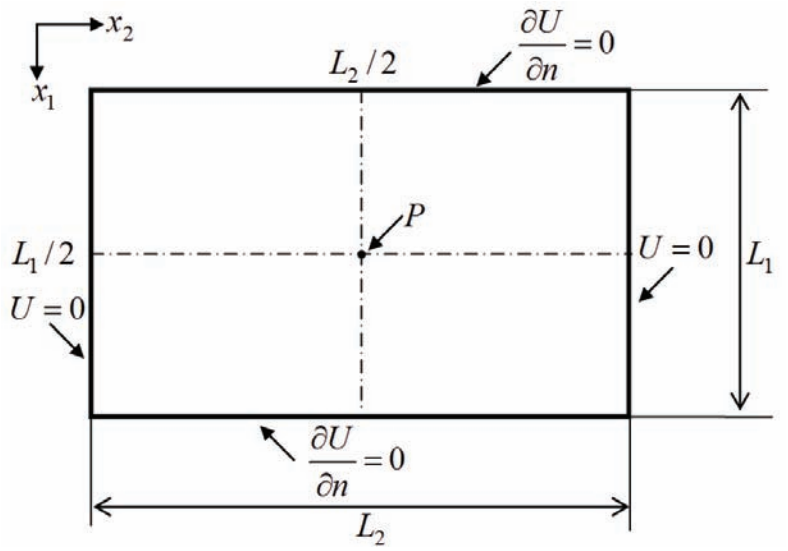

Figure 5.1. Example of analysis.

From (4.21)-(4.33) it follows

$$\overline{\alpha} = T_{N_p}^{-1}\overline{y}^{i_e}; \quad \overline{\beta} = T_{N_p}^{-1}\overline{z}^{ie}, \qquad (4.34)$$

where

$$T_{N_p} = \{T_{ij}\}_{i,j=1,..,N_p}, \quad T_{ij} = \varphi_j(t_i). \qquad (4.35)$$

Generally we have the following chain of equalities

$$(K_{\alpha\beta}\overline{\alpha},\overline{\beta}) = (K_{\alpha\beta}T_{N_p}^{-1}\overline{y}^{ie}, T_{N_p}^{-1}\overline{z}^{ie}) = \\ = ((T_{N_p}^{-1})^{\mathrm{T}} K_{\alpha\beta}T_{N_p}^{-1}\overline{y}^{ie}, \overline{z}^{ie}). \qquad (4.36)$$

Therefore, substituting (4.34) sequentially in (4.16), (4.18), we obtain local stiffness matrices K_{uu}^{ie} and K_{vv}^{ie}, corresponding to the operators L_{uu} and L_{vv}.

5. EXAMPLE OF ANALYSIS

5.1. Formulation of the problem.

Let us consider the problem shown at Figure 5.1.
Let us consider the following geometric parameters: $L_1 = 1.2$, $L_2 = 2.0$ is the thickness.
Let external load parameter be equal to $P = 100$.

5.2. Structural analysis with allowance for localization.

Let the number of elements be equal to $N_e = 4$.
Then we have the following element length:

$$h_e = \ell_1 / N_e = 1.2/4 = 0.3.$$

Let's define localization in the load area.
For the first element and for the fourth element we have $N_k = 1$ and third-order spline; distance between the coordinates of the nodes of the first element and the sixth element is equal to

$$h_1 = h_4 = 0.3/1 = 0.3.$$

For the second element and for the third element we have $N_k = 3$ and fifth-order spline; distance between the coordinates of the nodes of the second element and the third element is equal to

$$h_2 = h_3 = 0.3/5 = 0.06.$$

The total number of nodes for all elements is equal to

$$N_x = 2\cdot 1 + 2\cdot 5 + 1 = 13.$$

The total number of nodal unknowns is equal to

$$N_U = 2N_x = 2 \cdot 13 = 26.$$

5.3. Structural analysis without localization.
In this case, we will consider only the standard linear fulfilment. In this case, the length of the element is taken equal to the minimum distance between the nodes, i.e. $h_e = 0.06$. Then the number of elements is equal to

$$N_e = 1.2 / 0.06 = 20$$

and the total number of nodes is equal to $N_x = 21$. In this case the total number of nodal unknowns is equal to

$$N_U = 2N_x = 2 \cdot 21 = 42.$$

Graphical comparison of corresponding results of analysis is presented at Figures 5.2-5.4 (`U26(loc)` are nodal values computed with allowance for localization; `U2(lin)` are nodal values computed without localization).
As researcher can see, the results obtained are almost completely identical. Besides, the use of localization based on application of B-splines of various degrees leads to a significant decrease in the number of unknowns.

REFERENCES

1. **Tihonov A.N., Samarskij A.A.** Uravnenija matematicheskoj fiziki [Equations of mathematical physics]. Moscow, Nauka, 2004, 798 pages (in Russian).
2. **Ivlev D.D.** Mehanika plasticheskih sred. Tom 1. Teorija ideal'noj plastichnosti. [Mechanics of plastic media. Volume 1. The theory of ideal plasticity]. Moscow, Fizmatlit, 2001, 445 pages (in Russian).
3. **Ivlev D.D.** Mehanika plasticheskih sred. Tom 2. Obshhie voprosy. Zhestkoplasticheskoe i uprugoplasticheskoe sostojanie tel. Uprochnenie. Deformacionnye teorii. Slozhnye sredy. [Mechanics of plastic media. Volume 2. General problems. Rigid-plastic and elasto-plastic state of bodies. Strengthening. Deformation theories. Complex environments]. Moscow, Fizmatlit, 2002, 448 pages (in Russian).
4. **Ivlev D.D., Ershov L.V.** Metod vozmushhenij v teorii uprugoplasticheskogo tela [Perturbation method in the theory of an elastoplastic body]. Moscow, Nauka, 1978, 208 pages (in Russian).
5. **Lur'e A.I.** Teorija uprugosti [Theory of Elasticity]. Moscow, Nauka, 1970, 939 pages (in Russian).
6. **Aleksandrov V.M.** Zadachi mehaniki sploshnyh sred so smeshannymi granichnymi uslovijami [Problems of Continuum Mechanics with Mixed Boundary Conditions]. Moscow, Nauka, 1986, 329 pages (in Russian).
7. **Zolotov A.B., Akimov P.A., Mozgaleva M.L.** Mnogourovnevye diskretnye i diskretno-kontinual'nye realizacii variacionno-raznostnogo metoda [Multilevel discrete and discrete-continuous realizations of the variational-difference method]. Moscow, ASV, 2013, 416 pages (in Russian).
8. **Mingalev O.V., Mel'nik M.N.** Chislennoe reshenie kraevyh zadach dlja uravnenija Puassona metodom bystrogo preobrazovanija Fur'e s ispol'zovaniem parallel'nyh vychislenij [Numerical solution of boundary value problems for the Poisson equation by the fast Fourier transform method using parallel computations]. // *Trudy Kol'skogo nauchnogo centra RAN*, 2018, Issue 5-4(9), pp. 165-182 (in Russian).
9. **Akimov P.A., Belostotskiy A.M., Mozgaleva M.L., Mojtaba Aslami, Negrozov O.A.** Correct Multilevel Discrete-Continual Finite Element Method of Structural Analysis. // Advanced Materials Research Vol. 1040 (2014), pp. 664-669.
10. **Akimov P.A., Sidorov V.N.** Correct Method of Analytical Solution of Multipoint Boundary Problems of Structural Analysis for Systems of Ordinary Differential Equations with Piecewise Constant Coefficients. // Advanced Materials Research Vols. 250-253, 2011, pp. 3652-3655.

a)

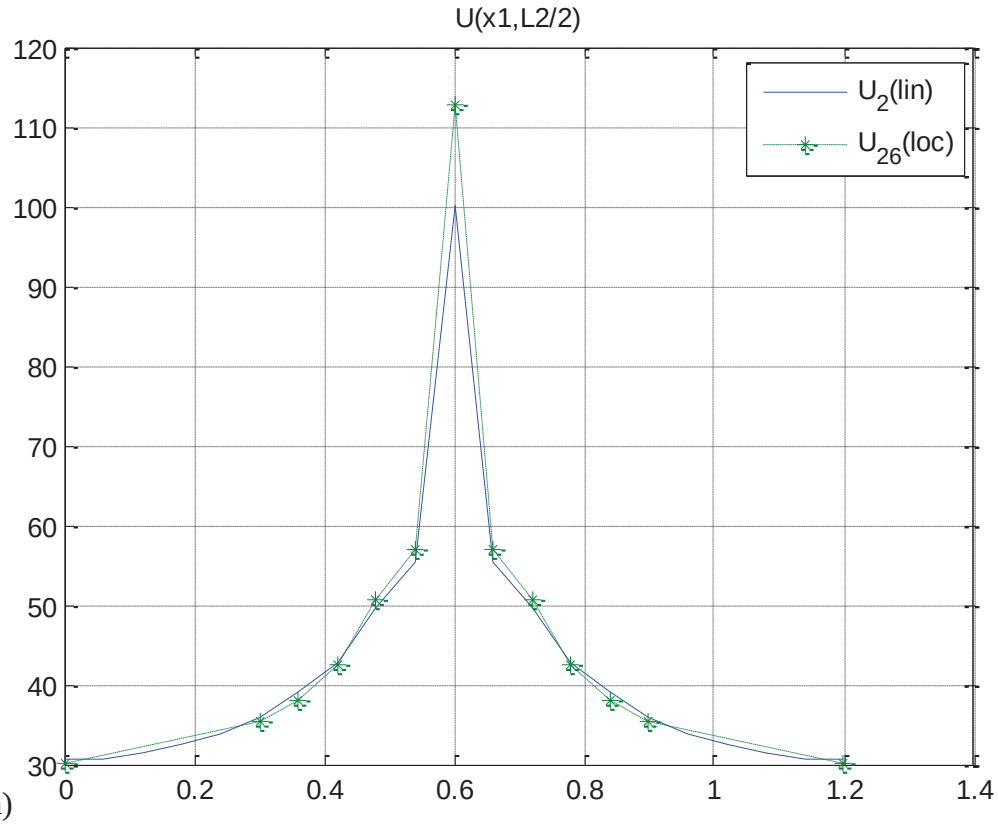

b)

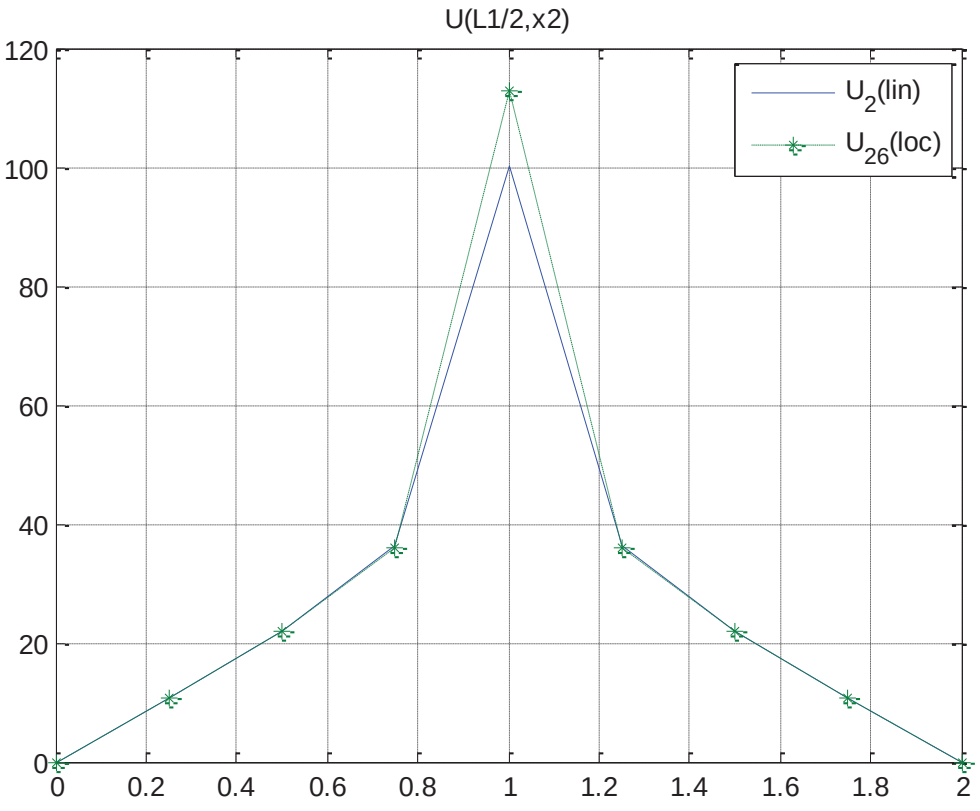

Figures 5.2. Comparison of the results of analysis in the middle sections:
a) along x_1 direction (discrete direction);
b) along x_2 direction (continual direction).

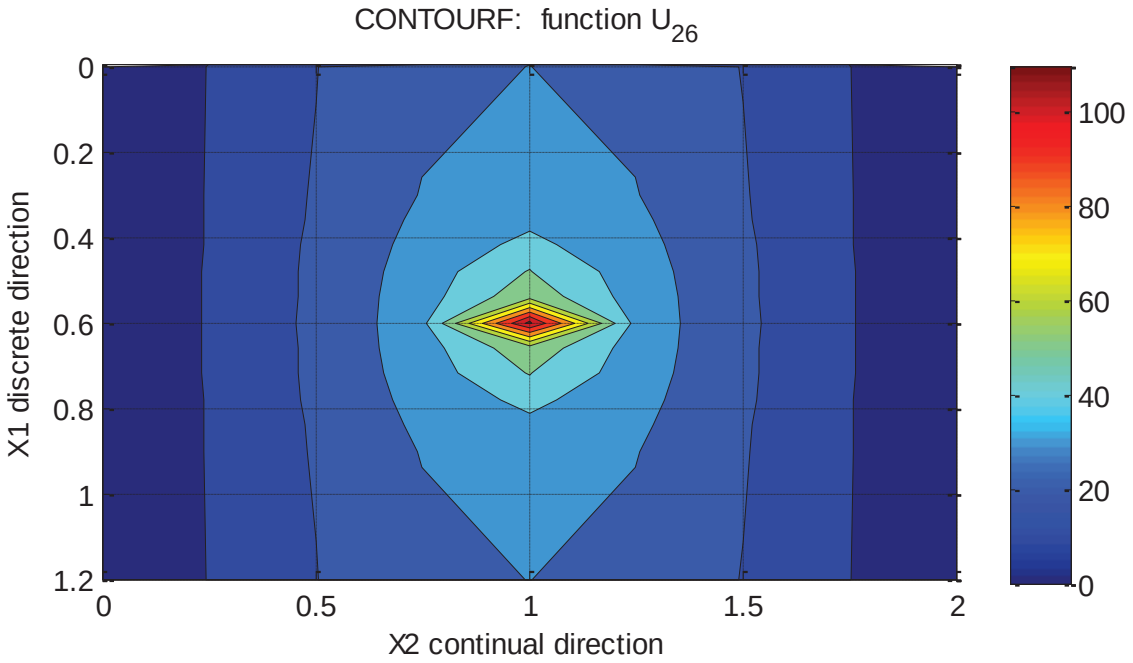

Figures 5.3. Solution with the use of localization.

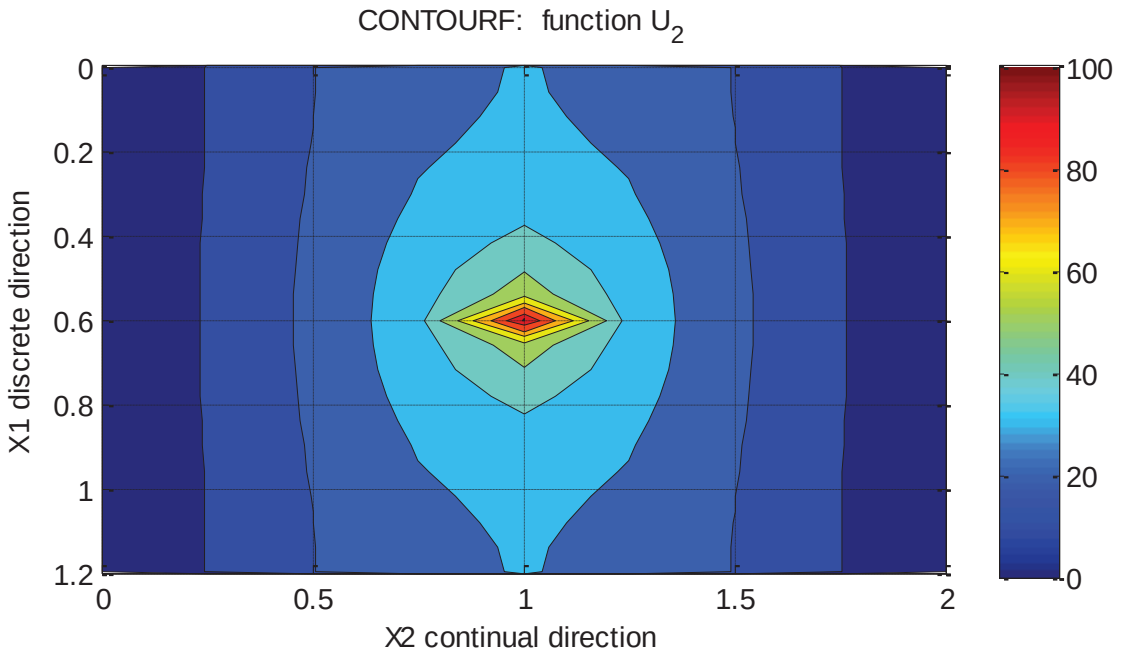

Figures 5.4. Solution with the use of standard (linear) approximation of function within the element.

11. **Sharfanec B.P., Sharfanec E.B.** O vybory metodov reshenija uravnenija Puassona v obshhem sluchae raspredelenija objemnoj plotnosti zarjada i o postanovke kraevyh uslovij v jelektrokineticheskih zadachah (obzor) [On the choice of methods for solving the Poisson equation in the general case of the distribution of the volume charge density and on the formulation of boundary conditions in electrokinetic problems (review)]. // *Nauchnoe priborostroenie*, 2015, Volume 25, Issue 1, pp. 65-75 (in Russian).
12. **Vladimirov V.S.** Uravnenija matematicheskoj fiziki [Equations of mathematical

physics]. Moscow, Nauka, 1981, 512 pages (in Russian).
13. **Koshljakov N.S., Gliner Je.B., Smirnov M.M.** Uravnenija v chastnyh proizvodnyh matematicheskoj fiziki [Partial differential equations of mathematical physics]. Moscow, Vysshaja shkola, 1970, 712 pages (in Russian).
14. **Vorozhcov E.V., Shapeev V.P.** Chislennoe reshenie uravnenija Puassona v poljarnyh koordinatah metodom kollokacij i naimen'shih nevjazok [Numerical solution of the Poisson equation in polar coordinates by the collocation and least residual method]. // *Modelirovanie i analiz informacionnyh sistem*, 2015, Volume 22, Issue 5, pp. 648-664 (in Russian).
15. **Knjazev S.Ju., Shherbakova E.E., Engibarjan A.A.** Chislennoe reshenie kraevyh zadach dlja uravnenija Puassona metodom tochechnyh istochnikov polja [Numerical solution of boundary value problems for the Poisson equation by the method of point field sources]. // *Vestnik DLGTU*, 2014, Volume 15, Issue 2(77), pp. 15-20 (in Russian).
16. **Dobeshi I.** Desjat' lekcij po vejvletam [Ten lectures on wavelets]. Izhevsk: NIC «Reguljarnaja i haoticheskaja dinamika», 2001, 464 pages (in Russian).
1. **Chui K.** Vvedenie v vejvlety [Introduction to wavelets]. Moscow, Mir, 2001, 412 pages (in Russian).
2. **Guo H., Chen W., Jiang X., Jiang D., Zhang X.** A discontinuous finite element method based on B-spline wavelet on the interval for solving first-order neutron transport equation with discrete ordinate (SN) angular discretization. // Annals of Nuclear Energy, 2021, Volume 162, 108511.
3. **Theodosiou T.C.** Derivative-orthogonal non-uniform B-Spline wavelets. // Mathematics and Computers in Simulation, 2021, Volume 188, pp. 368-388.
4. **Vadlamani S., Arun C.O.** A stochastic B-spline wavelet on the interval finite element method for beams. // Computers & Structures, 2020, Volume 233, 106246.
5. **Zhang X., Zeng W.** The regularization B-spline wavelet method for the inverse boundary problem of the Laplace equation from noisy data in an irregular domain. // Engineering Analysis with Boundary Elements, 2021, Volume 125, pp. 1-11.

СПИСОК ЛИТЕРАТУРЫ

1. **Тихонов А.Н., Самарский А.А.** Уравнения математической физики. – М.: Наука, 2004. – 798 с.
2. **Ивлев Д.Д.** Механика пластических сред. Том 1. Теория идеальной пластичности. – М.: Физматлит, 2001. – 445 с.
3. **Ивлев Д.Д.** Механика пластических сред. Том 2. Общие вопросы. Жесткопластическое и упругопластическое состояние тел. Упрочнение. Деформационные теории. Сложные среды. – М.: Физматлит, 2002. – 448 с.
4. **Ивлев Д.Д., Ершов Л.В.** Метод возмущений в теории упругопластического тела. – М.: Наука, 1978. – 208 с.
5. **Лурье А.И.** Теория упругости. – М.: Наука, 1970. – 939 с.
6. **Александров В.М.** Задачи механики сплошных сред со смешанными граничными условиями. – М.: Наука, 1986. – 329 с.
7. **Золотов А.Б., Акимов П.А., Мозгалева М.Л.** Многоуровневые дискретные и дискретно-континуальные реализации вариационно-разностного метода. – М.: АСВ, 2013. – 416 с.
8. **Мингалев О.В., Мельник М.Н.** Численное решение краевых задач для уравнения Пуассона методом быстрого преобразования Фурье с использованием параллельных вычислений. // Труды Кольского научного центра РАН, 2018, №5-4(9), с. 165-182.
9. **Akimov P.A., Belostotskiy A.M., Mozgaleva M.L., Mojtaba Aslami, Negrozov O.A.** Correct Multilevel Discrete-Continual

Finite Element Method of Structural Analysis. // Advanced Materials Research Vol. 1040 (2014), pp. 664-669.
10. **Akimov P.A., Sidorov V.N.** Correct Method of Analytical Solution of Multipoint Boundary Problems of Structural Analysis for Systems of Ordinary Differential Equations with Piecewise Constant Coefficients. // Advanced Materials Research Vols. 250-253, 2011, pp. 3652-3655.
11. **Шарфанец Б.П., Шарфанец Е.Б.** О выборы методов решения уравнения Пуассона в общем случае распределения объемной плотности заряда и о постановке краевых условий в электрокинетических задачах (обзор). // Научное приборостроение, 2015, том 25, №1, с. 65-75.
12. **Владимиров В.С.** Уравнения математической физики. – М.: Наука, 1981. – 512 с.
13. **Кошляков Н.С., Глинер Э.Б., Смирнов М.М.** Уравнения в частных производных математической физики. – М.: Высшая школа, 1970. – 712 с.
14. **Ворожцов Е.В., Шапеев В.П.** Численное решение уравнения Пуассона в полярных координатах методом коллокаций и наименьших невязок. // Моделирование и анализ информационных систем, 2015, том 22, №5, с. 648-664.
15. **Князев С.Ю., Щербакова Е.Е., Енгибарян А.А.** Численное решение краевых задач для уравнения Пуассона методом точечных источников поля. // Вестник ДЛГТУ, 2014, том 15, №2(77), с. 15-20.
16. **Добеши И.** Десять лекций по вейвлетам. – Ижевск: НИЦ «Регулярная и хаотическая динамика», 2001. – 464 с.
17. **Чуи К.** Введение в вейвлеты. – М.: Мир, 2001. – 412 с.
18. **Guo H., Chen W., Jiang X., Jiang D., Zhang X.** A discontinuous finite element method based on B-spline wavelet on the interval for solving first-order neutron transport equation with discrete ordinate (SN) angular discretization. // Annals of Nuclear Energy, 2021, Volume 162, 108511.
19. **Theodosiou T.C.** Derivative-orthogonal non-uniform B-Spline wavelets. // Mathematics and Computers in Simulation, 2021, Volume 188, pp. 368-388.
20. **Vadlamani S., Arun C.O.** A stochastic B-spline wavelet on the interval finite element method for beams. // Computers & Structures, 2020, Volume 233, 106246.
21. **Zhang X., Zeng W.** The regularization B-spline wavelet method for the inverse boundary problem of the Laplace equation from noisy data in an irregular domain. // Engineering Analysis with Boundary Elements, 2021, Volume 125, pp. 1-11.

Pavel A. Akimov, Full Member of the Russian Academy of Architecture and Construction Sciences, Professor, Dr.Sc.; Rector of National Research Moscow State University of Civil Engineering; 26, Yaroslavskoe Shosse, Moscow, 129337, Russia; phone: +7(495) 651-81-85; Fax: +7(499) 183-44-38; E-mail: AkimovPA@mgsu.ru, rector@mgsu.ru, pavel.akimov@gmail.com.

Marina L. Mozgaleva, Senior Scientist Researcher, Dr.Sc.; Professor of Department of Applied Mathematics, National Research Moscow State University of Civil Engineering; 26, Yaroslavskoe Shosse, Moscow, 129337, Russia; phone/fax +7(499) 183-59-94; Fax: +7(499) 183-44-38; Email: marina.mozgaleva@gmail.com.

Мозгалева Марина Леонидовна, старший научный сотрудник, доктор технических наук; профессор кафедры прикладной математики Национального исследовательского Московского государственного строительного университета; 129337, Россия, г. Москва, Ярославское шоссе, дом 26; телефон/факс: +7(499) 183-59-94; Email: marina.mozgaleva@gmail.com.

Акимов Павел Алексеевич, академик РААСН, профессор, доктор технических наук; ректор Национального исследовательского Московского государственного строительного университета; 129337, Россия, г. Москва, Ярославское шоссе, дом 26; телефон: +7(495) 651-81-85; факс: +7(499) 183-44-38; Email: AkimovPA@mgsu.ru, rector@mgsu.ru, pavel.akimov@gmail.com.

International Journal for Computational Civil and Structural Engineering, 17(3) 173–181 (2021)

DOI:10.22337/2587-9618-2021-17-3-173-181

BENDING WITH TORSION OF FIBER REINFORCED CONCRETE BEAM OF CIRCULAR CROSS SECTION

Sergey A. Bulkin

CJSC "GORPROEKT", Moscow, RUSSIA

Abstract. The article provides information about the tests of circle cross-section reinforced concrete beams made of high-strength steel-fiber concrete on combined torsion and bending. Given information contains the main results: a diagram of the cracks with an indication of their opening width, the values of support reactions at the moment of cracking and at the moment before destruction. It was found that as the load is applied in beams made of high-strength steel-reinforced concrete, in the case of several cracks at the first stage, there is one crack increases. The beams are modeled in the design complex and given description of the main design parameters. The results of the calculation are presented and a comparative analysis of the results obtained with the experiments results. It is noted that the adopted models in the computational complexes require the development of subroutines and refinement.

Keywords: reinforced concrete structures, combined bending and torsion, deformation, strength, circle cross section

КРУЧЕНИЕ С ИЗГИБОМ СТАЛЕФИБРОЖЕЛЕЗОБЕТОННОЙ БАЛКИ КРУГЛОГО СЕЧЕНИЯ

С.А. Булкин

ЗАО «ГОРПРОЕКТ», г. Москва, РОССИЯ

Аннотация. В статье приведена информация о проведенных испытаний железобетонных балок круглого сечения из высокопрочного сталефибробетона при действии кручения с изгибом. Приведена информация по основным полученным результатам: схема трещин с указанием их ширины раскрытия, значения опорных реакций в момент образования трещин и в момент, предшествующий разрушению образца. Установлено, что по мере приложения нагрузки в балках из высокопрочного сталефибробетона увеличивается в основном одна трещина, даже в случае возникновения нескольких трещин на первом этапе. Произведено моделирование балок в расчетном комплексе с описанием основных расчетных предпосылок. Приведены результаты расчета и выполнен сравнительный анализ полученных результатов с результатами проведенных экспериментов. Отмечено, что принятые модели в расчетных комплексах требуют разработки подпрограмм и уточнения.

Ключевые слова: железобетон, кручение с изгибом, деформации, прочность, квадратное сечение

INTRODUCTION

The designed elements of reinforced concrete structures, especially unique buildings and structures that operate in conditions of a complex stressed state - torsion with bending. A separate group of elements can be distinguished (beams with consoles, edge beams, stiffening cores of high-rise buildings, spatial frame structures, etc.) in which torsion plays a primary role in the work.

Work in the field of investigation of the torsion of reinforced concrete structures was carried out and is being carried out by many specialists, both Russian and foreign: V.M. Bondarenko, P.F. Vakhnenko, A.I. Demyanov, N.I. Karpenko, V.I. Kolchunov, V.I., A.M. Kuzmenko, V.I. Morozov, V.I. Travush, A. Bishara, H. Gesund, E. Rausch, T.T.C. Hsu et al. [1-15]. At the same time, only individual authors have dealt with the issue of the operation of structures with the combined action of torsion and bending, and the issue of the

operation of reinforced concrete structures made of high-strength fiber-reinforced concrete is at the initial stage.

Despite the fact that technological progress and existing needs require the use of new materials, regulatory documents cannot cover the entire range of emerging tasks, and the responsibility for the choice of both the design model and the obtained calculation results lies directly with the designer, who is faced with a difficult choice issue a calculation model that allows you to properly reflect the actual performance of the structures. In most cases, the solution to the problem arises comes down to assumptions, due to the lack of results of the conducted field experiments.

Considering the above, the development of a methodology for calculating reinforced concrete structures made of high-strength steel-fiber reinforced concrete in torsion with bending, taking into account the occurrence of cracks, is an urgent task. In this case, the refinement of the main design parameters (deflections and angles of rotation of sections, the scheme of cracks and their opening width, the moment of crack formation) adopted in the design model should be carried out on the basis of comparing the calculation results with the results of the experiments performed.

RESULTS AND DISCUSSION

A number of experiments were carried out to study the work of reinforced concrete beams of a circular cross-section on the joint action of bending with torsion to determine the actual bearing capacity.

For the study, beams of circular cross-section with a diameter of 20 cm and a length of 1.2 m were made. The beams were made of steel fiber reinforced concrete B130 with steel fiber 13 mm long, 0.3 mm in diameter and a temporary resistance of at least 1200 MPa.

Reinforcement of beams is made in the form of welded frames with longitudinal and transverse reinforcement A240 Ø6 mm. The longitudinal reinforcement is provided with eight rods, the transverse reinforcement is located in 100 mm increments. To be able to transmit torque, embedded parts were provided at the ends of the beams.

During the experiment, a beam with 720 mm long consoles welded to the embedded parts installed at the ends was installed by the middle part on a support, and a vertical force was transmitted to the consoles through the traverse (Fig. 1). The loading was carried out in stages - in steps equal to 10% of the cracking load. The fixation of instrument readings (indicators of deflection meters) was carried out at each stage before and after exposure.

In the course of the experiments, the moment of occurrence of cracks, as well as the moment of destruction of the samples, were recorded with the determination of the corresponding forces (Fig. 2).

According to the results of the experiment, data on the complex stress-strain state during bending with torsion in the studied areas of the beams were obtained and the main parameters were determined:

- the experimental value of the support reaction at the time of the formation of spatial cracks was 12.5 kN, with the destruction of reinforced concrete structures - 17.5 kN;
- coordinates of the formation of spatial cracks;
- deflections of the consoles and, accordingly, the angles of rotation;
- change in the length of the projections of spatial cracks, depending on the increase in the loading steps;

Based on the analysis results, a fracture pattern was drawn up. A diagram of cracks with indication of their numbers and opening width is shown in Fig. 3.

During the experiments, it was noted that as the load is applied in the beams made of high-strength steel-fiber reinforced concrete, mainly one crack increases, even if several cracks appear at the first stage.

The formation of a single spatial crack in the considered samples led to a rapid opening of

this crack, a significant increase in deformations, with a corresponding increase in deflections and angles of rotation.

For comparison with the results of the experiments carried out, the beam was modeled in the ANSYS environment and the calculation was performed.

As a design model, a beam with consoles was considered, which has a support in the middle. All dimensions are shown in the figure.

The formation of a geometric model in the software package was carried out on the basis of data on the samples used in the experiments. The geometric model is a concrete model of a circular beam with a diameter of 200 mm.

Inside the concrete is a reinforcing cage, consisting of longitudinal reinforcement - located at a distance of 25 mm from the edge to the center of the rods, and transverse reinforcement, located with a step of 100 mm.

Consoles in the form of elements of rectangular section 50x200 mm and length 720 mm were rigidly attached to the geometric models of concrete and reinforcement.

The next stage of computational modeling was the assignment of element types and the construction of a finite element mesh.

The concrete of the beam is represented by solid finite elements of the SOLID65 type, the beam reinforcement was modeled with bar finite elements of the BEAM188 type. The consoles and the supporting part of the beam are modeled with solid elements of the SOLID185 type.

Volumetric finite elements of the SOLID65 type are designed to simulate elements that allow cracking during tension, and they also allow the possibility of material destruction during compression. Taking into account the fact that, according to the results of the experiments, destruction occurs after the tensile reinforcement reaches the yield point, for the purposes of the research, the possibility of concrete destruction during compression was not considered (the option of destruction of compressed concrete was not used).

Additionally, shear transfer coefficients (0.7) are introduced, and the ultimate tensile stresses (9.6 MPa) and ultimate compressive stresses (132.5 MPa) are limited. The range of shear transfer ratio is set from 0 to 1, where 0 corresponds to no transfer of shear (smooth crack), and 1 corresponds to full transfer of shear.

For concrete modeling in the ANSYS environment, a combination of the following materials is adopted: Linear Isotropic, Multilinear Isotropic and Concrete. Linear Isotropic is used to set the initial modulus of elasticity and Poisson's ratio of concrete. The Multilinear Isotropic material implies the creation of a curvilinear diagram by multilinear approximation. Concrete material provides for the formation of cracks when the principal stresses exceed the specified tensile strength, as well as taking into account the triaxial stress state.

The physical and mechanical characteristics of concrete were determined from the results of statistical processing of tests of cubes and prisms. The results are shown in Table 1.

The modulus of elasticity, ultimate compressive strength and tensile strength in bending for concrete in this design study were taken in accordance with the data obtained on the samples made from high-strength fiber-reinforced concrete: Eb = 48.4 GPa, Rb = 132.5 MPa, Rbt = 9.6 MPa.

The diagram of work for reinforcing steel A240 was taken as two-line with hardening in accordance with the recommendations of SP 63.13330. The ultimate tensile and compressive strength in the calculations was taken equal to 240 MPa.

The load was applied to the ends of the cantilevers in accordance with a certain design scheme, making it possible to obtain a complex stress-strain state in the beam during torsion with bending.

Figure 1. Beam testing process

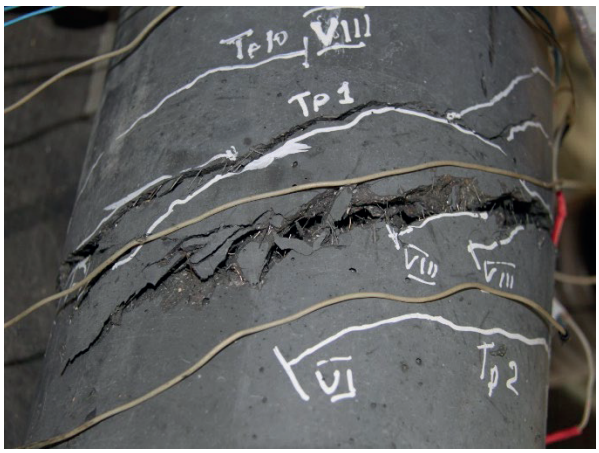

Figure 2. Crack in the beam at the time of destruction

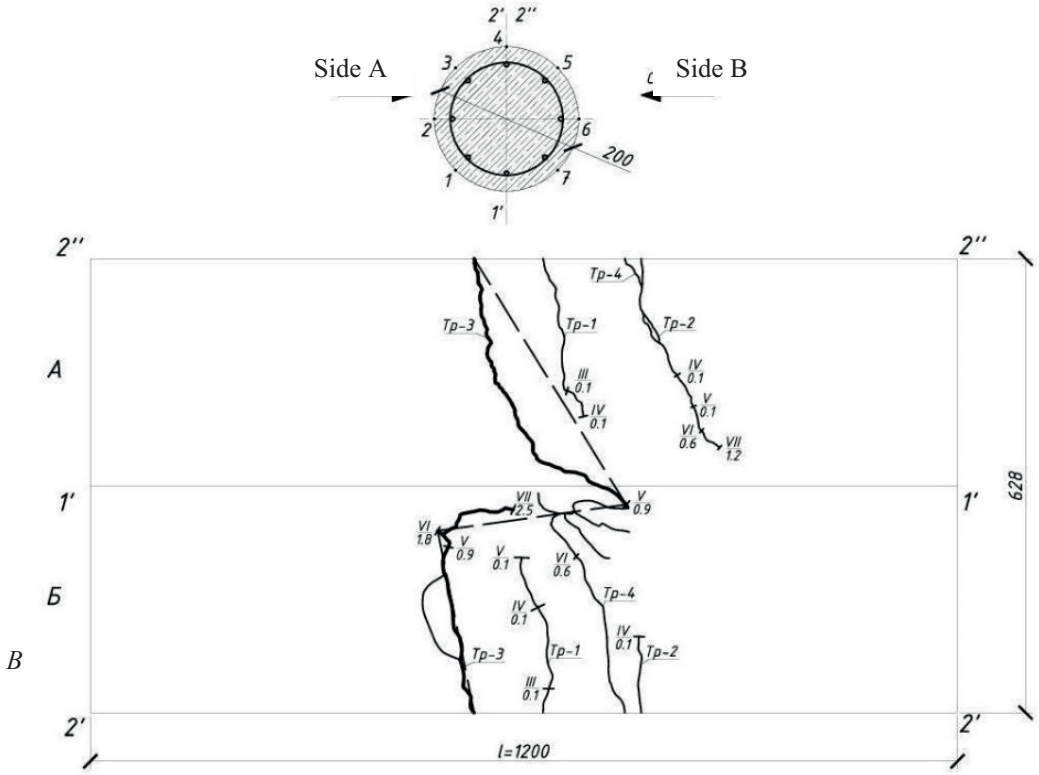

Figure 3. Crack diagram

Table 1. Physical and mechanical characteristics of concrete

No	Concrete type	Прочность бетона в 28 сут., МПа				Elastic modulus, GPa		Actual class of concrete at a coefficient of variation of 10%
		R	R_b	R_{bt}	R_{tt}	E_b	E_{dyn}	
Ultra high strength concrete								
1.	Fiber concrete	152.6	132.5	9.6	22.6	48.4	54.6	B134

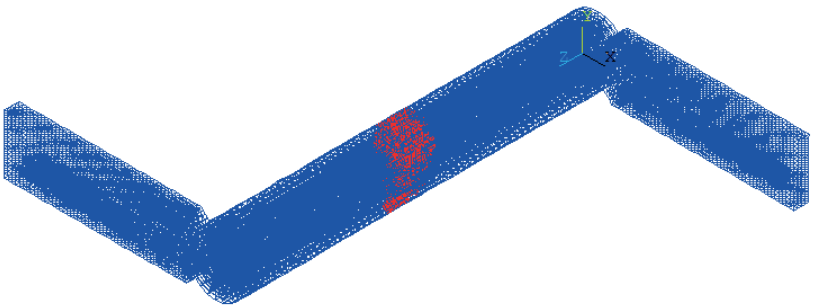

Figure 4. Arrangement of cracks in a beam

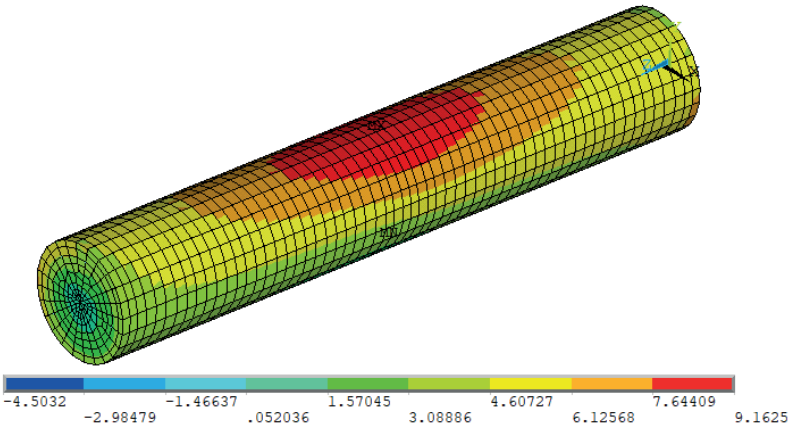

Figure 5. Principal stresses in concrete prior to cracking

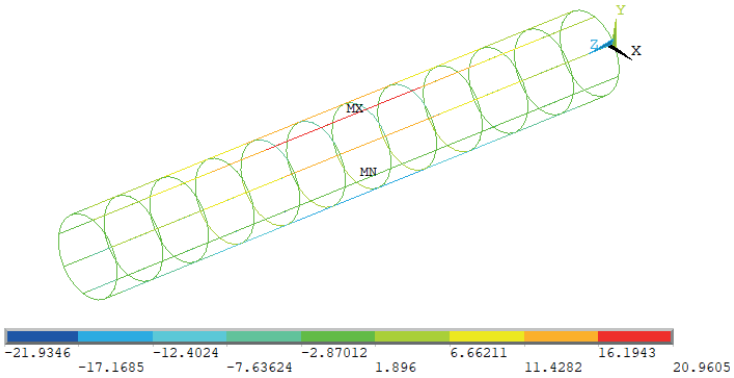

Figure 6. Reinforcement stresses preceding the moment of cracking in concrete

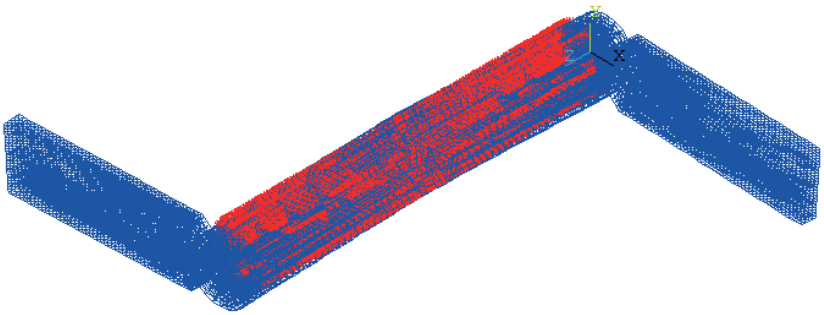

Figure 7. Arrangement of cracks in a beam

The loading of the model was carried out nonlinearly with the definition of an automatic step at the initial stages of 0.5 kN and a decrease in the step to 0.05 kN at the stage preceding the formation of cracks.
The fixing of the support platform of the beam was carried out by imposing displacement restrictions in three directions along the lower surface of the platform.
Based on the calculation results, the stresses in the beam elements, deformed schemes, crack locations at various loading stages were obtained, and the moment of crack initiation was determined.
The moment of crack initiation was determined at step 21 and corresponds to loads on the beam cantilevers of 9.8 kN. The crack locations at this moment are shown in Fig. 5.
Tensile stresses in concrete, preceding the moment of cracking, were 9.16 MPa (Fig. 5). Tensile stresses in reinforcement - 21 MPa (Fig. 6).
The displacement of the ends of the cantilevers at the moment of cracking was 1.4 mm.
The moment of failure of the beam is determined at step 149 and corresponds to loads on the beam cantilevers of 16.2 kN. The crack locations at this moment are shown in Fig. 7.
Tensile stresses in reinforcement in almost all longitudinal bars amounted to - 272 MPa.
The displacements of the ends of the consoles at this moment were 48 mm.
Based on the results of the calculations, the values of the forces transmitted to the beams' consoles at the moments of cracking and at the moment of destruction were determined. At the same time, the forces obtained at the time of cracking in the beam during the calculation (9.8 kN) are slightly lower than the values obtained as a result of the experiment (12.5 kN). Also, the efforts obtained at the moment of fracture in the calculation (16.2 kN) slightly differ from the experimental data (17.5 kN).
The deformed beam pattern is determined by significant displacements of the cantilevers, which is due to the rotation of the section with the formation of a plastic hinge (due to the reinforcement reaching the yield point) in the center of the beam, which corresponds to the moment of cracking and was 9.8 kN.
The actual destruction of the beam during the experiment, similar to the calculation, did not occur quickly, with the formation of plastic deformations and the absence of brittle fracture.
Also, one of the distinctive features revealed during the experiments was the growth of one main crack, however, according to the results of the calculations, a network of cracks is formed, which, as the load increases, captures an ever larger surface of the considered beam.
Such a significant difference requires the development of subroutines for the possibility of correcting the computational model and bringing the results obtained in line with the experimental data.

CONCLUSIONS

1. During the experiments, it was noted that as the load is applied in the beams made of high-strength steel-fiber reinforced concrete, mainly one crack increases, even if several cracks appear at the first stage.
2. The formation of a single spatial crack in the considered samples led to a rapid opening of this crack, a significant increase in deformations, with a corresponding increase in deflections and angles of rotation.
3. The ANSYS software package allows you to perform volumetric modeling of reinforced concrete elements, taking into account the reinforcement and the purpose of nonlinear diagrams of concrete and reinforcement work.
4. The ANSYS software package can be used to assess the performance of reinforced concrete elements, including to the stage of destruction.
5. The moment of cracking and the moment of fracture (transmitted force), obtained as a result of the calculation, differ slightly from the values obtained as a result of the experiments carried out.
6. In contrast to the experiment with the formation of one main crack, during the

calculation in the software package, a network of cracks is formed, which requires the development of subroutines.

REFERENCES

1. **Travush V.I., Karpenko N.I., Kolchunov VL.I., Kaprielov S.S., Demyanov A.I., Konorev A.V.** Rezul'taty eksperimental'nykh issledovaniy konstruktsiy kvadratnogo i korobchatogo secheniy iz vysokoprochnogo betona pri kruchenii s izgibom [Results of experimental studies of square and box-section structures made of high-strength concrete under torsion with bending]. Stroitel'stvo i rekonstruktsiya. 2018. No. 6. Pp. 32-43.
2. **Travush V.I., Karpenko N.I., Kolchunov VL.I., Kaprielov S.S., Demyanov A.I., Konorev A.V.** Osnovnyye rezul'taty eksperimental'nykh issledovaniy zhelezobetonnykh konstruktsiy iz vysokoprochnogo betona B100 kruglogo i kol'tsevogo secheniy pri kruchenii s izgibom [Main results of experimental studies of reinforced concrete structures made of high-strength concrete in the form of round and ring sections during torsion with bending]. Construction mechanics of engineering structures and structures. 2019. No. 15(1). Pp. 51-61.
3. **Demyanov A.I.** Osobennosti treschinoobrazovaniya v konstruktsiyah iz visokoprochnogo zhelezobetona pri slozhnom soprotivlenii – kruchenii s izgibom [Crack formation in high-strength reinforced concrete structures at complex resistance – torsion with bending]. Stroitel'stvo i rekonstruktsiya. 2019. No. 5. Pp. 3-10.
4. **V.I. Travush, N.I. Karpenko, VL.I. Kolchunov, S.S. Kaprielov, A.I. Demyanov, S.A. Bulkin, V.S. Moskovtseva**. Rezul`taty eksperimental’nykh issledovaniy slozhnj-napryazhennykh balok kruglogo poporechnogo secheniya iz visokoprochnogo fibrozhelezobetona [Results of experimental studies of high-strength fiber reinforced concrete beams with round cross-sections under combined bending and torsion]. Structural Mechanics of Engineering Constructions and Buildings. 2020. No. 16 (4). Pp. 290-297.
5. **Kolchunov VL.I., Salnikov A.S.** Eksperimental'nyye issledovaniya treshchinoobrazovaniya zhelezobetonnykh konstruktsiy pri kruchenii s izgibom [Experimental studies of crack formation of reinforced concrete structuresunder torsion with bending]. Stroitel'stvo i rekonstruktsiya. 2016. No. 3 (65). Pp. 24-32
6. **Morozov V.I., Bakhotsky I.V.** K raschetu fibrozhelezobetonnykh konstruktsiy, podverzhennykh sovmestnomu vozdeystviya krucheniyu s izgibom [To the calculation of fiber-reinforced concrete structures exposed to the joint effect of torsion with bending.] Sovremennye problem nauki I obrazovaniya. 2013. No. 5.
7. **Bondarenko V.M., Kolchunov V.I**. The computational model of a power resistance of reinforced concrete [Computational models of the force resistance of reinforced concrete: monograph]. Moskow, ASV Publ., 2004. 472 p.
8. **Salnikov A.S., Kolchunov Vl.I., Klyueva N.V.** Metod opredeleniya minimal'noj nagruzki i koordinat obrazovaniya prostranstvennoj treshchiny v zhelezobetonnyh konstrukciyah pri kruchenii s izgibom [Method for determining the minimum load and coordinates of spatial crack formation in reinforced concrete structures during torsion with bending]. Promyshlennoe i grazhdanskoe stroitelstvo. 2016. No.1. Pp. 52–57.
9. **Salnikov A.S., Kolchunov V.I., Kolchunov Vl.I.** Metodika rascheta predel'noj nagruzki i koordinat obrazovaniya prostranstvennoj treshchiny pervogo vida v zhelezobetonnyh

konstrukciyah pri kruchenii s izgibom [Method for calculating the maximum load and coordinates of the formation of a spatial crack of the first type in reinforced concrete structures during torsion with bending]. Stroitel'stvo i rekonstrukciya. 2015. No. 6(62). Pp. 49– 56.

10. **Demyanov A.I., Kolchunov Vl.I., Salnikov A.S., Mihajlov M. M.** Raschetnye modeli statikodinamicheskogo deformirovaniya zhelezobetonnoj konstruk-cii pri kruchenii s izgibom v moment obrazovaniya prostranstvennoj treshchiny [Computational models of static-dynamic deformation of a reinforced concrete structure during torsion with a bend at the moment of formation of a spatial crack]. Stroitel'stvo i rekonstrukciya. 2017. No.3 (71). Pp. 13–22.
11. **Salnikov A., Kolchunov Vl., Yakovenko I.** the computational model of spatial formation of cracks in reinforced concrete constructions in torsion with bending. Applied Mechanics and Materials. Vols. 725-726 (2015). Pp. 784-789.
12. **Awadh E.A.** Torsion plus bending and shear on reinforced concrete beams. Journal of Engineering and Sustainable Development. 2016. No.4. P. 277– 288
13. **Khaldoun Rahal.** Combined Torsion and Bending in Reinforced and Prestressed Concrete beams Using Simplified Method for Combined Stress-Resultants. ACI Structural Journal. 2007. Vol. 104. No. 4. Pp. 402–411
14. **Vishnu H. Jariwalaa, Paresh V. Patel, Sharadkumar P. Purohit**. Strengthening of RC Beams subjected to Combined Torsion and Bending with GFRP Composites // Procedia Engineering. 2013. Vol. 51. Pp. 282–289.
15. **David A.E., Thomas L.H., Simon A.N., Jonathan E.C.** Veering and nonlinear interactions of a clamped beam in bending and torsion. Journal of Sound and Vibration. 2018. Vol. 416. Pp. 1-16.

СПИСОК ЛИТЕРАТУРЫ

1. **Травуш В.И., Карпенко Н.И., Колчунов Вл.И., Каприелов С.С., Демьянов А.И., Конорев А.В.** Результаты экспериментальных исследований конструкций квадратного и коробчатого сечений из высокопрочного бетона при кручении с изгибом // Строительство и реконструкция. 2018. №6. С. 32-43.
2. **Травуш В.И., Карпенко Н.И., Колчунов Вл.И., Каприелов С.С., Демьянов А.И., Конорев А.В.** Основные результаты экспериментальных исследований железобетонных конструкций из высокопрочного бетона В100 круглого и кольцевого сечений при кручении с изгибом // Строительная механика инженерных конструкций и сооружений. 2019. №15(1). С.51-61.
3. **Демьянов А.И.** Особенности трещинообразования в конструкциях из высокопрочного железобетона при сложном сопротивлении – кручении с изгибом // Строительство и реконструкция. 2019. №5. С. 3-10.
4. **В.И. Травуш, Н.И. Карпенко, Вл.И. Колчунов, С.С. Каприелов, А.И. Демьянов, С.А. Булкин, В.С. Московцева.** Результаты экспериментальных исследований сложнонапряженных балок круглого поперечного сечения из высокопрочного фиброжелезобетона // Строительная механика инженерных конструкций и сооружений. 2020. №16 (4). С 290-297
5. **Колчунов Вл. И., Сальников А.С.** Экспериментальные исследования трещинообразования железобетонных конструкций при кручении с изгибом // Строительство и реконструкция. 2016. № 3(65). С. 24–32.
6. **Морозов В.И., Бахотский И.В.** К расчету фиброжелезобетонных конструкций, подверженных совместному воздействию кручения с

изгибом // Современные проблемы науки и образования. 2013. № 5.
7. **Бондаренко В.М., Колчунов В.И**. Расчетные модели силового сопротивления железобетона: монография. М.: Изд-во АСВ, 2004. 472 с.
8. **Сальников А.С., Клюева Н.В., Колчунов В.И.** Метод определения минимальной нагрузки и координат образования пространственной трещины в железобетонных конструкциях при кручении с изгибом // Промышленное и гражданское строительство. 2016. №1. С. 52–57.
9. **Сальников А.С., Колчунов Вл.И., Колчунов В.И.** Методика расчета предельной нагрузки и координат образования пространственной трещины первого вида в железобетонных конструкциях при кручении с изгибом // Строительство и реконструкция. 2015. №6(62). С. 49– 56.
10. **Демьянов А.И., Колчунов В.И., Сальников А.С., Михайлов М.М.** Расчетные модели статико-динамического деформирования железобетонной конструкции при кручении с изгибом в момент образования пространственной трещины // Строительство и реконструкция. 2017. №3 (71). С. 13–22.
11. **Salnikov A., Kolchunov Vl., Yakovenko I.** The computational model of spatial formation of cracks in reinforced concrete constructions in torsion with bending // Applied Mechanics and Materials. Vols. 725–726 (2015), pp 784–789.
12. **Awadh E.A.** Torsion plus bending and shear on reinforced concrete beams. Journal of Engineering and Sustainable Development. 2016. No.4. P. 277– 288.
13. **Khaldoun Rahal**. Combined Torsion and Bending in Reinforced and Prestressed Concrete beams Using Simplified Method for Combined Stress-Resultants. ACI Structural Journal. 2007. Vol. 104. No. 4. Pp. 402–411
14. **Vishnu H. Jariwalaa, Paresh V. Patel, Sharadkumar P. Purohit.** Strengthening of RC Beams subjected to Combined Torsion and Bending with GFRP Composites // Procedia Engineering. 2013. Vol. 51. Pp. 282–289.
15. **David A.E., Thomas L.H., Simon A.N., Jonathan E.C.** Veering and nonlinear interactions of a clamped beam in bending and torsion. Journal of Sound and Vibration. 2018. Vol. 416. Pp. 1-16.

Bulkin Sergey A. ZAO «GORPROJECT», Moscow, Russia, E-mail: sa.bulkin@gmail.com

Булкин Сергей Александрович. ЗАО «ГОРПРОЕКТ», г. Москва, Россия. E-mail: sa.bulkin@gmail.com

DOI:10.22337/2587-9618-2021-17-3-182-189

EVALUATION OF THE RELIABILITY OF BUILDING STRUCTURES IN SIMULIA ABAQUS: MODELING OF STOCHASTIC MATERIAL PROPERTIES

Alexander I. Khvostov [1], ***Sergei I. Zhukov*** [2], ***Sergey N. Tropkin*** [3], ***Andrey Y. Chauskin*** [4]

[1] LLC Auriga, Moscow, RUSSIA
[2] Research Computing Center of Moscow State University, Moscow, RUSSIA
[3] LLC "TESIS", Moscow, RUSSIA
[4] REM Systems LLC, Moscow, RUSSIA

Abstract. This article describes a software module component integrated with the SIMULIA Abaqus engineering analysis software package and designed to simulate random values of material parameters in a finite element model based on specified statistical characteristics, with the possibility of taking into account the physical nonlinearity of material behavior under various combinations of loads and influences. The target group of materials under study is materials of load-bearing elements of building structures, such as concrete, stone, steel. This software module can be recommended for use by specialists, engineers and scientists engaged in probabilistic analysis of the reliability of structures of buildings and structures, apparatus, machines, devices, with the combined use of complexes of computer modeling and engineering analysis. Has a certificate of state registration of the computer program "AS for modeling stochastic properties of materials" No. 2019667439 dated 12.24.2019.

Keywords: Finite element method, theory of reliability, random numbers, computer modeling, programming

ОЦЕНКА НАДЁЖНОСТИ СТРОИТЕЛЬНЫХ КОНСТРУКЦИЙ В SIMULIA ABAQUS: МОДЕЛИРОВАНИЕ СТОХАСТИЧЕСКИХ СВОЙСТВ МАТЕРИАЛА

А.И. Хвостов [1], ***С.И. Жуков*** [2], ***С.Н. Тропкин*** [3], ***А.Ю. Чаускин*** [4]

[1] ООО «Аурига», Москва, РОССИЯ
[2] НИВЦ МГУ, Москва, РОССИЯ
[3] ООО «ТЕСИС», Москва, РОССИЯ
[4] ООО «РЕМ Системс», Москва, РОССИЯ

Аннотация. В данной статье описывается компонент программного модуля интегрированный с программным комплексом инженерного анализа SIMULIA Abaqus и предназначенный для моделирования случайных значений параметров материала в конечно-элементной модели на основе заданных статистических характеристик, с возможностью учёта физической нелинейности поведения материала при различных сочетаниях нагрузок и воздействиях. Целевая группа исследуемых материалов – материалы несущих элементов строительных конструкций, такие как бетон, камень, сталь. Данный программный модуль может быть рекомендован для применения специалистами, инженерами и учёными, занимающимися вероятностным анализом надёжности конструкций зданий и сооружений, аппаратов, машин, приборов, при совместном использовании комплексов компьютерного моделирования и инженерного анализа. Имеет свидетельство государственной регистрации программы для ЭВМ «АС моделирования стохастических свойств материалов» №2019667439 от 24.12.2019.

Ключевые слова: Метод конечных элементов, теория надёжности, случайные числа, компьютерное моделирование, программирование

INTRODUCTION

Currently, ensuring the mechanical safety of buildings, structures and their structures is regulated by regulatory legal acts based on the semi-probabilistic method of limit states using reliability coefficients. The calculation methods laid down in the standards do not allow the designer to obtain quantitative indicators of the reliability of the facility being developed. The available qualitative characteristic of reliability is subjective, depends significantly on the qualifications of experts and often leads to inexpedient economic decisions, including those based on personal reinsurance of a specialist in the design process. On the other hand, there are cases when the reliability of objects of increased responsibility is lower than objects of the normal and reduced levels. It should also be noted that at present, damage and defects in structures are often the result of design errors. One of the significant "modern" factors affecting the probability of error is the lack of time – the generally accepted principles of finding optimal solutions based on iterative design and experimental verification are now becoming less and less relevant.

One of the effective solutions to this problem is the use of universal software systems for numerical modeling, which have flexible customization options: development of new types of material, finite elements, solver customization, and much more.

USING THE USER SUBROUTINE UMAT

The finite element method initially developed as a generalization and systematization of methods for solving problems in structural mechanics. Later it found wide application in other fields of science and technology [6]. It is rather difficult to create a universal graphical interface that would satisfy the highly specific requirements of an ever-growing number of extremely diverse problems solved using the finite element method. There are user subroutines for additional customization of the SIMULIA Abaqus software package. The principle of working with them is that the core of the software complex calls during the calculation a set of user-written subroutines that overload the corresponding functionality in Abaqus.

User subroutines are an extremely powerful tool that allows you to extend some of the functionality of the software package for which the usual interface for inputting initial data imposes too strict restrictions. Custom subroutines provide the ability to flexibly define material properties and behavior, initial and boundary conditions, and even directly calculate local stiffness matrices for custom finite element types.

User-defined routines are usually written in FORTRAN. Subroutines cannot call each other, but a number of utilities can be called from the Abaqus programming interface.

In Abaqus, the user can create his own type of material. A custom UMAT subroutine is used to set its behavior.

The UMAT subroutine is designed to simulate the nonlinear behavior of materials. In this article, we restrict ourselves to generating a model with random, locally given initial elastic properties. UMAT is called at each Gaussian integration point of the finite element when constructing its local stiffness matrix at each loading step. From the data passed by the Abaqus kernel to the UMAT subroutine, we need the stress tensor σ = *STRESS (NTENS)* and the strain tensor increment $\Delta\varepsilon$ = *DSTRAN (NTENS)*. We must obtain the Jacobi matrix:

$$J = DDSDDE(i,j) = \frac{\Delta\sigma}{\Delta\varepsilon} = E(i,j) = E_{ij}$$

which in our case is equal to the tensor of the elastic constants of the material and stress at the next loading step

$$\sigma_{k+1} = \sigma_k + E\Delta\varepsilon_k;$$

A detailed description and a complete list of arguments for the UMAT subroutine can be found in the documentation for the SIMULIA Abaqus software package.

BOX-MULLER TRANSFORM

Typically, algorithms for (pseudo) random number generators on personal computers generate a sequence of numbers that obeys a uniform distribution. However, many physical quantities have a distribution close to normal (and tending to it, according to the Lyapunov theorem), which is implemented by various kinds of special sensors used in cryptography. The question of converting a uniform distribution into a normal distribution has been studied in detail for a long time, and the method of polar coordinates proposed by George Box, Mervyn Mueller and George Marsaglia in 1958 has become the most widespread [9]. In this work, we used the following version of the Box-Muller transformation.

Let and be independent random variables uniformly distributed on the interval [–1; 1]. We calculated $s = x^2 + y^2$. If $s > 1$ or S = 0, then the values x and y should be regenerated again. If the condition $0<s\leq1$ is satisfied, then further by the formulas it is necessary to calculate:

$$z_0 = x\sqrt{\frac{-2\ln s}{s}},$$

$$z_1 = y\sqrt{\frac{-2\ln s}{s}};$$

Here z_0 and z_1 are independent quantities that satisfy the standard normal distribution.

The method considered above allows one to obtain a pair of independent normally distributed random variables with mathematical expectation 0 and variance 1. In order to obtain a distribution with other characteristics, it is sufficient to multiply the result of the function by the standard deviation and add the mathematical expectation.

Young's modulus for an isotropic material with normally distributed properties is calculated by the formula:

$$E = M[E] + \sigma[E] \cdot z,$$

where $M[E]$ is expected value and $\sigma[E]$ is standard deviation of the Young's modulus of the material.

MODELING MATERIAL WITH ACCUMULATED DAMAGE

As an example, the first approximation of modeling reinforced concrete structures with variable values of the modulus of elasticity of concrete is considered. The value of the modulus of elasticity in building structures is an important indicator both in determining the strength and deformation characteristics of load-bearing

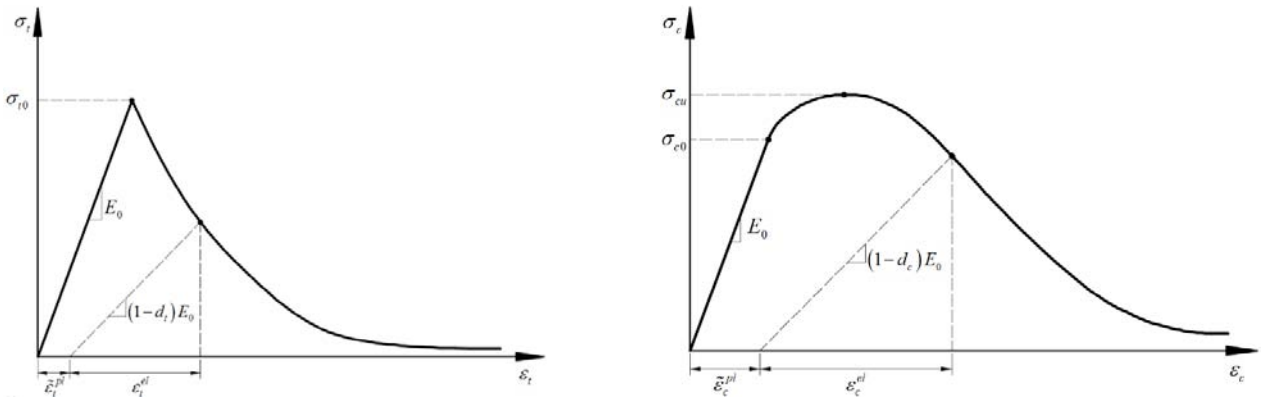

a) *b)*

Figure 1. Diagrams of concrete deformation described by the CDP model: a) in tension; b) in compression

structures, and is directly related to meeting the requirements for the first and second groups of limiting states. For example, Abaqus implements a model of fracture of brittle materials CDP [3, 4] (Concrete Damage Plasticity), in which the decrease in the elastic modulus is expressed through the scalar value of material damage d and the initial Young's modulus E_0:

$$E = (1 - d)E_0;$$

A formulation close to this implementation is also regulated by the Chinese standards GB 50010-2010 (applicable for concretes of the C20-C80 class with a density of 2200-2400 kg / m^3), for example, when determining tensile stresses:

$$\sigma = (1 - d_t)E_c\varepsilon;$$

Integrally, Young's modulus is also related to the dynamic characteristics of the object, which allows, on the basis of a comparison of the experimentally obtained natural frequencies of the structure and those obtained in the process of virtual tests, to speak about their residual resource after a long time of operation or after a seismic effect of high intensity, where there are residual damage to structures [10].

MODELING OF REINFORCED CONCRETE STRUCTURES WITH A RANDOM DISTRIBUTION OF YOUNG'S MODULUS OF HEAVY CONCRETE IN VOLUME

Based on the current regulatory legal acts, in particular GOST 28570-2019 for testing concrete samples taken from structures, the values of concrete compressive strength tend to the normal distribution law and are described by such indicators as standard deviation, coefficient of variation and mathematical expectation. It should be noted that for concretes with low strength indices, the application of the normal distribution law may be incorrect (for example, for aerated concrete, where there may be negative strength in a significant distribution range, which contradicts physical principles). The example presented below is a demonstrator of the previously described methods and is a prerequisite for the development of practical, verified methods for modeling such a class of problems.

Below is the procedure for user actions when using stochastic values of material parameters by the example of modeling an elementary structure – a pylon or a section of a wall. Omitting the classic, basic stages of developing a finite element model, the user specifies the required values in the parameters of the custom material, as well as the path to the

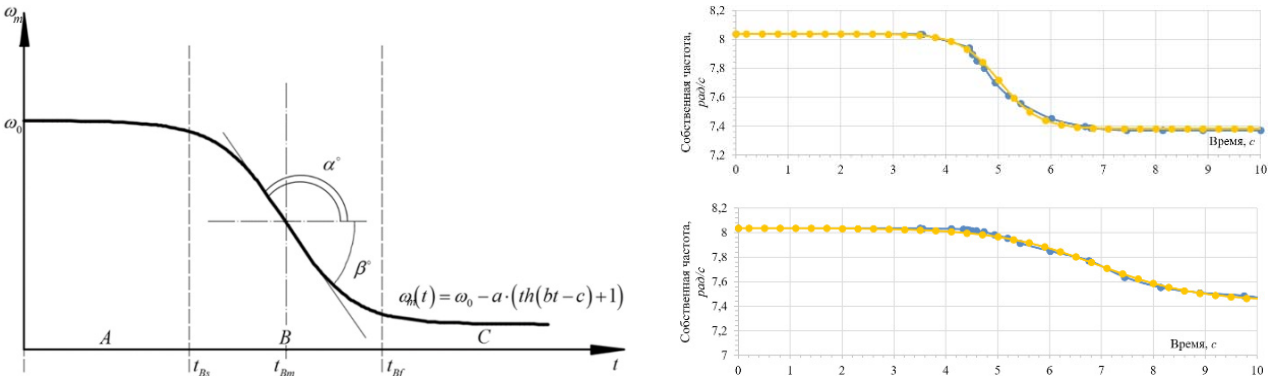

Figure 2. Derived function described in [10] and graphs of changes in the values of natural vibration frequency depending on Young's modulus for a reinforced concrete monolithic frame obtained in the process of virtual tests and calculated analytically without them

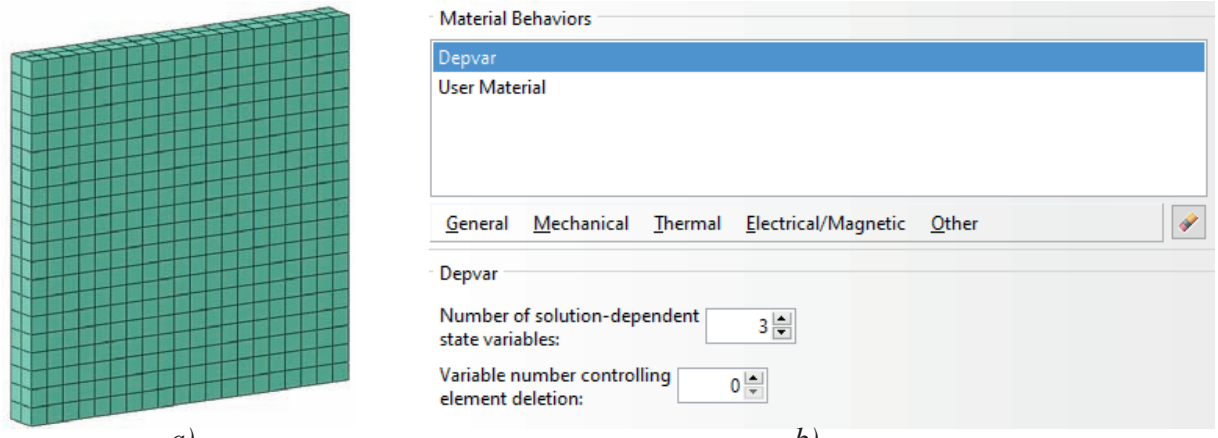

Figure 3. a) Finite element mesh of the test model, elements C3D8 - 8-node hexagonal FE of a continuous medium with a linear shape function; b) Setting the number of variables in the graphical interface; c) Description of variable values; d) Description of the path to the subroutine

custom subroutine in the menu for starting the calculation task in Abaqus. The mathematical expectation and standard deviation of Young's modulus are taken as variables $M[E]$and $\sigma[E]$, as well as Poisson's ratio μ.

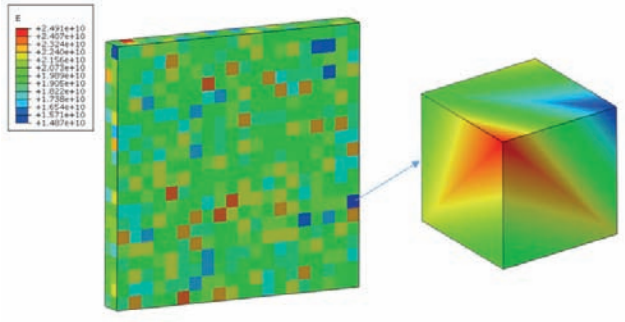

Figure 4. Mosaic of Young's modulus distribution for the test model, Pa

Based on the verification tests performed, the values of Young's modulus for the FE model were obtained, without taking into account the correlation of values in space, which in reality may be a random spread of poor quality of the material obtained during the production of work. Further, virtual tests were performed for two cases:

1. For the above-described elementary structure of a type of wall or pylon section, with the calculation of the calculated values of vertical stresses for concrete of class B40;
2. For a reinforced column (concrete class B25, steel A400), with a random value obtained for the entire volume of Young's modulus and subsequent analytical analysis of reliability over the entire height.

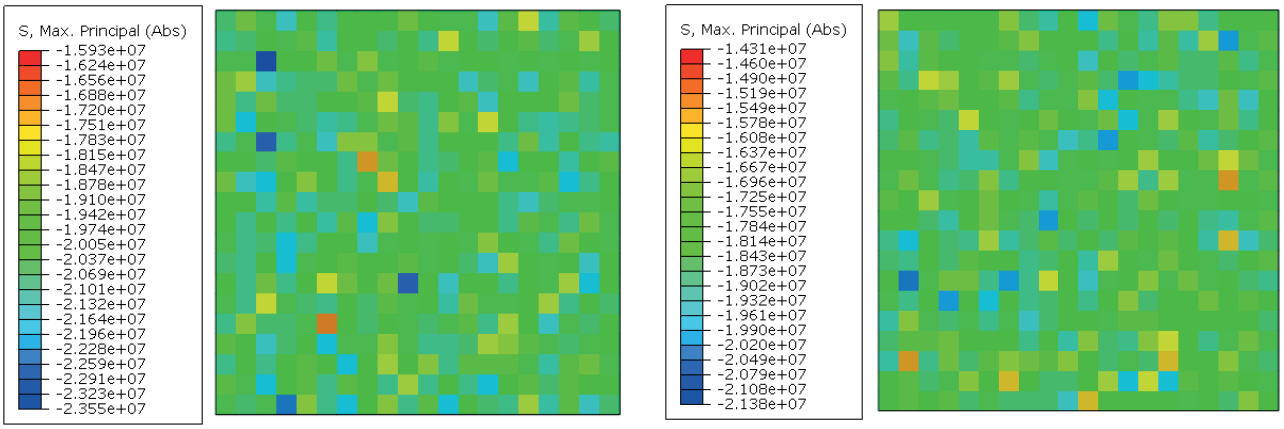

a) *b)*

Figure 5. Random design realizations of the mosaic of the distribution of the main stresses in concrete of class B40 of the wall model: a) Failure case (maximum compressive stress 23.55 MPa); b) Case to failure (maximum compressive stresses 21.38 MPa). Total failures for 500 virtual tests - 2. Reliability value 99.96% (β ≈ 3,35).

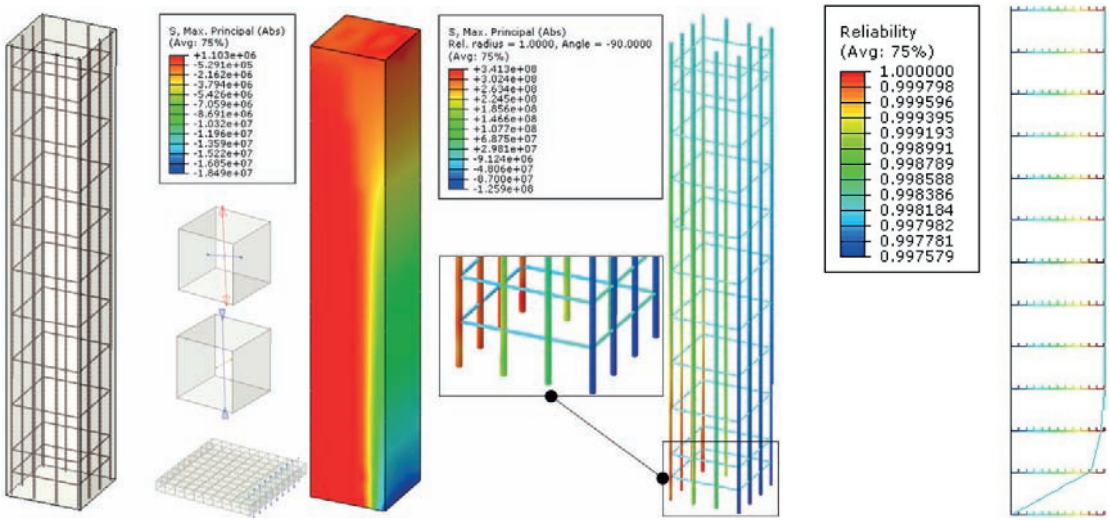

Figure 6. Control solution based on parametric optimization in a nonlinear formulation using volumetric finite elements (elements of the C3D8R and B31R types) (maximum stress in reinforcement 341 MPa, compressive stresses in concrete 18.5 MPa). Reliability diagram along the column height calculated for a bar analogue.

In the first case, after 500 virtual tests, local vertical internal stresses in concrete in 498 cases did not exceed the permissible design values. In 2 cases, these stresses were exceeded and can be identified as a local failure (but not a failure of the structure as a whole). At the same time, the reliability index $\beta = 3.35$, which is a relatively high indicator of reliability for load-bearing structures, based, for example, on the recommendation data of EN 1990: 2002 + A1. Eurocode - Basis of structural design (for objects of normal level of responsibility with an estimated service life of 50 years is 3.8).

In the second case, for one test, the distribution of the reliability value along the column height was obtained, taking into account the arising internal forces. For this example, using custom output data, for a bar analogue, a reliability diagram was

obtained for the entire structural element, which is a convenient integral indicator for assessing mechanical safety.

CONCLUSIONS

1. Based on the performed analytical and numerical studies, using the software module for generating random values of material parameters for numerical finite element models, the following conclusions can be drawn:

2. 1. A software module for generating random values of material parameters has been developed and verified, which allows for numerical analysis in a stochastic formulation both for the construction industry and for other technical areas, which is also important in the development of new products using modern materials that require study and appropriate certification;

3. 2. The practical application of the method in the universal complex of computer modeling Abaqus is shown: a series of virtual tests was performed with the calculation of the reliability value and the reliability index, a numerical-analytical method for constructing a reliability diagram was applied, which allows to evaluate sections of structures that do not meet the requirements of strength, stability and rigidity in an integrated manner in a convenient form.

REFERENCES

1. GB 50010-2010. Code for design of concrete structures. National standard of People's Republic of China. China architecture & building press – China – 2010. – 441 p.
2. ISO 2394:2015. General principles on reliability for structures [Text] – Switzerland, 2015. – 111 p.
3. **Lee J, Fenves GL.** Plastic-Damage Model for Cyclic Loading of Concrete Structures. J. Engng. Mech, – 1998. – Vol. 124 (8). – pp. 892–900.
4. **Lubliner J., Oliver J., Oller S., Onate E.** A Plastic-Damage Model for Concrete // Int. J. Solids Struct. – 1989. – Vol. 25 (3). – pp. 229–326.
5. **Shen S**. Stochastic material characterization of heterogeneous media with randomly distributed material properties. Doctor of Philosophy [Dissertation], 12.2012. – The Graduate Faculty of The University of Akron, USA, 2012. – 212 p.
6. **Zienkiewicz, O.C.** The Finite Element Method: vol.1 The Basis. [Text] / O.C. Zienkiewicz, R.L. Taylor // Butterworth-Heinemann, 2000. – 348 p.
7. Verifikatsionnyy otchot po PK Abaqus. Svidetel'stvo RAASN o verifikatsii PS № 05/ SIMULIA Abaqus/2014 ot 20.03.2014 goda.: v 4 t. [Verification report on PC Abaqus. RAASN certificate of verification of PS No. 05 / SIMULIA Abaqus / 2014 dated 03/20/2014: in 4 volumes] / FGBOU VPO «MGSU», LLC «TESIS». – Moscow, 2014
8. Standard of RF GOST 27751-2014. Nadezhnost' stroitel'nykh konstruktsiy. Osnovnyye polozheniya [Reliability for constructions and foundations. General principles]. – Moscow : Standartinform, 2015 – 16 p.
9. **Knut D.E**. Iskusstvo programmirovaniya. Tom 2. Poluchislennyye algoritmy (3-ye izdaniye, ispravlennoye i dopolnennoye) [The art of programming. Volume 2. Obtained algorithms (3rd edition, revised and enlarged)], Moscow: Dialektika, 2019.
10. **Chauskin A. YU.** Assessment of the reliability of a monolithic reinforced concrete building under the influence of a maximum flow rate earthquake [Tekst]. Candidate of Techn. Science: 05.23.17. Moscow, 2017 – 157 p.

СПИСОК ЛИТЕРАТУРЫ

1. GB 50010-2010. Code for design of concrete structures. National standard of People's Republic of China. China architecture & building press – China – 2010. – 441 p.
2. ISO 2394:2015. General principles on reliability for structures [Text] – Switzerland, 2015. – 111 p.

3. **Lee J, Fenves GL.** Plastic-Damage Model for Cyclic Loading of Concrete Structures. J. Engng. Mech, – 1998. – Vol. 124 (8). – pp. 892–900.
4. **Lubliner J., Oliver J., Oller S., Onate E.** A Plastic-Damage Model for Concrete // Int. J. Solids Struct. – 1989. – Vol. 25 (3). – pp. 229–326.
5. **Shen S**. Stochastic material characterization of heterogeneous media with randomly distributed material properties. Doctor of Philosophy [Dissertation], 12.2012. – The Graduate Faculty of The University of Akron, USA, 2012. – 212 p.
6. **Zienkiewicz, O.C.** The Finite Element Method: vol.1 The Basis. [Text] / O.C. Zienkiewicz, R.L. Taylor // Butterworth-Heinemann, 2000. – 348 p.
7. Верификационный отчёт по ПК Abaqus. Свидетельство РААСН о верификации ПС № 05/SIMULIA Abaqus/2014 от 20.03.2014 года.: в 4 т. [Текст] / ФГБОУ ВПО «МГСУ», ООО «ТЕСИС». – Москва, 2014
8. ГОСТ 27751-2014. Надежность строительных конструкций. Основные положения [Текст]. – Москва : Стандартинформ, 2015 – 16 с.
9. **Кнут Д.Э.** Искусство программирования. Том 2. Получисленные алгоритмы (3-е издание, исправленное и дополненное), Диалектика, 2019 г.
10. **Чаускин А. Ю.** Оценка надёжности монолитного железобетонного здания при воздействии максимального расчётного землетрясения [Текст]. Канд. техн. наук: 05.23.17: защищена 21.06.17: утв. 12.10.18 – Москва, 2017 – 157 с.

Alexander I. Khvostov, Lead Programmer, LLC Auriga, 117587 Moscow, Varshavskoe shosse, 125, building 16A; phone +7 (903) 685-79-91; E-mail: alexander.khvostov@auriga.com

Sergei I. Zhukov, PhD in Physics and Mathematics, Lead Programmer, Research Computing Center, Moscow State University, 119991 Moscow, Leninskie Gory, Building 1, Building 4; phone +7 (977) 333-56-07; E-mail: serge.zhukov@auriga.com

Sergey N. Tropkin, candidate of technical sciences, leading engineer of TESIS LLC; 127083 Moscow, st. Yunnatov, 18; phone: +7 (495) 612-44-22; E-mail: st@tesis.com.ru

Andrey Y. Chauskin, Candidate of Technical Sciences, General Director of REM Systems LLC; chief expert of OOO DPI Vostokproektverf; 121205 Russia, Moscow, Skolkovo Innovation Center; phone: +7 (977) 972-33-84; E-mail: a.chauskin@remsystems.ru

Александр Игоревич Хвостов, ведущий программист ООО «Аурига», 117587 Москва, Варшавское шоссе, д. 125, стр. 16А; телефон +7(903)685-79-91; E-mail: alexander.khvostov@auriga.com

Сергей Иванович Жуков, кандидат физико-математических наук, ведущий программист НИВЦ МГУ, 119991 Москва, Ленинские горы, дом 1, стр. 4; телефон +7(977)333-56-07; E-mail: serge.zhukov@auriga.com

Сергей Николаевич Тропкин, кандидат технических наук, ведущий инженер ООО «ТЕСИС»; 127083 Москва, ул. Юннатов, д. 18; телефон: +7(495)612-44-22; E-mail: st@tesis.com.ru

Андрей Юрьевич Чаускин, кандидат технических наук, генеральный директор ООО «РЕМ Системс»; главный эксперт ООО ДПИ «Востокпроектверфь»; 121205 Россия, г. Москва, Инновационный центр «Сколково»; телефон: +7(977)972-33-84; E-mail: a.chauskin@remsystems.ru

REVIEW

on educational and practical tutorial: **«DESIGN OF BASE, FOUNDATIONS AND UNDERGROUND STRUCTURES»**, prepared by R.A. Mangushev, A.I. Osokin, V.V. Konyushkov, I.P. Dyakonov, S.V. Lanko
(Saint Petersburg State University of Architecture and Civil Engineering)

The educational-practical manual, submitted for review, was prepared by the staff of the Department of Geotechnics of Saint Petersburg State University of Architecture and Civil Engineering. The work was carried out under the editorship of Corresponding Member. RAACS, Dr. Sciences, Professor R.A. Mangushev in A5 format and contains 594 pages of text, a bibliography of 61 titles and two appendices.

The tutorial under review was prepared for students of construction universities (bachelors, specialists and undergraduates), as well as for engineering workers of design and construction organizations. When writing it, the authors set themselves the task of showing students, university graduates and engineering and technical workers of design and construction organizations the main stages of calculation, design of foundations of buildings and underground structures; teach them to make competent decisions in the design, construction and reconstruction of various objects.

A feature of the tutorial under review is a wide range of issues under consideration including the range from the assessment of construction conditions, design of various types of foundations, underground parts of buildings and structures, to calculations and design of deep-laid foundations, foundations of high-rise buildings and structures, foundations in conditions of reconstruction and restoration of buildings. The main part of the issues under consideration is supported by practical examples of design.

There is a comment to tutorial. The tutorial does not cover the issues of monitoring the technical condition of buildings in the context of their reconstruction.

Evaluating the paper, it should be noted that despite the comment made, a full-fledged educational and practical tutorial has been prepared for students studying in the specialty 08.05.01 "Construction of unique buildings and structures", students studying in the direction "Construction" (bachelor's programs 08.03.01 and master's programs 08.04.01). The tutorial is also intended for employees of design and construction organizations in the construction industry. The presented work is written in workable manner, the main material of the tutorial is well illustrated by drawings, practical examples. The considered educational and practical tutorial "Design of base, foundations and underground structures" is recommended to be published in the presented form.

Head of the Department of "Bases and Foundations"
Kuban State Agrarian University, Honored Builder of the Russian Federation, Doctor of Tech. Sciences, Professor
A.I. Polischuk